Southern Illinois University Carbondale
OpenSIUC

Dissertations | Theses and Dissertations

5-1-2015

Towards Combined Computational and Experimental Studies on Toxicity of Silver Nanoparticles

Pamela Cabalu Ubaldo
Southern Illinois University Carbondale, pamela.ubaldo@outlook.com

Follow this and additional works at: http://opensiuc.lib.siu.edu/dissertations

Recommended Citation
Ubaldo, Pamela Cabalu, "Towards Combined Computational and Experimental Studies on Toxicity of Silver Nanoparticles" (2015). *Dissertations.* Paper 992.

This Open Access Dissertation is brought to you for free and open access by the Theses and Dissertations at OpenSIUC. It has been accepted for inclusion in Dissertations by an authorized administrator of OpenSIUC. For more information, please contact opensiuc@lib.siu.edu.

TOWARDS COMBINED COMPUTATIONAL AND EXPERIMENTAL STUDIES ON TOXICITY OF SILVER NANOPARTICLES

by

Pamela C. Ubaldo

B.S. Chemical Engineering,
University of Santo Tomas, Manila, Philippines, 2003

A Dissertation
Submitted in Partial Fulfillment of the Requirements for the
Doctor of Philosophy Degree

Department of Chemistry and Biochemistry
in the Graduate School
Southern Illinois University Carbondale
May 2015

DISSERTATION APPROVAL

TOWARDS COMBINED COMPUTATIONAL AND EXPERIMENTAL STUDIES ON TOXICITY OF SILVER NANOPARTICLES

By

Pamela C. Ubaldo

A Dissertation Submitted in Partial

Fulfillment of the Requirements

for the Degree of

Doctor in Philosophy
in the field of Chemistry

Approved by:

Lichang Wang, Chair

Qingfeng Ge

Kyle N. Plunkett

Zhihua Du

Dale Buck Hales

Graduate School
Southern Illinois University Carbondale
April 2015

AN ABSTRACT OF THE DISSERTATION OF

PAMELA C. UBALDO, for the Doctor of Philosophy degree in CHEMISTRY, presented on April 7, 2015 at Southern Illinois University Carbondale.

TITLE: TOWARDS COMBINED COMPUTATIONAL AND EXPERIMENTAL STUDIES ON TOXICITY OF SILVER NANOPARTICLES

MAJOR PROFESSOR: Dr. Lichang Wang

Despite the growing applications of silver nanoparticles, toxicity information on this nanomaterial is still deficient. Conclusions on the toxicity of silver nanoparticles vary and atomic level toxicity mechanisms are not yet achieved. Consequently, our group conducted combined computational and experimental toxicity studies of silver nanoparticles (AgNPs). Toxicity of 10 nm citrate stabilized AgNPs on HepG2 cells were investigated. Experimental results show that the 10 nm citrate stabilized AgNPs begin to be toxic to HepG2 cells at a dosage that exceeds 1 ppm and LD50 was observed at 3 ppm. Elevated reactive oxygen species levels were seen upon exposure to AgNPs with the maximum at the LD50 concentration of 3 ppm. Normal protein regulation of HepG2 cells were affected by exposure to AgNPs. TEM images of HepG2 cells exposed to AgNPs reveal that AgNPs can penetrate and agglomerate inside the cells.

Our preliminary computational study was guided by one of the widely accepted toxicity mechanism of AgNPs in which the nanoparticles dissolute to Ag^+. The computational model was composed of a 1:1 ratio of silver and phospholipid head. The silver employed are in atomic and anionic form while the phospholipid head are the phosphocholine (PC) and phosphoethanolamine (PE), which are abundant in HepG2

cells. Computational study shows that the presence of Ag^+ results in partial oxidation of both the phospholipid heads.

Our preliminary experimental and computational studies lead us to develop new computational methods that can accurately predict oxidation potentials (HOMO), reduction potentials (LUMO), and absorption spectra that can be used in studying toxicity mechanism of AgNPs through the oxidation pathway.

Thus, computational methods for cyclic voltammetry and absorption spectroscopy that use DFT and TD-DFT, respectively, were improved to provide more accurate electronic and optical properties.

Cyclopenta-fused polycyclic hydrocarbons (CP-PAHs) with available experimental data for HOMO, LUMO, ΔE_{gap} and absorption spectra and have potential application as AgNP stabilizers were used in developing the improved computational methods for cyclic voltammetry and absorption spectroscopy. The improved computational method for cyclic voltammetry was developed by accounting for the anion species that occur experimentally and by using B3LYP the best density functional in predicting the HOMO, LUMO and ΔE_{gap} of CP-PAHs with overall MAE of 014 eV. The best absorption spectra otef CP-PAHs were predicted using B3LYP for geometry optimizations followed by TD-CAMB3LYP with MAE of 29 nm. All calculations of CP-PAHs were implemented using the 6-311g (d,p) basis set and tetrahydrofuran (THF) as solvent.

These two developed computational methods were tested on a group of methyl triphenyl amine (MTPA) derivatives with available experimental data for HOMO, LUMO, ΔE_{gap} and absorption spectra and have potential application as AgNP stabilizers. The

new computational methods for cyclic voltammetry and absorption spectroscopy also provided the most accurate predicted electronic and optical properties of MTPA derivatives. Among the ten density functionals employed, prediction of HOMO, LUMO and ΔE_{gap} were most accurate using B3LYP and B3PW91 with overall MAE of 0.31 eV and 0.27 eV, respectively. Absorption spectra of MTPA derivatives were still best predicted using the B3LYP/TD-CAMB3LYP method with MAE of 13 nm. All calculations of MTPA were implemented using the 6-31+g (d,p) basis set and dichloromethane as solvent.

DEDICATION

This dissertation is dedicated to the most important people in my life

Elisa de Leon

Carlos Ubaldo

Purificacion Ubaldo

Ella Ubaldo

Patty Ubaldo

CJ Ubaldo

Ulik Augustine

ACKNOWLEDGMENTS

Completion of this work is not possible without the guidance, encouragement and expertise invested by my mentors and committee members both former and present.

I would like to thank Dr. Lichang Wang for her expertise, guidance and patience in mentoring me to learn the skills needed to complete this dissertation. Her innovative ideas, hard work and enthusiasm in physical and quantum chemistry has been contagious and helped me survive the six years of graduate school in chemistry.

I would like to thank Dr. Qingfeng Ge, for always asking challenging questions in my group meeting presentations which contributed to improving my analytical and problem solving skills.

I would like to thank Dr. Jay Means and Dr. Dale Buck Hales for their guidance and expertise in completing the experimental toxicity studies of this dissertation.

I would like to thank Dr. Kyle N. Plunkett for helping me understand cyclopenta-fused polycyclic aromatic hydrocarbons (CP-PAHs) and cyclic voltammetry better.

I would like to thank all my students who have helped me complete this work, Nathan D. Colley, Breanne L. Harell, Betsy J. Dick, Franklin Cavender, Ryan Chun, and Christian Mason.

I would like to thank my group members and colleagues who have challenged my ideas that helped improve my work and my friends Michael Fralaide and Kyle Klitzing who have dedicated a Saturday night to help with the table of contents.

TABLE OF CONTENTS

CHAPTER PAGE

ABSTRACT i

DEDICATION iv

ACKNOWLEDGMENTS v

LIST OF TABLES xiv

LIST OF FIGURES xvi

CHAPTERS

CHAPTER 1 – Introduction 1

1.1 Studies on the Dissolution of AgNPs to Ag^+ 3

1.2 Studies on the Effect of Stabilizers on Toxicity of AgNPs 5

1.3 Studies on the Effect of Size on Toxicity of AgNPs 6

1.4 Computational Studies on Toxicity of AgNPs 8

1.5 Objectives of this Work 9

CHAPTER 2 – Overview of Experimental and Computational Methods in Studying AgNP Toxicity.....10

2.1 Experimental Approaches in AgNP Toxicity Studies.....10

2.1.1 Cell Viability Tests.....11

2.1.2 Reactive Oxygen Species Assays 13

2.2 Computational Approaches in AgNP Toxicity Studies.....14

CHAPTER 3 – Overview of Density Functional Theory Methods.. 15

3.1 DFT and Time Dependent DFT.....….16

3.2 Characterization Methods Based on DFT and TD-DFT……..…… 23

3.2.1 Computational and Experimental Cyclic Voltammetry …..……..……..26

3.2.2 Computational and Experimental Absorption Spectroscopy……. 27

3.3 Accuracy Improvement of the DFT and TD-DFT Methods ……..……..……28

CHAPTER 4 – Experimental and Computational Studies of AgNP Toxicity…….31

4.1 Design of Experimental Studies on AgNP Toxicity…….……31

4.2 Measurement of AgNPs Toxicity on HepG2 cells…….…. 32

4.2.1 HepG2 Cell Culture…….…..32

4.2.2 HepG2 Cell Viability Test…….…... 33

4.2.3 Measurement of Oxidative Stress……..…….……..33

4.2.4 Extraction and Determination of Affected Proteins……. 34

4.2.5 TEM Experiments…… 35

4.3 Experimental Results of AgNP Toxicity on HepG2 cells……...36

4.3.1 HepG2 Cell Viability Curve and LD50 ……...……37

4.3.2 Oxidative Stress Caused by Exposure to AgNPs……...….....….38

4.3.3 Proteins Affected by AgNPs …… .....….39

4.3.4 TEM Results ……..... ……43

4.4 Computational Design in Studying AgNP Toxicity ……43

4.5 Computational Design of Measuring Ag^+ Toxicity ……..……..45

4.5.1 The Phospholipid-Silver Models…….46

4.5.2 Predicted Binding Energies and Absorption Spectra ……..... 46

4.6 Computational Results of Ag^+ and Ag^0 Toxicity on the Phospholipids …....47

4.6.1 Effects of Ag^+ or Ag^0 on the Phospholipids……..……..……47

4.6.2 Binding Energies of the Phospholipid-Silver Models…….……....51

4.6.3 Electronic Properties, Molecular Orbitals and Contour Plots ……..52

4.6.4 Absorption Spectra of the Phospholipid-Silver Models ……..56

4.7 Summary……. .....….57

CHAPTER 5 – Improved Computational Cyclic Voltammetry and Absorption Spectroscopy …….……. .....….59

5.1 Effects of the Different Alkyl –R groups on CP-PAHs ……..….60

5.2 Effects of Different Density Functionals on Accuracy of Computational Cyclic Voltammetry ……63

5.3 The Improved Computational Cyclic Voltammetry……..….67

5.4 Accounting for the Neutral and Anion State of the CP-PAH model……...72

5.5 The Improved Computational Absorption Spectroscopy …… 75

5.6 Summary…….…..82

CHAPTER 6 – The Improved Computational Cyclic Voltammetry and Absorption Spectroscopy on MTPA derivatives…… 84

6.1 Accuracies of the Density Functionals in Predicting Electronic Properties…85

6.2 Accuracies of the Density Functionals in Predicting Absorption Spectra.....93

6.3 Functional Group (-R) Dependent Accuracy of Predicted Electronic and Optical Properties of MTPA Derivatives …….98

6.3.1 Predicted Optical Properties MTPA Derivatives ……..……..… 99

6.3.2 Predicted Electronic Properties of MTPA Derivatives ……..…… 101

6.4 Summary ……..…. 104

CHAPTER 7– Conclusions and Future Work……..…… 106

REFERENCES……. 110

APPENDICES

APPENDIX A – Abbreviations…….123

APPENDIX B – Proteins Affected Upon Exposure to 5ppm 10 nm AgNP ……130

APPENDIX C – Optimized Geometries of the 8 CP-PAHS (Neutral and Anion) using B3LYP/6-311g(d,p)…..……...…… ….171

C1. CP-PAH1 Neutral Optimized Geometry ..…… ….171

C2. CP-PAH1 Anion Optimized Geometry ..…….. ….172

C3. CP-PAH2 Neutral Optimized Geometry ..…..…….....……173

C4. CP-PAH2 Anion Optimized Geometry ..……..… .175

C5. CP-PAH3 Neutral Optimized Geometry ..……176

C6. CP-PAH3 Anion Optimized Geometry ..……..… .178

C7. CP-PAH4 Neutral Optimized Geometry ..…… ….179

C8. CP-PAH4 Anion Optimized Geometry ..…….. ….180

C9. CP-PAH5 Neutral Optimized Geometry ..……181

C10. CP-PAH5 Anion Optimized Geometry ..……..…..... .182

C11. CP-PAH6 Neutral Optimized Geometry ..……183

C12. CP-PAH6 Anion Optimized Geometry ..……..…184

C13. CP-PAH7 Neutral Optimized Geometry ..……185

C14. CP-PAH7 Anion Optimized Geometry ..……..…186

C15. CP-PAH8 Neutral Optimized Geometry ..……186

C16. CP-PAH8 Anion Optimized Geometry ..……..…187

APPENDIX D- Vibrational Frequencies of the 8 CP-PAHs (Neutral and Anion) using B3LYP/6-311g (d,p)…… 188

D1. CP-PAH1 Neutral Vibrational Frequencies ..…… .. 188

D2. CP-PAH1 Anion Vibrational Frequencies..…….. 192

D3. CP-PAH2 Neutral Vibrational Frequencies..……196

D4. CP-PAH2 Anion Vibrational Frequencies..…….. 200

D5. CP-PAH3 Neutral Vibrational Frequencies..…… 203

D6. CP-PAH3 Anion Vibrational Frequencies..…….. 206

D7. CP-PAH4 Neutral Vibrational Frequencies..…… 208

D8. CP-PAH4 Anion Vibrational Frequencies..…….. 211

D9. CP-PAH5 Neutral Vibrational Frequencies……..214

D10. CP-PAH5 Anion Vibrational Frequencies..……..…..216

D11. CP-PAH6 Neutral Vibrational Frequencies..…… . 219

D12. CP-PAH6 Anion Vibrational Frequencies..……220

D13. CP-PAH7 Neutral Vibrational Frequencies..…… . 222

D14. CP-PAH7 Anion Vibrational Frequencies..…… 224

D15. CP-PAH8 Neutral Vibrational Frequencies..…… . 226

D16. CP-PAH8 Anion Vibrational Frequencies..…… 228

APPENDIX E- Predicted Excitation Energies of the 8 CP-PAHs using B3LYP/TD-CAMB3LYP and 6-311g(d,p) basis set.....230

E1. Excited State Energies with Oscillator Strength of CP-PAH1..... 230

E2. Excited State Energies with Oscillator Strength of CP-PAH2..... 233

E3. Excited State Energies with Oscillator Strength of CP-PAH1..... 237

E4. Excited State Energies with Oscillator Strength of CP-PAH1..... 240

E5. Excited State Energies with Oscillator Strength of CP-PAH1..... 243

E6. Excited State Energies with Oscillator Strength of CP-PAH1..... 246

E7. Excited State Energies with Oscillator Strength of CP-PAH1..... 248

E8. Excited State Energies with Oscillator Strength of CP-PAH1..... 252

APPENDIX F- Optimized Geometries of the 7 MTPA derivatives (Neutral and Anion) using B3LYP/6-31+g(d,p) 256

F1. MTPAa Neutral Optimized Geometry 256

F2. MTPAa Anion Optimized Geometry 257

F3. MTPAo Neutral Optimized Geometry 258

F4. MTPAo Anion Optimized Geometry ..... .260

F5. MTPA Neutral Optimized Geometry ..... .261

F6. MTPA Anion Optimized Geometry ..... .262

F7. MTPAcl Neutral Optimized Geometry 263

F8. MTPAcl Anion Optimized Geometry 265

F9. MTPAc Neutral Optimized Geometry 266

F10. MTPAc Anion Optimized Geometry ..... .267

F11. MTPAcc Neutral Optimized Geometry 268

F12. MTPAcc Anion Optimized Geometry 270

F13. MTPAn Neutral Optimized Geometry 271

F14. MTPAn Anion Optimized Geometry 272

APPENDIX G- Vibrational Frequencies of the 7 MTPA derivatives (Neutral and Anion) using B3LYP/6-31+g (d,p) 274

G1. MTPAa Neutral Vibrational Frequencies 274

G2. MTPAa Anion Vibrational Frequencies..... 277

G3. MTPAo Neutral Vibrational Frequencies..... 281

G4. MTPAo Anion Vibrational Frequencies..... 284

G5. MTPA Neutral Vibrational Frequencies..... 287

G6. MTPA Anion Vibrational Frequencies..... 291

G7. MTPAcl Neutral Vibrational Frequencies..... 295

G8. MTPAcl Anion Vibrational Frequencies..... 298

G9. MTPAc Neutral Vibrational Frequencies..... 302

G10. MTPAc Anion Vibrational Frequencies..... 305

G11. MTPAcc Neutral Vibrational Frequencies..... 308

G12. MTPAcc Anion Vibrational Frequencies..... 312

G13. MTPAn Neutral Vibrational Frequencies..... 315

G14. MTPAn Anion Vibrational Frequencies..... 319

APPENDIX H- Predicted Excitation Energies of the 7 MTPA derivatives using B3LYP/TD-CAMB3LYP and 6-311g(d,p) basis set..... 323

H1. Excited State Energies with Oscillator Strength of MTPAa..... 323

H2. Excited State Energies with Oscillator Strength of MTPAo..... 324

H3. Excited State Energies with Oscillator Strength of MTPA..... 326

H4. Excited State Energies with Oscillator Strength of MTPAcl..... 328

H5. Excited State Energies with Oscillator Strength of MTPAc..... 329

H6. Excited State Energies with Oscillator Strength of MTPAcc..... 331

H7. Excited State Energies with Oscillator Strength of MTPAn..... 333

VITA 336

LIST OF TABLES

TABLE PAGE

Table 2.1 IUPAC name and λ_{max} Detection of formazan formed using the tetrazolium compounds 12

Table 3.1 E_{XC} Approximations in the Jacob's Ladder 19

Table 3.2 Formalism of E_{XC} Approximations of the Ten Functionals 20

Table 4.1 Published LD50 of AgNP 37

Table 4.2 Identified Tubulin Family Proteins Affected by AgNP 41

Table 4.3 Identified Heat Shock Proteins affected by AgNP 42

Table 4.4 Binding Energies of PC-Ag^+ and PC- Ag^0 interactions 51

Table 4.5 Binding Energies of PE-Ag^+ and PE- Ag^0 interactions 52

Table 4.6 Contour plots of PC, PE and their interaction with Ag^+ and Ag^0 55

Table 5.1 Electronic properties of 1 and 2 with varying alkyl –R groups 61

Table 5.2 Errors and MAE of predicted HOMO 64

Table 5.3 Errors and MAE of predicted LUMO 65

Table 5.4 Errors and MAE of predicted ΔE_{gap} 66

Table 5.5 Errors and MAE of predicted LUMO using the proposed methods 69

Table 5.6 Errors and MAE of predicted ΔE_{gap} using the proposed methods 70

Table 5.7 Overall MAE for predicted HOMO, LUMO and ΔE_{gap} using the proposed and traditional method 72

Table 5.8 Change in C-C bond lengths as **1** is reduce 73

Table 5.9 Errors of Predicted λ_{max} of **1-7** 77

Table 5.10 Contour plots of the eight CP-PAHs 81

Table 6.1 HOMO Errors and MAE 87

Table 6.2 Predicted LUMO Errors and MAE 88

Table 6.3 Predicted ΔE_{gap} Errors and MAE 89

Table 6.4 Average MAE of HOMO, LUMO and ΔE_{gap} 91

Table 6.5 Predicted λ_{max} errors and MAE 95

Table 6.6 Contour plots of HOMO and LUMO of MTPA derivatives 100

Table 6.7 Predicted HOMO of MTPA derivatives relative to MTPA 101

Table 6.8 Predicted LUMO of MTPA derivatives relative to MTPA 103

Table 6.9 Predicted ΔE_{gap}, of MTPA derivatives relative to MTPA 103

LIST OF FIGURES

FIGURE PAGE

Figure 3.1 Jacob's Ladder of the ten density functionals..... 18

Figure 4.1 HepG2 cell viability curve upon exposure to 10 nm AgNP at 24 h 37

Figure 4.2 ROS level HepG2 cells exposed to 10 nm AgNPs at 24 h 38

Figure 4.3 TEM images of control (A) 5ppm dosed HepG2 cells (B & C)..... 43

Figure 4.4 Computational models of the phospholipids..... 44

Figure 4.5 PC-Ag^+ models with distances 48

Figure 4.6 PC- Ag^0models with distances 49

Figure 4.7 Ag^+ - PE models with distance 50

Figure 4.8 Ag^0 - PE models with distances 50

Figure 4.9 Energy Diagram of PC, PE, Ag^+, Ag^0 and their interactions..... 53

Figure 4.10 Predicted absorption spectra of PC, PE, their interaction with Ag^+ and Ag^0, and Ag^0..... 56

Figure 5.1 CP-PAHs structures 60

Figure 5.2 Predicted absoption spectra of **1** and **2** with varying –R groups using B3LYP/6-311g (d,p) on neutral model 62

Figure 5.3 The proposed method for computational cyclic voltammetry 68

Figure 5.4 Accuracy of predicted HOMO using the six density functionals 69

Figure 5.5 Comparison of predicted LUMO and ΔE_{gap} using traditional and proposed method 71

Figure 5.6 Contour plots and energy levels of A) oxidized, B) neutral, and C) reduced **1** calculated using B3LYP/6-311g (d,p) 74

Figure 5.7 Summary of the improved absorption spectra in silico and predicted

absorption spectra of **1** and **2** 75

Figure 5.8 Accuracy of predicting λ_{max} using seven CP-PAHs 78

Figure 5.9 Predicted absorption spectra of **3-8** 79

Figure 6.1. Chemical structure of MTPA derivatives 84

Figure 6.2 Predicted HOMO and LUMO in comparison to experimental values..... 86

Figure 6.3 Predicted HOMO, LUMO, ΔE_{gap} and overall MAE of MTPA derivatives..... 92

Figure 6.4 Predicted absorption spectra of MTPA derivatives..... 94

Figure 6.5 MAE of each density functional for absorption wavelength (λ_{max}) 96

Figure 6.6 Predicted absorption spectra trend of the different MTPA derivatives 98

CHAPTER 1

INTRODUCTION

Silver is generally low in toxicity (*1*). However, when decreased to nanoscale size, the toxicity of silver nanoparticles (AgNPs) is unknown. Yet they are present in topical wound dressings, cosmetics, textiles, detergent, food packaging, clothing, laundry detergent, water filters, electronics and many consumer products we use daily (*2-5*). The rapid growth of the application of this nanomaterial is attributed to its antimicrobial properties (*6-12*), good optical, conductive and other outstanding properties (*5*). Despite the growing applications of this material, information about its toxicity is still lacking (*5, 13*)**.** The lack of rigorous toxicity studies of AgNPs makes them prone to catastrophic failure in their potentially important applications.

In 2008, the International Center for Technology Assessment (CTA) and a coalition of consumer, health, and environmental groups filed a legal action for Environmental Protection Agency (EPA), to stop selling over two hundred (200) nanosilver products (*14*). This event resulted in more curiosity and controversy in the toxicity of AgNPs. Today, several experimental toxicity studies are available. However, conclusions vary due to the differences in parameters used in the toxicity studies such as nanoparticles size, shape, stabilizers, dosages, cell type and biochemical assays employed (*15*).

AgNPs exists in different sizes, shapes and are protected by capping agents such as citrate, PVP (polyvinylpyrrolidone), DDT (1-dodecanethiol), and many others depending on the purpose. Particle size that ranges from 1 nm to 100nm (*16*) and

shapes can be triangular, hexagonal, polyhedrons and others (*17*). Several studies show that these physical properties of AgNPs factor into its toxicity.

Toxicity of AgNPs was found to be dependent on the size, shape, concentration, pH, stabilizers, and the species it is exposed to (*18-22*). For instance, toxicity of AgNPs was found to increase as they become smaller or have stabilizers with more positive surface charges (*5, 23*). Toxicity of AgNP also decreases as the pH of the media used increases (*21, 24*). These toxicity trends can also vary depending on the species that the AgNPs are exposed to. Contreras, et. al. observed that 10nm AgNPs are more toxic to caenorhabditis elegans compared to 2 nm AgNPs (*18*). Other studies attribute the toxicity to the Ag^+ that possibly leaks out of the AgNPs (*19, 20, 25-28*).

In humans, AgNPs are known to affect differentiation of stem cells (*29*), induce oxidative stress, cause DNA damage, cell cycle arrest and apoptosis (*30*). Exposure to high concentration of AgNPs can result in diffuse pulmonary fibrosis that can be visible on chest radiograms (*31*). Argyria, which is a permanent blue-gray discoloration of skin, eyes and mucous membranes is a condition caused by silver. The permissible exposure limit to silver (metal and soluble compounds) by the Occupational Safety & Health Administration (OSHA) is 0.01 mg/m3 (*32*).

A total of 96,344 publications on silver nanoparticles in ISI Web of Science is available from 2002 to March 28, 2015. However, only 6,466 publications of these publications are dedicated to studying toxicity of silver nanoparticles. Majority of the toxicity studies on silver nanoparticles are done using different species and cell lines.

Despite the available toxicity studies, information about AgNP toxicity mechanisms is still lacking (*29*).

Computational studies that can provide molecular or atomic level toxicity mechanisms and properties of AgNPs are scarce and not well explored. Most computational studies in toxicity (including nanoparticles) often use Quantitative Structure Activity Relationship (QSAR) or other similar methods that employs statistical approach in measuring toxicity. These computational methods provide very good toxicity prediction relative to other nanoparticles with very similar structure. However, atomic level toxicity information specific to a particular nanoparticle is not provided.

In the next three sections, summary of experimental results of the three most common toxicity aspects of AgNPs are discussed. Section 1.4 describes the work in computational studies of toxicity of AgNPs. The last section of this chapter states the objectives of this work.

1.1 Studies on the Dissolution of AgNPs to Ag^+

The release of silver ion from AgNPs is one of the widely accepted toxicity mechanisms of AgNPs on different cell lines and species. Its antibacterial property can be attributed to this same mechanism. Studies of beneficial and adverse effects of the dissolution of silver nanoparticles to Ag^+ are often performed on different cell lines. However, its holistic effect is often overlooked and not well understood. The toxicity study by Sengstock et. al. suggested that AgNPs even at a non-toxic, very low concentration can impair human mesenchymal stem cell differentiation due to ionic

silver (*29*). Comfort and his co-workers observed a modification of the epidermal growth factor (EGF) signaling response caused by the slow dissolution of AgNPs into silver ions (*33*). Park and coworkers conducted toxicity study of AgNPs using He La cells and observed that sedimentation of aggregated AgNPs has a significant contribution to the toxicity of AgNPs at the early state of exposure. As exposure time to AgNPs prolongs, the toxicity is enhanced by the increase in silver ions (*34*). The group of Cronholm, et. al. studied toxicity of AgNPs on human lung cell lines A549 and BEAS-2B. Their results show that silver ions are released in a faster rate from $AgNO_3$ and are toxic to the cells compared to AgNPs that have a comparably slower release of silver ions (*35*).

On the other hand, other research groups are focused on beneficial effects of AgNPs such as its possible treatment for cancer. AgNPs are found to inhibit growth of different bacterial cells and cancer cells and are used as antibacterial agents and still being studied as a possible treatment for cancer.

Biosynthesized AgNPs shows toxicity on different human breast cancer cell lines (*36-38*). Locatelli, et al. studied the synergistic toxicity effect of AgNPs and alisertib on glioblastoma, which is the most aggressive malignant brain tumor. They used U87MG or human glioblastoma-astrocytoma epithelial like cell line and mice as well. Tumor reduction was observed in their study (*39*). Guo et. al, studied the toxic effects of AgNPs on chronic myeloid leukemia cells (CML) taken from patients. Their results show that AgNPs inhibited growth of these cancer cells and caused cellular and molecular alterations of the patient's cells, which is reversible by using vitamin C (*40*).

1.2 Studies on the Effect of Stabilizers on the Toxicity of AgNPs

A wide variety of stabilizers or capping agents are used in the synthesis of AgNPs. These capping agents prevent the fast leakage of silver ions and aggregation of the AgNPs (*41*). Several studies attribute toxicity of AgNPs to the stabilizers or capping agents.

A study done by Nguyen and coworkers showed that uncoated AgNPs are more toxic than coated AgNPs on J774A.1 macrophage and HT29 epithelial cells (*42*). The capping agents or stabilizers contribute to the final surface properties of AgNPs, which affects its toxicity properties. Sulfurized AgNPs decrease the toxicity of AgNPs due to the lower solubility of silver sulfide (*43*). The more positive surface charge, the more toxic the AgNPs will be. Polymer stabilizers that are cationic can form complexes with the DNA (negative charged) and bind to the plasma membrane (also negative charged) stronger than a neutral of anionic molecules (*44*).

Schlinkert, et. al. studied the toxicity of 7 – 10 nm AgNPs . They used sodium citrate or chitosan as AgNP coating, which provided surface charges of -50 mV to +70 mV on A549 cells and BEAS-2B cells, and primary lung epithelial cells. Results show that AgNPs with more positive surface charges are more toxic to the cells (*23*).

Shannahan, et. al. studied how protein corona functionalized AgNPs can modify its activity, bio-distrubution, cellular uptake, clearance and toxicity. Their choice of adding protein corona to the surface of AgNPs was based on their hypothesis that AgNPs will associate to proteins that are common in human serum and cell culture media forming a protein corona that can affect cell activation and cytotoxicity. AgNPs

with the protein corona showed decreased uptake by rat lung epithelial and rat aortic endothelial cells and were observed to activate cells by inducing IL-6 mRNA expression (*45*). Suresh and coworkers also studied toxicity of silver nanocrystallites with different capping agents on mouse macrophage (RAW-264.7) and lung epithelial (C-10) cell lines. Their group used poly(diallyldimethylammonium), chloride-Ag, biogenic-Ag, uncoated colloidal-Ag and oleate-Ag with different zeta potentials. In their study, the poly(diallylmethylammonium) coated AgNPs was the most toxic and the uncoated colloidal AgNPs were the least toxic.(*46*).

In summary, the degree that the stabilizers or capping agents contribute to silver nanoparticle toxicity is still not known.

1.3 Studies on the Effect of Size on Toxicity of AgNPs

Few groups have observed that the toxicity of AgNPs can be dependent on its size. This effect is related to the increased surface area of the AgNPs that interacts with ongoing chemical reactions in the cells. Toxicity studies of different sizes of AgNPs on different cell lines provide different conclusions.

Huk and coworkers studied toxicity of 50, 80 and 20 nm PVP stabilized AgNPs on human lung carcinoma epithelial cells (A549) and Chinese hamster fibroblast cells (V79-4). They observed that 50nm AgNPs resulted in strong cytotoxicity and genotoxicity but the 200nm AgNPs has the most mutagenic effect (*47*). Gilga, et. al also studied toxicity of 10, 40 , 75 nm citrate stabilized and 10 nm and 50 nm PVP stabilized AgNPs on BEAS-2B lung cells and observed that only the 10 nm AgNPs are cytotoxic to

the cells independent of their stabilizers. However, all their AgNPs caused increased DNA damage to the cells, which is independent of the size (*48*). Prasad and coworkers used HepG2 cells in studying the toxicity of 10 nm and 75 nm citrate stabilized and PVP stabilized AgNPs. Their results showed that the 10 nm AgNPs were more potent and that higher concentration of citrate stabilized AgNPs were found in the cells compared to PVP stabilized AgNPs. Their group also attributed this toxicity mechanism to the release of silver ions due the similar toxicity of $AgNO_3$ and AgNPs (*49*).

Meithling-Graff and coworkers studied toxicity of 10, 20, 40, 60 and 100 nm AgNPs and observed that cellular uptake was regulated by size. The smaller AgNPs penetrated the human LoVo cells while the 100 nm was not able to penetrate the cells (*50*). The group of Ivask, et. al studied size dependent toxicity of AgNPs to bacteria, yeast, crustaceans and mammalian cells in vitro. Their results show that toxicity of AgNPs was dependent on the nanoparticle dissolution and AgNPs that are less than10 nm tends to interact with cells and are more bioavailable either outside or inside the cells (*51*). Hamilton and coworkers studied toxicity of 20 -110 nm sizes of AgNPs that are stabilized with citrate and PVP. AgNPs that are 20 nm in size showed the most toxicity towards macrophage and lung epithelial cell lines. Their group also attributes the size dependent toxicity of AgNPs to the nanoparticle dissolution that release silver ions (*52*).

1.4 Computational Studies on Toxicity of AgNPs

Literature-available computational methods in modeling nanoparticle toxicity use statistical or mathematical approach in the study of nanoparticle toxicity. Important computational modelling methods by different groups are discussed below.

Kleandrova and coworkers developed a Quantitative Structure Toxicity Relationship (QSTR) perturbation model that can be used in simultaneously predicting ecotoxicity and cytotoxicity of coated and uncoated nanoparticles under multiple experimental conditions. Their model was derived from 36488 nanoparticle pairs and has an accuracy of > 98%. Their QSTR perturbation model was consists of nine descriptors (*53*).

Busse and coworkers developed a model for nanoparticles toxicity by using the Hodgkin-Huxley equations on the dynamic changes in membrane conductance and used Differential Evolution Algorithm for fitting their experimentally measured sodium-currents data. Their toxicity model measures toxicity of AgNPs using the coefficients in the Hodgkin-Huxley equations that change due to the impact of AgNPs. Unexposed and AgNPs dosed chromaffin cells, a type of neuronal cells, were used in their calculations (*54*).

The group of Silva, et. al. uses the general linear model (GLM) approach in predicting toxicity properties of three different kinds of nanoparticles each with different stabilizers namely citrate, polyvinylpyrrolidone and polyethyleneimine. Their model using GLM was able to explain 99.9% variation of toxicity in E. coli and 99.8% variation of toxicity in D. magna (*55*).

All these computational approaches discussed above provide a good toxicity model for AgNPs. However, it does not provide a clear atomic level understanding on the toxicity mechanism of AgNPs.

1.5 Objectives of This Work

One of the objectives of this work is to present an improved methodology in studying toxicity of AgNPs that combines experimental and computational tools to accurately predict toxicity properties. Our experimental toxicity study of AgNPs uses 10 nm citrate stabilized AgNPs on HepG2 cells. HepG2 cell line is often used in studying liver cell function in vitro (*56*) and is the organ where bioaccumulation of AgNPs are highest (*25, 57*).

This dissertation also aims to provide an atomic level toxicity mechanism of AgNPs using the Density Functional Theory (DFT) method. One pathway of toxicity of AgNPs in the cells is through oxidative stress or oxidation of different biological molecules that can result into higher level of reactive oxygen species. Lastly, this dissertation aims to establish computational methods that can accurately predict electronic and optical properties of different systems that can provide a toxicity information and mechanism of AgNPs through the possible oxidation of biological molecules.

CHAPTER 2

OVERVIEW OF EXPERIMENTAL AND COMPUTATIONAL METHODS IN STUDYING AGNP TOXICITY

Experimental methods for studying toxicity of AgNPs are similar to those used for toxicity measurements of any other toxic substances. In this chapter an overview of experimental and computational methods used in studying toxicity of AgNPs is presented. Implementation of these methods is also discussed the next sections.

2.1 Experimental Approaches in AgNP Toxicity Studies

Experimental methods used in the study of AgNP toxicity are similar to the general experimental approaches used in studying toxicity of any possible toxic substance. Most AgNP toxicity studies available are conducted using exposure studies on different species or cell lines. These species or cell lines are exposed to AgNPs with varying sizes, shapes, capping agents, media, and other variables that can affect toxicity. Preliminary toxicity measurement is done by probing how much of the species survived after exposure. In the case of cell cultures, live cells are measured after a certain exposure time using a cell counter or cell viability assays.

The presence of reactive oxygen species (ROS) in the cells, DNA damage and abnormal levels of proteins related to immune and inflammatory responses are also indication of toxicity (*58, 59*), which can lead to infertility (*60*), cancer and other diseases. Different toxicity assays and test kits are available and are coupled with analytical methods such as absorption spectroscopy, fluorescence spectroscopy,

luminescence, electrochemical measurements, and dynamic light scattering to measure the degree of a specific toxicity pathway. These different toxicity tests are further discussed below.

2.1.1 Cell Viability Tests

Numerous cell viability tests are available for determination of toxicity. Lethal dosage 50 (LD50) is one of the goals of the cell viability test. LD50 is the concentration at which 50% of the cells or species are still alive upon exposure to a possibly toxic substance for a certain time. Below are some of the most methods used for determination of cell viability

Tryphan Blue Exclusion Test is an old fashioned way of counting viable cell is through staining with a dye such as tryptophan blue followed by counting the stained live cells under a microscope using a hemocytometer. A faster way of counting the viable cells is through the use of an automated cell counter that provides results of viable cells in seconds (*61*).

Tetrazolium Reduction Assays is a colorimetric assay, which viable cells reduced the tetrazolium dye into a colored formazan. Cell viability is directly proportional to formazan measured by difference in absorbance intensity at a specific wavelength using a microplate reader. Commonly used tetrazolium compounds for measuring cell viability are MTT, MTS, XTT and WST-1. Their IUPAC names are available in Table 2.1. MTT carries a positive charge providing easy penetration to viable eukaryotic cells. The quantity of formazan formed using MTT is measured at

using a microplate reader. The latter three, MTS, XTT and WST-1, are all negatively charge, making them difficult to transport inside the cells. MTS, XTT and WST-1 (water soluble tetrazolium salt) require an intermediate electron acceptor that can transfer electrons from the cytoplasm or cell membrane to help reduce the tetrazolium to the colored formazan product. IUPAC names of the four tetrazolium salts and the suggested detection wavelength of the formazan dye formed is summarized in Table 2.1.

Table 2.1: IUPAC name and λ_{max} Detection of formazan formed using the tetrazolium compounds

Tetrazolium Compound	IUPAC Name	λ_{max} Detection
MTT	3-(4,5-dimethylthiazol-2-yl)-2,5-diphenyltetrazolium bromide	570 nm
MTS	3-(4,5-dimethylthiazol-2-yl)-5-(3-carboxymethoxyphenyl)-2-(4-sulfophenyl)-2H-tetrazolium	490 nm
XTT	2,3-bis-(2-methoxy-4-nitro-5-sulfophenyl)-2H-tetrazolium-5-carboxanilide	450 nm
WST-1	4-(3-(4-Iodophenyl)-2-(4-nitrophenyl)-2H-5-tetrazolio) 1,3-benzene disulfonate	420 – 480 nm

Resazurin Reduction Assays. This fluorescence assay is cell permeable like MTT. Resazurin (7-hydroxy-3H-phenoxazin-3-one-10-oxide) is blue in color. Its reduction in the cell results into resorufin, which is pink in color and highly fluorescent. The cell viability is directly proportional to the fluorescence intensity measured using a microplate reader at excitation wavelength of 530-560 nm and emission wavelength of 590 nm (*62*).

2.1.2 Reactive Oxygen Species Assays

Reactive oxygen species (ROS) in the cells is another way of measuring toxicity on a level deeper than the cell viability test. The interaction between cells and nanoparticles can cause the increased level of ROS that leads to an imbalance pro-oxidative state. Excessive amount of ROS can be damaging to the cell membrane, organelles and can be a direct source of genotoxicity. Accurate measurement of ROS is important to monitor cellular stress levels. The most common ROS are O_2^-, H_2O_2, $HO^\cdot$, $^1O_2$, all are more reactive than oxygen (*63*). Discussed below are some of the most commonly used assays developed to measure ROS levels.

H_2DCF-DA Assay is a fluorescent assay where 2',7'-dichlorodihydrofluorescein diacetate (H_2DCF-DA) a nonfluorescent molecule permeates the cells and is oxidized by ROS available in the cells to form of a fluorescent 2',7'-dichlorofluorescein (DCF). Upon permeation in the cell, acetate groups of H2DCF-DA are cleaved by unspecific esterases in the cell resulting to DCF. ROS level corresponds to the fluorescent intensity.

Homovanillic Acid (4-Hydroxy-3-methoxyphenylacetic acid, HVA) is a reagent used to detect oxidative enzymes available in the cells such as glucose oxidase. HVA is a major metabolite in the body and is associated to dopamine levels in the brain. The oxidative enzyme level corresponds to the fluorescent intensity as well.

Amplex Red is reagent used to detect the presence of H_2O_2 available in the cells. This reagent is colorless and reacts with H_2O_2 with a 1:1 stoichiometry to yield a

fluorescent resorufin. The resorufin can be detected using an excitation wavelength of 570 nm and emission wavelength of 585 nm. The fluorescent intensity corresponds to the H_2O_2 level.

2.2 Computational Approaches in AgNP Toxicity Studies

Common computational methods used in predicting toxicity of nanoparticles employ statistical approach or mathematical modelling in predicting toxicity such as Quantitative Structure Activity Relationship (QSAR), Quantitative Structure Toxicity Relationship (QSTR), and Quantitative Structure Property Relationship (QSPR). These methods use available experimental activity, property or toxicity information of different nanoparticles with similar structures in literature and correlate this information to different descriptors of the nanoparticles such as molecular weight, electronegativity, size and others. The correlation between the activity, property or toxicity information and descriptors is represented by a linear equation that can be used to predict activity, property or toxicity of other nanoparticles. These methods provide information about AgNPs relative to other kinds of nanoparticles with the similar structures. However, detailed toxicity information on the atomic level cannot be obtained using these methods. As such, we have chosen to employ DFT method in studying AgNP toxicity that will be discussed extensively in Chapter 3.

CHAPTER 3

OVERVIEW OF DFT METHODS

Density Functional Theory (DFT) has been the most successful and commonly used electronic structure calculation method for a wide range of systems. Its application includes, but not limited to, catalysis, solar energy harvesting and conversion, drug design and many more problems in science and technology (*64*). Unlike ab initio methods that use wavefunction, DFT uses function of electron density in solving complex electronic and molecular properties. Its success can be attributed to several people who have been dedicated in improving DFT and its implementation to various quantum mechanical problems and chemical systems.

In 1964, Pierre Hohenberg and Walter Kohn first introduced the use of density functional in calculating ground state of inhomogeneous electron gas systems(*65*) . The following year, Walter Kohn with Ju Leu Sham further improved the Hohenberg-Kohn DFT by using self-consistent equations that include exchange and correlation effects(*66*). In 1992, John A. Pople, Peter M. W. Gill and Benny G. Johnson formulated the Kohn-Sham DFT using a finite orbital basis expansion (*67*), which is used in all versions of the Gaussian Software. In 1998, the Noble Prize in Chemistry was awarded to Walter Kohn and John A. Pople for the development of DFT and computational methods in quantum chemistry, respectively, which commenced significant growth in the field of Computational Chemistry. In 2013, three more computational chemists, Martin Karplus, Michael Levitt, and Ariel Warshel, shared the Noble Prize in Chemistry for the development of multi-scale models for complex chemical systems.

These recognitions amplify the importance of computational work as much as experimental work. The application of the DFT computational methods pioneered by Kohn and Pople has expanded from solving simple chemical systems to more complex ones. As DFT provides atomic level description of a chemical system, we choose to use DFT to study toxicity of AgNPs. Since the accuracy of the DFT method is dependent on several factors, we also developed more accurate computational characterization techniques that can be employed towards the toxicity studies of AgNPs.

3.1 DFT and Time Dependent-DFT

DFT is a computational modelling method that uses concepts of quantum mechanics in solving the ground state electronic structure of a many body system. The system can be an atom, molecule or units of molecular structures. It originates from the Schrodinger equation shown in Eq. (3.1). The wavefunction (ψ) is replaced by functionals of electron density.

$$\hat{H}\psi = E\psi \tag{3.1}$$

where $\hat{H}$ is the Hamiltonian operator and E is the energy.

The version of DFT coded in the Gaussian Software is the Kohn-Sham DFT proposed by Pople's group in 1992, as defined in Eq. (3.2).

$$E_{KS}=E_T + E_V + E_J + E_{XC} \tag{3.2}$$

E_T, E_V and E_J are the kinetic, electron-nuclear interactions and Coulomb interaction energies of the electron densities respectively. E_{XC} is the exchange and correlation energy approximated using different density functionals (*67*). Since DFT solves the total energy of a system as a function of electron density, Eq. (3.2) can be further expanded as

$$E[\rho] = T[\{\Phi_i[\rho]\}] + \int dr\, \rho(r) v(r) + \frac{1}{2} \iint dr\, dr' \frac{\rho(r)\, \rho(r')}{|r - r'|} + E_{XC} \tag{3.3}$$

The success or failure of application of DFT is dependent on how well this term is approximated (*64*).

Similarly, the Time Dependent DFT (TD-DFT) originates from the time dependent Schrodinger equation shown in Eq. (3.4) and utilizes the functional of the electron density instead of the wavefunction (ψ) in its formalism.

$$i\hbar \frac{\partial}{\partial t} \psi = H\psi \tag{3.4}$$

TD-DFT is an extension of the ground state DFT into the excited states. The most critical choice in DFT and TD-DFT calculations is the selection of the density functionals.

Development of different density functionals used in DFT is inspired by the desire for increased chemical accuracy. In 2001, John P. Perdew and Karla Schimidt introduced the Jacob's ladder of density approximations in the world of Computational Chemistry, which has served as a guide in choosing the suitable density functional(*68*). Figure 3.1 shows the Jacob's ladder with the ten density functionals that were assessed in search

for the best computational method that can be employed in studying the toxicity of silver nanoparticles.

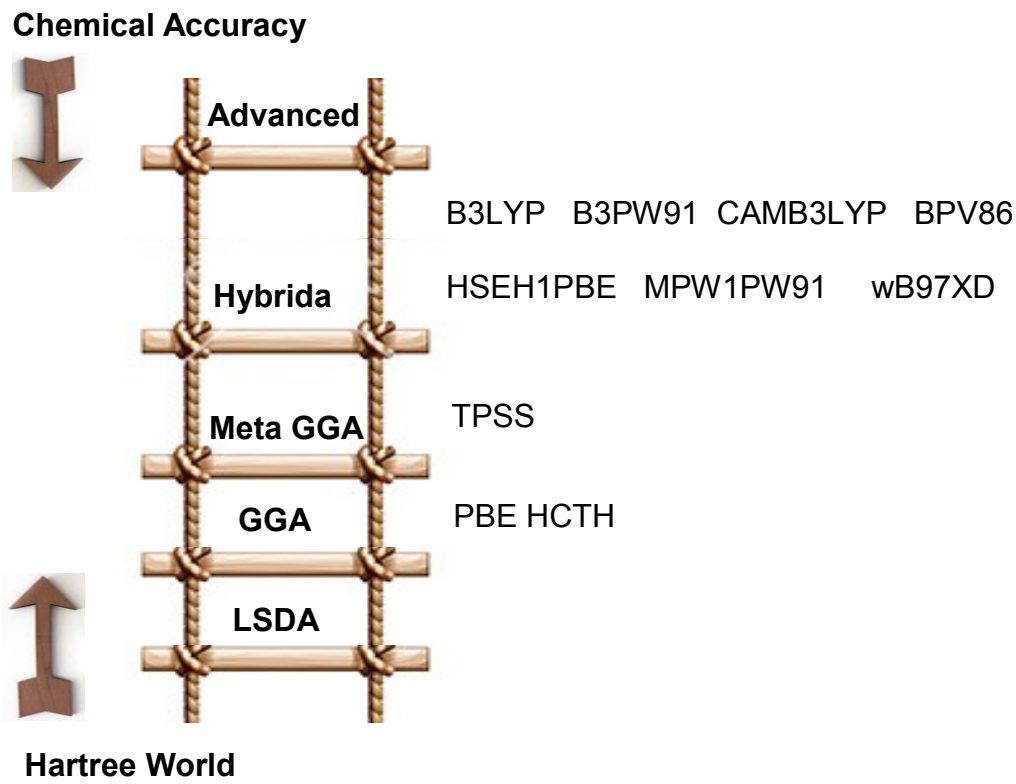

Figure 3.1: Jacob's Ladder of the ten density functionals

Each rung of the Jacob's ladder represents an approximation improved from the previous rung and higher chemical accuracy. The lowest rung of the ladder is the Local Spin Density Approximation (LSDA), which approximates E_{XC} as a function of spin densities ($n_{\uparrow} n_{\downarrow}$). The second rung is the Generalized Gradient approximation (GGA), which approximates the E_{XC} as a function of spin densities ($n_{\uparrow,} n_{\downarrow}$) and the density gradient ($\nabla n_{\uparrow}, \nabla n_{\downarrow}$). The meta-GGA on the third rung approximates the E_{XC} as a function of spin densities ($n_{\uparrow,} n_{\downarrow}$), density gradient ($\nabla n_{\uparrow}, \nabla n_{\downarrow}$) and the kinetic energy density ($\tau_{\uparrow,} \tau_{\downarrow}$). Hybrids in the higher rung of the ladder approximate E_{XC} using different

ratios of the exact exchange and local DFT exchange energies combined with chosen correlation energy approximation. Table 3.1 summarizes how the E_{XC} is approximated on each rung of the Jacob's ladder.

Table 3.1: E_{XC} Approximations in the Jacob's Ladder

Approximations	**Exchange and Correlation Energy (E_{XC})**
LSDA	$\int dr\, n(r)\, \varepsilon_{XC}(n_{\uparrow}, n_{\downarrow},)$
GGA	$\int dr\, n(r)\, \varepsilon_{XC}(n_{\uparrow}, n_{\downarrow}, \nabla n_{\uparrow}, \nabla n_{\downarrow})$
Meta-GGA	$\int dr\, n\, \varepsilon_{XC}(n_{\uparrow}, n_{\downarrow}, \nabla n_{\uparrow}, \nabla n_{\downarrow}, \tau_{\uparrow,}\tau_{\downarrow})$
Hybrids	$\frac{X}{100} E_X^{HF} + \left(1 - \frac{X}{100}\right) E_X^{local\ DFT} + E_C$

Understanding the derivation of E_{XC} on any density functional can be challenging but possible by first learning approximations in Table 3,1 in which developed density functionals were rooted. Different density functionals for the DFT method are available and new density functionals are continuously being developed in search for the best density functional. The background, formalism and key features of the ten density functionals employed in most of my work will be discussed in the next paragraphs. Table 3.2 shows all the ten density functionals with the formalism of the exchange and correlation energies.

Table 3.2: Formalism of E_{XC} Approximations of the Ten Functionals

Functional	Exchange Energy (E_X)	Correlation Energy (E_C)
B3LYP(*69-71*)	$0.2E_X^{HF}$+$0.8E_x^{LSDA}$+$0.72\Delta E_x^{B88}$	$0.81\ E_c^{LYP} + 0.19E_C^{VWN}$
B3PW91(*69*)	$0.2E_X^{HF} + 0.8E_X^{LSDA} + 0.72\Delta E_x^{B88}$	$E_C^{LSDA} + 0.81\Delta E_C^{PW91}$
HSEH1PBE(*72, 73*)	$0.25E_x^{SR-HF} + 0.75E_x^{SR-PBE} + E_x^{LR-PBE}$	E_C^{PBE}
MPW1PW91(*74*)	$0.25E_x^{HF} + 0.75E_x^{LSDA} + \Delta E_x^{GGA}$	$E_C^{LSDA} + E_C^{GGA}$
CAM-B3LYP(*75*)	$0.19E_X^{HF}$+$0.81E_x^{LSDA}$+$0.81\ \Delta E_x^{B88}$	$0.81\ E_c^{LYP} + 0.19E_C^{VWN}$
ωB97XD(*76*)	$0.22E_x^{SR-HF} + E_x^{LR-HF} + E_x^{SR-B97} + E_{disp}$	E_C^{B97}
BPV86(*71, 77, 78*)	$E_X^{LSDA} - \beta \sum_\sigma \int \rho_\sigma^{4/3} \frac{x_\sigma^2}{1 + 6\beta x_\sigma \sinh^{-1} x_\sigma}$	$E_C^{local\ VWN5} + E_C^{non-localP86}$
PBE(*79*)	$\int d^3r\ n\epsilon_x^{unif}(n)F_x$(s)	$\int d^3r\ n[\epsilon_c^{unif}(r_s, \zeta)$ +$H(r_s, \zeta$, t)]
TPSS(*80*)	$\int d^3r\ n\epsilon_x^{unif}(n)F_x$(p,z)	$\int d^3r\ n\epsilon_c^{revPKZB}$ x [1+ $d\epsilon_c^{revPKZB}(\tau^W/\tau)^3$]
HCTH(*81*)	$\sum_\sigma \int e_{X\sigma}^{LSDA}(\rho_\sigma) g_{X\sigma}(s_\sigma^2)dr$	$\sum_\sigma E_{C\sigma\sigma} + E_{C\alpha\beta}$

B3LYP or Becke's three-parameter (B3) exchange functional(*69*) with the Lee-Yang-Parr (LYP) correlation functional(*70*) is the most famous and commonly used density functional in the DFT method. The name B3LYP is almost synonymous to DFT. Derived from B3PW91 that is originally proposed by Becke, B3LYP was created and when Gaussian 94 software implemented different combinations of exchange and correlation functionals.(*82*)

B3PW91 or Becke's three-parameter (B3) exchange functional(*69*) with Perdew and Wang's 1991 correlation functional(*83-87*) is the functional proposed by Becke in 1993. The correlation energy of B3PW91 uses a LSDA with the Perdew and Wang's 1991 gradient correction for correlation energy. Atomization energies calculated using this functional provides a small average absolute deviation of 2.4 kcal/ mol from experimental values(*69*).

HSEH1PBE or Heyd- Scuseria-Ernzerhof exchange functional (HSE06 in literatures)(*72, 73, 88, 89*) with the Perdew- Burke-Ernzerhof (PBE) correlation functional(*78*) is a range separated hybrid functional with a screened Coulomb potential that is based on splitting the Coulomb operator into short and long range operators shown below

$$\frac{1}{r} = \frac{erfc(\omega r)}{r} + \frac{\mathrm{erf}(\omega r)}{r} \tag{3.5}$$

Computation time using HSEH1PBE functional is faster than regular hybrid functionals and is accounted to the short-range nature of its exchange integrals(*88*).

MPW1PW91 is an Adamo and Barone modified Perdew-Wang 1991 exchange functional with the Perdew and Wang's 1991 correlation functional. This functional has a mixing ratio of 0.25 : 0.75 exact to DFT exhange(*74*).

CAM-B3LYP or Coulomb Attenuating Method - B3LYP functional is developed to improve three important applications that B3LYP fails. These three applications include 1) polarizability of long chains, 2) excitations using TDDFT(*90, 91*) and 3) charge transfer excitations(*92-94*). The key step to the Coulomb Attenuating Method (CAM) is

the partitioning of the r_{12}^{-1} operator, in the exchange interaction into two parts as shown below

$$\frac{1}{r_{12}} = \frac{1-[\alpha+\beta\cdot\mathrm{erf}(\mu r_{12})]}{r_{12}} + \frac{1-\alpha+\beta\cdot\mathrm{erf}(\mu r_{12})}{r_{12}} \quad (3.6)$$

where α=0.19, α+β=0.65 and μ=0.33. The first term accounts for the short range interaction and the second term accounts for the long range interaction(*75*).

ωB97XD is a long range corrected hybrid functional that includes empirical atom-atom dispersion corrections. This functional includes 100% long-range exact exchange, 22% short-range exact exchange, a modified B97 exchange functional for short range interaction, the B97 correlation functional and an empirical dispersion correction(*76*).

BPV86 Is Becke's 1988 exchange functional(*77*) with Perdew's 1986 correlation functional modified by replacing local correlation with Vosko-Wilk-Nusair correlation functional(*71*).

PBE. Perdew- Burke-Ernzerhof exchange and correlation functional is a simple derivation of the exchange and correlation functional from Generalized Gradient Approximation (GGA) where all parameters, other than those in LSDA, are fundamental constants(*79*).

TPSS or Tao-Perdew-Staroverov- Scuseria exchange and correlation functional is derived from the Perdew-Kurth-Zupan-Blaha (PKZB) meta-GGA. The key step in the development of TPSS is that the meta-GGA exchange potential is set finite at the nucleus for ground-state one and two electron densities, an exact constraint satisfied by LSD (Local Spin Density) but lost in GGA(*80*).

HCTH or Hamprecht-Cohen-Tozer and Handy functional is a stand-alone functional developed from GGA using a least-squares procedure involving numerical exchange-correlation potentials and experimental energetics and nuclear gradients (*81*).

The performance of DFT depends critically on the accuracy of the density functional chosen in the calculations. Other factors that can affect accuracy are the basis set, type of systems or interaction being modelled, and fraction of exact exchange for hybrid functionals.

3.2 Characterization Methods Based on DFT and TD-DFT

As a chemical sample can be synthesized and characterized experimentally, so can it be computationally. Visualization software such as Gaussview and computing software packages such as Gaussian, VASP, ADF, NWChem, Quantum Espresso and etc. make it possible to synthesize a chemical sample with the use of computers or "*in silico"*.

Synthesis of a sample *in silico* involves three steps. The first step is identifying the chemical composition and structure of your sample followed by drawing it using the visualization software. Second step is geometry optimization where the most stable chemical structure with minimum energy is calculated using DFT (or other methods) and done with the aid of computing software. Choosing the appropriate level of theory (best density functional, basis set, solvation model, etc.) that will give an accurate result is essential in this step. Lastly, the optimized geometry must be probed for convergence

and any negative frequencies before performing any characterization techniques *in silico*.

Known experimental characterization techniques that can also be done computationally include X-ray crystallography, cyclic voltammetry, absorption spectroscopy, fluorescence spectroscopy, Raman spectroscopy, calorimetry, FTIR, NMR and more(*95*). A brief description of how these characterization methods and how they are done *in silico* are discussed below.

X-Ray Crystallography is a characterization technique often used for atomic or molecular structure determination of a crystal. A beam of x-rays is bombarded to the crystal producing diffraction pattern used to solve the crystal structure. *In silico*, solving the atomic or molecular structure of a chemical sample is completed using the three steps for synthesis *in silico* step discussed above. DFT optimized geometries using B3LYP are in good agreement with crystal structured solved using X-Ray crystallography.

Fluorescence Spectroscopy is another characterization technique similar to absorption spectroscopy. This spectroscopic technique involves measurements of radiation emitted by excited atoms or molecules. *In silico*, fluorescence spectroscopy is done by performing TD-DFT calculations on the excited state structure of the chemical sample.

Raman Spectroscopy is another spectroscopic technique that measures the inelastic scattering of monochromatic light produced by the interaction of light with the

molecular frequencies and excitation of the system. Raman spectroscopy can be done *in silico* by performing a frequency calculation on chemical sample synthesized *in silico*.

Calorimetry is a characterization technique that determines the changes in state of a system by measuring the amount of heat gained or lost by a system when subjected to different reactions. *In silico*, this method is done by calculating the ground state energy of each chemical components of the reaction and calculating the difference between the products and reactants.

FTIR is an abbreviation for Fourier Transform Infrared Spectroscopy is an important characterization technique used for structure determination. Absorption peaks in infrared spectrum represents vibrational frequencies of bonds that exist between atoms in the chemical sample. *In silico*, FTIR is done by performing frequency calculations after the ground state geometry calculations.

NMR is an abbreviation for nuclear magnetic resonance. It is a spectroscopy technique that based on chemical shifts of atoms that becomes present upon exposure to a static magnetic field and introduced to a second oscillating magnetic field. *In silico*, NMR spectroscopy can be performed in Gaussian09 software using the calculated ground state geometry of the chemical sample. Calculation of NMR shielding tensors and magnetic susceptibilities are essential to generate the predicted NMR spectrum. These two properties can be calculated using DFT together with the Continuous Set of Gauge Transformation (CSGT) or the Gauge Independent Atomic Orbital (GIAO) method(*95*).

The focus of this work is to improve the cyclic voltammetry and absorption spectroscopy computational methods that can be used in toxicity studies. These two characterization methods are discussed in detail in the next subsections. Computational results can serve as a guide to experimentalist, confirm experimental results or in some cases explain phenomena that cannot be explained using experiments alone. The use of DFT and TD-DFT provides an electronic and molecular level of characterization that is sometimes not possible experimentally for certain chemical samples.

3.2.1 Computational and Experimental Cyclic Voltammetry

Cyclic voltammetry is a versatile electroanalytical quantitative technique use in studying redox behavior of electroactive species(*96*). Important characteristics of the sample such as oxidation potential (HOMO), corresponding to the highest occupied molecular orbital and reduction potential (LUMO), corresponding to the lowest unoccupied molecular orbital, which are used in calculating the electrochemical band gap, can be extracted from a cyclic voltammogram. The most common cyclic voltammetry experimental set-up uses three electrodes namely the counter electrode, working electrode and the reference electrode. All these electrodes are connected to a potentiostat and immersed in an unstirred solution containing the solvent, electrolyte and a small concentration of the reactant or sample(*97*). A controlled potential is then applied across the working and reference electrode and is scanned between two values. As the potential scans in the negative direction, current rises to a peak and then

decays in a regular manner. The current response is dependent on the 1) electron transfer reaction and 2) the movement of electroactive material to the surface by diffusion. When the potential scan direction is reversed, the reduced form of the sample is oxidized back to the original starting material (*98*). The HOMO and LUMO energy levels are extracted from the first oxidation and first reduction potentials respectively. Frequently, -4.8 eV, HOMO energy level of ferrocene in vacuum is used as reference in calculating the HOMO and LUMO energy levels of a sample (*99*).

Conventionally, cyclic voltammetry is performed using software such as Gaussview and Gaussian 09. A neutral chemical sample is first synthesized *in silico*, i.e. geometry optimization. After geometry optimization step, the HOMO and LUMO energy levels can be directly extracted from an output file. Accuracy of the calculated HOMO and LUMO is dependent on factors such as density functional, basis set, solvation model and type of systems being studied. The HOMO-LUMO band gap is calculated from the predicted HOMO and LUMO. In general, there is a big discrepancy between the experimental and calculated HOMO-LUMO band gaps.

3.2.2 Computational and Experimental Absorption Spectroscopy

Absorption spectroscopy is a technique that measures the absorption of radiation as function of wavelength or frequency. Different molecules will have different absorption wavelengths upon exposure to radiation. Absorption bands in absorption spectrum represent electronic transitions that occur due to excitation of outer electrons upon absorption of radiation. Absorbance also increases as concentration of a

chemical sample increases. Quantitative measurement of radiation absorption is defined by the Beer-Lambert's Law in Eq. (3.7)

$$I\ (\lambda) = I_0\ (\lambda) e^{-L\sigma(\lambda)c} \tag{3.7}$$

where I_0 is initial intensity, I is the radiation intensity after passing light through a cuvette with a thickness *L* and a sample concentration *c* and $\sigma(\lambda)$ is the absorption cross section(*100*).

Computational absorption spectroscopy is obtained by performing TD-DFT calculations after the *in silico* synthesis of a chemical sample and specifying how many excited states (N) needed to be involved.

3.3 Accuracy Improvement of the DFT and TD-DFT Methods

Several groups have been working on improving the accuracy of DFT and TDDFT. Development of new hybrid density functionals that can accurately various properties are ongoing. In addition, correction methods that can increase accuracy of the different density functionals are also being investigated.

Double hybrid functionals have been developed and now used by a few for DFT calculations. Su et. al. studied accuracy of conventional hybrid functionals and new doubly hybrid functionals in predicting fractional charge behavior, ionization potential (IP), electron affinity (EA) and ΔE_{gap} using a data set of seven atoms and five molecular species. XY3G, a doubly hybrid density functional with the cc-PVQZ basis set provided the best predicted IP, EA and E_{gap} with MAE of 0.10, 0.37 and 0.39 eV respectively.

B3LYP predicted IP, EA and bandgap resulted in MAE of 0.37, 0.25 and 0.59 eV, respectively, in their study (*101*).

Some correction methods for DFT calculations were studied by Zhang and Musgrave. They used eleven different density functionals that include LSDA, five GGA, three hybrid GGA, one hybrid and one hybrid meta GGA on a set of twenty seven molecules in aim to improve accuracy of predicting HOMO, LUMO and ΔE_{gap}. Their group predicted HOMO more accurately using a correction formula: $-HOMO_{corr} = A + B \times (-HOMO_{cal})$ where A and B are determined using a linear correlation of each functional with experimental values. Their uncorrected ΔE_{gap} is calculated using HOMO and LUMO eigenvalues and corrected ΔE_{gap} using TD-DFT. Their corrected LUMO is determined by subtracting the corrected HOMO from the corrected ΔE_{gap}. KMLYP, BH&HLYP, and B3LYP are the top three in in their list of predicting HOMO with MAE of 0.73, 1.48 and 3.10 eV before correction and MAE of 0.24, 0.25 and 0.37 after correction. All eleven density functionals inaccurately predicted experimental electron affinity from LUMO eigenvalues due to the poor description of virtual orbitals that result from extensive relaxation of occupied orbitals. MAE of predicted E_{gap} using KMLYP, BH&HLYP, B3LYP are 4.96, 4.29 and 1.63 eV before correction and 1, 0.95 and 0.85 eV after correction. Predicted ΔE_{gap} using GGA functionals are relatively accurate (~0.73 eV) despite their inaccuracy in predicting HOMO and LUMO (*102*).

Several studies on improving accuracy of TDDFT prediction of absorption spectra and excited state energies are also available. In the work done by Rabilloud in the absorption spectra prediction of silver clusters, it was found that long range correction of the exchange functional is essential in the description of absorption

spectra of large silver clusters. CAM-B3LYP and ωB97x are two of the most accurate density functionals in calculating absorption spectra and lowest excitation energy of silver clusters with MAD of 0.08 and 0.09 eV, respectively, for Ag_n clusters with n= 4, 6, 8, 12, 18, and 20 (*103*).

Peach and coworkers studied prediction of excitation energies of eighteen molecules that range from N_2 to a tripeptide using PBE, B3LYP and CAM-B3LYP. Their group correlated the errors in calculation of excitation energy to the overlap parameter (Λ), the spatial overlap between the HOMO and LUMO. Their study showed that CAM-B3LYP is best in predicting the excitation energy of range of molecules from N_2 to a tripeptide with no correlation between Λ and errors, while PBE, and to a lesser extent B3LYP resulted in an increase in excitation energy errors as the overlap parameter (Λ) reduces (*104*).

Dev et. al observed the same correlation between the choice of functional and overlap parameter (Λ) of different organic dyes where CAM-B3LYP outperformed the functionals PBE, M06L, B3LYP and wB97XD in most of their organic dyes (*105*). Our group improved the prediction of LUMO energy of organic dyes using TD-B3LYP with the basis sets 6-31+g(d,p) and 6-311+g(d,p) by accounting for all the optically active molecular orbitals (OAMOs) involved in the excitation aside from the HOMO and LUMO (*106*). A few groups now use TD-CAM-B3LYP on B3LYP optimized ground state structures that provide excitation energies, absorption and emission spectra that are in good agreement with experimental values (*107-109*).

CHAPTER 4

EXPERIMENTAL AND COMPUTATIONAL STUDIES OF AGNP TOXICITY

A variation of experimental results is available on toxicity of silver nanoparticles with the same sizes and stabilizers. However, computational studies are not well explored. As such, we have conducted experimental toxicity studies on 10 nm citrate stabilized AgNPs on HepG2 cells, which is presented in sections 4.1 to 4.3. Our computational studies on AgNP toxicity are presented in sections 4.4 to 4.6.

4.1 Design of Experimental Studies on AgNP Toxicity

When AgNPs are absorbed in the body, the target organ for accumulation is the liver (*110*). Liver is a vital organ responsible for metabolism and detoxification in the body. In vitro studies of the liver often use HepG2 cell line, which is widely accepted as a valuable and informative model system for studying human liver cell functions(*13*). This cell line is also preferred as an in vitro model of the liver for drug metabolism studies (*111, 112*).

HepG2 cell culture was conducted and the responses of these cells to different concentrations of 10 nm citrate stabilized AgNPs purchased from NanoComposix was observed. The effects of AgNP to the cell viability, morphology, oxidative stress, and protein expressions were determined. The concentration of AgNP was varied to the following: 0.3, 0.5, 0.75, 1, 1.5, 3, and 5 ppm. Each AgNP concentration was introduced to HepG2 cells. Viable cells were measured using tryphan blue exclusion

test and TC10 automated cell counter from BioRad. LD50 was determined using the cell viability curve.

Oxidative stress caused by different concentrations of AgNPs was also probed using H_2DCFDA fluorescent assay that measures the amount of reactive oxygen species present in HepG2 cells. The morphology and integrity of HepG2 cells upon exposure to AgNPs and the location of AgNPs in HepG2 cells were also studied using transmission electron microscope (TEM). In addition, protein expression studies were conducted to determine which proteins in HepG2cells are affected upon exposure to 10 nm citrate stabilized AgNPs.

4.2 Measurement of AgNP Toxicity on HepG2 cells

Measurement of AgNP toxicity on HepG2 cells entails a series of steps before observing toxic effects of AgNPs. This section provides a detailed protocol employed in HepG2 cell culture, cell viability test, oxidative stress measurements, identification of affected proteins, and TEM imaging of HepG2 cells.

4.2.1 HepG2 Cell Culture

HepG2 cells were purchased from ATCC. A complete growing media containing 10% fetal bovine serum, 1% non-essential amino acids, 1% of 100mM sodium pyruvate, 1% Penicillin-Streptomycin 10/10 from Atlanta Biologicals, 2.5% of 1M HEPES buffer solution and 84.5 % minimum essential media was used in the cell culture. Cells were

grown to approximately 85% confluent and subcultured to a ratio of 1:4 every three days. HepG2 cells were grown at 37°C in a 5% CO_2 humidified incubator.

4.2.2 HepG2 Cell Viability Test

An estimate of 4x10^{4} cells were seeded in 48 well plates and grown to approximately 60% confluent upon dosing with different dosages of citrate stabilized AgNP for 24 h. The cells were exposed to 0.3, 0.5, 0.75, 1, 1.5, 3, and 5 ppm of citrate stabilized 10 nm AgNP. The HepG2 cells with 0.1μM citrate dosed for 24 hours and AgNP and citrate free HepG2 cells were the two controls used to observe cytotoxic effect of increasing dosage of 10 nm citrate stabilized AgNP. After 24 hours of treatment, cells were washed with MEM, trypsinized, incubated at 37 ^{o}C in 5% CO_2 humidified incubator for a minute and resuspended in complete growing media. Cells were dyed with tryphan blue, which penetrates dead cells. The dead cells were counted using TC10 automated cell counter from BioRad to determine cell viability of HepG2 cells exposed to different concentrations of 10 nm citrate stabilized AgNPs.

4.2.3 Measurement of Oxidative Stress

Approximately about 2x10^{4} cells were seeded to a 96 well plate and grown to 70% confluent upon dosing with different dosages of citrate stabilized AgNP for 24 hrs. The cells were exposed to 0.3, 0.5, 0.75, 1, 1.5, 3, and 5 ppm of citrate stabilized AgNP and incubated at 37 ^{o}C in 5% CO_2 incubator upon treatment. The HepG2 cells with 0.1

μM citrate dosed for 24 hours and AgNP and citrate free HepG2 cells were the two controls used to observe how different dosages of AgNP will affect oxidative stress level in the cells. After 24 hours of treatments, cells were further incubated with 200 μL of 100 mM H2DCFDA (2,7-dichlorodihydrofluorescein), a nonfluorescent and reduced form of flourescein, and dispersed in HBSS for 30 min. The cells were washed with PBS and then switched back to complete growing media. The fluorescence intensity for each well was monitored using excitation at 485nm and emission at 528nm.

All fluorescence intensity measurements were normalized by total protein present on each well. After the fluorescence measurements, the cells were suspended in PBS and lysed by sonication. Total amount of protein on each well was then determined using bicinchoninic acid (BCA) protein assay reagent.

4.2.4 Extraction and Determination of Affected Proteins

About $4x10^6$ cells were seeded in a 135mm dish and grown to approximately 70% confluent upon dosing with 5ppm citrate stabilized silver nanoparticles for 24h. Undosed cells were used as control. After 24h of treatment, cells were washed with ice cold PBS and gently scraped from the dish. Cells were then centrifuged at 450xg for 5 min at 4^oC. Cell pellet formed was chemically lysed using Qproteome mammalian protein preparation kit from Qiagen. Total protein of each sample was determined and normalized using BCA protein assay reagent. The unfractionated samples were then sent to MSBioworks LLC for analysis.

Each protein sample was extracted and lysed from equal numbers of HepG2 cells and was then mixed with LDS buffer and loaded onto a 4-12% SDS-PAGE gel. A gel electrophoresis experiment was then conducted to separate proteins according to molecular weight. At the end of the gel electrophoresis experiment, the SDS-page gel with the separated protein was stained with coommassie blue. Each gel band was digested with trypsin and profiled using protein-works protein profiling unfractionated in preparation for the liquid chromatography (LC) - mass spectroscopy (MS) experiments. The gel digests were analyzed using nano LC/MS/MS with Waters NanoAcquity HPLC system interfaced to a ThermoFisher Orbitrap Velos Pro. Peptides were loaded on a trapping column and eluted over a 75μM analytical column at 350nL/min with both columns packed with Jupiter Proteo Resin (Phenomenex) employing a 1 hr gradient. The mass spectrometer was operated in data-dependent mode, with MS performed in the Orbitrap at 60,000 FWHM resolution and MS/MS performed in the LTQ. The fifteen most abundant ions were selected for MS/MS. The Mascot database containing peptide mass fingerprints from Matrix Science Ltd. London was used in identifying proteins characterized using MS/MS.

Spectral counting, a non-labeling relative protein quantification technique, was used in this study. Spectral counting proteomics is an emerging technique and has been very useful for its simplicity and low cost compared to isotope labeling approaches. In spectral counting relative amount of protein in a sample is correlated with number of peptide spectrums which belong to that protein.

4.2.5. TEM Experiments

TEM was used to observe the morphological differences between cells treated for 24h with 5ppm AgNP and untreated cells. Cells were fixed using 4% gluteraldehyde in 0.1 M PBS overnight and post-fixed with 1% OsO4 in 0.1M PBS for 1 h. Cell pellets were dehydrated by suspending into 25%, 50%, 75%, 100% ethanol and 100% propylene oxide consecutively for 15 min in each solution, 1:1, 2:1 and 0:1 EMBed 812 and propylene oxide, for 2h and overnight respectively. After dehydration, cell pellets were embedded in beam capsules and dried in the oven at 60 ^{o}C for 48 h, followed by sectioning. Ultrathin sections (50-100 nm) were collected and images were obtained using TEM (Hitachi-7500, Hitachi, Ltd. Tokyo Japan).

4.3 Experimental Results of AgNP Toxicity on HepG2 cells

Other groups have done cell viability experiments on 24 h AgNPs treated HepG2 cells using different nanoparticle size, stabilizers, manufacturers and assays. Table 4.1 shows a summary of their results.

Published LD50 results shown in Table 4.1 for 24 h exposure vary and some are significantly different from the others. Hence, our group also conducted cell viability experiments to determine the LD50 of 10 nm citrate stabilized AgNPs in HepG2 cells.

Table 4.1: Published LD50 of AgNP

Author	AgNP size	Stabilizer	Manufacturer	Method	LD50
Nowrouwzi, et. al.(*113*)	10 nm	Water	Biocera in South Korea	MTT & XTT assays	2.5 - 3 ppm
Kawata, et. al.(*19*)	7 - 10 nm	Polyethyl-enimine	Kyoto Nanochemical Co., Ltd., Japan	neutral red uptake assay	2.5 ppm
Lin, et. al.(*114*)	5 nm	Water & SMA	Gold Nanotech Industries	MTT assay	> 30ppm
Eom, et. al.(*30*)	2 nm	PVP	-not mentioned	MTT assay	> 20 ppm

* Some abbreviations above are SMA for poly(styrene-co-maleic anhydride)-grafting poly(oxylkyalkylene), PVP for polyvinylpryrrolidone

4.3.1 HepG2 Cell Viability Curve and LD50

Upon 24 h exposure of HepG2 cells to 10nm citrate stabilized AgNP, a positive dose-response is established between AgNP and its toxicity. Similar viability were observed on cells exposed to 0.1 uM citrate and with AgNP concentration of 0, 0.3, 0.5, 0.75 and 1 ppm. Significant cell death is noticeable at a dosage of 1.5 ppm after 24h of treatment. LD50 where only fifty percent of HepG2 cells survived was observed at the dosage of 3ppm (Figure 4.1). HepG2 cell viability decreases with increasing dosage of the 10 nm citrate stabilized AgNPs. This LD50 is in the range with the results from other groups that used 10nm AgNPs shown in Table 4.1. Considering all these cell viability information, the toxic dosage for 10 nm citrate stabilized AgNPs is >1ppm.

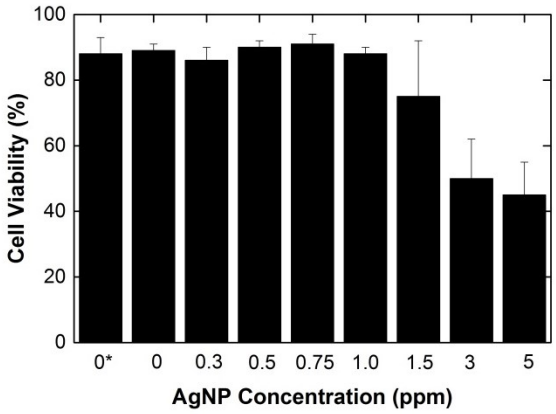

Figure 4.1: HepG2 cell viability curve upon exposure to 10 nm AgNP at 24 h , 0* has 0.1 uM citrate solution

4.3.2 Oxidative Stress Caused by Exposure to AgNPs

Oxidative stress level in cells is a reliable indication of toxicity and an earlier step to cell death. In our study, oxidative stress was measured using H_2DCFDA. The 24 h exposure of HepG2 cells to 10 nm citrate stabilized AgNPs generated a positive dose-response between AgNP and ROS. Increasing dosage of AgNPs resulted in elevation of ROS levels (Figure 4.2). At low dosage of 0.3 ppm of AgNPs, an increase in ROS level compared to two controls (citrate and 0ppm) is noticeable. A maximum ROS level was reached at 3ppm and went back down at 5ppm where major population of cells was dead. Pairing this information with cell viability response curve (Figure 4.1) where a noticeable decreased in cells begins at 1.5ppm is indicative of HepG2 cells ability to withstand higher level of reactive oxygen species before cell death.

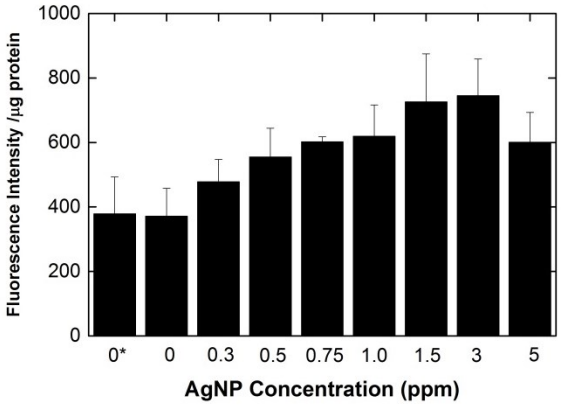

Figure 4.2: ROS level of HepG2 cells exposed to 10 nm AgNPs at 24 h, 0* has 0.1 uM citrate solution

Previous studies of oxidative stress induced by AgNP on HepG2 cells resulted on elevated ROS and decreased antioxidant level as the dosage is increased(*113*). Kim, et. al. emphasized that toxicity of AgNP in HepG2 cells is mainly due to oxidative stress(*45*). Other groups that used different cell lines such as human dermal and cervical cancer cell lines yielded the same effect of AgNP to the cells (*50*). Though different methods, cells and AgNPs were used in measurement of oxidative stress levels, all these findings clearly agree that exposure of cells to AgNP can lead to generation of elevated ROS levels followed by in the cell death. Compared to previous studies, similar scenario was observed in our oxidative stress study.

4.3.3 Proteins Affected by AgNPs

Using LC tandem mass spectrum and spectral counting approach we were able to identify a total of 1218 proteins from both the treated (5ppm of 10 nm citrate stabilized AgNP) and control HepG2 cells. The number of proteins identified from the

control was 1026, which was slightly more than those identified from the treated, which was 987. In both samples, the false discovery rate (FDR) was 0.1%. The proteins which were affected were membrane proteins, cytoplasmic, cytoskeletal and some nuclear proteins. It was interesting to observe mitochondrial proteins such as 60 kDa Heat shock protein being affected significantly. Among the identified proteins, it was observed that regulation of fatty acid synthase, heat shock proteins, the tubulin beta chain, the histone family proteins, spectrin family proteins and other numerous proteins were affected by exposure to AgNPs. Interestingly, some of the proteins which show large spectral count differences are involved in calcium dependent movement of the cytoskeletal membrane, cell motility, protein structure control, ATPase cycle, glycolysis, participate in RNA transcription and ribosome assembly, and involved in RNA metabolism both in nucleus and mitochondria, and others.

The control and treated cells culture were started from equal numbers and upon harvest we tried to keep the number of cells comparable. In addition to minimize the difference in cells we used proportional amount of protein extraction kits. Furthermore, an equal amount of sample was loaded onto the SDS gel. These steps would minimize or control the differences caused by sample handling and preparation and maintain the original expression differences. The tubulin family proteins as a whole were observed to be down expressed in the treated cells when compared to the control cells shown in (Table 4.2). As a family, these proteins are cytoskeletal proteins in the cytoplasm and are major constituents of microtubules. Microtubules are key components of the cytoskeleton. They are long, filamentous, tube-shaped protein polymers that are essential in all eukaryotic cells. They are crucial in the development and maintenance of

cell shape, in the transport of vesicles, mitochondria and other components throughout cells, in cell signaling, and in cell division and mitosis. They are composed of alpha and beta tubulin dimers and their functionality is determined by the expression and post translational modification of tubulin proteins (*41*).

Table 4.2: Identified Tubulin Family Proteins Affected by AgNP

Protein Accession Number	M.W.	Spectral count		Change in Regulation
		0 ppm	5 ppm	
sp|Q9BQE3|TBA1C_HUMAN	50 kDa	60	39	-21
sp|P07437|TBB5_HUMAN	50 kDa	77	53	-53
sp|Q13885|TBB2A_HUMAN	50 kDa	59	0	-59
sp|P68371|TBB2C_HUMAN	50 kDa	73	50	-23
sp|Q13509|TBB3_HUMAN	50 kDa	40	32	-8

The ribosomal protein family (40 S ribosomal protein) was also down expressed. They are proteins of the ribosome, large ribonucleo-protein particles where the translation of messenger RNA (mRNA) into protein occurs. They are both free in the cytoplasm and attached to membranes of eukaryotic and prokaryotic cells. A total of 26 proteins were identified and quantified in this family and all were found to be expressed low in the treated sample compared to the control. Depending on their post translational modification they have different functionality and importance.

Four heat shock proteins were identified and quantified. All were highly expressed in the treated sample relative to the control shown in Table 4.3.

Table 4.3: Identified Heat Shock Proteins affected by AgNP

Protein Accession Number	M.W.	Spectral count		Change in Regulation
		0 ppm	5 ppm	
sp|P08107|HSP71_HUMAN	70 kDa	28	51	+23
sp|P11142|HSP7C_HUMAN	71 kDa	30	41	+11
sp|P07900|HS90A_HUMAN	85 kDa	62	79	+17
sp|P08238|HS90B_HUMAN	83 kDa	90	98	+8

The change in protein expressions of the identified proteins upon exposure to AgNP provides a deeper level of toxicity information in comparison to just the cell viability curve.

Several groups have studied effects of AgNPs on gene and protein expressions on different cells. Xin and coworkers has also detected up regulation of heat shock protein 70 (HSP70) on A549 cells and HepG2 cells upon exposure to 20-50 nm AgNPs. The up regulation of HSP70 in HepG2 cells is dosage dependent (*115*). Huang, et. al observed that 3-5 nm AgNPs can alter gene and protein expression of amyloid beta on mouse brain neural cells and induce Alzheimer's disease (*116*). Junpeng, et. al studied the injury and dysfunction caused by AgNPs on human umbilical vein endothelial cells (HUVECs) through oxidative stress pathway via IKK/NF-kappaB pathways. Up regulation of inflammatory cytokines, adhesion molecules and chemokines of HUVECs were observed (*117*).

4.3.4 TEM Results

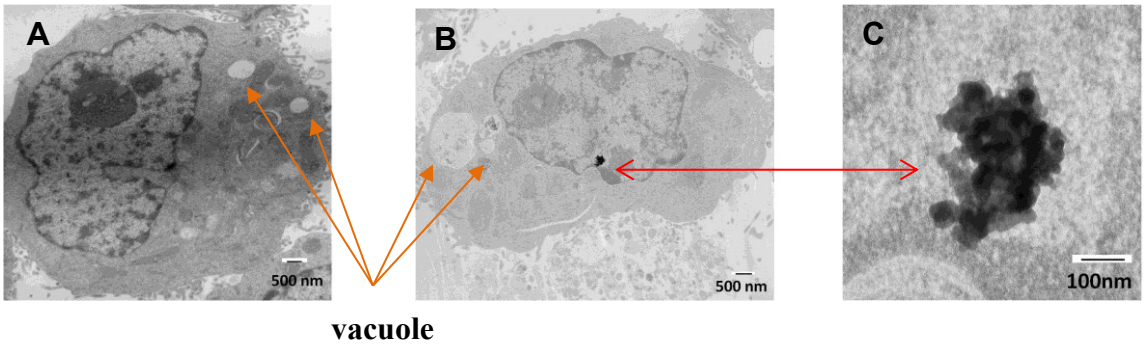

Figure 4.3: TEM images of control (A) 5ppm dosed HepG2 cells (B & C)

Agglomerated citrate stabilized AgNP were found to penetrate the treated HepG2 cells. Figure 4.3 B and C show that an agglomeration found in the nucleus is about 300 nm in size. The treated cells were observed to shrink in size having a smaller diameter (≈7nm) than control (10-13nm). Moreover, an expansion of vacuole containing large amount of lysosome responsible in intracellular digestion of waste were also noticeable in the treated cells. This change in cell morphology in the treated cells is an indication that the dosage used (5ppm) is extremely toxic to the cells.

4.4 Computational Design in Studying AgNP Toxicity

Even though some toxicity information on AgNPs is available on the cellular level toxicity, numerous groups still claim that there is little information known about its toxicity mechanism. Computational studies on AgNP toxicity that can provide molecular level toxicity information of AgNPs are not readily available. Our preliminary toxicity model is based on several studies on that account AgNP toxicity to the Ag^+ that

leaks over time as discussed in Chapter 2. Using Ag^+ as part of the computational model can also represent this phenomena. Both the Ag^+ and Ag^0 were used to determine how these two states of silver that possibly leak out of AgNPs and interact with HepG2 cells. Before anything permeates inside the cells, it will need to interact and pass by the cell membrane, which protects the integrity of the cell and is composed of lipid bilayers. The major lipid components of HepG2 cells are 1-palmitoyl-2-oleoyl-sn-glycero-3-phosphocholine (POPC) and 1-palmitoyl-2-oleoyl-sn-glycero-3-phosphoethanolamine (POPE) (*118-120*). These two lipids both have a hydrophobic tail (oleic acid, palmitic acid and part of glycerol) and a hydrophilic head containing a choline or ethanol amine group with a phosphate group, which are more likely to interact with silver.

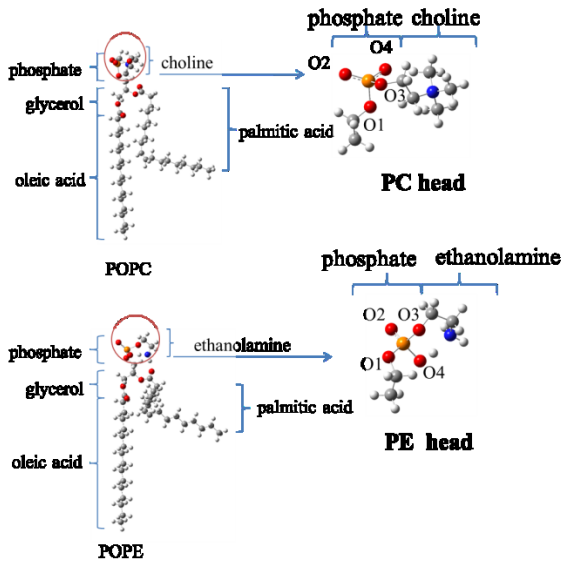

Figure 4.4: Computational models of the phospholipids

Our computational models represents interaction between the two phospholipid heads with Ag^+ and Ag^0. The phosphocholine (PC) and phosphoethanolamine (PE) heads of POPC and POPE respectively shown in Figure 4.4 were used chosen. A 1:1 ratio of phospholipid to silver, which translates to a high silver concentration, is used in our interaction models. Ag^+ or Ag^0 is located near one of the four oxygens in both phospholipids to identify the preferred location of silver. Each of these four positions were labeled as P1, P2, P3 and P4 where the number represents which oxygen of the phosphate the Ag^+ or Ag^0 was initially introduced. A total of sixteen phospholipid head-silver models were established. These sixteen are composed of the four different positions using PC-Ag^+, PC-Ag^0, PE-Ag^+, and PE-Ag^0 interactions.

Oxidation of the phospholipid heads by the Ag^+ or Ag^0 corresponds to toxicity. Computational measurement of toxicity was done using the calculated electronic properties, binding energies and contour plots of the models. Electronic properties together with the contour plots can provide information on the oxidation or reduction of the phospholipid heads caused by Ag^+ or Ag^0. The calculated binding energy can be used to determine the interaction that exists between the phospholipid heads and silver. In addition, changes in the structure of the two phospholipids upon exposure to Ag^+ or Ag^0 and their absorption spectra were studied as well.

4.5 Computational Design of Measuring Ag^+ Toxicity

In our computational design a 1:1 ratio of silver (neutral and anion states) and phospholipid head (PC and PE) model were employed. The computational details

employed in studying toxicity of Ag^+ that leaks from AgNPs are discussed in the next sections.

4.5.1 The Phospholipid-Silver Models

Density Functional Theory (DFT) in the Gaussian 09 software was used in the geometry optimization of the sixteen phospholipid-silver models. B3LYP was used for all DFT calculations. Hybrid basis sets were used in the interaction of the phospholipid heads with silver. The 6-311g (d,p) basis set was used for two phospholipid heads while the LANL2DZ basis set was used for Ag^+ and Ag^0. GaussView05 was used to visualize geometries and interaction between the phospholipid heads and silver. All optimized models were done in water and were inspected for structural conformational changes caused by Ag^+ or Ag^0. Electronic properties and contour plots of HOMO and LUMO were also generated using the optimized phospholipid – silver models.

4.5.2. Predicted Binding Energies and Absorption Spectra

Among the sixteen phospholipid head- silver models, the most stable geometries for the PC-Ag^+, PC-Ag^0, PE-Ag^+, and PE-Ag^0 interaction were used to calculate the binding energies and absorption spectra. The binding energies generated by the interaction of Ag^+ or Ag^0 with the phospholipid heads were calculated using the total energy of each of the sixteen phospholipid head- silver model, the PC and PE head, and Ag^+ and Ag^0. The binding energy is defined by Eq. (4.1) below.

$$E_{binding} = E_{phospholipid\ head - silver\ model} - [E_{phospholipid\ head} + E_{silver}] \quad (4.1)$$

where the phospholipid head can be PC or PE and silver can be Ag^+ or Ag^0. A negative value of the binding energy defined in Equation 4.1 represents an attraction between the silver and phospholipid head while a positive number represents a repulsion interaction.

Time Dependent Density Functional Theory (TDDFT) was used to calculate all absorption spectra. B3LYP with the hybrid basis sets of 6-311g (d,p) for the phospholipid heads and LANL2DZ for silver were also used in all TDDFT calculations. The solvent used in all calculations is water.

4.6 Computational Results of Ag^+ and Ag^0 Toxicity on the Phospholipids

Computational results of the exposure of a phospholipid heads to Ag^+ and Ag^0 are presented in this section. The effect of Ag^+ and Ag^0 on conformational structure of phospholipids, binding energies, contour plots, electronic properties and absorption spectra are discussed in the next sections.

4.6.1 Effects of Ag^+ or Ag^0 on the Phospholipids

The presence of Ag^+ caused structural conformational changes to the two phospholipid heads. The interaction of PC-Ag^+ (Figure 4.5), resulted in the straightening of PC, which has a bent structure in the absence of Ag^+ (Figure 4.4). In the PC-Ag^+ interaction represented in Figure 4.5, the silver ion's preferred positions are ranked as

P4>P1>P3>P2, where the first two (P4 and P1) have both straight conformation. All these four possible positions shows that the silver ion prefers interaction with O2 and O4, two oxygen in the phosphate group that can freely bind, yielding the shortest distance of silver ion to the phosphate group of 2.28 Å for all four positions. Partial oxidation of the PC was also observed in the PC-Ag^+ interaction. The partial electron gained by PC from the Ag^+ ranges from 0.141 to 0.164.

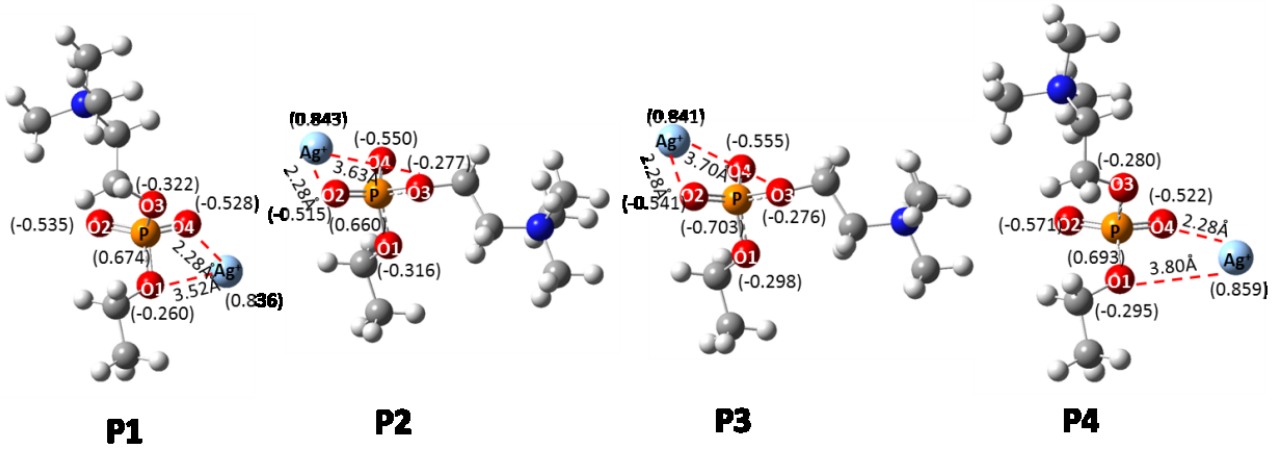

Figure 4.5: PC-Ag^+ models with distances, Mulliken atomic charges. Red - oxygen, orange - phosphorus, gray - carbon, white - hydrogen, royal blue – nitrogen, and light blue – silver

The PC-Ag^0 interaction (Figure 4.6) shows that the preferred position of the silver atom is P3>P1>P2>P4 with bent-straight-bent-straight conformation pattern. The shortest distance observed between the silver atom and phosphate group of PC is 4.72 Å (P4 in Figure 4.6), which is about twice the distance of PC-Ag^+ interaction. This

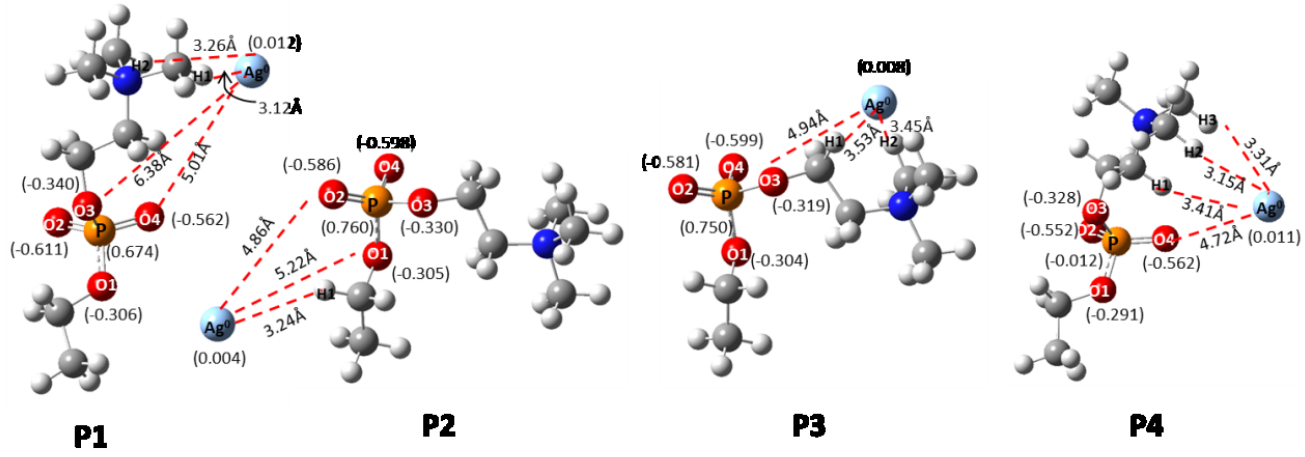

Figure 4.6: PC- Ag^0models with distances, Mulliken atomic charges. Red - oxygen, orange - phosphorus, gray - carbon, white - hydrogen, royal blue – nitrogen, and light blue – silver

indicates that silver atom does not bind to PC as strongly as the ion state and possibly repelled by the PC. A partial reduction of the PC was also observed in the presence of Ag^0. The PC lost partial electrons ranging from 0.004 - 0.012.

The interaction of PE-Ag^+ is shown in Figure 4.7. No drastic structural change was observed in the PE head. In the presence or absence of the silver ion, PE still prefers to have a bend conformation. The preferred positions of Ag^+ around PE shown in Figure 4.7 is rank as P4>P3>P1>P2 where all four has a bent conformation. The shortest distance of silver ion to PE is 2.29 Å for positions P1, P3, and P4 in Figure 4.7. This distance of 2.29 Å is very similar to that of PC-Ag^+ interaction with the shortest distance of 2.28 Å for all four positions. The silver ion was observed to partially oxidized PE. The partial gain of electron by PE in the presence of silver ion ranges from 0.124 to 0.137.

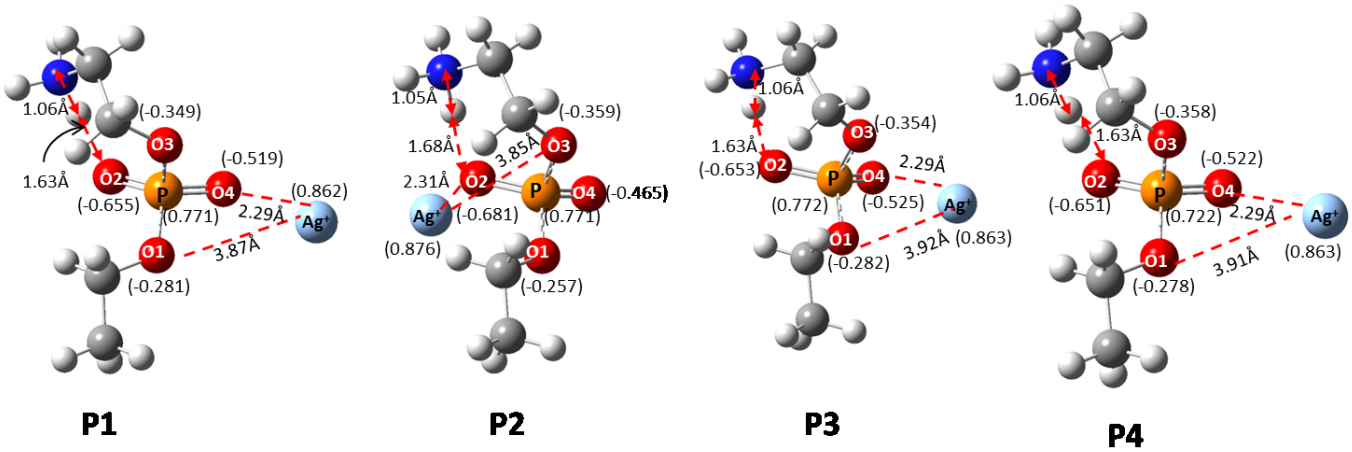

Figure 4.7: Ag^+ - PE models with distances, Mulliken atomic charges. Red - oxygen, orange - phosphorus, gray - carbon, white - hydrogen, royal blue – nitrogen, and light blue – silver

PE-Ag^0 interaction is shown in Figure 4.8. No structural conformation change was observed in PE in the presence or absence of Ag^0. The silver atom preference around POPE is P3>P4>P1>P2. The distance PE and the silver atom range from 4.89Å to 5.26Å. This distance is twice as long as that of the PE-Ag^+ interaction. This longer distance between PE-Ag^0 indicates that the silver atom is possibly repelled by PE.

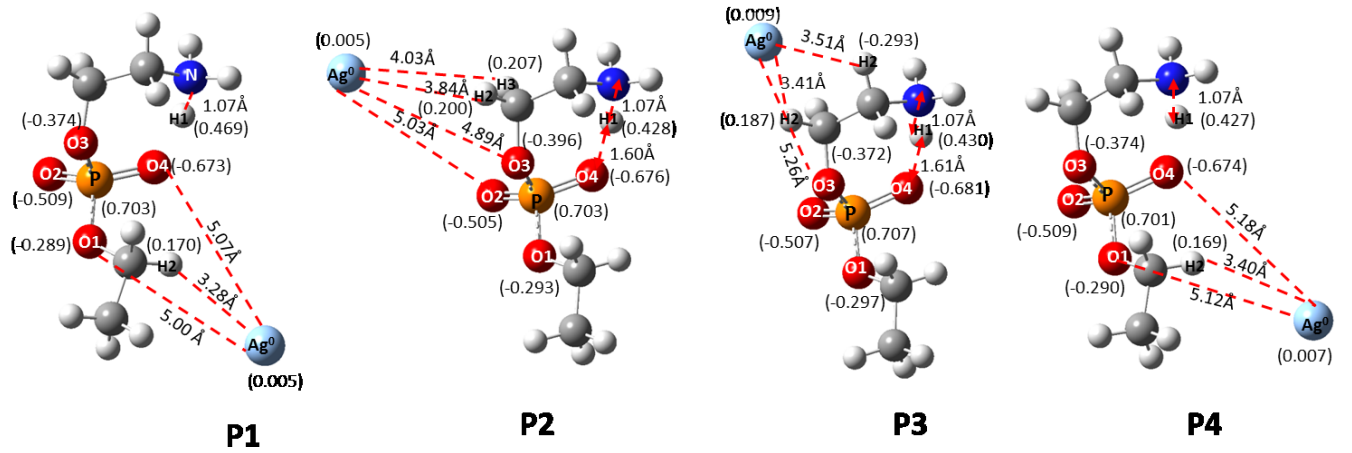

Figure 4.8: Ag^0 - PE models with distances, Mulliken atomic charges. Red - oxygen, orange - phosphorus, gray - carbon, white - hydrogen, royal blue – nitrogen, and light blue – silver

In addition, partial reduction of PE was also observed in the presence of the silver atom. PE lost partial electrons ranging from 0.005-0.009.

Overall, the ionic state of silver can cause partial oxidation of both the PC and PE heads while the atomic state of silver causes partial reduction. Distance between the phospholipid head and silver is the closest when silver is in ionic form. Structural conformational change is observed in PC in the presence of silver ion or atom while no change is observed in PE.

4.6.2 Binding Energies of the Phospholipid-Silver Models

Binding energies of the PC-Ag^+, PC-Ag^0, PE-Ag^+, and PE-Ag^0 interactions were calculated to determine the kind of interaction that exist. The silver ion interaction with both the PC and PE heads results in a shorter distance, which indicates a stronger binding energy compared to silver atom. This is confirmed in the binding energy results in Tables 4.4 and 4.5.

Table 4.4: Binding Energies of PC-Ag^+ and PC- Ag^0 interactions

	Binding Energy (kcal/mol)	
Position	**PC-Ag^+**	**PC-Ag^0**
P1	-5.84	-1.83
P2	-5.16	-1.70
P3	-5.74	-2.24
P4	-7.30	-1.48

All binding energies shown in Tables 4.4 and 4.5 are all positive indicating an attraction, not a repulsion interaction. Binding energies of PC and PE with Ag^+ are greater than with Ag^0 confirming that the ionic form of silver binds strongly to PC and PE that the atomic form. The binding energies of Ag^+ with PC and PE were three to five times that of with Ag^0, which explains its strong interaction with the PC and PE head marked by the shorter distance between Ag^+ and PC or PE.

Table 4.5: Binding Energies of PE-Ag^+ and PE- Ag^0 interactions

	Binding Energy (kcal/mol)	
Position	**PC-Ag^+**	**PC-Ag^0**
P1	-4.84	-1.70
P2	-3.38	-1.45
P3	-4.91	-1.94
P4	-4.92	-1.72

4.6.3 Electronic Properties, Molecular Orbitals and Contour Plots

Figure 4.9 shows an energy diagram of the molecular orbitals of PC, PE, Ag^+, Ag^0 and their interactions. Illustration of the highest occupied molecular orbital (HOMO), lowest occupied molecular orbital (LUMO) and corresponding ΔE_{gaps} are also shown. The LUMO of Ag^+ is lower than that of PC or PE making it easier for the two phospholipid heads to loose electron to Ag^+, which is an oxidation process.

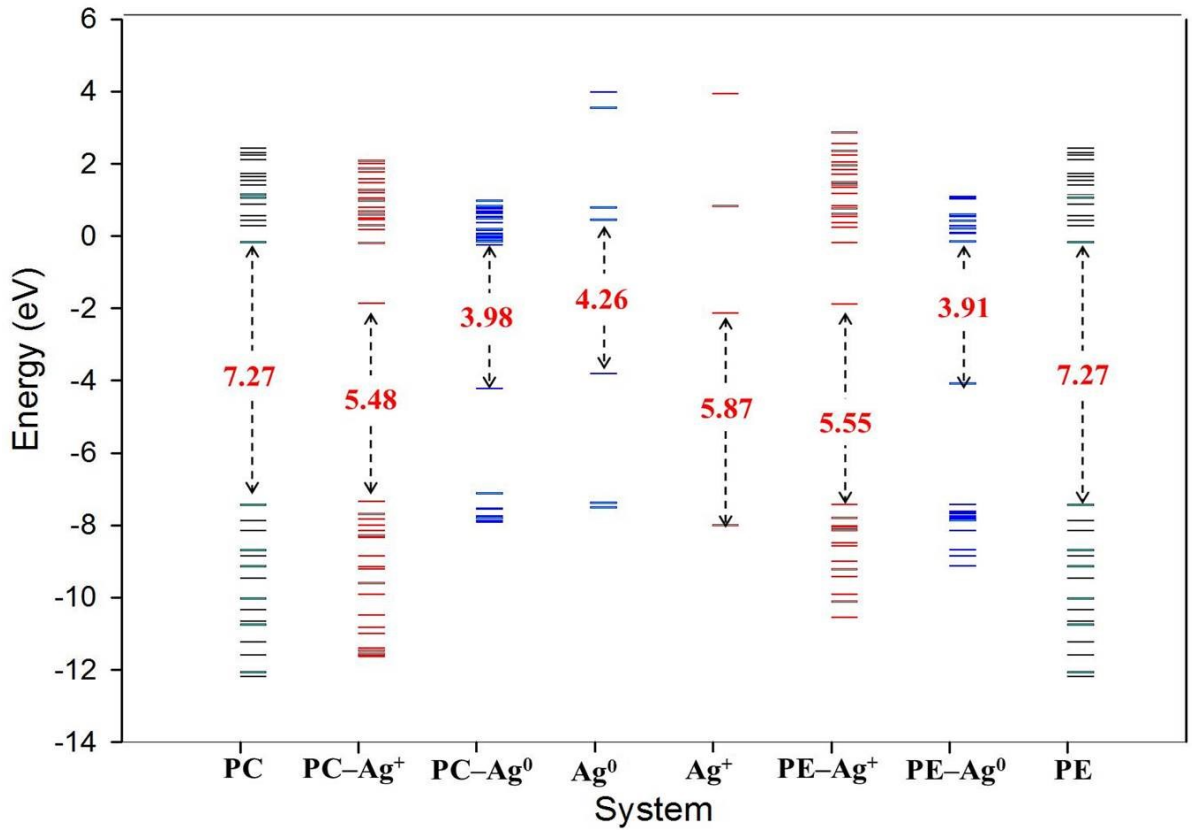

Figure 4.9: Energy Diagram of PC, PE, Ag^+, Ag^0 and their interactions

On the other hand, LUMO of Ag^0 is slightly higher than that of PC and PE making it easier for the two phospholipid head to gain electron, which is a reduction process. Though only partial oxidation and reduction were observed in the PC-Ag^+, PE-Ag^+, PC-Ag^0 and PE-Ag^0, the energy diagram provides a guide on the direction of the electron.

In addition, it was also observed that both the PC and PE heads possess the same ΔE_{gap} (7.27 eV). The presence of Ag^+ or Ag^0 resulted in a decrease in ΔE_{gap} in both PC and PE. In the presence of Ag^+ , the ΔE_{gap} of PC and PE were lowered by the lowering their LUMO energy, which resembles the LUMO of Ag^+ while the HOMO energy remains similar as shown in the PC-Ag^+ and PE-Ag^+ interaction in Figure 4.9. In the presence of Ag^0, the LUMO energy remains similar to that of PC and PE while the

HOMO energy is increased and resembles that of Ag^0 as shown in the PC-Ag^0 and PE-Ag^0 interaction in Figure 4.9. The ΔE_{gap} decreased the most when the PC and PE heads interact with Ag^0.

Contour plots were also calculated for PC, PE and their interaction with Ag^+ and Ag^0 as shown in Table 4.6. Excitation mechanism of both PC and PE are very similar. Upon HOMO-LUMO excitation, the electron density migrates from the phosphate group to the choline or ethanolamine group of PC and PE. In the presence of Ag^+ and Ag^0, the excitation mechanism change. Introduction of Ag^+ to PC or PE results in a HOMO-LUMO excitation where the electron density is shared by Ag^+ and the phosphate group of PC or PE at HOMO to an increased electron density on the Ag^+ upon excitation to LUMO. In the PC-Ag^+ and PE-Ag^+ interactions, the HOMO resembles the HOMO of the PC and PE heads while the LUMO resembles that of the Ag^+ , which is also seen in the energy diagram in Figure 4.9 and Table 4.6.

In the presence of Ag^0, its interaction with PC and PE results in a HOMO-LUMO excitation where the majority of the electron density is at Ag^0 at HOMO and migrate to the choline or ethanolamine group of the PC and PE at LUMO. In the PC-Ag^0 and PE-Ag^0 interactions, the HOMO resembles the HOMO of the Ag^0 while the LUMO resembles the LUMO of the PC and PE as shown in Table 4.6 and Figure 4.9 as well.

Table 4.6: Contour plots of PC, PE and their interaction with Ag^+ and Ag^0

System	HOMO	LUMO
PC	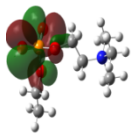 MO 57 (-7.40 eV)	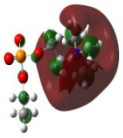 MO 58 (-0.22 eV)
PE	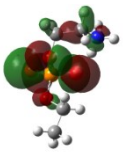 MO 45 (-7.43 eV)	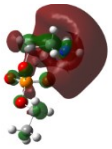 MO 46 (-0.14eV)
PC-Ag^+	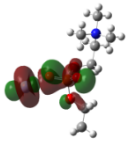 MO 66 (-7.32 eV)	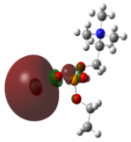 MO 67 (-1.85 eV)
PC-Ag^0	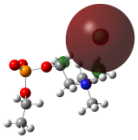 MO 67 (4.14 eV)	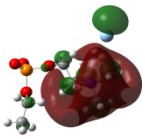 MO 68 (0.22 eV)
PE-Ag^+	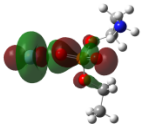 MO 54 (-7.40 eV)	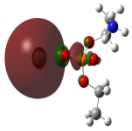 MO 55 (-1.85 eV)
PE-Ag^0	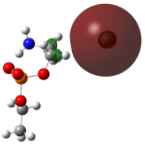 MO 55 (-4.05 eV)	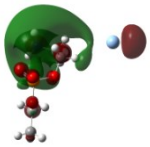 MO 56 (-0.14 eV)

4.6.4 Absorption Spectra of the Phospholipid-Silver Models

Predicted absorption spectra of the two phospholipid heads, their interaction with the ionic and atomic state of silver, and silver atom were calculated using TDDFT. Predicted absorption spectrum for silver ion is characterized with no peak and is not included in the calculated spectra shown in Figure 4.10. The 10 nm citrate stabilized AgNP from Nanocomposix is characterized by an intense absorption peak at 385 nm. The predicted absorption peak for Ag^0 using B3LYP/LANL2DZ is 366 nm, which is 19 nm away from experimental value.

The presence of Ag^+ and Ag^0 in both PC and PE resulted in a bathochromic shifts. The presence of Ag^0 in the PC and PE is characterized by more intense absorption peaks and larger redshift of 185 nm and 200 nm respectively. Absorption spectra of PC-Ag^0 and PE-Ag^0 interactions resulted in an absorption wavelength similar to Ag^0. On the contrary, the presence of Ag^+ in both PC and PE resulted in weak

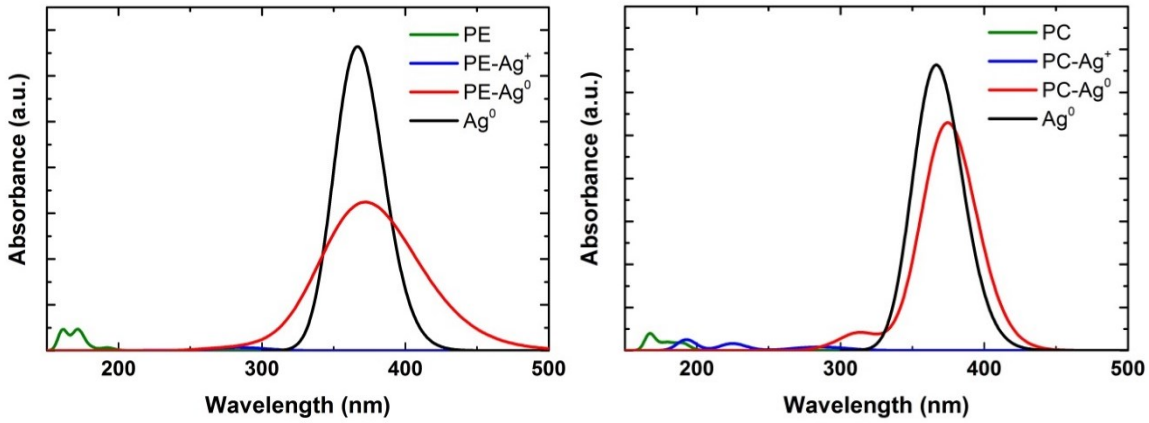

Figure 4.10: Predicted absorption spectra of PC, PE, their interaction with Ag^+ and Ag^0, and Ag^0

peaks defined by smaller redshifts of 103 nm and 40 nm respectively compared to the presence of Ag^0.

These predicted absorption spectra suggest that the presence of Ag^0 around the two phospholipid heads can be easily detected using absorption spectroscopy and will be characterized by intense peaks near 372-376 nm. However, the presence of Ag^+, though can be identified by a redshift of 40-103 nm, may be difficult to characterized using absorption spectroscopy due to less intense peaks. Other characterization methods such as cyclic voltammetry and other electrochemical characterization methods will be more ideal to use in identifying the presence of Ag^+ around the two phospholipids.

4.7 Summary

Experimental results show that the presence of 10 nm citrate stabilized AgNP can be harmful to HepG2 cells at a dosage that is > 1ppm. Cell viability curve generated from the tryphan blue exclusion test results test resulted in an LD50 of 3ppm, which is similar to other groups' LD50 results for the same size AgNP. Oxidative stress levels were observed to increase in HepG2 cells as the concentration of AgNP increases until 3ppm and started to decline at 5ppm, where most of the cells were dead. Maximum ROS level was observed the LD50 of 3ppm, which indicates that the cells can tolerate high ROS level before apoptosis.

Computational results show possible toxicity mechanism caused by the Ag^+ that can possibly leak in AgNPs. Effects of the presence of atomic and ionic form of silver on

two phospholipid heads, PC and PE, were studied. The presence of Ag^+ around the PC and PE caused partial oxidation on the two phospholipid heads. Oxidation of lipids usually happens when a toxic chemical such as a radical steals electrons from the lipids, which can result in the activation of inflammation in cells (*121*). The presence of Ag^+ around PC and PE is characterized by a red shift of 40-103 nm using absorption spectroscopy but weak peak intensities. The presence of Ag^0 causes a slight reduction to the PC and PE heads and can be characterized by a redshift of 185-200 nm and intense absorption peak around 372 nm – 376 nm.

CHAPTER 5

IMPROVED COMPUTATIONAL CYCLIC VOLTAMMETRY AND ABSORPTION SPECTROSCOPY

The redox recycling reactions of different compounds involved in normal biological function of cells can be the source of generation of multiple free radicals. Reaction of these free radicals with oxygen can form reactive oxygen species that can give rise to further oxidants and induce oxidative stress in the cells (*122*). Metal mediated formation of free radicals can interact with DNA bases, enhance lipid peroxidation, alter calcium and sulfhydryl homeostasis, and can produce mutagenic and carcinogenic by products(*123*). The potential toxicity of a metal nanoparticle can be measured through its ability to oxidize or reduce different compounds, lipids, proteins, and other complex biological molecules in the cells.

Cyclic voltammetry and absorption spectroscopy are two characterization methods that can detect the occurrence of oxidation and reduction. Improvement of cyclic voltammetry and absorption spectroscopy computational methods can provide the tools to accurately study atomic level toxicity mechanism for AgNPs and other kinds of nanoparticles. Improving the accuracy of these two computational methods requires the availability of experimental results of electronic properties and absorption spectra to which computational results can be compared. As such we employed a set of eight cyclopenta fused polycyclic aromatic hydrocarbons (CP-PAHs) shown in Figure 5.1 as their experimental data are available (*124*).

Conventional computational studies of these molecules used B3LYP density functional and found large discrepancies between experimental and calculated results. Therefore, it is important to investigate computational tools and develop better methods. Different density functionals available in the Gaussian 09 software were tested and more accurate representations of experimental phenomena were explored in search for more accurate computational techniques to predict cyclic voltammetry and absorption spectroscopy results.

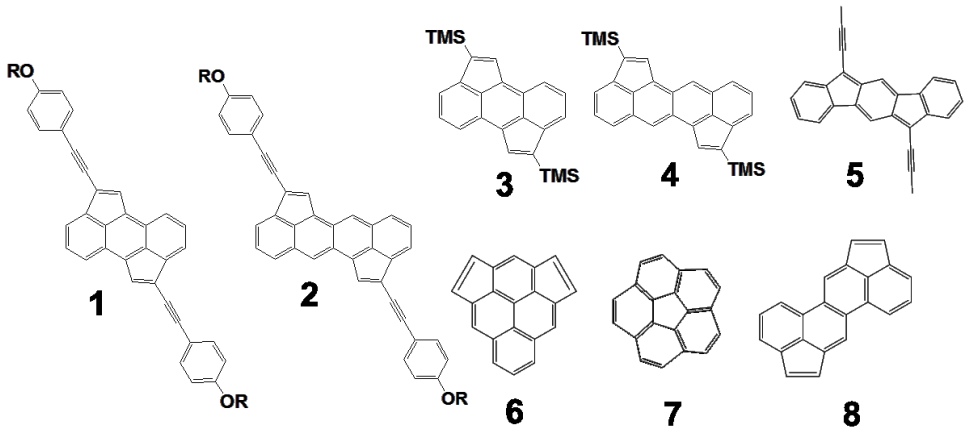

Figure 5.1: CP-PAH structures of ,7-bis((4-(alkoxyphenyl)ethynyl) cyclopenta[*hi*] aceanthrylene (1, R=H, CH_3, C_2H_5, $CH_2CH_2CH_3$); 2,8-bis((4-alkoxyphenyl)ethynyl) dicyclopenta[*de,mn*] tetracene (2); 2,7-bis (trimethylsilyl)cyclopenta[*hi*]aceanthrylene (3); 2,8-bis(trimethylsilyl) dicyclopenta[de,mn]tetracene (4); 6,12-diethynylindeno[1,2-b]fluorine (5); dicyclopenta[*cd,mn*] pyrene (6); corannulene (7); dicyclopenta[*hi,qr*] chrysene (8).

5.1 Effects of the Different Alkyl –R groups on CP-PAHs

The -R groups attached to **1** and **2** are $C_{10}H_{21}$ upon their synthesis experimentally. The long alkyl groups attached to **1** and **2** are necessary for their

solubility in tetrahydrofuran (THF). However, the theoretical model used in this study contains only $–CH_3$ as the –R groups. To justify the use of $–CH_3$ in the DFT and TD-DFT calculations, the effects of different alkyl –R groups on the electronic properties and absorption spectra of **1** and **2** were investigated. The different –R groups used in the calculations were –H, $-CH_3$, $-C_2H_5$ and $-C_3H_7$. All calculations to study the effect of these different –R groups were performed in THF solvent treated using the polarized continuum model (PCM) and carried out using B3LYP/6-311g (d, p) level of theory.

Table 5.1 is a summary of the electronic properties of **1** and **2** as the –R groups increase in length. As the–R groups increase in length, the HOMO, LUMO and ΔE_{gap} remained very similar for the two CP-PAHs. The absence of significant change as the length of alkyl chain attached to **1** and **2** increases indicates that alkyl –R groups do not have influence in the electronic properties of functionalized CP-PAHs and similar models. Thus, the replacement of long alkyl chains functional groups in a CP-PAH with $–CH_3$ is sufficient in modeling its electronic properties.

Table 5.1: Electronic properties of 1 and 2 with varying alkyl –R groups

-R	**1**			**2**		
Groups	**HOMO**	**LUMO**	**ΔE_{gap}**	**HOMO**	**LUMO**	**ΔE_{gap}**
-H	-5.19	-3.31	1.88	-5.14	-3.32	1.82
$-CH_3$	-5.18	-3.31	1.87	-5.13	-3.31	1.82
$-C_2H_5$	-5.17	-3.30	1.87	-5.12	-3.31	1.81
$-C_3H_7$	-5.17	-3.30	1.87	-5.12	-3.31	1.81

* Calculated using B3LYP/6-311g (d,p) on neutral model

* All values are in eV

The effect of the different alkyl –R groups on the absorption spectra of **1** and **2** were also probed using predicted absorption spectra shown in Figure 5.1. The change in length of the different –R groups attached to **1** and **2** produced similar and almost overlapping absorption spectra. However, as the alkyl –R groups increase in length from –H to C_3H_7 small shifts in the absorption spectra were observed. The replacement of the –R groups in **1** from –H to CH_3, CH_3 to C_2H_5 and C_2H_5 to C_3H_7 produced a red shift of 6 nm, a red shift of 3nm, and a blue shift of 1nm respectively. An average of 3 nm redshift per addition of a methyl group was observed as the –R group length in **1** increase. Similarly, the change of the –R groups in **2** from –H to CH_3, CH_3 to C_2H_5 and C_2H_5 to C_3H_7 produced a red shift of 5 nm, a red shift of 1 nm, and no shift respectively. The average redshift of 2 nm per addition of methyl group was observed in **2**. These small red shifts of 2-3 nm per addition of methyl group suggest that the model containing -CH_3 instead of the longer alkyl chain is sufficient to represent absorption spectra of alkyl functionalized CP- PAHs.

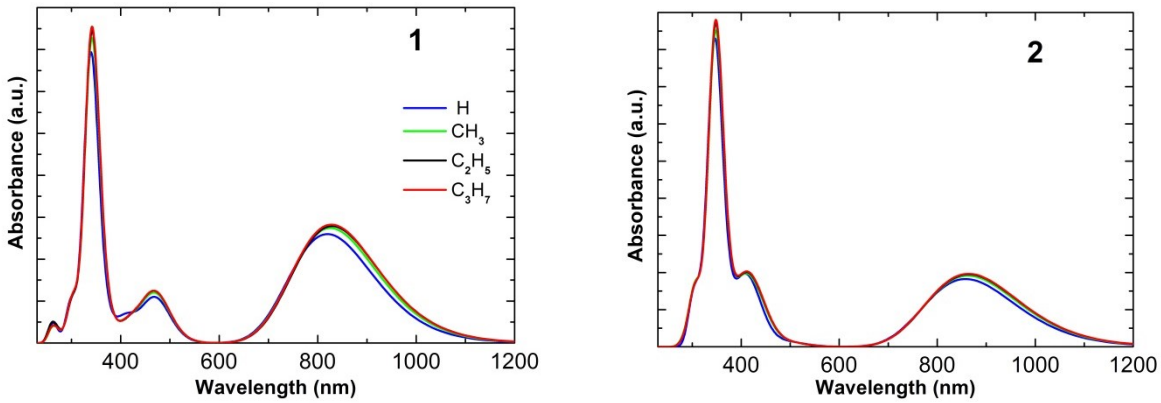

Figure 5.2: Predicted absoption spectra of 1 and 2 with varying –R groups using B3LYP/6-311g (d,p) on neutral model

5.2 Effects of Different Density Functionals on Accuracy of Computational Cyclic Voltammetry

Accurate prediction of electronic properties is important in the development of materials and improving toxicity studies that can be measured electrochemically. Six density functionals namely B3LYP, CAM-B3LYP, PBE, TPSS, HCTH, and HSEH1PBE were implemented with the 6-311g (d,p) basis set on all ground state structure and frequency calculations of all the eight CP-PAHs in Figure 1. The solvent used for **1 - 5** is tetrahydrofuran (THF) and **6 - 8** used acetonitrile (CH_3CN). The solvents were treated using PCM in all calculations.

Experimentally, the measurement of the first reduction (LUMO) and oxidation (HOMO) potentials in cyclic voltammetry involves the neutral and anion state of a chemical sample. Computationally, the anion state of the chemical sample is not really accounted for. Traditional computational method of predicting HOMO, LUMO and ΔE_{gap} uses only the neutral state of a chemical sample. The six density functionals were employed to determine which predicts these three properties the best. The accuracy of each of the six density functionals in predicting the HOMO, LUMO and ΔE_{gap} using the traditional method are summarized in Tables 5.2 – 5.4. The deviations of predicted HOMO, LUMO and ΔE_{gap} from experimental values and their calculated errors are presented in the tables below. Mean Absolute Errors (MAE) for all eight CP-PAHs were also used as a measure of accuracy.

Table 5.2: Errors and MAE of predicted HOMO

Functional	1	2	3	4	5	6	7	8	MAE
Experiment	-5.19	-5.19	-5.59	-5.36	-5.88	-6.06	-6.37	-6.16	
B3LYP	0.01	0.06	-0.15	-0.06	0.34	0.20	0.02	0.11	0.12
HSEH1PBE	0.15	0.61	0.02	0.07	0.47	0.32	0.10	0.23	0.19
CAMB3LYP	-1.24	-1.12	-1.43	-1.21	-0.81	0.32	-1.40	-1.20	1.09
PBE	0.60	0.61	0.49	0.46	0.83	0.86	0.65	0.76	0.66
TPSS	0.64	0.66	0.52	0.51	0.88	0.90	0.70	0.80	0.70
HCTH	0.53	0.55	0.42	0.41	0.76	0.80	0.59	0.70	0.60

*Experimental HOMO values are taken from references (*124-126*)

*All errors values are in eV

Among the six density functionals, B3LYP provided the best predicted HOMO with lowest MAE of 0.12 eV. HSEH1PBE is the second best functional for predicting HOMO with a similar accuracy to B3LYP. CAMB3LYP resulted in a significantly underestimated HOMO with the highest MAE of 1.09 eV. The other three density functionals which originated from GGA namely PBE, TPSS and HCTH provided all provided similar accuracy with MAE > 0.5 eV.

Accuracy of predicted LUMO using the different density functionals is also probed. Among the six density functionals, TPSS provided the best predicted LUMO with MAE of 0.11 eV. Likewise, all the GGA functionals (PBE, TPSS and HCTH) and HSEH1PBE provided similar accuracy. Predicted LUMO using CAMB3LYP were all overestimated with an MAE of 1.50 eV and B3LYP provided a LUMO with MAE of almost 0.5 eV.

Table 5.3: Errors and MAE of predicted LUMO

Functional	1	2	3	4	5	6	7	8	MAE
Experiment	-3.64	-3.62	-3.41	-3.45	-4.00	-3.48	-2.55	-3.35	
B3LYP	0.33	0.31	0.34	0.32	0.52	0.68	0.55	0.63	0.46
HSEH1PBE	0.05	-0.01	0.05	0.02	0.24	0.39	0.28	0.35	0.17
CAMB3LYP	1.30	1.28	1.39	1.35	1.52	1.76	1.69	1.74	1.50
PBE	-0.13	-0.18	-0.24	-0.25	0.04	0.06	-0.11	0.01	0.13
TPSS	-0.03	-0.07	-0.12	-0.13	0.15	0.20	0.03	0.15	0.11
HCTH	-0.17	-0.22	-0.27	-0.28	-0.01	0.04	-0.12	-0.01	0.14

*Experimental LUMO values are taken from references (*124-126*)

*All errors values are in eV

The accuracy of calculated HOMO and LUMO can affect the predicted ΔE_{gap} as well. Among the six density functionals, HSEH1PBE provided the best predicted ΔE_{gap} with the lowest MAE of 0.13 eV. All the three GGA functionals still provided similar accuracy for ΔE_{gap}. ΔE_{gap} calculated using CAMB3LYP was way overestimated with MAE of 2.52 eV and that of B3LYP was also overestimated with MAE of 0.46 eV.

Table 5.4: Errors and MAE of predicted ΔE_{gap}

Functional	1	2	3	4	5	6	7	8	MAE
Experiment	1.55	1.57	2.18	1.91	1.88	2.58	3.82	2.81	
B3LYP	0.32	0.25	0.49	0.38	0.18	0.48	0.57	0.52	0.40
HSEH1PBE	-0.10	-0.79	0.06	-0.05	-0.23	0.07	0.18	0.12	0.13
CAMB3LYP	2.55	2.40	2.82	2.56	2.32	1.43	3.10	2.93	2.52
PBE	-0.73	-0.79	-0.73	-0.71	-0.79	-0.80	-0.77	-0.74	0.76
TPSS	-0.66	-0.73	-0.64	-0.64	-0.73	-0.70	-0.66	-0.65	0.68
HCTH	-0.70	-0.76	-0.69	-0.68	-0.77	-0.77	-0.71	-0.71	0.72

*Experimental ΔE_{gap} values are taken from references (*124-126*)

*All errors values are in eV

Three different density functionals resulted to be the best in predicting three electronic properties using the traditional method. B3LYP, TPSS and HSEH1PBE were best in predicting HOMO, LUMO and ΔE_{gap} respectively. Calculating the HOMO, LUMO and ΔE_{gap} using three different functionals is computationally expensive and means synthesizing three ground state structure of a chemical sample in silico using the three mentioned density functionals, which can result in more complexity and confusion in interpretation of results.

Looking back to the states that a chemical sample undergoes upon cyclic voltammetry characterization made us revisit the veracity of the neutral computational model often used and lead us to propose a more realistic method to calculate the HOMO, LUMO and ΔE_{gap} of a chemical sample as described in the next section

5.3 The Improved Computational Cyclic Voltammetry

In a simple cyclic voltammetry experiment, upon measurement of reduction and oxidation potential, a neutral chemical sample is subjected to a potential scan towards the negative direction. As the potential scans towards the negative direction the sample is reduced to an anion state at the reduction potential, which is observed as a negative peak (reduction peak) in the voltammogram. The scan will continue until a specified potential is reached and then followed by a reverse potential scan. As the potential scans to the reverse direction the chemical sample in anion state will be oxidized back to original neutral state that is observed as a positive peak (oxidation peak). Using neutral and anion models of a chemical sample is a more accurate representation cyclic voltammetry experiments. However, traditional computational cyclic voltammetry uses only the neutral model.

Our group implemented the use of neutral and anion models in characterization of a chemical sample using computational cyclic voltammetry. The six density functionals with the 6-311g (d,p) basis set were used on all ground state structure and frequency calculations of the neutral and anion state of the eight CP-PAHs in Figure 5.1. The solvent used for **1 - 5** is tetrahydrofuran (THF) and **6 - 8** used acetonitrile (CH_3CN) and the solvents were treated using the polarized continuum model (PCM) for all calculations.

The proposed method for computational cyclic voltammetry is summarized and illustrated in Figure 5.3.

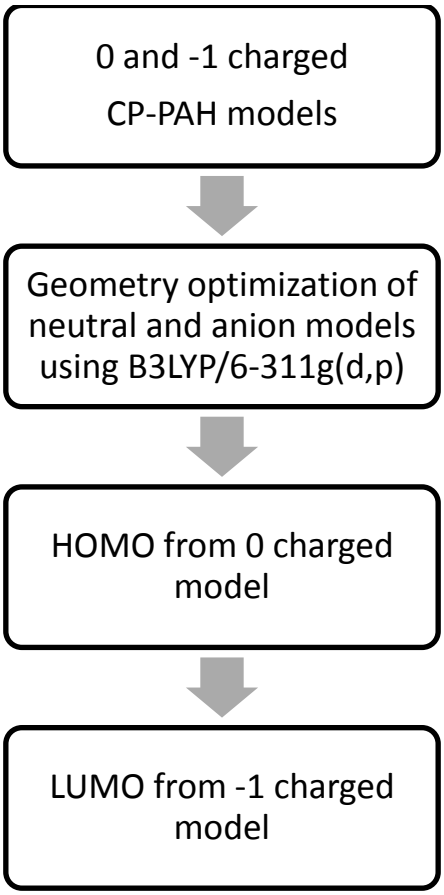

Figure 5.3: The proposed method for computational cyclic voltammetry

Electronic properties using the proposed computational cyclic voltammetry were compared to that of the traditional method. The accuracy of the predicted HOMO using the proposed method is the same as that of the traditional method since both methods calculates HOMO using a neutral model. Figure 5.4 shows the accuracy of predicted HOMO using the six density functionals.

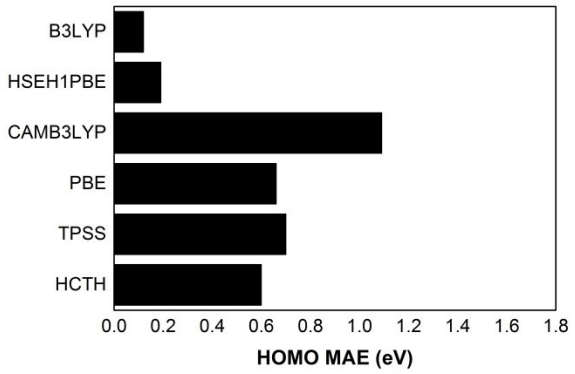

Figure 5.4: Accuracy of predicted HOMO using the six density functionals

Only the LUMO and ΔE_{gap} were improved by accounting for the anion state of the chemical sample. Errors and MAE of predicted LUMO and ΔE_{gap} using the proposed method are shown in Tables 5.5 and 5.6.

Table 5.5 Errors and MAE of predicted LUMO using the proposed methods

Functional	**1**	**2**	**3**	**4**	**5**	**6**	**7**	**8**	**MAE**
Experiment	-3.64	-3.62	-3.41	-3.45	-4.00	-3.48	-2.55	-3.35	
B3LYP	0.16	0.12	0.16	0.16	0.38	0.21	0.06	0.14	0.17
HSEH1PBE	0.27	0.23	0.29	0.27	0.50	0.32	0.21	0.27	0.30
CAMB3LYP	-0.85	-0.81	-0.89	-0.81	-0.70	-0.80	-0.87	0.80	0.82
PBE	0.55	0.47	0.60	0.52	0.87	0.61	0.40	0.48	0.56
TPSS	0.61	0.53	0.65	0.58	0.91	0.66	0.47	0.55	0.62
HCTH	0.51	0.43	0.57	0.49	0.82	0.57	0.39	0.45	0.53

*Experimental LUMO values are taken from references (*124-126*)

*All errors values are in eV

Improvement in the LUMO accuracy using the proposed method was observed using B3LYP and CAMB3LYP. LUMO predicted using HSEH1PBE, PBE, TPSS and HCTH with the proposed method resulted in higher MAE than the traditional method. The prediction of LUMO using the proposed method is most accurate using B3LYP with MAE of 0.11 eV and provides an improvement of the traditional method by reducing the MAE by more than 50%.

Table 5.6: Errors and MAE of predicted ΔE_{gap} using the proposed methods

Functional	**1**	**2**	**3**	**4**	**5**	**6**	**7**	**8**	**MAE**
Experiment	1.55	1.57	2.18	1.91	1.88	2.58	3.82	2.81	
B3LYP	0.14	0.06	0.3	0.22	0.05	0.01	0.08	0.03	0.11
HSEH1PBE	0.13	-0.14	0.3	0.20	0.03	-0.01	0.11	0.03	0.11
CAMB3LYP	0.39	0.31	0.54	0.41	0.11	-1.12	0.53	0.39	0.47
PBE	-0.04	-0.14	0.11	0.06	0.04	-0.25	-0.25	-0.28	0.15
TPSS	-0.02	-0.12	0.13	0.07	0.03	-0.24	-0.22	-0.24	0.14
HCTH	-0.02	-0.12	0.14	0.08	0.05	-0.23	-0.20	-0.25	0.14

*Experimental ΔE_{gap} values are taken from references (*124-126*)

*All errors values are in eV

The majority of the predicted ΔE_{gap} using the six density functionals were improved and all ΔE_{gap} MAE were lower than that of the traditional method. Among the six density functionals, B3LYP and HSEH1PBE provided the best predicted $\Delta E_{gap.}$

A comparison of accuracy of predicted LUMO and ΔE_{gap} using the traditional method and proposed method are shown in Figure 5.5. The proposed method shows an

improvement in predicted LUMO using B3LYP and CAMB3LYP. Conversely, the traditional method provided better predicted LUMO for the three GGA functionals and HSEH1PBE. However, the proposed method shows a significant improvement in predicted ΔE_{gap} using all the six density functionals. B3LYP and HSEH1PBE provided similar accuracy both with MAE of 0.11 eV as shown in Table 5.7.

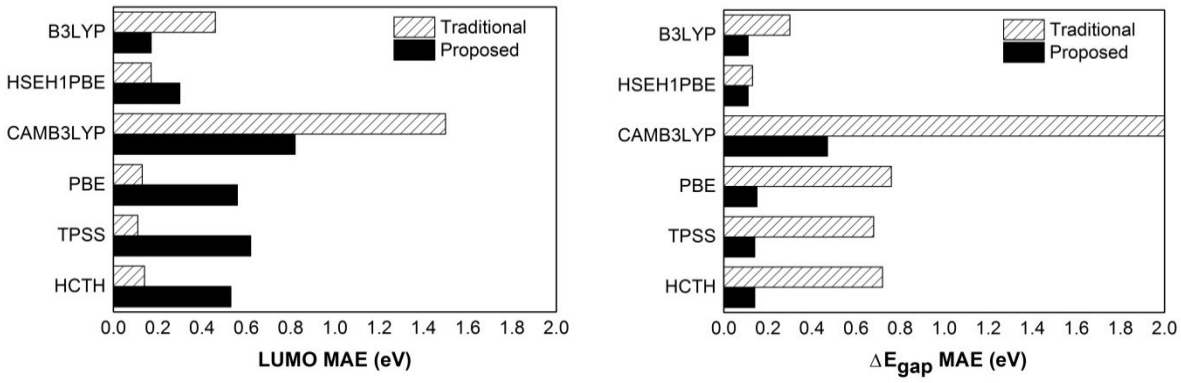

Figure 5.5: Comparison of predicted LUMO and ΔE_{gap} using traditional and proposed method

Overall MAE for all three properties were also calculated to determine which density functional compensates the least error and is best for calculating HOMO, LUMO and ΔE_{gap}. Table 5.7 provides a summary of all calculated MAE. Among the six density functionals, B3LYP predicts all three properties the best using the proposed method with MAE of 0.14 eV as shown in Table 5.7.

Table 5.7: Overall MAE for predicted HOMO, LUMO and ΔE_{gap} using the proposed and traditional method

Functional	HOMO MAE	LUMO MAE	ΔE_{gap} MAE	Overall MAE
B3LYP	0.12	0.17 (0.46)	0.11 (0.30)	0.14 (0.33)
HSEH1PBE	0.19	0.30 (0.17)	0.11 (0.13)	0.20 (0.16)
CAMB3LYP	1.09	0.82 (1.50)	0.47 (2.52)	0.80 (1.70)
PBE	0.66	0.56 (0.13)	0.15 (0.76)	0.46 (0.51)
TPSS	0.70	0.62 (0.11)	0.14 (0.68)	0.49 (0.50)
HCTH	0.60	0.53 (0.14)	0.14 (0.72)	0.42 (0.49)

*MAE from traditional method in parenthesis

*All values are in eV

These results shows that it is possible to accurately predict the HOMO, LUMO and ΔE_{gap} using one density functional and also confirms our choice of using B3LYP in the proposed method in Figure 5.3, which is the best in predicting all three properties. Moreover, accounting for the anion state of a chemical sample in cyclic voltammetry improves the accuracy of overall predicted electronic properties.

5.4 Accounting for the Neutral and Anion State of the CP-PAH model

Optimized geometries of 0 and -1 charged **1** using the six density functionals were evaluated to understand the effect of the electron gained upon reduction on the atomic bond lengths. Results showed that upon gaining an electron atomic bond distances in the cyclopenta[hi]aceanthrylene center changes the most. Eight out of the

twenty two C-C bonds in the cyclopenta[hi]aceanthrylene center decreased significantly using B3LYP, HSEH1PBE, PBE, TPSS and HCTH. Using CAMB3LYP, ten out of twenty-two C-C bonds in the cyclopenta[hi]aceanthrylene center decreased significantly. Adjacent C-C bonds present in both cyclopentene regions decreased and increased the most for all the six density functionals. The range of the change in bond length in that occurred in the cyclopenta[hi]aceanthrylene center of **1** is summarized in Table 5.8.

Table 5.8: Change in C-C bond lengths as 1 is reduced to 1^-

Functional	**Increase Å**	**Decrease Å**
B3LYP	0.0003- 0.0240	0.0128 – 0.0257
CAMB3LYP	0.0011 – 0.0283	0.0029 - 0.0347
HSEH1PBE	0.0004 - 0.0229	0.0121 - 0.0242
PBE	0.001 – 0.0179	0.0091 - 0.0165
TPSS	0.0008 – 0.0195	0.0094 – 0.0184
HCTH	0.0009 – 0.0179	0.0092 – 0.0170

*This change is only on the cyclopenta[hi]aceanthrylene center

Among the six functionals, CAMB3LYP resulted in the shortest bond length with a maximum decrease of 0.0347 Å. In addition, CAMB3LYP resulted in the highest number of decreased atomic bond lengths as **1** is reduced to $\mathbf{1}^-$. Contour plots and energy levels of the +1, 0 and -1 charged **1** can provide a clearer view of electronic changes that occurs in a cyclic voltammetry experiments. Figure 5.7 illustrates the contour plots and energy levels of **1** when it is oxidized, neutral and reduced.

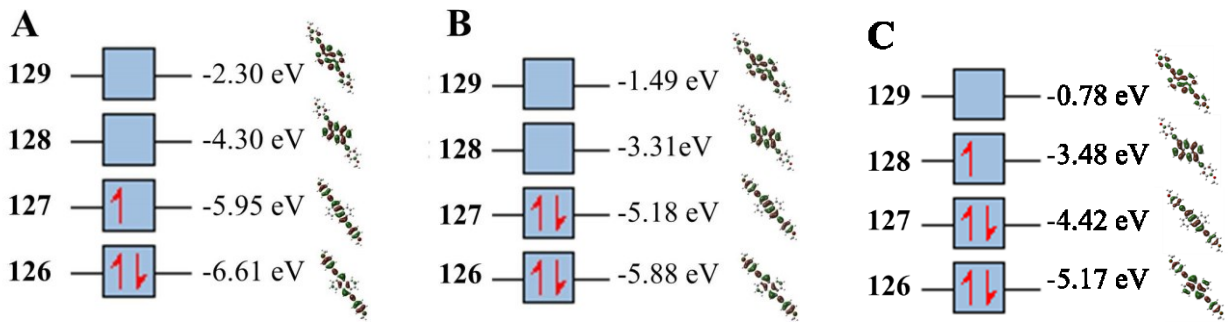

Figure 5.6: Contour plots and energy levels of A) oxidized, B) neutral, and C) reduced 1 calculated using B3LYP/6-311g (d,p)

The neutral state of **1** has an even number of electrons filling up to molecular orbital (MO) 127 (Figure 5.6 B). The gain or removal of electron produced an odd total number of electrons resulting in an unpaired electron. Figure 5.6 shows that when **1** is oxidized to $\mathbf{1}^+$ or reduced to $\mathbf{1}^-$**,** the energies of each MO will be different. Upon oxidation (**1** to $\mathbf{1}^+$), the energies of MO127 and MO 128 were decreased. Upon reduction, (**1** to $\mathbf{1}^-$), the energy of MO 127 increased while MO 128 decreased. This confirms that the presence of an unpaired electron in a certain MO will result in a lowering of MO energy. Moreover, the reduced form of a sample when characterized using cyclic voltammetry experiments has different electronic behavior from the neutral form and should be accounted upon prediction of HOMO and LUMO. Using 0 and -1 charged CP-PAH models that closely represent the sample in cyclic voltammetry experiments provides more accurately predicted LUMO and ΔE_{gap} summarized in Figure 5.5 and Table 5.7.

5.5 The Improved Computational Absorption Spectroscopy

The six different density functionals were also employed in the TD-DFT calculations in search for the best functional in predicting absorption spectra of a chemical sample. Predicted absorption spectra of **1** and **2** published in 2010 were generated using B3LYP/6-311g (d,p) on a neutral model for both DFT and TD-DFT calculations (*124*). In addition to employing the six density functionals, TD-CAMB3LYP using a B3LYP optimized chemical structure was also implemented. Summary of the improved computational absorption spectroscopy and predicted spectra of **1** and **2** using the six density functionals and B3LYP/TD-CAMB3LYP are all shown in Figure 5.7.

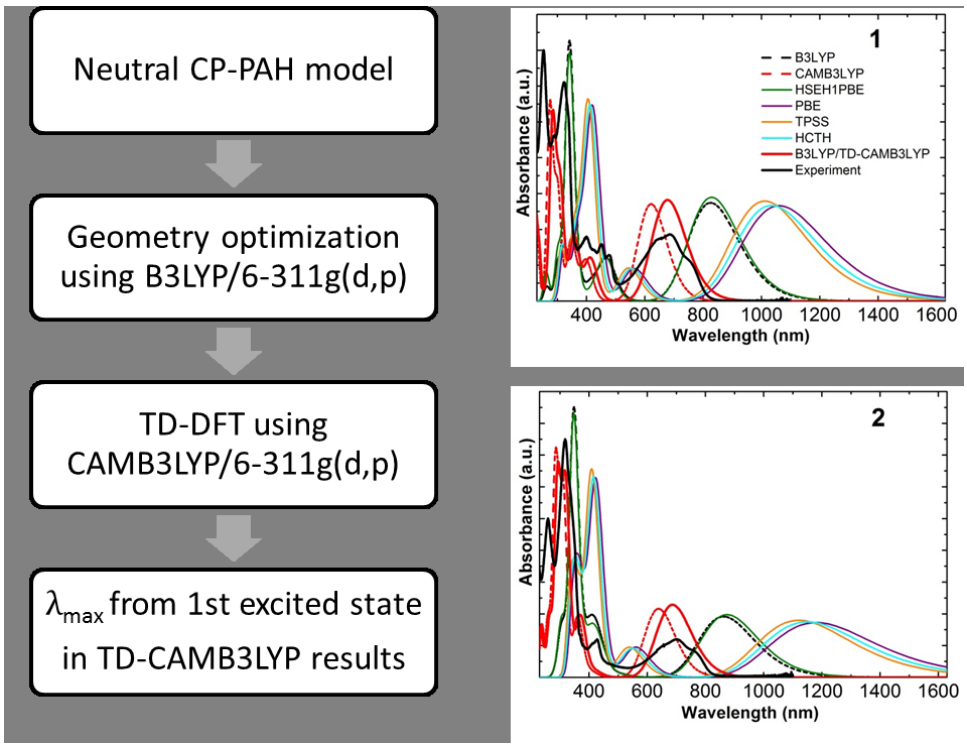

Figure 5.7: Summary of the improved computational absorption spectroscopy and predicted absorption spectra of 1 and 2

Among the six density functionals, CAMB3LYP provided the better predicted absorption spectra than previously published absorption spectra of **1** and **2** using B3LYP. However, B3LYP/TD-CAMB3LYP provided the best predicted spectra of both **1** and **2**.

Several groups have used the B3LYP/TD-CAMB3LYP in predicting absorption spectra of different systems. Fitri, et. al used this method in studying ten thiazolothiazole based dyes (*108*) and thienpyrazine based dyes that resulted in predicted excitation energies, absorption and emission spectra that are reasonable and in good agreement with experimets(*127*). Kumar, et. al studied hydroxyl radical reaction with guanine in an aqueous environment using B3LYP/TD-CAMB3LYP with the 6-31g(d) and 6-311+g(d,p) basis set for absorption spectra calculation and results are in good agreement with experiments (*109*). The use of TD-CAMB3LYP in absorption spectra prediction is preferred over TD-B3LYP because B3LYP is not appropriate to use for ion pair or species involving charge transfer excited states where transition energies are greatly underestimated while TD-CAMB3LYP has been very successful in studying these mentioned systems (*75, 93, 109, 128, 129*).

In a similar way, the long range corrected exchange functional included in CAMB3LYP is proven to work better in the TD-DFT study of **1** and **2** in comparison with TD-B3LYP and resulted in predicted absorption spectra of **1** and **2** that are in good agreement with experiment. However, B3LYP still provides good predicted geometry, but is not a good functional to use in TD-DFT and for systems with charge transfer mechanism. Combining these strengths of B3LYP and CAMB3LYP can provide the best absorption spectra of CP-PAHs such as that of **1** and **2** as shown in Figure 5.8.

Thus, the more accurate way of predicting absorption spectra of CP-PAHs is by using TD-CAMB3LYP preceded by B3LYP optimized CP-PAH neutral model.

The B3LYP/TD-CAMB3LYP and the six density functionals were also employed on the six other CP-PAHs for validation. Accuracy of predicted absorption spectra were also calculated and summarized in Table 5.9. Accuracy of only seven CP-PAHs (**1-7**) is reported in Table 5.9. Experimental absorption spectrum is not available for **8** excluding it in the calculation of MAE for λ_{max}. However, predicted absorption spectra of **8** can still serve as a guide for future experiments since experimental absorption spectrum of **8** is not available. The difference in accuracy of predicted λ_{max} is also illustrated in Figure 5.8.

Table 5.9: Errors of Predicted λ_{max} of 1-7

Method	**1**	**2**	**3**	**4**	**5**	**6**	**7**	**MAE**
Experimental	**686**	**699**	**548**	**603**	**568**	**363**	**286**	
TD-B3LYP	139	164	47	61	129	153	63	108
TD-CAMB3LYP	-65	-61	-48	-53	-21	56	23	47
TD-HSEH1PBE	142	174	39	55	118	146	56	104
TD-PBE	374	481	165	200	262	275	104	266
TD-TPSS	325	421	132	167	229	247	94	231
TD-HCTH	348	450	149	184	249	265	98	249
B3LYP/TD-CAMB3LYP	-9	-13	-25	-29	29	70	30	29

*Experimental values of λ_{max} are taken from references (*124, 130, 131*)

*All values are in nm

Among the seven methods employed, the B3LYP/TD-CAMB3LYP still resulted to be the best at predicting absorption spectra of seven CP-PAHs with MAE of 29 nm. TD-B3LYP, which is the previously used method for **1** and **2** provided a higher MAE of 108 nm. Predicted absorption spectra of the other six CP-PAHs using the seven methods are shown in Figure 5.9.

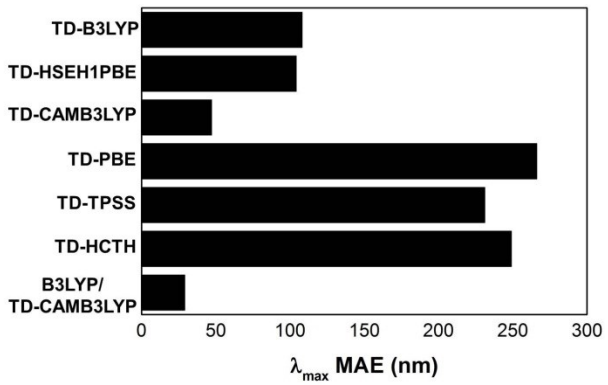

Figure 5.8: Accuracy of predicting λ_{max} using seven CP-PAHs

Predicted absorption spectra together with the predicted HOMO, LUMO and ΔE_{gap} in section 5.3 and 5.4 also confirm that the six density functionals can be grouped into three according to accuracy. These three groups are Group 1 - CAMB3LYP, Group 2 - B3LYP and HSEH1PBE and Group 3 – PBE, TPSS and HCTH.

These three groups can be easily observed in Table 5.9, Figure 5.8 and 5.9. Group 1 with CAMB3LYP has predicted λ_{max} on the shortest wavelength and the smallest MAE of 47 nm. Group 2 with B3LYP and HSEH1PBE has very similar accuracy with MAE of 108 nm and 104 nm respectively and both overestimated λ_{max} by

more than 100 nm. Group 3 with the GGA functionals namely PBE, TPSS and HCTH also have similar accuracy and provided overestimated λ_{max} greater than 200 nm.

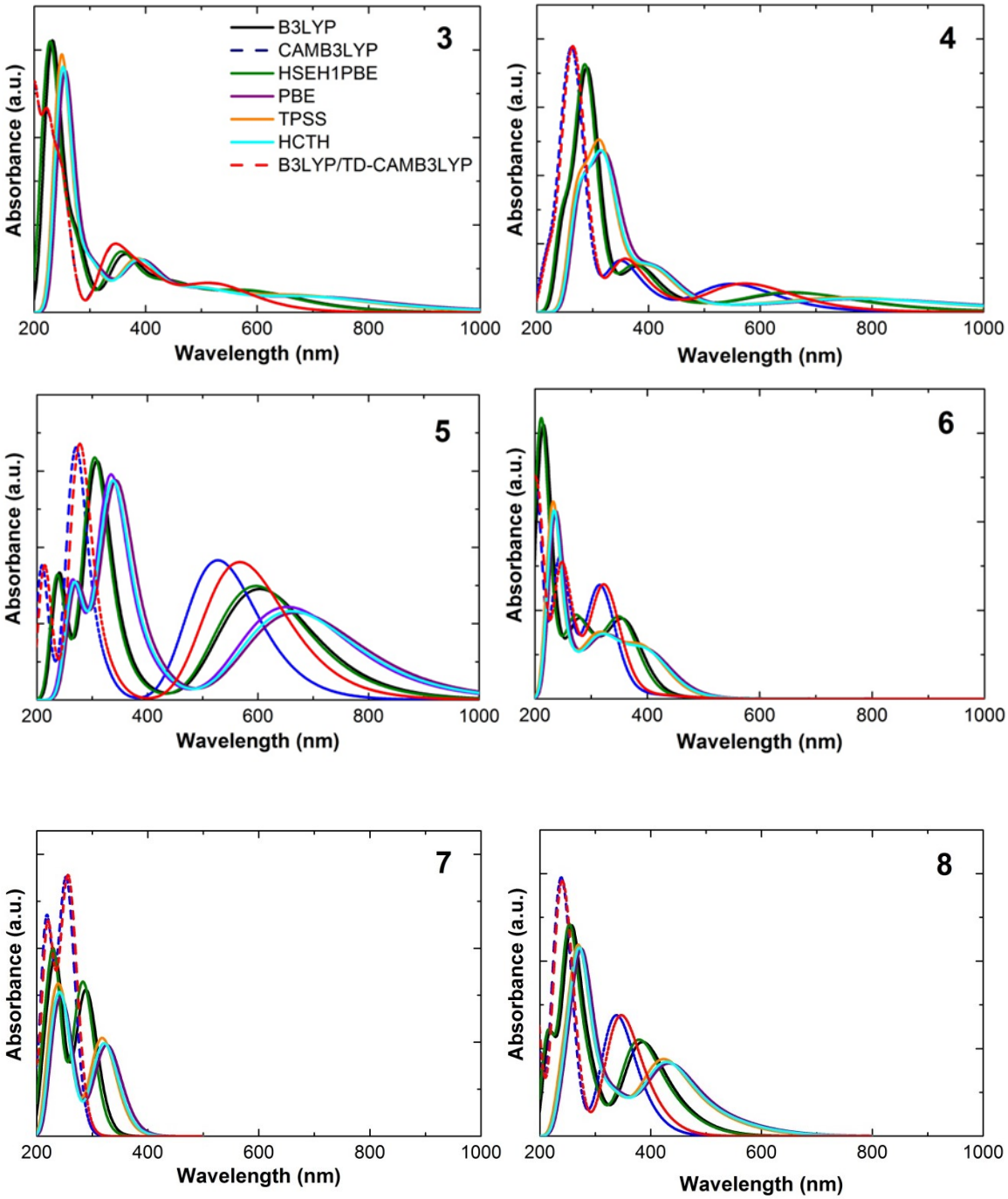

Figure 5.9: Predicted absorption spectra of 3-8

Error trends of predicted λ_{max} were observed as well by comparing similar CP-PAHs and probing the excitation mechanism with the help of contour plots shown in Table 5.10. Among the eight CP-PAHs, **1** & **3**, **2** & **4**, with similar centers, and **6** &**7** can be compared. Contour plots of HOMO for **1** and **2** both have a distributed electron density stretched to the alkyl functional group. Upon excitation to LUMO, the electron density that is stretched to the functional groups migrates to the center providing less spatial overlap between HOMO and LUMO. On the other hand, **3** and **4** have shorter groups attached to the CP-PAH center providing a greater spatial overlap between HOMO and LUMO.

λ_{max} errors of **3** and **4** were almost three times less than that of **1** and **2,** respectively, (shown in Table 5.9) which follows the same phenomena observed by Peach, et. al. on overlap parameters where the less spatial overlap between HOMO and LUMO the greater the excitation energy or wavelength error. The same was observed in **6** and **7,** which are $C_{20}H_{10}$ isomers. A greater spatial overlap between HOMO and LUMO can be seen in **7** compared to **6** (see Table 5.9 and 5.10) providing a smaller λ_{max} error.

Table 5.10: Contour plots of the eight CP-PAHs

CP-PAH	HOMO	Neutral LUMO	-1 Charged LUMO
1	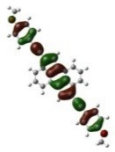 -5.18 eV	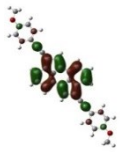 -3.31 eV	-3.48 eV
2	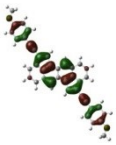 -5.13 eV	-3.31 eV	-3.50 eV
3	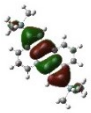 -5.74 eV	-3.07 eV	-3.25 eV
4	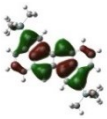 -5.42 eV	-3.13 eV	-3.29 eV
5	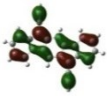 -5.54 eV	-3.48 eV	-3.62 eV
6	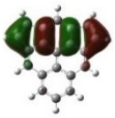 -5.86 eV	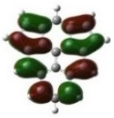 -2.80 eV	-3.27 eV
7	-6.39 eV	-2.00 eV	-2.49 eV
8	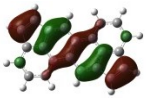 -6.05 eV	-2.72 eV	-3.21 eV

*Calculated using B3LYP/6-311g (d,p)

Contour plots in Table 5.10 shows that there is no significant change in the shape of LUMO of the neutral and anion model. However, the LUMO energy values were lowered using an anion model.

5.6 Summary

This chapter has presented our proposed computational methods for more accurate cyclic voltammetry and absorption spectroscopy (Figures 5.3 and 5.8) using eight CP-PAHs with available experimental results. Both improved computational methods involve choosing the best density functional that will accurately predict experimental results. The more accurate computational cyclic voltammetry uses B3LYP/6-311g(d,p) improved the predicted LUMO and ΔE_{gap} by accounting for the neutral and anion states of CP-PAHs that occur in experiments. In doing so, predicted LUMO and ΔE_{gap} were significantly improved with MAE of 0.17 eV and 0.11 eV while using traditional method provides an MAE of 0.46 eV and 0.40 eV respectively.

In predicting absorption spectra, CAMB3LYP resulted to be the best in predicting λ_{max} of CP-PAHs among the six density functionals. However, by using a good predicted structure of CP-PAHs from B3LYP followed by CAMB3LYP that performs the best in TD-DFT calculations, the most accurate λ_{max} is achieved. This B3LYP/TD-CAMB3LYP method that is already used by other groups provided the least MAE of 29 nm for predicting λ_{max} of seven CP-PAHs.

Molecular level toxicity of AgNPs and other nanoparticles that often involve redox reactions can be accurately predicted using the improved computational cyclic

voltammetry and absorption spectroscopy. Prediction of electronic and optical properties of the silver clusters and the type of capping agent or stabilizers for designing AgNPs for specific application can provide potential toxicity information and possible interaction with biological molecules.

CHAPTER 6

THE IMPROVED COMPUTATIONAL CYCLIC VOLTAMMETRY AND ABSORPTION SPECTROSCOPY ON MTPA DERIVATIVES

Another group of molecules were used to test the accuracy of the improved computational cyclic voltammetry and absorption spectroscopy. Electronic and optical properties of methyltriphenylamine (MTPA) and six other MTPA derivatives in Figure 6.1 were predicted using the improved computational methods discussed in Chapter 5. These set of molecules are often used as an electron donor molecules for organic semiconductor (*132*) and also has the potential application as stabilizers for AgNPs. The electron donor–acceptor mechanism often used in designing efficient organic solar cells can be extended to toxicity studies of AgNPs and other nanoparticles. Recycling redox reactions in biological systems entails donating and accepting electrons and toxicity takes part when the electrons are donated or accepted by the unintended electron donor or acceptor biological molecules.

The MTPA derivatives were chosen as they are the most difficult systems to be calculated accurately. Availability of HOMO, LUMO, ΔE_{gap} and absorption spectra experimental values of MTPA derivatives from our previous studies(*133*) provides a possible measurement of accuracy both for the improved computational methods and the different density functionals.

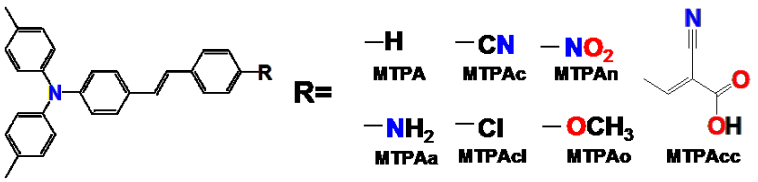

Figure 6.1. Chemical structure of MTPA derivatives

The ten different density functionals namely B3LYP, B3PW91, HSEH1PBE, MPW1PW91, CAMB3LYP, WB97XD, BPV86, PBE, TPSS and HCTH were used in predicting electronic and optical properties of MTPA and its derivatives. The improved computational cyclic voltammetry that accounts for the anion state of the model was performed using B3LYP, B3PW91, HSEH1PBE and HCTH, which have good agreement with experimental values of MTPA derivatives. Accuracy of predicted HOMO, LUMO and ΔE_{gap} were all determined using the traditional and the improved computational method for cyclic voltammetry. In addition, effects of the –R functional group on electronic properties, optical properties and errors of generated using the different density functional were studied.

6.1 Accuracies of the Density Functionals in Predicting Electronic Properties

Synthesis of all the MTPA derivatives in silico was performed using the ten density functionals prior to probing any other properties. Geometry optimization of neutral MTPA derivatives were implemented using the 6-31g+(d,p) basis set and dichloromethane as the solvent treated using the conductor-like polarizable continuum model (CPCM). All geometry optimizations followed the convergence criteria for SCF, gradient and energy of 10^{-8}, 10^{-6} and 10^{-6} a. u. respectively. Each geometry optimization is followed by a frequency calculation and probed for the absence of imaginary frequency to ensure that the structure is the energetic minimum. In addition, the anion state of all the MTPA derivatives were also optimized using B3LYP, B3PW91, HSEH1PBE, and HCTH for the application of the improved computational cyclic voltammetry.

All predicted HOMO, LUMO and ΔE_{gap} values were compared to experimental values taken from literatures. Figure 3 illustrates the predicted HOMO and LUMO using the ten density functionals using the traditional cyclic voltammetry method and the improved method using B3LYP, B3PW91, HSEH1PBE, HCTH and their deviation from experimental values. It clearly shows how wB97XD (dark yellow) and CAMB3LYP (magenta) are the two least density functional in predicting the HOMO, LUMO and ΔE_{gap} of MTPA derivatives. Both density functionals underestimate HOMO and overestimate the LUMO substantially. However, wB97XD is the worst to predict these three properties.

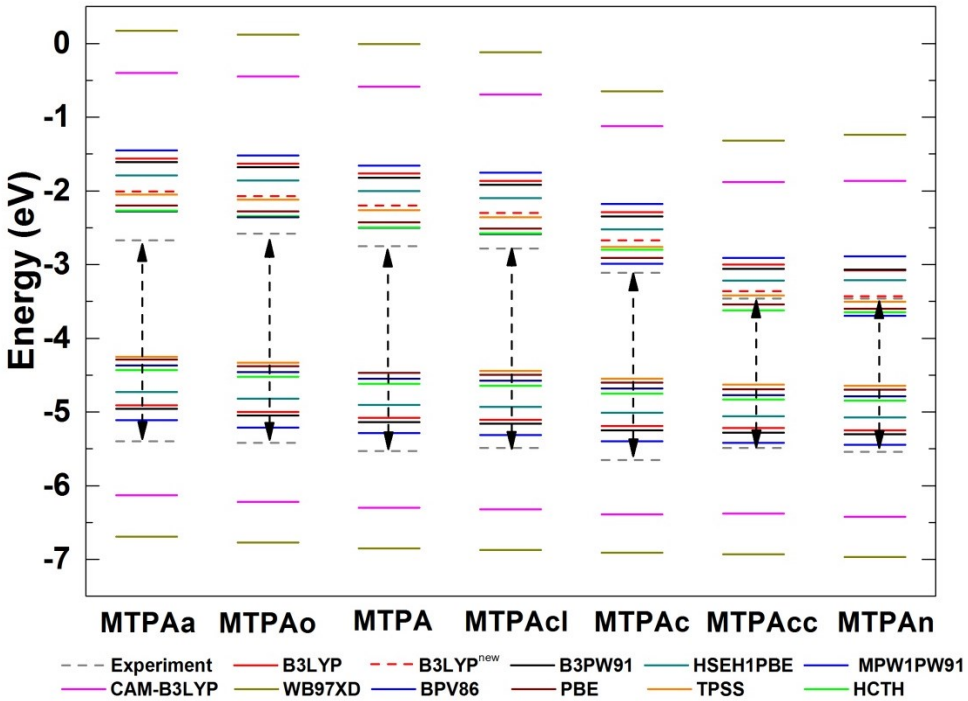

Figure 6.2 Predicted HOMO and LUMO in comparison to experimental values (with arrows showing ΔE_{gap})

Table 6.1 summarizes how each of the ten density functional calculates HOMO of MTPA and its derivatives. All the density functionals overestimate HOMO except for CAMB3LYP and wB97XD that underestimates HOMO remarkably. The top three functionals in estimating HOMO of MTPA and its derivatives are MPW1PW91, B3PW91, and B3LYP, all with MAE < 0.50 eV. Among these three functional MPW1PW91 predicted HOMO the best with the smallest MAE of 0.19 eV also shown in

Table 6.1: HOMO Errors and MAE

Functional	MTPAa	MTPAo	MTPA	MTPAcl	MTPAc	MTPAcc	MTPAn	MAE
Experiment	**-5.40**	**-5.42**	**-5.53**	**-5.49**	**-5.65**	**-5.49**	**-5.54**	
B3LYP	0.49	0.42	0.45	0.39	0.46	0.27	0.29	0.40
B3PW91	0.44	0.37	0.39	0.33	0.40	0.21	0.24	0.34
HSEH1PBE	0.67	0.60	0.62	0.56	0.63	0.43	0.46	0.57
MPW1PW91	0.29	0.21	0.24	0.17	0.25	0.07	0.09	0.19
CAMB3LYP	-0.74	-0.8	-0.77	-0.83	-0.74	-0.9	-0.88	0.81
WB97XD	-1.29	-1.35	-1.32	-1.39	-1.26	-1.44	-1.43	1.35
BPV86	1.03	0.96	0.98	0.91	0.97	0.72	0.75	0.90
PBE	1.11	1.04	1.06	1.00	1.05	0.8	0.84	0.99
TPSS	1.15	1.09	1.11	1.05	1.10	0.86	0.89	1.04
HCTH	0.97	0.90	0.91	0.85	0.89	0.65	0.70	0.84

*All HOMO errors and MAE are in eV

*Experimental HOMO values are provided above

The accuracy of the ten density functional in predicting LUMO using the neutral state of the MTPA derivatives and the anion state using B3LYP, B3PW91, HSEH1PBE and HCTH are summarized in Table 6.2 and Figure 6.3. LUMO calculation using the ten density functionals were overestimated except for LUMO of MTPAn and MTPAcc using BPV86, PBE, and HCTH and LUMO of MTPAn using TPSS. MTPAn and

MTPAcc contain –R groups that have strong electron withrawing abilities. The best density functional in calculating LUMO of MTPA and its derivatives using only a neutral model are BPV86 and HCTH with MAE of 0.22 eV. Accounting for the anion state MTPA snd its derivatives resulted in an improved predicted LUMO for B3LYP, B3PW91, HSEH1PBE but not HCTH.

Table 6.2: Predicted LUMO Errors and MAE

Functional	MTPAa	MTPAo	MTPA	MTPAcl	MTPAc	MTPAcc	MTPAn	MAE
Experiment	**-2.67**	**-2.58**	**-2.77**	**-2.78**	**-3.11**	**-3.46**	**-3.46**	
B3LYP	1.11	0.95	1.00	0.92	0.82	0.46	0.38	0.81
B3PW91	1.06	0.90	0.95	0.86	0.76	0.40	0.39	0.76
HSEH1PBE	0.88	0.72	0.77	0.68	0.59	0.24	0.25	0.59
MPW1PW91	1.22	1.06	1.11	1.02	0.93	0.55	0.57	0.92
CAMB3LYP	2.27	2.13	2.17	2.09	1.99	1.58	1.60	1.98
WB97XD	2.84	2.46	2.76	2.66	2.46	2.14	2.22	2.51
BPV86	0.39	0.22	0.27	0.20	0.12	-0.16	-0.23	0.23
PBE	0.46	0.30	0.34	0.27	0.20	-0.08	-0.14	0.26
TPSS	0.61	0.45	0.50	0.42	0.34	0.04	-0.05	0.34
HCTH	0.39	0.23	0.27	0.20	0.13	-0.16	-0.19	0.22
B3LYP^{new}	0.66	0.51	0.57	0.48	0.44	0.10	0.03	0.40
B3PW91^{new}	0.60	0.45	0.50	0.42	0.37	0.03	0.05	0.35
HSEH1PBE^{new}	0.82	0.68	0.73	0.65	0.59	0.25	0.26	0.57
HCTH^{new}	0.94	0.80	0.85	0.77	0.70	0.26	0.59	0.70

* All LUMO errors and MAE are in eV

*Experimental LUMO values are provided above

Table 6.3 and Figure 6.3 shows the accuracy of the ten density functional in predicting ΔE_{gap} of MTPA and it's derivatives. ΔE_{gap} calculated using B3LYP, B3PW91, MPW1PW91, CAMB3LYP and wB97XD were all overestimated. CAMB3LYP and

wB97XD provide the considerably overestimated ΔE_{gap}. BPV86, PBE, TPSS and HCTH provide underestimated ΔE_{gap}. HSEH1PBE provides an overestimated ΔE_{gap} for MTPA, MTPAa, MTPAo and MTPAcl while an underestimation for MTPAc, MTPAn and MTPAcc. The top three best functional for prediction of ΔE_{gap} are HSEH1PBE, B3LYP

Table 6.3: Predicted ΔE_{gap} Errors and MAE

Functional	MTPAa	MTPAo	MTPA	MTPAcl	MTPAc	MTPAcc	MTPAn	MAE
Experiment	**2.73**	**2.84**	**2.76**	**2.71**	**2.54**	**2.03**	**2.08**	
B3LYP	0.62	0.53	0.55	0.53	0.36	0.19	0.09	0.41
B3PW91	0.62	0.53	0.56	0.53	0.36	0.19	0.15	0.42
HSEH1PBE	0.21	0.12	0.15	0.12	-0.04	-0.19	-0.21	0.15
MPW1PW91	0.93	0.85	0.87	0.85	0.68	0.48	0.48	0.73
CAMB3LYP	3.01	2.93	2.95	2.92	2.73	2.48	2.48	2.79
WB97XD	4.13	3.81	4.06	4.05	3.72	3.58	3.65	3.86
BPV86	-0.64	-0.74	-0.71	-0.71	-0.85	-0.88	-0.98	0.79
PBE	-0.65	-0.74	-0.72	-0.73	-0.85	-0.88	-0.98	0.79
TPSS	-0.54	-0.64	-0.61	-0.63	-0.76	-0.82	-0.94	0.71
HCTH	-0.58	-0.67	-0.64	-0.65	-0.76	-0.81	-0.89	0.71
B3LYP^{new}	0.16	0.09	0.11	0.10	-0.02	-0.17	-0.26	0.13
B3PW91^{new}	0.16	0.08	0.11	0.09	-0.03	-0.17	-0.19	0.12
HSEH1PBE^{new}	0.15	0.08	0.10	0.09	-0.04	-0.18	-0.21	0.12
HCTH^{new}	-0.03	-0.10	-0.07	-0.07	-0.19	-0.22	-0.11	0.11

* All ΔE_{gap} errors and MAE are in eV

*Experimental ΔE_{gap} values are provided above

and B3PW91. Among these three HSEH1PBE is the best functional in calculating ΔE_{gap} of MTPA and its derivatives using the neutral model. The improved computational cyclic voltammetry using B3LYP, B3PW91, HSEH1PBE and HCTH with the neutral and anion

state for calculation of HOMO and LUMO respectively provided the most accurate predicted ΔE_{gap} of MTPA and its derivatives.

There is not one density functional that can predict all electronic properties of MTPA and its derivatives accurately. Calculation of the MAE for HOMO, LUMO and ΔE_{gap} shows that each of these three properties is predicted the best by different density functionals using the traditional computational method for cyclic voltammetry. The HOMO, LUMO and ΔE_{gap} were predicted the best by MPW1PW91, BPV86 & HCTH, and HSEH1PBE respectively using the traditional computational method fot cyclic voltammetry. The improved computational cyclic voltammetry provided a significantly improved LUMO and ΔE_{gap} using B3LYP, B3PW91 and HSEH1PBE and provided very similar accuracy for all three electronic properties.

Determining one best functional in predicting all these three optical properties will provide efficiency in studying similar systems theoretically. Considering all MAE of predicted HOMO, LUMO and ΔE_{gap} using the traditional and improved computational methods for cyclic voltammetry, the most accurate predicted HOMO, LUMO and ΔE_{gap} can be achieced using B3LYP and B3PW91 with very similar MAE of 0.31 eV and 0.27 eV respectively as shown in Table 6.4.

Table 6.4 Average MAE of HOMO, LUMO and ΔE_{gap}

Functional	HOMO MAE	LUMO MAE	ΔE_{gap} MAE	Overall MAE
B3LYP	0.40	0.81	0.41	**0.54**
B3PW91	0.34	0.76	0.42	**0.51**
HSEH1PBE	0.57	0.59	0.15	**0.44**
MPW1PW91	0.19	0.92	0.73	**0.61**
CAMB3LYP	0.81	1.98	2.79	**1.86**
WB97XD	1.35	2.51	3.86	**2.57**
BPV86	0.90	0.23	0.79	**0.64**
PBE	0.99	0.26	0.79	**0.68**
TPSS	1.04	0.34	0.71	**0.70**
HCTH	0.84	0.22	0.71	**0.59**
B3LYP^{new}	0.40	0.40	0.13	**0.31**
B3PW91^{new}	0.34	0.35	0.12	**0.27**
HSEH1PBE^{new}	0.57	0.57	0.12	**0.42**
HCTH^{new}	0.19	0.70	0.11	**0.33**

* All MAE are in eV

The accuracy of the ten density functionals in predicting electronic properties of MTPA and its derivatives using the traditional computational method for cyclic voltammetry is illustrated in Figure 6.3. The comparison of the traditional and improved computational methods using B3LYP, B3PW91, HSEH1PBE and HCTH is also shown in Figure 6.3. Using the traditional computational method, the HOMO, LUMO and ΔE_{gap} are predicted the best using HSEH1PBE. However, using the improved computational method for cyclic voltammetry, HOMO, LUMO and ΔE_{gap} are predicted most accurately using B3LYP and HSEH1PBE as shown in Figure 6.3D. Accounting for the anion state of the model that exists experimentally significantly improved the

prediction of LUMO and ΔE_{gap} of MTPA. This improved method discussed in Chapter 5 also provided significant improvements in predicted LUMO and ΔE_{gap} of CP-PAH systems.

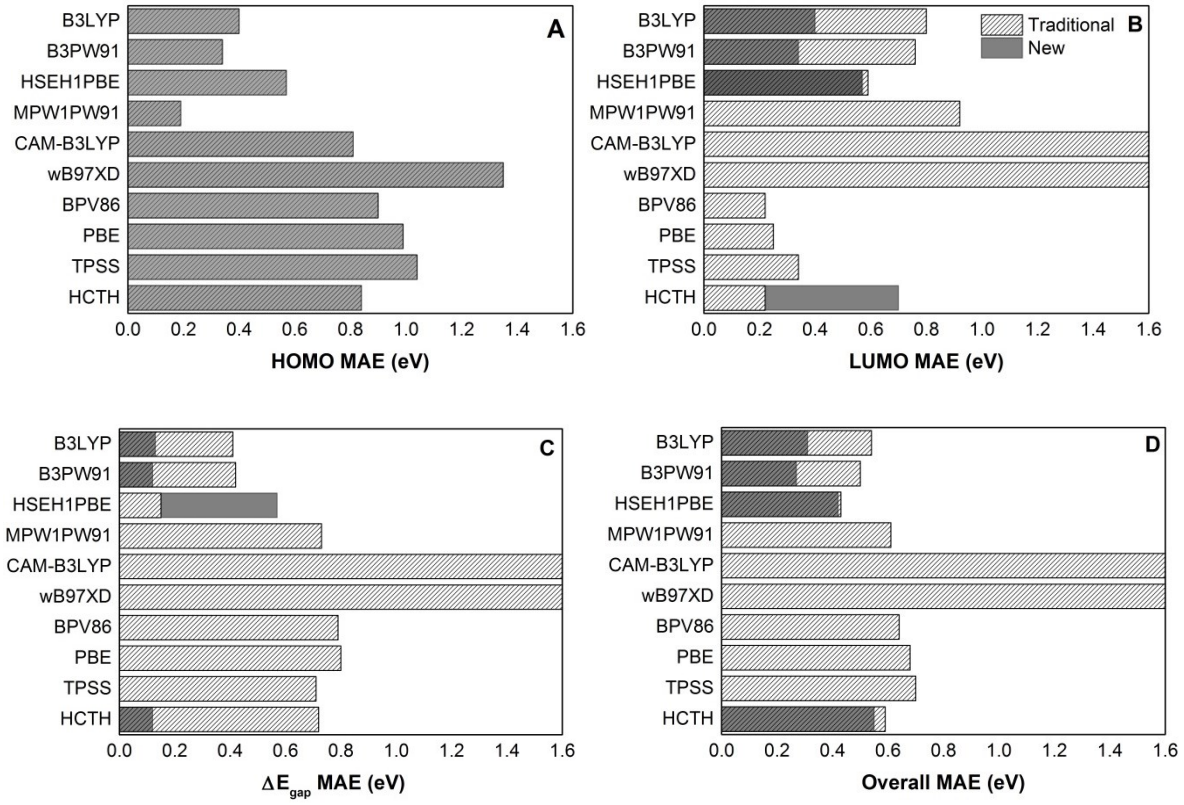

Figure 6.3: Predicted HOMO, LUMO, ΔE_{gap} and overall MAE of MTPA derivatives

Accuracy of predicted HOMO, LUMO and ΔE_{gap} using the ten functionals can be grouped into three (see Tables 6.1 to 6.4 and Figure 6.3). These three groups are Group 1 – B3LYP, B3PW91, HSEH1PBE & MPW1PW91, Group 2 – CAMB3LYP & wB97XD, and Group 3 – PBE, TPSS, HCTH and BPV86. Group 1 members are all hybrid density functionals with similar accuracy to B3LYP and provides good esttimation of HOMO with MAE < 0.6 eV. Group 2 members are all hybrid as well with long range correction for the exchange functional and are the worst in predicting HOMO, LUMO

and ΔE_{gap}. Group 3 includes one hybrid, one meta-GGA and two GGA functionals, and is the best group in calculating LUMO with MAE < 0.4 eV.

6.2 Accuracies of the Density Functionals in Predicting Absorption Spectra

Absorption spectra of MTPA and its derivatives were calculated using the ten density functionals. In addition, the improved computational absorption spectroscopy that uses a B3LYP/TD-CAMB3LYP was also employed. All absorption spectra were generated using twelve states on all TDDFT calculations. All TDDFT calculations were implemented using the 6-31g+(d,p) basis set and dichloromethane as the solvent treated using the conductor-like polarizable continuum model (CPCM).

All predicted absorption spectra in comparison to experimental values are shown in Figure 6.4. Predicted absorption spectra also suggest that the ten density functionals employed can be grouped into three according to accuracy. Predicted absorption spectra belonging to the same group are almost overlapping. On all the predicted spectra in Figure 6.4, predicted absorption using Group 1 density functionals are in the middle. Predicted absorption spectra using Group 2 density functionals are closer to experiment and appear on the shorter wavelength while Group 3 are on the longer wavelength and provided the worst prediction. Among the ten density functionals, CAMB3LYP provided the best predicted absorption spectra. However, the improved computational method for absorption spectroscopy that uses B3LYP/TD-CAMB3LYP provided more accurate predicted absorption spectra than using just CAMB3LYP.

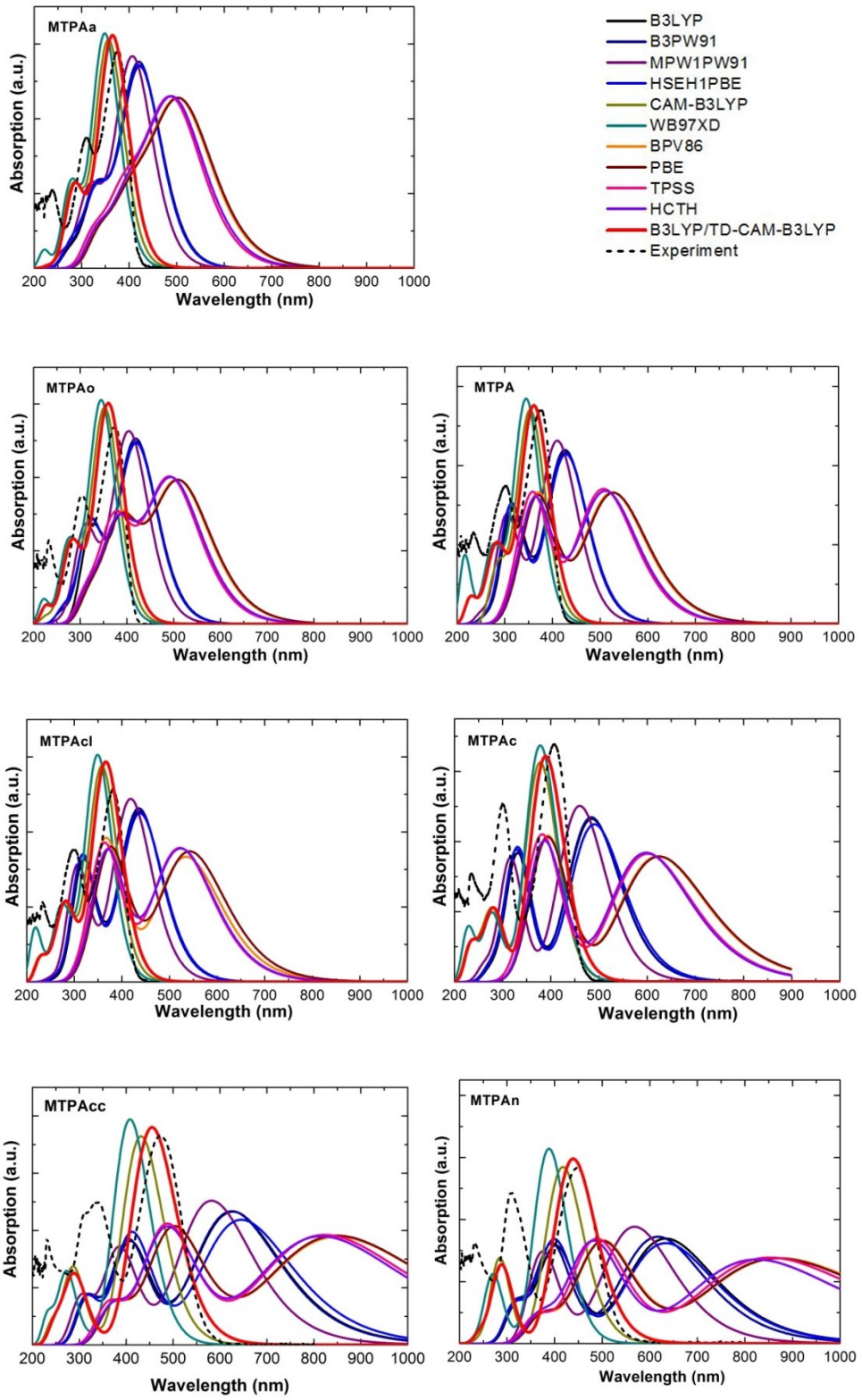

Figure 6.4: Predicted absorption spectra of MTPA derivatives

Experimental λ_{max} and errors of each of the ten density functionals and the B3LYP/TD-CAMB3LYP method in predicting absorption spectra are shown in Table 6.5. Group 1 density functionals provided predicted λ_{max} that were overestimated with MAE between 50 to 100 nm. Group 3 density functionals produced the worst predicted absorption spectra that were overestimated by >200 nm. Group 2 density functionals – CAMB3LYP & wB97xD performed the best among the three groups in calculating absorption spectra of MTPA and its derivatives with λ_{max} underestimated by less than 40 nm.

Table 6.5: Predicted λ_{max} errors and MAE

Functional	MTPAa	MTPAo	MTPA	MTPAcl	MTPAc	MTPAcc	MTPAn	MAE
Experiment	**375**	**375**	**375**	**380**	**407**	**472**	**448**	
B3LYP	48	47	53	57	78	156	186	89
B3PW91	47	45	52	56	77	153	169	86
HSEH1PBE	48	46	54	58	83	174	186	93
MPW1PW91	33	30	35	39	53	110	120	60
CAMB3LYP	-18	-22	-21	-22	-29	-40	-30	26
WB97XD	-26	-29	-30	-31	-29	-64	-60	38
BPV86	135	137	152	155	225	380	426	230
PBE	137	139	154	163	218	378	422	230
TPSS	118	119	133	143	194	352	405	209
HCTH	123	123	137	145	191	342	387	206
B3LYP/TD-CAMB3LYP	-10	-14	-13	-13	-18	-17	-9	13

*All errors and MAE are in nm

The B3LYP/TD-CAMB3LYP method provided underestimated but the best λ_{max} of MTPA and its derivatives with MAE of 13.4 nm. Accuracy of predicted absorption spectra are illustrated in Figure 6.5. Group 3 composed of mostly GGA functionals and one hybrid functional BPV86 provided the highest MAE. Density functionals that has a long ranged corrected exchange function such as those that belongs to Group 2 and the B3LYP/TD-CAMB3LYP method provided very good absorption spectra prediction, which suggest the importance of long range correction for TDDFT calculations.

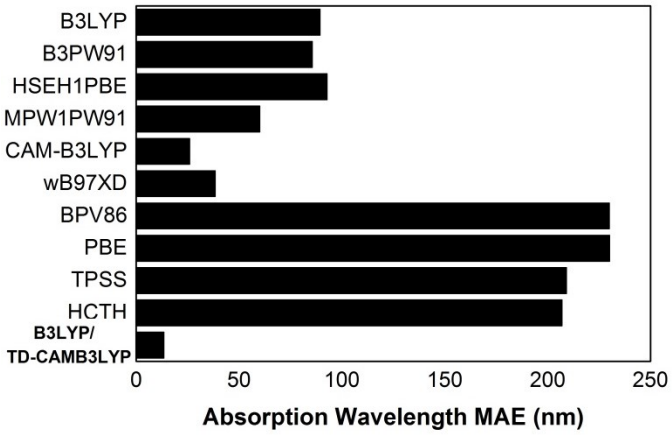

Figure 6.5: MAE of each density functional for absorption wavelength (λ_{max})

Experimental results λ_{max} ranks the seven MTPA derivatives from highest to lowest absorption wavelength as such MTPAcc > MTPAn > MTPAc > MTPAcl > MTPAo = MTPAa = MTPA. This suggest that as the increase in electron withdrawing ability of the –R group attached to MTPA results into a red shift. Among the ten density functionals employed, B3PW91, HSEH1PBE, MPW1PW91, CAMB3LYP and WB97XD was able to predict this trend. Group 3 density functionals- BPV86, PBE, TPSS and HCTH were not able to predict the proper trend for MTPAcc and MTPAn. Calculation

using Group 3 functionals provide an absorption wavelength of MTPAn that is higher than MTPAcc. Figure 6.6 shows how each of the ten density functional predict the absorption trend of the seven MTPA derivatives. Among the 10 functionals, CAMB3LYP still provided the best prediction of the trend of effects of different –R groups on MTPA.

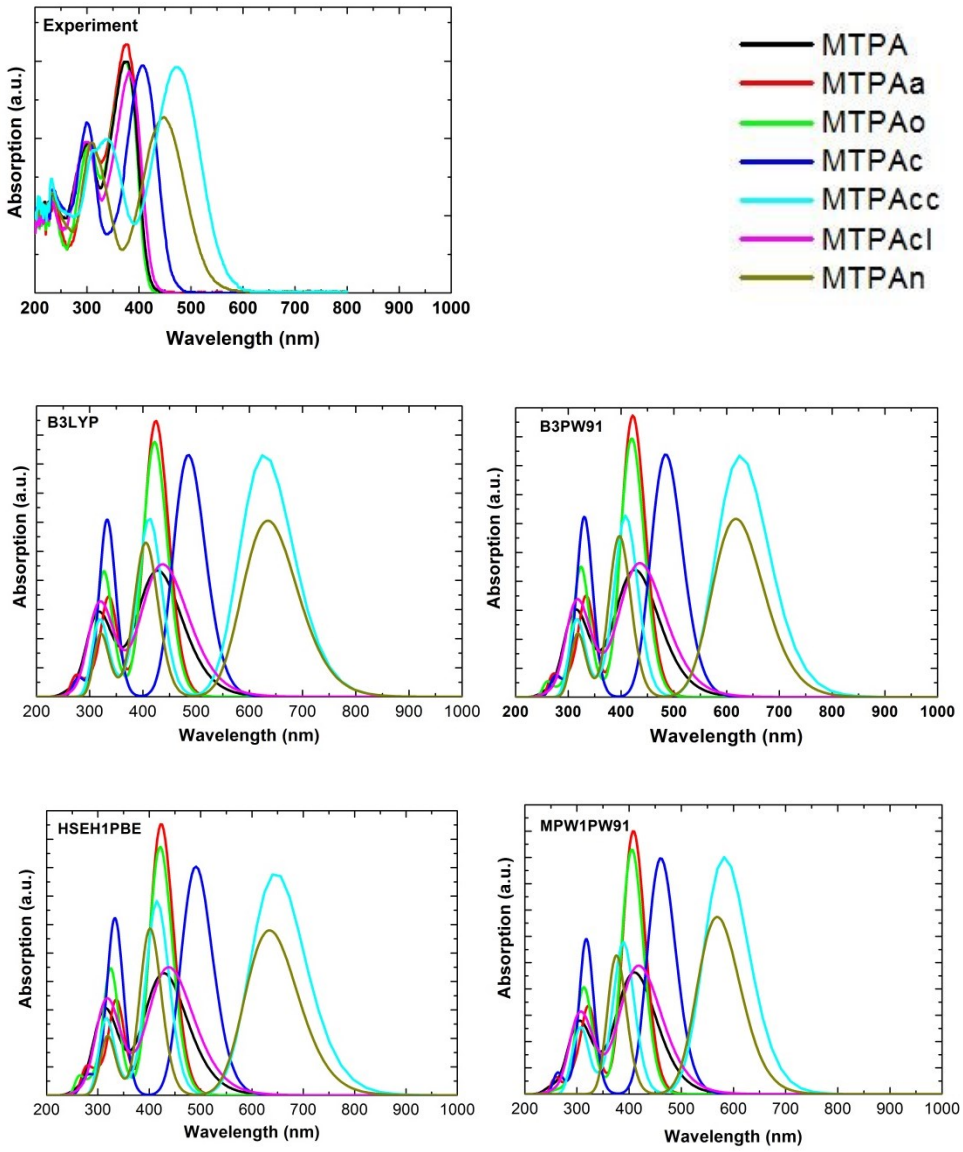

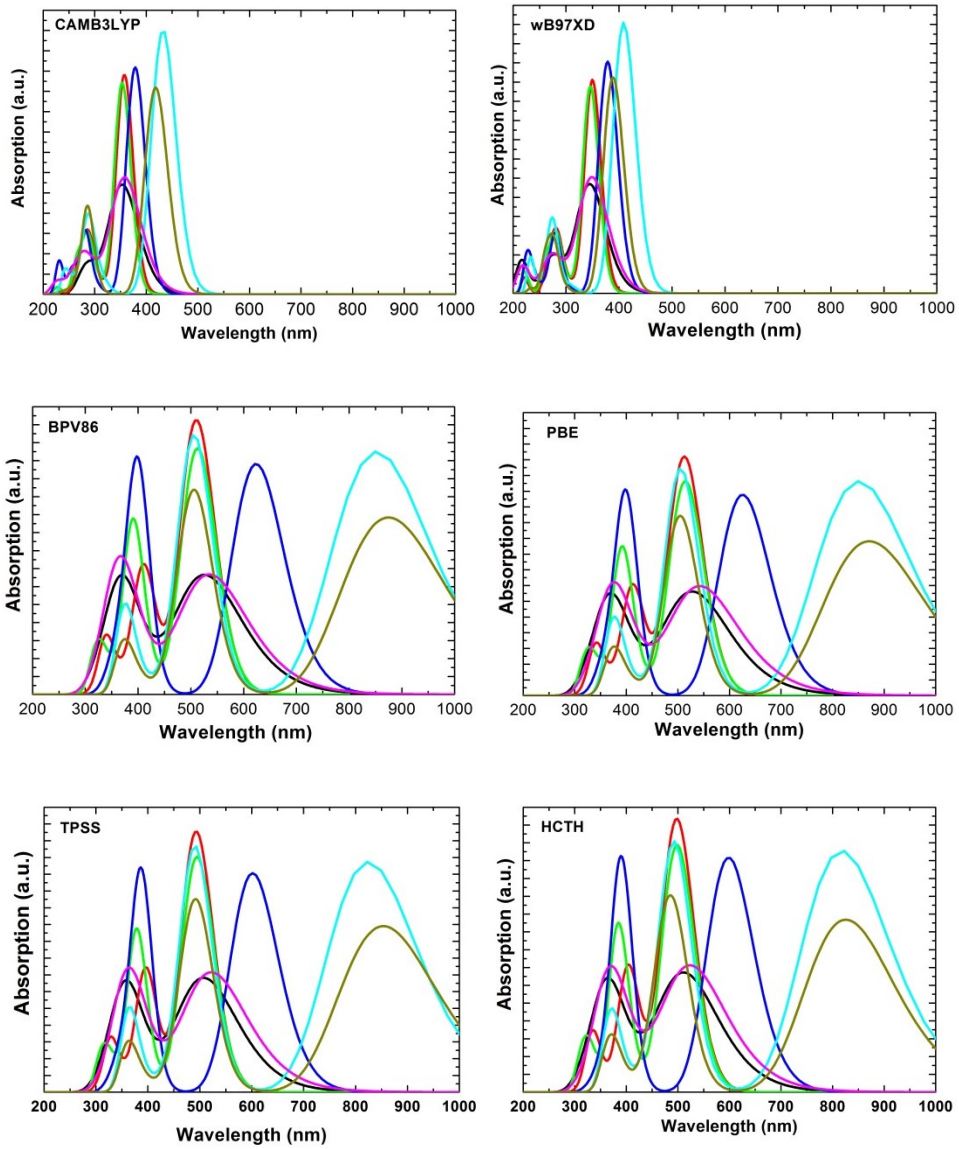

Figure 6.6: Predicted absorption spectra trend of the different MTPA derivatives

6.3 Functional Group (-R) Dependent Accuracy of Predicted Electronic and Optical Properties of MTPA Derivatives

The different MTPA derivatives included in this study contains a variety of –R groups from electron donating to electron withdrawing groups. $–NH_2$ and $–OCH_3$ are

electron donating when attached to an aromatic ring while –Cl, –CN, -COOH, NO_2 are all electron withdrawing groups. The ranking from most electron withdrawing to least electron donating ability of the MTPA derivatives employed in this study is MTPAn > MTPAcc > MTPAc > MTPAcl > MTPA > MTPAo > MTPAa.

6.3.1. Predicted Optical properties MTPA derivatives

Varying of –R groups attached to MTPA was observed to have an effect in accuracy of predicting absorption spectra of MTPA derivatives. Errors of predicted absorption spectra using the different density functionals increased as the –R group attached to MTPA becomes more electron withdrawing. MTPAn and MTPAcc with strong electron withdrawing –R groups resulted in the high MAE for any density functional (see Table 6.5). On the contrary, MTPAo and MTPAa with electron donating groups resulted in the low MAE for any density functional (see Table 6.5). This trend can be correlated to the degree of spatial overlap between the occupied and virtual orbitals involved in excitation of MTPA and its derivatives. As the spatial overlap between the occupied and virtual orbitals involved in excitation reduces excitation energy errors increase(*104, 129*). This spatial overlap for MTPA and its derivatives can be visually inspected using contour plots of HOMO and LUMO shown in Figure 6.6. Spacial overlap between HOMO and LUMO decreases as the –R group changes from being electron donating to electron withdrawing, which explains the increase in MAE.

Table 6.6: Contour plots of HOMO and LUMO of MTPA derivatives

	HOMO	LUMO
MTPAa	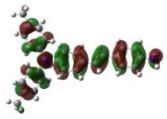 MO104 (-4.73 eV)	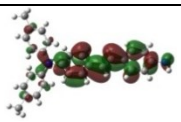 MO 105 (-1.79 eV)
MTPAo	MO 108 (-4.82 eV)	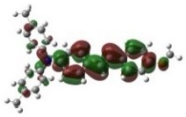 MO 109 (-1.86 eV)
MTPA	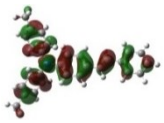 MO 100 (-4.91 eV)	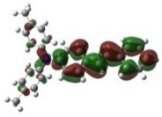 MO 101 (-2.00 eV)
MTPAcl	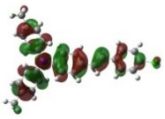 MO 108 (-4.93 eV)	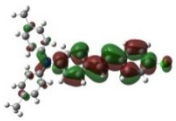 MO 109 (-2.10 eV)
MTPAc	MO 106 (-5.02 eV)	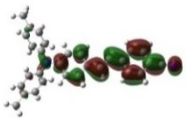 MO107(-2.52 eV)
MTPAcc	MO 124 (-5.06 eV)	MO 125 (-3.22 eV)
MTPAn	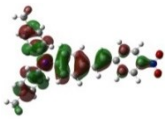 MO 111 (-5.08 eV)	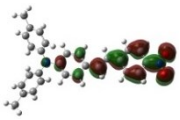 MO 112 (-3.21 eV)

6.3.2 Predicted Electronic Properties of MTPA Derivatives

The variation of functional group attached to MTPA also affected accuracy of predicted electronic properties. If predicted absorption spectra becomes less accurate as the –R group attached to MTPA becomes a more electron withdrawing, the opposite is observed for predicted electronic properties. Errors of predicted HOMO, LUMO and ΔE_{gap} using any density functional tends to decrease as the –R group attached to MTPA increased in electron withdrawing ability (see Table 6.1 to 6.3).

Table 6.7: Predicted HOMO of MTPA derivatives relative to MTPA

Functional	MTPAa	MTPAo	MTPA	MTPAcl	MTPAc	MTPAcc	MTPAn
Experiment	**0.13**	**0.11**	**0**	**0.04**	**-0.12**	**0.04**	**-0.01**
B3LYP	0.17	0.08	0	-0.02	-0.11	-0.14	-0.17
B3PW91	0.18	0.09	0	-0.02	-0.11	-0.14	-0.16
HSEH1PBE	0.18	0.09	0	-0.02	-0.11	-0.15	-0.17
MPW1PW91	0.18	0.08	0	-0.03	-0.11	-0.13	-0.16
CAMB3LYP	0.16	0.08	0	-0.02	-0.09	-0.09	-0.12
WB97XD	0.16	0.08	0	-0.03	-0.06	-0.08	-0.12
BPV86	0.18	0.09	0	-0.03	-0.13	-0.22	-0.24
PBE	0.18	0.09	0	-0.02	-0.13	-0.22	-0.23
TPSS	0.17	0.09	0	-0.02	-0.13	-0.21	-0.23
HCTH	0.19	0.10	0	-0.02	-0.14	-0.22	-0.22

*All values are in eV

Using MTPA as a reference, Table 6.6 to 6.8 show how the different –R groups can affect the HOMO, LUMO and ΔE_{gap}. Experimental results in Table 6.7 show that MTPA with –R group of strong to moderate electron donating ability can provide an increase in HOMO to as high as 0.13 eV (MTPAa). Changing the –R group to an

electron withdrawing group produced a slight increase of HOMO to 0.04 eV (MTPAcl and MTPAcc) to a deacrease of 0.12 eV (MTPAc). A similar trend was observed for predicted HOMO using the ten density functionals. All calculated HOMO increase as the –R group attached to MTPA becomes more electron donating while it decrease as the –R group becomes more electron withdrawing as shown in Table 6.7

Experimental trend of LUMO in Table 6.8 shows that an increase in LUMO is present for MTPA with electron donating groups while a decreasing LUMO as the –R group becomes more electron withdrawing is observed. Predicted LUMO using the ten density functionals provide the same trend except for wB97XD that produced a decrease in LUMO for MTPAo with an electron donating group. Predicted LUMO shows an increase in LUMO as the –R group in MTPA becomes more electron donating and a decrease in LUMO as the –R group becomes more electron withdrawing.

Experimental trend of ΔE_{gap} in Table 6.9 shows that ΔE_{gap} for electron donating groups is increased to as high as 0.06 eV (MTPAo) and decreased to as low as 0.05 eV (MTPAa) while a decreasing ΔE_{gap} from as low as 0.07 eV (MTPAcl) to 0.75 eV (MTPAcc) was observed as the –R group attached to MTPA becomes more electron withdrawing group. Predicted ΔE_{gap} using the all density functionals show a slight increase as the –R group attached becomes electron donating except for wB97XD that resuled in a decrease for MTPAo. A decreasing ΔE_{gap} is observed as the –R group becomes more electron withdrawing group is observed for all density functionals employed.

Table 6.8: Predicted LUMO of MTPA derivatives relative to MTPA

Functional	MTPAa	MTPAo	MTPA	MTPAcl	MTPAc	MTPAcc	MTPAn
Experiment	**0.10**	**0.19**	**0**	**-0.01**	**-0.34**	**-0.69**	**-0.69**
B3LYP	0.21	0.14	0	-0.09	-0.52	-1.23	-1.31
B3PW91	0.21	0.14	0	-0.10	-0.53	-1.24	-1.25
HSEH1PBE	0.21	0.14	0	-0.10	-0.52	-1.22	-1.21
MPW1PW91	0.21	0.14	0	-0.10	-0.52	-1.25	-1.23
CAMB3LYP	0.19	0.14	0	-0.10	-0.53	-1.29	-1.27
WB97XD	0.18	-0.11	0	-0.11	-0.64	-1.31	-1.23
BPV86	0.22	0.14	0	-0.08	-0.49	-1.12	-1.19
PBE	0.22	0.15	0	-0.08	-0.48	-1.11	-1.17
TPSS	0.21	0.14	0	-0.09	-0.50	-1.15	-1.24
HCTH	0.22	0.15	0	-0.08	-0.48	-1.12	-1.15

*All values are in eV

Table 6.9 Predicted ΔE_{gap} of MTPA derivatives relative to MTPA

Functional	MTPAa	MTPAo	MTPA	MTPAcl	MTPAc	MTPAcc	MTPAn
Experiment	**-0.03**	0.08	**0**	-0.05	-0.22	**-0.73**	**-0.68**
B3LYP	0.04	0.06	0	-0.07	-0.41	-1.09	-1.14
B3PW91	0.03	0.05	0	-0.08	-0.42	-1.10	-1.09
HSEH1PBE	0.03	0.05	0	-0.08	-0.41	-1.07	-1.04
MPW1PW91	0.03	0.06	0	-0.07	-0.41	-1.12	-1.07
CAMB3LYP	0.03	0.06	0	-0.08	-0.44	-1.20	-1.15
WB97XD	0.02	-0.19	0	-0.08	-0.58	-1.23	-1.11
BPV86	0.04	0.05	0	-0.05	-0.36	-0.90	-0.95
PBE	0.04	0.06	0	-0.06	-0.35	-0.89	-0.94
TPSS	0.04	0.05	0	-0.07	-0.37	-0.94	-1.01
HCTH	0.03	0.05	0	-0.06	-0.34	-0.90	-0.93

*All values are in eV

Overall, accuracy of electronic properties of MTPA derivatives were affected by the different –R groups. The calculated accuracy of the ten density functional in predicting the HOMO, LUMO and ΔE_{gap} of MTPA derivatives can be used as a guide in choosing the best functional for studying a system with known HOMO to LUMO excitation mechanism.

6.4 Summary

In this chapter the improved computational cyclic voltammetry and absorption spectroscopy discussed in chapter 5 were also used in predicted electronic and optical properties of MTPA derivatives. The ten different density functional available in the DFT method in the Gaussian 09 software were employed. Electronic properties of MTPA derivatives were best predicted using B3LYP or B3PW91 on the improved computational cyclic voltammetry. The B3LYP/TD-CAMB3LYP method still resulted to be the best in predicting absorption spectra of MTPA derivatives.

Moreover, the varying –R groups attached to the MTPA can affect the accuracy of predicted electronic and optical properties. More accurate predicted HOMO, LUMO and ΔE_{gap} were observed as the –R group attached to MTPA becomes more electron withdrawing. On the other hand, predicted absorption spectra tends to be less accurate as the –R group attached to MTPA becomes more electron withdrawing group, which is explained by decrease in spacial overlap between the HOMO and LUMO that has a trend of decrease accuracy in excitation energy calculations.

Results presented in this chapter can be a guide in the accurate prediction of electronic and optical properties. Overall results also suggest that the application of the improved computational methods for cyclic voltammetry and absorption spectra can be expanded to other systems and not only confined to CP-PAHs. Application of these two improved computational methods can also be extended to predicting molecular level toxicity mechanisms of silver nanoparticles in which the electronic properties of the surface can define its toxicity. Prediction of electronic and optical properties of silver nanoparticle stabilizers or capping agents can also provide toxicity information for these materials.

CHAPTER 7

CONCLUSIONS AND FUTURE WORK

Though thousands of toxicity studies on AgNPs are available, most of these studies claim that toxicity information on AgNPs are still insufficient. Hence, our group conducted a combination of experimental and computational studies of AgNP toxicity that can provide atomic level toxicity mechanism of AgNPs. The experimental results show that toxicity of 10 nm citrate stabilized silver nanoparticles to HepG2 cells starts at a dosage that exceeds 1ppm and LD50 is at 3ppm. Reactive oxygen species level is elevated upon introduction of increasing concentration of silver nanoparticles and is at maximum at the LD50 of 3ppm concentration of AgNPs. Normal protein regulation of HepG2 cells were affected upon exposure to the AgNPs. TEM images of the AgNP dosed HepG2 cells reveal that the AgNPs can penetrate and agglomerate inside the cells.

Our preliminary computational study was guided by toxicity mechanism that attributes the toxicity of AgNPs to its dissolution to Ag^+. Our computational models were composed of 1:1 ratio of silver and phospholipid head. The silver is in atomic or anionic form and the phospholipid heads were phosphocholine (PC) and phosphoethanolamine (PE). Computational results show that the presence Ag^+ around PC or PE, results in partial oxidation of the phospholipid heads. Oxidation of phospholipids produces an imbalanced pro-oxidative stress state that provides an easier access for the formation of reactive oxygen species. The presence of Ag^0 caused partial reduction to the phospholipids. Calculated binding energies suggest that Ag^+ binds to the phospholipid

heads three to five times stronger than Ag^0, which is marked by shorter distance between Ag^+ and PC or PE. The presence of Ag^+ and Ag^0 around the phospholipids was predicted to have bathochromic shifts of 40 -103 nm and 185 – 200 nm, respectively, in the predicted absorption spectra. However, absorption intensities due to the presence of silver ion were weak and electrochemical method may be a better choice of detection.

Prior to further studying AgNP toxicity computationally, we recognized the need for improving computational methods to accurately predict properties of AgNPs and its toxicity mechanisms. Since both preliminary experimental and computational studies of AgNP toxicity indicate an oxidation toxicity mechanism, we have chosen to improve the accuracy of computational methods for cyclic voltammetry and absorption spectroscopy that use DFT and TD-DFT, respectively. Cyclopentafused-polycyclic aromatic hydrocarbonds (CP-PAHs), a group of electron acceptors that has a potential application as stabilizers for AgNPs were used in developing the more accurate computational methods. Availability of HOMO, LUMO, ΔE_{gap} and absorption spectra experimental data of CP-PAHs made possible to develop more accurate computational methods. The improved computational method for cyclic voltammetry was developed by accounting the anion species of CP-PAHs that occur experimentally and B3LYP resulted to be the best density functional, among the six density functional employed. Overall MAE of 0.14 eV was achieved for predicting electronic properties using B3LYP in the improved computational method, which is a significant improvement of the conventional method with overall MAE of 0.50 eV. Absorption spectra of the CP-PAHs were best predicted using B3LYP in geometry optimizations followed by TD-CAMB3LYP

with MAE of 29nm. Errors in absorption spectra were observed to increase as the spatial overlap between the HOMO and LUMO decreases.

The developed computational cyclic voltammetry and absorption spectroscopy were tested on a set of methyl triphenyl amine (MTPA) derivatives with available experimental data and have a potential application as stabilizers of AgNP. The –R group (functional group) attached to the MTPA derivatives are $–NH_2$, $-OCH_3$, -H, -Cl, -CN, -CN(COOH), $-NO_2$, which are arranged from most electron donating to most electron withdrawing in ability. Ten density functionals available in the Gaussian 09 were employed in both the improved computational cyclic voltammetry and absorption spectroscopy. The developed computational cyclic voltammetry used for CP-PAHs that accounts for the anionic species also provided the accurate electronic properties of MTPA derivatives using B3LYP/6-311g (d,p) with overall MAE of 0.31 eV (B3PW91 resulted similar accuracy as B3LYP), which is significantly improved from conventional method with overall MAE of 0.54 eV. Absorption spectra of MTPA derivatives were best calculated using the B3LYP/TD-CAMB3LYP method among the other ten density functionals employed with MAE of 13 nm. I was also observed that as the functional group attached to MTPA increases in electron withdrawing ability, accuracy of predicted electronic properties increases while accuracy of predicted absorption spectra decreases.

In the future, we intend to use our two improved computational methods in studying possible oxidation of other biological molecules caused by silver nanoparticles and different stabilizers. Accurately predicting the HOMO and LUMO of biological molecules such as adenosine triphosphate (ATP), adenosine diphosphate (ADP),

stabilizers like PVP, citrate, and different clusters of silver can provide a map of possible oxidation pathway that leads to toxicity. This map can be illustrated using an energy diagram of all the HOMO and LUMO of the biological molecules, stabilizers and silver clusters and possible detection of oxidation pathway can be probed by the possibility of electron transfer from the silver clusters or stabilizers to a particular biological molecules.

As part of the future work, we also want to study the possible catalytic role of silver nanoparticles in Fenton reactions that causes generation of ROS, and other recycling redox reactions in the body such as those that are involve in the Krebs cycle.

REFERENCES

1. J. C. Merill, Morton, J.J.P. and Solleau, S.D., *Metals*. A. W. Hayes, Ed., Principles and Methods of Toxicology (Taylor & Francis Group, Boca Raton, 2008).

2. M. Li, Al-Jamal, K.T., Kostarelos, K., Reineke, J., Review: Physiologically based pharmacokinetic modelling of nanoparticles. *ACS nano* **4**, 6303 (2010).

3. W. Lu, Senapati, D., Wang, S., Tovmachenko, O., Singh. A. K., Yu, H., and Ray, P. C., Effect of surface coating on the toxicity of silver nanomaterials on human skin keratinocytes. *Chem. Phys. Lett.* **487**, 92 (2010).

4. P. V. Ashani, Low Kah Mun, G., and Hande, M.P., Cytotoxicity and genotoxicity of silver nanoparticles in human cells *ACS nano* **3**, 279 (2009).

5. A. M. El Badawy, Silva, R. V., Morris, B., Scheckel, K. G., Suidan, M. T., Tolaymat, T. M., Surface Charge-Dependent Toxicity of Silver Nanoparticles. *Environ. Sci. Technol.* **45**, 283 (2011).

6. S. K. Gogoi, Gopinath, P., Paul, A., Ramesh, A., Ghosh, S.S., and Chattopadhyay, A., Green flourescent protein-expressing Escherichia coli as a model system for investigating the antimicrobial activities of silver nanoparticles. *Langmuir* **22**, 9322 (2006).

7. M. Singh, Singh, S., Prasad, S., and Gambhir, I. S., Nanotechnology in medicine and antibacterial effect of silver nanoparticles. *Dig. J. Nanomater. Biostructures* **3**, 115 (2008).

8. I. Sondi, and Salopek-Sondi, B., Silver nanoparticles as antimicrobial agent: A case study on E. coli as a model for gram-negative bacteria. *J. Colloid Interface Sci.* **275**, 177 (2004).

9. M. Ugyun, Kahveci, M.U., Odaci, D., Tumur, S., and Yagci, Y., Antibacterial acrylamide hydrogels containing silver nanoparticles by simultaneous photoinduced free radical polymerization and electron transfer process. *Macromol. Chem. Phys.* **210**, 1867 (2009).

10. J. S. Kim, Kuk, E., Yu, K.N., Kim, J. H., Park, S. J., Lee, H.J., Kim, S. H., Park, Y. K., Park, Y. H., and Hwang, C.Y., Antibacterial effects of silvernanoparticles. *Nanomedicine* **3**, 95 (2007).

11. C. Lok, N., Ho, C.M., Chen, R., He, Q.Y., Yu, W.Y., Sun, H., Tam, P. K., Chiu, J. F. and Chen, C. M., Proteomic analysis of the mode of antibacterial action of silver nanoparticles. *J. Proteome. Res.* **5**, 916 (2006).

12. A. Travan, Pelillo, C., Donati., I., Marsich, E., Benincasa, M., Scarpa, T., Semeraro, S., Turco, G., Gennaro, R., and Paoletti, S., Noncytotoxic silver nanoparticles-polysaccharide nanocomposite with antimicrobial activity. *Biomacromolecules* **10**, 1429 (2009).

13. J. Kramer, Bell, R., Smith, S., and Gorsuch, J., Silver nanoparticle toxicity and biocides: Need for chemical speciation. *Integr. Environ. Asses. Manag.* **4**, 720 (2009).

14. Berger, M. (Jun 6, 2008). Problematic new findings regarding toxicity of silver nanoparticles. Nanowerk. [Online]. Available:http://www.nanowerk.com/spotlight/spotid=5966.php [Acess date: Mar 20, 2013].

15. A. Lankoff, Sandberg, W. J., Wegierek-Ciuk, A., Lisowska, H., Sartowska, B., Schwarze, P. E., Meczynska-Wielgosz, S., and Wojewodzka, M., The effect of agglomeration state of silver and titanium oxide nanoparticles on cellular response of of HepG2, A549 and THP-1 cells. *Toxicol. Lett.* **208**, 197 (2012).

16. N. Sanvicens, and Marco, M.P., Review: Multifunctional nanoparticles-properties and prospects for their use in human medicine. *Trends Biotechnol.* **8**, 425 (2008).

17. Y. Yang, Matsubara, S., Xiong, L., Hayakawa, T., and Nogami, M., Solvothermal synthesis of multiple shapes of silver nanoparticle and their SERS properties. *J. Phys. Chem.* **111**, 9095 (2007).

18. E. Q. Contreras, H. L. Puppala, G. Escalera, W. W. Zhong, V. L. Colvin, SIZE-DEPENDENT IMPACTS OF SILVER NANOPARTICLES ON THE LIFESPAN, FERTILITY, GROWTH, AND LOCOMOTION OF CAENORHABDITIS ELEGANS. *Environ. Toxicol. Chem.* **33**, 2716 (2014).

19. K. Kawata, Osawa, M., and Okabe, S., In Vitro toxicity of silver nanoparticles at noncytotoxic doses to HepG2 human hepatoma cells. *Environ. Sci. Technol.* **43**, 6046 (2009).

20. S. Kittler, Greulich, C., Diendorf, J., Koller, M., Epple, M, Toxicity of silver nanoparticles increases during storage because if slow dissolution under release of silver ions. *Chem. Mater.* **22**, 4548 (2010).

21. F. Seitz., Rosenfeldt, R. R., Storm, K., Metreveli, G., Schaumann, G. E., Schulz, R., Bundschuh, M. Effects of silver nanoparticle properties, media pH and dissolved organic matter on toxicity to Daphnia magna. *Ecotoxicology and environmental safety* **111**, 263 (2015).

22. X. Yujie, Brunson, M., Juyoung, H., Huang, A., Coster, A., Wendt, K., Fay, J., Dong, Q. The Role of Surface Chemistry on the Toxicity of Ag Nanoparticles. *Small* **9**, 2628 (2013).

23. P. Schlinkert, Casals, E., Boyles, M., Tischler, U., Hornig, E., Tran, N., Zhao, J. Y., Himly, M., Riediker, M., Oostingh, G. H., Puntes, V., Dischl, A. The oxidative potential of differently charged silver and gold nanoparticles on three human lung epithelial cell types. *J. Nanobiotechnol.* **13**, 1 (2015).

24. T. S. Peretyazhko, Q. B. Zhang, V. L. Colvin, Size-Controlled Dissolution of Silver Nanoparticles at Neutral and Acidic pH Conditions: Kinetics and Size Changes. *Environ. Sci. Technol.* **48**, 11954 (2014).

25. L. Garza-Ocanas, Ferrer, D. A., Burt, J., Diaz-Torres, L. A., M. R. Cabrera, Rodrı´guez, V. T., Rangel, R. L., Romanovicze, D., Jose-Yacaman, M., Biodistribution and long term fate of silver nanoparticles functionalized with bovine serum albumin in rats. *Metallomics* **2**, 204 (2010).

26. N. R. Panyala, Pena-Mendez, E. M., and Havel, J., Review: Silver or silver nanoparticles: A hazardous threat to the environment and human health? *J. Appl. Biomed.* **6**, 117 (2008).

27. H. Bouwmeester, Poortman, J., Peters, R., Wijima, E., Kramer., E., Makama, S., Puspitaninganindita, K., Marvin, H. J. P., Peingjnenburg, A. A. C. M and Hendriksen, J. M., Characterization of translocation of silver nanoparticles and effects on whole genome gene expression using in vitro intestinal epithelium coculture model *ACS nano* **5**, 4091 (2011).

28. C. Beer, Foldbjerg, R., Hayashi, Y., Sutherland, D. S., Autrup, H., Toxicity of silver nanoparticles - Nanoparticle or silver ion. *Toxicol. Lett.* **208**, 286 (2012).

29. C. Sengstock, J. Diendorf, M. Epple, T. A. Schildhauer, M. Koller, Effect of silver nanoparticles on human mesenchymal stem cell differentiation. *Beilstein J. Nanotechnol.* **5**, 2058 (2014).

30. H. Eom, and Choi., J., p38 MAPK activation, DNA damage, cell cycle arrest and apoptosis as mechanism of toxicity of silver nanoparticles in Jurkat T. cells. *Environ. Sci. Technol.* **44**, 8337 (2010).

31. American Conference of Governmental Industrial Hygienist: Documentation of the Threshold Limit Values (TLVs) and Biological Exposure Indices (BEIs)- Silver and Compounds (2001).

32. Occupational Safety & Health Administration (Sep 6, 2012). Silver, Metal and Soluble Compounds (as Ag). OSHA. [Online].Available: https://www.osha.gov/dts /chemicalsampling/data/CH_267300.html [Access Date: Mar 20, 2013].

33. K. K. Comfort, E. I. Maurer, S. M. Hussain, Slow release of ions from internalized silver nanoparticles modifies the epidermal growth factor signaling response. *Colloid Surf. B-Biointerfaces* **123**, 136 (2014).

34. M. S. Park, J. Park, S. K. Jeon, T. H. Yoon, The Effects of Sedimentation and Dissolution on the Cytotoxicity of Ag Nanoparticles. *J. Nanosci. Nanotechnol.* **13**, 7264 (2013).

35. P. Cronholm *et al.*, Intracellular Uptake and Toxicity of Ag and CuO Nanoparticles: A Comparison Between Nanoparticles and their Corresponding Metal Ions. *Small* **9**, 970 (2013).

36. B. Gajendran, A. Chinnasamy, P. Durai, J. Raman, M. Ramar, Biosynthesis and characterization of silver nanoparticles from Datura inoxia and its apoptotic effect on human breast cancer cell line MCF7. *Mater. Lett.* **122**, 98 (2014).

37. S. Gurunathan, J. Raman, N. A. Malek, P. A. John, S. Vikineswary, Green synthesis of silver nanoparticles using Ganoderma neo-japonicum Imazeki: a potential cytotoxic agent against breast cancer cells. *Int. J. Nanomed.* **8**, 4399 (2013).

38. S. Gurunathan, J. W. Han, V. Eppakayala, M. Jeyaraj, J. H. Kim, Cytotoxicity of Biologically Synthesized Silver Nanoparticles in MDA-MB-231 Human Breast Cancer Cells. *Biomed Res. Int.*, (2013).

39. E. Locatelli *et al.*, Targeted delivery of silver nanoparticles and alisertib: in vitro and in vivo synergistic effect against glioblastoma. *Nanomedicine* **9**, 839 (2014).

40. D. W. Guo *et al.*, The Cellular Uptake and Cytotoxic Effect of Silver Nanoparticles on Chronic Myeloid Leukemia Cells. *J. Biomed. Nanotechnol.* **10**, 669 (2014).

41. A. Jebali, S. Hekmatimoghaddam, B. Kazemi, The cytotoxicity of silver nanoparticles coated with different free fatty acids on the Balb/c macrophages: an in vitro study. *Drug Chem. Toxicol.* **37**, 433 (2014).

42. K. C. Nguyen *et al.*, Comparison of toxicity of uncoated and coated silver nanoparticles. *Nanosafe 2012: International Conferences on Safe Production and Use of Nanomaterials* **429**, (2013).

43. C. Levard, E. M. Hotze, G. V. Lowry, G. E. Brown, Environmental Transformations of Silver Nanoparticles: Impact on Stability and Toxicity. *Environmental Science & Technology* **46**, 6900 (2012).

44. E. Frohlich, The role of surface charge in cellular uptake and cytotoxicity of medical nanoparticles. *Int. J. Nanomed.* **7**, 5577 (2012).

45. J. H. Shannahan *et al.*, Formation of a protein corona on silver nanoparticles mediates cellular toxicity via scavenger receptors. *Toxicological sciences : an official journal of the Society of Toxicology* **143**, 136 (2015).

46. A. K. Suresh *et al.*, Cytotoxicity Induced by Engineered Silver Nanocrystallites Is Dependent on Surface Coatings and Cell Types. *Langmuir* **28**, 2727 (2012).
47. A. Huk *et al.*, Is the toxic potential of nanosilver dependent on its size? *Part. Fibre Toxicol.* **11**, (2014).

48. A. R. Gliga, S. Skoglund, I. O. Wallinder, B. Fadeel, H. L. Karlsson, Size-dependent cytotoxicity of silver nanoparticles in human lung cells: the role of cellular uptake, agglomeration and Ag release. *Part. Fibre Toxicol.* **11**, (2014).

49. R. Y. Prasad *et al.*, Investigating oxidative stress and inflammatory responses elicited by silver nanoparticles using high-throughput reporter genes in HepG2 cells: Effect of size, surface coating, and intracellular uptake. *Toxicol. Vitro* **27**, 2013 (2013).

50. R. Miethling-Graff *et al.*, Exposure to silver nanoparticles induces size- and dose-dependent oxidative stress and cytotoxicity in human colon carcinoma cells. *Toxicol. Vitro* **28**, 1280 (2014).

51. A. Ivask *et al.*, Size-Dependent Toxicity of Silver Nanoparticles to Bacteria, Yeast, Algae, Crustaceans and Mammalian Cells In Vitro. *PLoS One* **9**, (2014).

52. R. F. Hamilton, S. Buckingham, A. Holian, The Effect of Size on Ag Nanosphere Toxicity in Macrophage Cell Models and Lung Epithelial Cell Lines Is Dependent on Particle Dissolution. *Int. J. Mol. Sci.* **15**, 6815 (2014).

53. V. V. Kleandrova *et al.*, Computational ecotoxicology: Simultaneous prediction of ecotoxic effects of nanoparticles under different experimental conditions. *Environ. Int.* **73**, 288 (2014).

54. M. Busse *et al.*, Modeling the Effects of Nanoparticles on Neuronal Cells: From Ionic Channels to Network Dynamics. *2010 Annual International Conference of the Ieee Engineering in Medicine and Biology Society (Embc)*, 3816 (2010).

55. T. Silva *et al.*, Particle size, surface charge and concentration dependent ecotoxicity of three organo-coated silver nanoparticles: Comparison between general linear model-predicted and observed toxicity. *Sci. Total Environ.* **468**, 968 (2014).

56. M. Bokhari, R. J. Carnachan, N. R. Cameron, S. A. Przyborski, Culture of HepG2 liver cells on three dimensional polystyrene scaffolds enhances cell structure and function during toxicological challenge. *J. Anat.* **211**, 567 (2007).

57. Y. P. Buzulukov *et al.*, Bioaccumulation of silver and gold nanoparticles in organs and tissues of rats studied by neutron activation analysis. *Biol. Bull* **41**, 255 (2014).

58. Y. A. Suliman *et al.*, Evaluation of Cytotoxic, Oxidative stress, Proinflammatory and Genotoxic Effect of Silver Nanoparticles in Human Lung Epithelial Cells. *Environ. Toxicol.* **30**, 149 (2015).

59. U. Vattanasit *et al.*, Oxidative DNA damage and inflammatory responses in cultured human cells and in humans exposed to traffic-related particles. *International Journal of Hygiene and Environmental Health* **217**, 23 (2014).

60. T. Diemer, D. B. Hales, W. Weidner, Immune-endocrine interactions and Leydig cell function: the role of cytokines. *Andrologia* **35**, 55 (2003).

61. I. Bio-Rad Laboratories. (2015), vol. 2015.

62. M. R. Riss TL, Niles ALet al., in *Assay Guidance Manual [Internet]* C. N. Sittampalam GS, Nelson H, et al., Ed. (Eli Lilly & Company and the National Center for Advancing Translational Sciences, Bethesda (MD), 2013), vol. 2015.

63. M. Roesslein, C. Hirsch, J.-P. Kaiser, H. F. Krug, P. Wick, Comparability of in Vitro Tests for Bioactive Nanoparticles: A Common Assay to Detect Reactive Oxygen Species as an Example. *International Journal of Molecular Sciences* **14**, 24320 (2013).

64. A. J. Cohen, P. Mori-Sanchez, W. T. Yang, Challenges for Density Functional Theory. *Chemical Reviews* **112**, 289 (2012).

65. P. Hohenberg, W. Kohn, Inhomogeneous Electron Gas. *Phys. Rev. B* **136**, B864 (1964).

66. W. Kohn, L. J. Sham, Self Consistent Equations Including Exchange and Correlation Effects. *Phys. Rev. A* **140**, A1133 (1965).

67. J. A. Pople, Gill, P. M. W., Johnson, G. G., Kohn-Sham density functional theory within a finite basis set. *Chem. Phys. Lett.* **199**, 557 (1992).

68. J. P. Perdew, K. Schmidt, Jacob's Ladder of density functional approximations for the exchange-correlation energy. *AIP Conf. Proc* **577**, 1 (2001).

69. A. D. Becke, Density-functional thermochemistry. III. The role of exact exchange. *J. Chem. Phys.* **98**, 5648 (1993).

70. C. Lee, Yang, W., Parr, R. G., Development of the Colle-Salvetti correlation-energy formula into a functional of the electron density. *Phys. Rev. B* **37**, 785 (1988).

71. S. H. W. Vosko, L.; Nusair, M., Accurate spin-depdendent electron liquid correlation energies for local spin density calculations: a critical analysis. *Can. J. Phys.* **58**, 1200 (1980).

72. J. Heyd, G. E. Scuseria, Assessment and Validation of a screened Coulumb hybrid density functional. *J. Chem. Phys.* **120**, 7274 (2004).

73. J. Heyd, G. E. Scuseria, Efficient hybrid functional calculations in solids: assessment of the Heyd Scuseria Ernzerhof screened coulomb hybrid functional. *J. Chem. Phys.* **121**, 1187 (2004).

74. C. B. Adamo, V, Exchange functionals with improved long range behaviour and adiabatic connection methods without adustable parameters: The mPW and mPW1PW models. *J. Chem. Phys.* **108**, 664 (1998).

75. T. T. Yanai, D. P.; Handy, N. C., A new hybrid exchange-correlation functional using Coulomb attenuating method (CAM-B3LYP). *Chem. Phys. Lett.* **393**, 51 (2004).

76. C. Jeng-Da, M. Head-Gordon, Long-range corrected hybrid density functionals with damped atom-atom dispersion corrections. *Physical Chemistry Chemical Physics* **10**, 6615 (28, 2008).

77. A. D. Becke, Density-Functional Exchange-Energy Approximation with Correct Asymptotic Behavior. *Phys. Rev. A.* **38**, 3098 (1988).

78. N. Nath Ghosh, A. Chakraborty, S. Pal, A. Pramanik, P. Sarkar, Modulating triphenylamine-based organic dyes for their potential application in dye-sensitized solar cells: a first principle theoretical study. *Physical chemistry chemical physics : PCCP* **16**, 25280 (2014).

79. J. P. Perdew, Burke, K., Ernzerhof, M., Generalized Gradient Approximation Made Simple. *Phys. Rev. Lett.* **77**, 3865 (1996).

80. J. Tao, Perdew, J. P., Staroverov, V. N., Scuseria, G. E., , Climbing the Density Functional Ladder: Nonemperical Meta-Generalized Gradient Approximation Designed for Solecules and Solid. *Phys. Rev. Lett.* **91**, 146401 (2003).

81. F. A. Hamprecht, Cohen, A. J., Tozer, D. J., Handy, N. C., Development and assessment of new exchange-correlation functionals. *J. Chem. Phys.* **109**, 6264 (1998).

82. K. Raghavachari, Perspective on "Density Functional Thermochemistry. III. The Role of Exact Exchange" Becke A D (1993) J Chem Phys 98:5648-52. *Theor. Chem. Acc.* **103**, 361 (2000).

83. E. Torres, G. A. DiLabio, A (Nearly) Universally Applicable Method for Modeling Noncovalent Interactions Using B3LYP. *Journal of Physical Chemistry Letters* **3**, 1738 (2012).

84. Y. Zhao, D. G. Truhlar, Density functionals with broad applicability in chemistry. *Accounts Chem. Res.* **41**, 157 (2008).

85. V. N. Staroverov, G. E. Scuseria, J. M. Tao, J. P. Perdew, Comparative assessment of a new nonempirical density functional: Molecules and hydrogen-bonded complexes. *Journal of Chemical Physics* **119**, 12129 (2003).

86. T. J. Seiders, K. K. Baldridge, J. S. Siegel, R. Gleiter, Ionization of corannulene and 1,6-dimethylcorannulene: photoelectron spectra, electrochemistry, charge transfer bands and ab initio computations. *Tetrahedron Letters* **41**, 4519 (Jun 12, 2000).

87. K. Sheehy, A. Casey, A. Murphy, G. Chambers, Antimicrobial properties of nano-silver: A cautionary approach to ionic interference. *Journal of colloid and interface science* **443**, 56 (2015).

88. J. Heyd, J. E. Peralta, G. E. Scuseria, Energy band gaps and lattice parameters evaluated with HSE screnned hybrid functional. *J. Chem. Phys.* **123**, 174101 (2005).

89. S. F. Sousa, P. A. Fernandes, M. J. Ramos, General performance of density functionals. *Journal of Physical Chemistry A* **111**, 10439 (2007).

90. D. J. Tozer, Handy, N. C., Improving virtual Kohn-Sham orbitals and eigenvalues: application to excitation energies and static polarizabilities. *J. Chem. Phys.* **109**, 10180 (1998).

91. R. A. Bauernschmitt, R., , Treatment of electronic excitations within the adiabatic approximation of time dependent density functional theory. *Chem. Phys. Lett.* **256**, 454 (1996).

92. D. J. A. Tozer, R. D.; Handy, N.C.; Roos, B. O.; Serrano-Andres, L., Does Density Functional Theory Contribute to the Understanding of Excited States of Unsaturated Organic Compounds? *Mol. Phys.* **97**, 859 (1999).

93. A. W. Dreuw, J. L.; Head-Gordon, M., Long-Range Charge-Transfer Excited States in Time Dependent Density Functional Theory Require Non-local Exchange. *J. Chem. Phys.* **119**, 2943 (2003).

94. L. S. Bernasconi, M.; Hutter, J., Time Dependent Density Functional Theory Study of Charge-Transfer and Intramolecular Electronic Excitations in Acetone-Water Systems. *J. Chem. Phys.* **119**, 12417 (2003).

95. L. Wang, P. C. Ubaldo, in *Functional Nanometer-Sized Clusters of Transition Metals: Synthesis, Properties and Applications,* W. Chen, S. Chen, Eds. (Royal Society of Chemistry, Cambridge, U. K. , 2014), pp. 323-351.

96. P. T. Kissinger, Cyclic Voltammetry. *J. Chem Ed.* **60**, 702 (1983).

97. F. N. Marken, A.; Bond, A. M., in *Electroanalytical Methods, 2nd Ed* F. Scholz, Ed. (Springer-Verlag Berlin Heidelberg, New York, 2010).

98. K. Lim, S. Y. Lee, K. Song, G. D. Sharma, J. Ko, Synthesis and properties of low bandgap star molecules TPA- DTS-PyBTTh3 (3) and DMM-TPA DTS-PyBTTh3 (3) for solution-processed bulk heterojunction organic solar cells. *Journal of Materials Chemistry C* **2**, 8412 (2014).

99. M. M. Ahmida, S. H. Eichhorn, *Measurements and Prediction of Electronic Properties of Discotic Triphenylenes and Phtalocyanines* M. J. Deen, H. Klauk, Eds., Organic Semiconductor Materials, Devices, and Processing 2 (The Electrochemical Society New Jersey, USA, 2010), vol. 25.

100. U. Platt, J. Stutz, *Differential Optical Absorption Spectroscopy*. Principles and Applications (Springer, Heidelberg, Germany, 2008), pp. 597.

101. N. Q. Su, W. T. Yang, P. Mori-Sanchez, X. Xu, Fractional Charge Behavior and Band Gap Predictions with the XYG3 Type of Doubly Hybrid Density Functionals. *J. Phys. Chem. A* **118**, 9201 (2014).

102. Z. Gang, C. B. Musgrave, Comparison of DFT methods for molecular orbital eigenvalue calculations. *J. Phys. Chem. A* **111**, 1554 (2007).

103. F. Rabilloud, Assessment of the Performance of Long-Range-Corrected Density Functionals for Calculating the Absorption Spectra of Silver Clusters. *J. Phys. Chem. A* **117**, 4267 (2013).

104. M. J. G. Peach, P. Benfield, T. Helgaker, D. J. Tozer, Excitation energies in DFT: An evaluation and diagnostic test. *J. Chem. Phys.* **128**, (2008).

105. P. Dev, S. Agrawal, N. J. English, Determining the appropriate exchange-correlation functional for time-dependent density functional theory studies of charge-transfer excitations in organic dyes. *J. Chem. Phys.* **136**, 224301 (2012).

106. L. L. Walkup *et al.*, Importance of Dynamics in Electron Excitation and Transfer of Organic Dyes. *J. Phys. Chem.C* **114**, 19521 (2010).

107. A. T. B. Fitri, A.; Benzakour, M.; Mcharfi, M.; Sfaira, M.; Hamidi, M.; Bouachrine, M., New Materials based on thiazolothiazole and thiophene candidates for

optoelectronic device applications: theoretical investigations. *Res. Chem. Intermed.* **39**, 2679 (2013).

108. A. T. B. Fitri, A.; Benzakour, M.; Mcharfi, M.; Sfaira, M.; Hamidi, M.; Bouachrine, M., Theoretical Investigation of New Thiazolothiazole-based D-pi-A organic Dyes for efficient DSSC. *Spectrochimica Acta Part A: Mol. Biomol. Spectrosc.* **124**, 646 (2014).

109. A. P. V. S. Kumar, MD., Hydroxy rarical (OH) reaction with guanine in an aqueous environment: A DFT Study. *J. Phys. Chem. B* **115**, 15129 (2011).

110. J. H. Cho, Kulkarni, A., Kim, H., Yoon, J. U., Sung, J. H., Yu, I.J., and Kim, T. , Numerical study on spatial distribution of silver nanoparticles inside whole-body type inhilation toxicity chamber. *J. Mech. Sci. Tech.* **24**, 2215 (2010).

111. S. Wilkening, F. Stahl, A. Bader, Comparison of primary human hepatocytes and hepatoma cell line HEPG2 with regard to their biotransformation properties. *Drug Metab. Dispos.* **31**, 1035 (2003).

112. J. Zhang, J. Wu, H. Li, Q. Chen, J.-M. Lin, An in vitro liver model on microfluidic device for analysis of capecitabine metabolite using mass spectrometer as detector. *Biosensors & bioelectronics* **68**, 322 (2015).

113. A. Nowrouzi, Meghrazi, K., Golmohammadi, T., Golestani, A., Ahmadian, S., Shafiezadeh, M., Shajary, Z., Khaghani, S., and Amiri, A. N., Cytotoxicity of Subtoxic AgNP in Human Hepatoma Cell Line (HepG2) after Long-Term Exposure. *Iranian Biomedical Journal* **14**, 23 (2010).

114. J. Lin, Lin, W., Dong, R., and Hsu, S., The cellular responses and antibacterial activities of silver nanoparticles stabilized by different polymers. *Nanotechnology* **23**, 1 (2012).

115. L. Xin, J. Wang, Y. Wu, S. Guo, J. Tong, Increased oxidative stress and activated heat shock proteins in human cell lines by silver nanoparticles. *Hum. Exp. Toxicol.* **34**, 315 (2015).

116. C. L. Huang *et al.*, Silver nanoparticles affect on gene expression of inflammatory and neurodegenerative responses in mouse brain neural cells. *Environ. Res.* **136**, 253 (2015).

117. S. Junpeng *et al.*, Endothelial cell injury and dysfunction induced by silver nanoparticles through oxidative stress via IKK/NF-kappaB pathways. *Biomaterials* **35**, 6657 (2014).

118. M. Ahmed, Posgai, R., Gorey, T., J., Nielsen, M., Hussain, S. M., and Rowe, J.J., Silver nanoparticles induced heat shock protein 70, oxidative stress and apoptosis in Drosophilia Melanogaster. *Tox. App. Pharma.* **242**, 263 (2009).

119. S. Leekumjorn, Wu, Y., Sum, A. K., and Chan, C., Experimental and computational studies investigating trehalose protection of HepG2 cells from palmitate-induced toxicity. *Biophys. J.* **94**, 2869 (2008).

120. Y. She, Narindrasorasak, S., Yang, S., Spitale, N., Roberts, E. A., and Sarkar, B., Identification of Metal-binding Proteins in Human Hepatoma Cell Lines by Immobilized Metal Affinity Chromatography and Mass Spectrometry. *Molecular & Cellular Proteomics* **2.12**, 1306 (2003).

121. T. M. McIntyre, S. L. Hazen, Lipid Oxidation and Cardiovascular Disease: Introduction to a Review Series. *Circ.Res.* **107**, 1167 (Nov, 2010).

122. W. A. Schulz, P. Eickelmann, H. Sies, *Free radicals in toxicology: Redox cycling and NAD(P)H:quinone oxidoreductase*. J. P. Seiler, O. Kroftova, V. Eybl, Eds., Toxicology - from Cells to Man (Springer-Verlag Berlin, Berlin 33, 1996), vol. 18, pp. 217-222.

123. M. Valko, H. Horris, M. T. D. Cronin, Metals, Toxicity and Oxidative Stress. *Current Medicinal Chemistry* **12**, 1161 (2005).

124. J. D. J. Wood, J. L.; Finke, A.D.; Wang, L.; Plunkett, K.N., Electron Acceptors Based on Functionalizable Cyclopenta[hi]aceanthrylenes and Dicyclopenta[de,mn]tetracenes. *J. Am. Chem. Soc.* **134**, 15783 (2010).

125. D. T. Chase *et al.*, Electron-Accepting 6,12-Diethynylindeno[1,2-b]fluorenes: Synthesis, Crystal Structures, and Photophysical Properties. *Angewandte Chemie-International Edition* **50**, 11103 (2011).

126. C. Koper, M. Sarobe, L. W. Jenneskens, Redox properties of non-alternant cyclopenta-fused polycyclic aromatic hydrocarbons: The effect of peripheral pentagon annelation. *Physical Chemistry Chemical Physics* **6**, 319 (2004).

127. M. F. Bourass, A.; Benjelloun, A. T.; Benzakour, M.; Mcharfi, M.; Hamidi, M.; Serein-Spirau, F.; Jarrosson, T.; Lere-Porte, J. P.; Sotiropoulos, J. M.; Bouacharine, M., DFT and TDDFT investigations of new thienpyrazine-based dyes for solar cells: Effects of electron donor groups. *Der Pharma Chemica* **5**, 144 (2013).

128. A. H.-G. Dreuw, M., Single-Reference ab Initio Methods for the Calculation of Excited States of Large Molecules. *Chem. Rev.* **105**, 4009 (2005).

129. M. J. G. L. S. Peach, C. R.; Ruud, K.; Guillaume, M. ;Tozer, D. J., TDDFT diagnostic testing and functional assessment for triazene chromophores. *J. Chem. Chem. Phys.* **2009**, 4465 (2009).

130. A. L. Lafleur *et al.*, Identification of C20H10 dicyclopentapyrenes in flames: Correlation with corannulene and fullerene formation. *J. Phys. Chem.* **100**, 17421 (1996).

131. T. J. Seiders, E. L. Elliott, G. H. Grube, J. S. Siegel, Synthesis of corannulene and alkyl derivatives of corannulene. *J. Am. Chem. Soc.* **121**, 7804 (1999).

132. T. Y. Wang *et al.*, Ambipolar organic semiconductors with cascades of energy levels for generating long-lived charge separated states: a donor-acceptor1-acceptor2 architectural triarylamine dye. *Journal of Materials Chemistry C* **2**, 5466 (2014).

133. T. Y. Wang *et al.*, Tuning electron-hole distance of the excitons in organic molecules using functional groups. *Chemical Physics Letters* **618**, 142 (2015).

APPENDICES

APPENDIX A

ABBREVIATIONS

a.u.	Atomic Unit
A549	Human lung carcinoma epithelial cells
ADF	Amsterdam Density Functional Software
ADP	Adenosine Diphosphate
Ag^+	Silver ion
Ag^0	Silver atom
$AgNO_3$	Silver nitrate
AgNPs	Silver Nanoparticles
ATCC	American Type Culture Collection
ATP	Adenosine Triphosphate
ATPase	Adenosine Triphosphate enzymes
B3LYP	Becke's three parameter exchange functional and Lee-Yang Parr correlation functional
B3PW91	Becke's three parameter exchange functional and Perdew- Wang 1991 correlation functional
BCA	Bicinchoninic acid
BEAS-2B	Human lung carcinoma cell line infected with adenovirus 12-SV4
BH&HLYP	Becke's Half & Half exchange functional and Lee-Yang Parr correlation functional
BPV86	Becke's 1988 exchange functional with Perdew's
CAMB3LYP	Coulomb Attenuating Method Becke's three parameter exchange

	functional and Lee-Yang-Parr correlation functional
cc-PVQZ	Correlation Consistent Polarized Valence only Quadrupole Zeta
CML	Chronic Myeloid Leukemia cells
CPCM	Conductor-Like Polarizable Continuum Model
CP-PAHs	Cyclopenta fused Polycyclic Aromatic Hydrocarbons
CSGT	Continuous Set of Gauge Transformation
CTA	Center for Technology Assessment
DCF	2',7'-dichlorofluorescein
DDT	1-dodecanethiol
DFT	Density Functional Theory
DNA	Deoxyribonucleic Acid
EA	Electron Affinity
EGF	Epidermal Growth Factor
EMBed	Embedding Resin for Transmission Electron Microscopy
EPA	Environmental Protection Agency
eV	Electron Volts
E_{xc}	Exchange and correlation energy
FDR	False Discovery Rate
FTIR	Fourier Transform Infrared Spectroscopy
FWHM	Full Width at Half Maximum
GGA	Generalized Gradient Approximation
GIAO	Gauge Independent Atomic Orbital
GLM	General Linear Model

H_2DCF-DA	2',7'-dichlorodihydrofluorescein diacetate
H_2O_2	Hydrogen Peroxide
HBSS	Hank's Balanced Salt Solution
HCTH	Hamprecht-Cohen-Tozer and Handy functional
HEPES	4-(2-hydroxyethyl)-1-piperazineethanesulfonic acid
HepG2	Hepatocellular carcinoma cells
HOMO	Highest Occupied Molecular Orbital
HPLC	High Performance Liquid Chromatography
HSE06	Heyd- Scuseria-Ernzerhof functional
HSEH1PBE	Heyd- Scuseria-Ernzerhof exchange functional and Perdew- Burke-Ernzerhof correlation functional
HSP70	Heat Shock Protein 70 kDa
HT29	Colorectal adenocarcinoma cells
HUVECs	Human Umbilical Vein Endothelial Cells
HVA	Homovanillic Acid
IKK/NF-kappaB	IkappaB kinase/NF-kappaB signaling pathway
IL-6 mRNA	Interleukin 6 Messenger Ribonucleic Acid
IP	Ionization Potential
IUPAC	International Union of Pure and Applied Chemistry
J774A.1	Macrophage cell line derived from tumor in female BALC/c mouse
KMLYP	Kang-Musgrave exchange functional and Lee-Yang-Parr correlation functional

LANL2DZ	Los Alamos National Laboratory effective core potentials combined with valence basis set with Double Zeta quality
LC	Liquid Chromatography
LC/MS/MS	Liquid Chromatograph / Mass Spectroscopy / Mass Spectroscopy
LD50	Lethal Dosage 50
LoVo	Duke's Type C, grade IV colorectal adenocarcinoma cells
LSDA	Local Spin Density Approximation
LTQ	Linear Ion Trap with Quadrupole mass filter instrument for MS
LUMO	Lowest Unoccupied Molecular Orbital
LYP	Lee-Yang-Parr correlation functional
M.W.	Molecular Weight
M06L	Minnesota 06 Local functional
MAD	Mean Absolute Deviation
MAE	Mean Absolute Error
meta-GGA	Meta Generalized Gradient Approximation
MO	Molecular Orbital
MPW1PW91	Adamo and Barone modified Perdew-Wang 1991 exchange functional with the Perdew and Wang's 1991 correlation functional
mRNA	Messenger Ribonucleic Acid
MS	Mass Spectroscopy
MTPA	Methyltriphenylamine
MTPAa	Methyltriphenylamine with -R=NH_2 (amine group)
MTPAc	Methyltriphenylamine with -R=CN (cyanine group)

MTPAcc	Methyltriphenylamine with -R=$C_2H_4CNCOOH$ (cyanine and carboxylic acid group)
MTPAcl	Methyltriphenylamine with -R=Cl (cyanine)
MTPAn	Methyltriphenylamine with -R=NO_2 (nitro group)
MTPAo	Methyltriphenylamine with -R=OCH_3 (methoxy group)
MTS	3-(4,5-dimethylthiazol-2-yl)-5-(3-carboxymethoxyphenyl)-2-(4-sulfophenyl)-2H-tetrazolium
MTT	3-(4,5-dimethylthiazol-2-yl)-2,5-diphenyltetrazolium bromide
nm	Nanometer
NMR	Nuclear Magnetic Resonance
OAMOs	Optically Active Molecular Orbitals
OSHA	Occupational Safety & Health Administration
PBE	Perdew- Burke-Ernzerhof exchange and correlation functional
PBS	Phosphate Buffer Saline
PC	Phosphocholine
PC-Ag^+	Phosphocholine and silver ion model
PC-Ag^0	Phosphocholine and silver atom model
PCM	Polarized Continuum Model
PE	Phosphoethanolamine
PE-Ag^+	Phosphoethanolamine and silver ion model
PE-Ag^0	Phosphoethanolamine and silver atom model
PKZB	Perdew-Kurth-Zupan-Blaha functional
POPC	1-palmitoyl-2-oleoyl-sn-glycero-3-phosphocholine

POPE	1-palmitoyl-2-oleoyl-sn-glycero-3-phosphoethanolamine
PVP	Polyvinylpyrrolidone
QSAR	Quantitative Structure Activity Relationship
QSPR	Quantitative Structure Property Relationship
QSTR	Quantitative Structure Toxicity Relationship
RAW-264.7	Mouse macrophage cell line
RNA	Ribonucleic Acid
ROS	Reactive Oxygen Species
SCF	Self Consistent Field
SDS-PAGE	Sodium Dodecyl Sulfate – Polyacrylamide Gel Electrophoresis
SMA	Poly(styrene-co-maleic anhydride)-grafting poly(oxylkyalkylene)
TD-B3LYP	Time Dependent DFT using B3LYP functional
TD-CAMB3LYP	Time Dependent DFT using CAMB3LYP functional
TD-DFT	Time Dependent Density Functional Theory
TD-HCTH	Time Dependent DFT using HCTH functional
TD-HSEH1PBE	Time Dependent DFT using HSEH1PBE functional
TD-PBE	Time Dependent-DFT using PBE functional
TD-TPSS	Time Dependent-DFT using TPSS functional
TEM	Transmission Electron Microscope
THF	Tetrahydrofuran
TMS	Tetramethylsilane
TPSS	Tao-Perdew-Staroverov- Scuseria functional
U87MG	Human glioblastoma-astrocytoma epithelial like cell line

V79-4 Chinese hamster fibroblast cells

VASP Vienna Ab-initio Simulation Package

ωB97XD Head-Gordon functional with modified Becke's 97 exchange functional with atom-atom damp dispersion

WST-1 Water Soluble Tetrazolium Salt -1

XTT 2,3-bis-(2-methoxy-4-nitro-5-sulfophenyl)-2H-tetrazolium-5-carboxanilide

XY3G Xu-Yin-Goddard with 3 mixing parameters functional

APPENDIX B

PROTEINS AFFECTED UPON EXPOSURE TO 5ppm 10 nm AgNPs

Identified Proteins (1218)	Accession Number	Molecular Weight	12781 SpC	12782 SpC
Fatty acid synthase OS=Homo sapiens GN=FASN PE=1 SV=3	sp|P49327|FAS_HUMAN	273 kDa	154	67
60 kDa heat shock protein, mitochondrial OS=Homo sapiens GN=HSPD1 PE=1 SV=2	sp|P10809|CH60_HUMAN	61 kDa	140	229
Endoplasmin OS=Homo sapiens GN=HSP90B1 PE=1 SV=1	sp|P14625|ENPL_HUMAN	92 kDa	117	115
Actin, cytoplasmic 2 OS=Homo sapiens GN=ACTG1 PE=1 SV=1	sp|P63261|ACTG_HUMAN	42 kDa	110	92
78 kDa glucose-regulated protein OS=Homo sapiens GN=HSPA5 PE=1 SV=2	sp|P11021|GRP78_HUMAN	72 kDa	99	120
Glyceraldehyde-3-phosphate dehydrogenase OS=Homo sapiens GN=GAPDH PE=1 SV=3	sp|P04406|G3P_HUMAN	36 kDa	91	62
Heat shock protein HSP 90-beta OS=Homo sapiens GN=HSP90AB1 PE=1 SV=4	sp|P08238|HS90B_HUMAN	83 kDa	90	98
Elongation factor 2 OS=Homo sapiens GN=EEF2 PE=1 SV=4	sp|P13639|EF2_HUMAN	95 kDa	86	46
Alpha-enolase OS=Homo sapiens GN=ENO1 PE=1 SV=2	sp|P06733|ENOA_HUMAN	47 kDa	85	95
Tubulin beta chain OS=Homo sapiens GN=TUBB PE=1 SV=2	sp|P07437|TBB5_HUMAN	50 kDa	77	53
Pyruvate kinase isozymes M1/M2 OS=Homo sapiens GN=PKM2 PE=1 SV=4	sp|P14618|KPYM_HUMAN	58 kDa	77	45
Tubulin beta-2C chain OS=Homo sapiens GN=TUBB2C PE=1 SV=1	sp|P68371|TBB2C_HUMAN	50 kDa	73	50
(Bos taurus) similar to alpha-tubulin I isoform 1	IPI:CON_00700865.3|ENSEMBL:ENSBTAP00000016242 (+1)	50 kDa	71	39
L-lactate dehydrogenase A chain OS=Homo sapiens GN=LDHA PE=1 SV=2	sp|P00338|LDHA_HUMAN	37 kDa	71	48
Clathrin heavy chain 1 OS=Homo sapiens GN=CLTC PE=1 SV=5	sp|Q00610|CLH1_HUMAN	192 kDa	68	41
Elongation factor 1-alpha 1 OS=Homo sapiens GN=EEF1A1 PE=1 SV=1	sp|P68104|EF1A1_HUMAN	50 kDa	67	76
Leucine-rich PPR motif-containing protein, mitochondrial OS=Homo sapiens GN=LRPPRC PE=1 SV=3	sp|P42704|LPPRC_HUMAN	158 kDa	66	87
Heterogeneous nuclear ribonucleoprotein U OS=Homo sapiens GN=HNRNPU PE=1 SV=6	sp|Q00839|HNRPU_HUMAN	91 kDa	64	28
Aldo-keto reductase family 1 member C1 OS=Homo sapiens GN=AKR1C1 PE=1 SV=1	sp|Q04828|AK1C1_HUMAN	37 kDa	63	39
Heat shock protein HSP 90-alpha OS=Homo sapiens GN=HSP90AA1 PE=1 SV=5	sp|P07900|HS90A_HUMAN	85 kDa	62	79
Nucleolin OS=Homo sapiens GN=NCL PE=1 SV=3	sp|P19338|NUCL_HUMAN	77 kDa	62	32
Protein disulfide-isomerase OS=Homo sapiens GN=P4HB PE=1 SV=3	sp|P07237|PDIA1_HUMAN	57 kDa	60	68
Tubulin alpha-1C chain OS=Homo sapiens GN=TUBA1C PE=1 SV=1	sp|Q9BQE3|TBA1C_HUMAN	50 kDa	60	39
Tubulin beta-2A chain OS=Homo sapiens GN=TUBB2A PE=1 SV=1	sp|Q13885|TBB2A_HUMAN	50 kDa	59	0
Protein disulfide-isomerase A3 OS=Homo sapiens GN=PDIA3 PE=1 SV=4	sp|P30101|PDIA3_HUMAN	57 kDa	57	63
Fructose-bisphosphate aldolase A OS=Homo sapiens GN=ALDOA PE=1 SV=2	sp|P04075|ALDOA_HUMAN	39 kDa	51	48
ATP synthase subunit beta, mitochondrial OS=Homo sapiens GN=ATP5B PE=1 SV=3	sp|P06576|ATPB_HUMAN	57 kDa	49	65

Ribosome-binding protein 1 OS=Homo sapiens GN=RRBP1 PE=1 SV=4	sp|Q9P2E9|RRBP1_HUMAN	152 kDa	46	41
Histone H4 OS=Homo sapiens GN=HIST1H4A PE=1 SV=2	sp|P62805|H4_HUMAN	11 kDa	45	26
Histone H3.1 OS=Homo sapiens GN=HIST1H3A PE=1 SV=2	sp|P68431|H31_HUMAN	15 kDa	45	11
Protein disulfide-isomerase A4 OS=Homo sapiens GN=PDIA4 PE=1 SV=2	sp|P13667|PDIA4_HUMAN	73 kDa	44	57
DNA-dependent protein kinase catalytic subunit OS=Homo sapiens GN=PRKDC PE=1 SV=3	sp|P78527|PRKDC_HUMAN	469 kDa	43	15
60S ribosomal protein L3 OS=Homo sapiens GN=RPL3 PE=1 SV=2	sp|P39023|RL3_HUMAN	46 kDa	42	9
Histone H2B type 1-D OS=Homo sapiens GN=HIST1H2BD PE=1 SV=2	sp|P58876|H2B1D_HUMAN (+5)	14 kDa	41	21
Spectrin beta chain, brain 1 OS=Homo sapiens GN=SPTBN1 PE=1 SV=2	sp|Q01082|SPTB2_HUMAN	275 kDa	41	7
UDP-glucose 6-dehydrogenase OS=Homo sapiens GN=UGDH PE=1 SV=1	sp|O60701|UGDH_HUMAN	55 kDa	40	31
ATP-dependent RNA helicase A OS=Homo sapiens GN=DHX9 PE=1 SV=4	sp|Q08211|DHX9_HUMAN	141 kDa	40	11
Tubulin beta-3 chain OS=Homo sapiens GN=TUBB3 PE=1 SV=2	sp|Q13509|TBB3_HUMAN	50 kDa	40	32
Histone H2B type 1-O OS=Homo sapiens GN=HIST1H2BO PE=1 SV=3	sp|P23527|H2B1O_HUMAN (+2)	14 kDa	39	0
Transitional endoplasmic reticulum ATPase OS=Homo sapiens GN=VCP PE=1 SV=4	sp|P55072|TERA_HUMAN	89 kDa	39	27
Alpha-actinin-4 OS=Homo sapiens GN=ACTN4 PE=1 SV=2	sp|O43707|ACTN4_HUMAN	105 kDa	38	42
ATP synthase subunit alpha, mitochondrial OS=Homo sapiens GN=ATP5A1 PE=1 SV=1	sp|P25705|ATPA_HUMAN	60 kDa	36	40
Heterogeneous nuclear ribonucleoprotein A3 OS=Homo sapiens GN=HNRNPA3 PE=1 SV=2	sp|P51991|ROA3_HUMAN	40 kDa	36	27
Dehydrogenase/reductase SDR family member 2 OS=Homo sapiens GN=DHRS2 PE=1 SV=3	sp|Q13268|DHRS2_HUMAN	27 kDa	36	35
Glutamate dehydrogenase 1, mitochondrial OS=Homo sapiens GN=GLUD1 PE=1 SV=2	sp|P00367|DHE3_HUMAN	61 kDa	35	35
Calreticulin OS=Homo sapiens GN=CALR PE=1 SV=1	sp|P27797|CALR_HUMAN	48 kDa	35	39
60S ribosomal protein L4 OS=Homo sapiens GN=RPL4 PE=1 SV=5	sp|P36578|RL4_HUMAN	48 kDa	35	18
Aldo-keto reductase family 1 member C2 OS=Homo sapiens GN=AKR1C2 PE=1 SV=3	sp|P52895|AK1C2_HUMAN	37 kDa	35	29
Delta-1-pyrroline-5-carboxylate synthase OS=Homo sapiens GN=ALDH18A1 PE=1 SV=2	sp|P54886|P5CS_HUMAN	87 kDa	35	38
Heterogeneous nuclear ribonucleoproteins A2/B1 OS=Homo sapiens GN=HNRNPA2B1 PE=1 SV=2	sp|P22626|ROA2_HUMAN	37 kDa	34	30
Insulin-like growth factor 2 mRNA-binding protein 1 OS=Homo sapiens GN=IGF2BP1 PE=1 SV=2	sp|Q9NZI8|IF2B1_HUMAN	63 kDa	34	19
Phosphoglycerate kinase 1 OS=Homo sapiens GN=PGK1 PE=1 SV=3	sp|P00558|PGK1_HUMAN	45 kDa	33	36
Trifunctional enzyme subunit alpha, mitochondrial OS=Homo sapiens GN=HADHA PE=1 SV=2	sp|P40939|ECHA_HUMAN	83 kDa	33	37
Heterogeneous nuclear ribonucleoprotein M OS=Homo sapiens GN=HNRNPM PE=1 SV=3	sp|P52272|HNRPM_HUMAN	78 kDa	33	8
Elongation factor Tu, mitochondrial OS=Homo sapiens GN=TUFM PE=1 SV=2	sp|P49411|EFTU_HUMAN	50 kDa	32	27
Coatomer subunit alpha OS=Homo sapiens GN=COPA PE=1 SV=2	sp|P53621|COPA_HUMAN	138 kDa	32	10
Heterogeneous nuclear ribonucleoprotein L OS=Homo sapiens GN=HNRNPL PE=1 SV=2	sp|P14866|HNRPL_HUMAN	64 kDa	31	19
60S ribosomal protein L6 OS=Homo sapiens	sp|Q02878|RL6_HUMAN	33 kDa	31	11

GN=RPL6 PE=1 SV=3				
Long-chain-fatty-acid--CoA ligase 3 OS=Homo sapiens GN=ACSL3 PE=1 SV=3	sp|O95573|ACSL3_HUMAN	80 kDa	30	20
Heat shock cognate 71 kDa protein OS=Homo sapiens GN=HSPA8 PE=1 SV=1	sp|P11142|HSP7C_HUMAN	71 kDa	30	41
Spectrin alpha chain, brain OS=Homo sapiens GN=SPTAN1 PE=1 SV=3	sp|Q13813|SPTA2_HUMAN	285 kDa	30	9
Keratin, type I cytoskeletal 18 OS=Homo sapiens GN=KRT18 PE=1 SV=2	sp|P05783|K1C18_HUMAN	48 kDa	29	31
60S ribosomal protein L7 OS=Homo sapiens GN=RPL7 PE=1 SV=1	sp|P18124|RL7_HUMAN	29 kDa	29	12
Protein disulfide-isomerase A6 OS=Homo sapiens GN=PDIA6 PE=1 SV=1	sp|Q15084|PDIA6_HUMAN	48 kDa	29	29
Phosphoenolpyruvate carboxykinase [GTP], mitochondrial OS=Homo sapiens GN=PCK2 PE=1 SV=3	sp|Q16822|PCKGM_HUMAN	71 kDa	29	27
Tax_Id=9606 Gene_Symbol=KRT8 Keratin, type II cytoskeletal 8	IPI:CON_IPI00554648.3|SWISS-PROT:P05787 (+1)	54 kDa	28	34
Dolichyl-diphosphooligosaccharide--protein glycosyltransferase subunit 1 OS=Homo sapiens GN=RPN1 PE=1 SV=1	sp|P04843|RPN1_HUMAN	69 kDa	28	32
Heat shock 70 kDa protein 1A/1B OS=Homo sapiens GN=HSPA1A PE=1 SV=5	sp|P08107|HSP71_HUMAN	70 kDa	28	51
X-ray repair cross-complementing protein 5 OS=Homo sapiens GN=XRCC5 PE=1 SV=3	sp|P13010|XRCC5_HUMAN	83 kDa	28	31
Neutral alpha-glucosidase AB OS=Homo sapiens GN=GANAB PE=1 SV=3	sp|Q14697|GANAB_HUMAN	107 kDa	28	32
Serotransferrin OS=Homo sapiens GN=TF PE=1 SV=3	sp|P02787|TRFE_HUMAN	77 kDa	27	37
Heterogeneous nuclear ribonucleoprotein A1 OS=Homo sapiens GN=HNRNPA1 PE=1 SV=5	sp|P09651|ROA1_HUMAN (+1)	39 kDa	27	31
Filamin-A OS=Homo sapiens GN=FLNA PE=1 SV=4	sp|P21333|FLNA_HUMAN	281 kDa	27	12
Myosin-10 OS=Homo sapiens GN=MYH10 PE=1 SV=3	sp|P35580|MYH10_HUMAN	229 kDa	27	0
Matrin-3 OS=Homo sapiens GN=MATR3 PE=1 SV=2	sp|P43243|MATR3_HUMAN	95 kDa	27	5
T-complex protein 1 subunit gamma OS=Homo sapiens GN=CCT3 PE=1 SV=4	sp|P49368|TCPG_HUMAN	61 kDa	27	21
Peroxiredoxin-1 OS=Homo sapiens GN=PRDX1 PE=1 SV=1	sp|Q06830|PRDX1_HUMAN	22 kDa	27	24
Isocitrate dehydrogenase [NADP] cytoplasmic OS=Homo sapiens GN=IDH1 PE=1 SV=2	sp|O75874|IDHC_HUMAN	47 kDa	26	26
Transketolase OS=Homo sapiens GN=TKT PE=1 SV=3	sp|P29401|TKT_HUMAN	68 kDa	26	29
Heterogeneous nuclear ribonucleoprotein H OS=Homo sapiens GN=HNRNPH1 PE=1 SV=4	sp|P31943|HNRH1_HUMAN	49 kDa	26	17
Stress-70 protein, mitochondrial OS=Homo sapiens GN=HSPA9 PE=1 SV=2	sp|P38646|GRP75_HUMAN	74 kDa	26	37
Trifunctional enzyme subunit beta, mitochondrial OS=Homo sapiens GN=HADHB PE=1 SV=3	sp|P55084|ECHB_HUMAN	51 kDa	26	25
T-complex protein 1 subunit epsilon OS=Homo sapiens GN=CCT5 PE=1 SV=1	sp|P48643|TCPE_HUMAN	60 kDa	25	16
Heterogeneous nuclear ribonucleoprotein K OS=Homo sapiens GN=HNRNPK PE=1 SV=1	sp|P61978|HNRPK_HUMAN	51 kDa	25	18
60S ribosomal protein L7a OS=Homo sapiens GN=RPL7A PE=1 SV=2	sp|P62424|RL7A_HUMAN	30 kDa	25	12
40S ribosomal protein S4, X isoform OS=Homo sapiens GN=RPS4X PE=1 SV=2	sp|P62701|RS4X_HUMAN	30 kDa	25	12
40S ribosomal protein S6 OS=Homo sapiens GN=RPS6 PE=1 SV=1	sp|P62753|RS6_HUMAN	29 kDa	25	7
Guanine nucleotide-binding protein subunit beta-2-like 1 OS=Homo sapiens GN=GNB2L1	sp|P63244|GBLP_HUMAN	35 kDa	25	17

PE=1 SV=3				
Glucosamine--fructose-6-phosphate aminotransferase [isomerizing] 1 OS=Homo sapiens GN=GFPT1 PE=1 SV=3	sp|Q06210|GFPT1_HUMAN	79 kDa	25	15
ATP-dependent RNA helicase DDX3X OS=Homo sapiens GN=DDX3X PE=1 SV=3	sp|O00571|DDX3X_HUMAN	73 kDa	24	6
Filamin-B OS=Homo sapiens GN=FLNB PE=1 SV=2	sp|O75369|FLNB_HUMAN	278 kDa	24	10
Histone H2A type 1-B/E OS=Homo sapiens GN=HIST1H2AB PE=1 SV=2	sp|P04908|H2A1B_HUMAN (+1)	14 kDa	24	15
ADP/ATP translocase 2 OS=Homo sapiens GN=SLC25A5 PE=1 SV=7	sp|P05141|ADT2_HUMAN	33 kDa	24	21
Calnexin OS=Homo sapiens GN=CANX PE=1 SV=2	sp|P27824|CALX_HUMAN	68 kDa	24	30
60S ribosomal protein L5 OS=Homo sapiens GN=RPL5 PE=1 SV=3	sp|P46777|RL5_HUMAN	34 kDa	24	10
ATP-citrate synthase OS=Homo sapiens GN=ACLY PE=1 SV=3	sp|P53396|ACLY_HUMAN	121 kDa	24	15
Exportin-2 OS=Homo sapiens GN=CSE1L PE=1 SV=3	sp|P55060|XPO2_HUMAN	110 kDa	24	23
Triosephosphate isomerase OS=Homo sapiens GN=TPI1 PE=1 SV=2	sp|P60174|TPIS_HUMAN	27 kDa	24	27
Heterogeneous nuclear ribonucleoprotein R OS=Homo sapiens GN=HNRNPR PE=1 SV=1	sp|O43390|HNRPR_HUMAN	71 kDa	23	14
Long-chain-fatty-acid--CoA ligase 4 OS=Homo sapiens GN=ACSL4 PE=1 SV=2	sp|O60488|ACSL4_HUMAN	79 kDa	23	15
Sodium/potassium-transporting ATPase subunit alpha-1 OS=Homo sapiens GN=ATP1A1 PE=1 SV=1	sp|P05023|AT1A1_HUMAN	113 kDa	23	37
Glucose-6-phosphate isomerase OS=Homo sapiens GN=GPI PE=1 SV=4	sp|P06744|G6PI_HUMAN	63 kDa	23	25
Bifunctional aminoacyl-tRNA synthetase OS=Homo sapiens GN=EPRS PE=1 SV=5	sp|P07814|SYEP_HUMAN	171 kDa	23	12
NADPH--cytochrome P450 reductase OS=Homo sapiens GN=POR PE=1 SV=2	sp|P16435|NCPR_HUMAN	77 kDa	23	30
Aldo-keto reductase family 1 member C3 OS=Homo sapiens GN=AKR1C3 PE=1 SV=4	sp|P42330|AK1C3_HUMAN	37 kDa	23	22
40S ribosomal protein S7 OS=Homo sapiens GN=RPS7 PE=1 SV=1	sp|P62081|RS7_HUMAN	22 kDa	23	9
T-complex protein 1 subunit beta OS=Homo sapiens GN=CCT2 PE=1 SV=4	sp|P78371|TCPB_HUMAN	57 kDa	23	29
Cytoplasmic dynein 1 heavy chain 1 OS=Homo sapiens GN=DYNC1H1 PE=1 SV=5	sp|Q14204|DYHC1_HUMAN	532 kDa	23	4
Thioredoxin domain-containing protein 5 OS=Homo sapiens GN=TXNDC5 PE=1 SV=2	sp|Q8NBS9|TXND5_HUMAN	48 kDa	23	18
UDP-glucose:glycoprotein glucosyltransferase 1 OS=Homo sapiens GN=UGGT1 PE=1 SV=3	sp|Q9NYU2|UGGG1_HUMAN	177 kDa	23	32
Dolichyl-diphosphooligosaccharide--protein glycosyltransferase subunit 2 OS=Homo sapiens GN=RPN2 PE=1 SV=3	sp|P04844|RPN2_HUMAN	69 kDa	22	23
T-complex protein 1 subunit zeta OS=Homo sapiens GN=CCT6A PE=1 SV=3	sp|P40227|TCPZ_HUMAN	58 kDa	22	18
Actin, alpha cardiac muscle 1 OS=Homo sapiens GN=ACTC1 PE=1 SV=1	sp|P68032|ACTC_HUMAN (+1)	42 kDa	22	25
Histone H3.2 OS=Homo sapiens GN=HIST2H3A PE=1 SV=3	sp|Q71DI3|H32_HUMAN	15 kDa	22	0
T-complex protein 1 subunit eta OS=Homo sapiens GN=CCT7 PE=1 SV=2	sp|Q99832|TCPH_HUMAN	59 kDa	22	16
Fibronectin OS=Homo sapiens GN=FN1 PE=1 SV=4	sp|P02751|FINC_HUMAN	263 kDa	21	0
2',3'-cyclic-nucleotide 3'-phosphodiesterase OS=Homo sapiens GN=CNP PE=1 SV=2	sp|P09543|CN37_HUMAN	48 kDa	21	14
Aspartyl-tRNA synthetase, cytoplasmic OS=Homo sapiens GN=DARS PE=1 SV=2	sp|P14868|SYDC_HUMAN	57 kDa	21	13

T-complex protein 1 subunit alpha OS=Homo sapiens GN=TCP1 PE=1 SV=1	sp|P17987|TCPA_HUMAN	60 kDa	21	18
Liver carboxylesterase 1 OS=Homo sapiens GN=CES1 PE=1 SV=2	sp|P23141|EST1_HUMAN	63 kDa	21	27
Splicing factor, proline- and glutamine-rich OS=Homo sapiens GN=SFPQ PE=1 SV=2	sp|P23246|SFPQ_HUMAN	76 kDa	21	4
40S ribosomal protein S3 OS=Homo sapiens GN=RPS3 PE=1 SV=2	sp|P23396|RS3_HUMAN	27 kDa	21	20
Aldehyde dehydrogenase X, mitochondrial OS=Homo sapiens GN=ALDH1B1 PE=1 SV=3	sp|P30837|AL1B1_HUMAN	57 kDa	21	22
Isocitrate dehydrogenase [NADP], mitochondrial OS=Homo sapiens GN=IDH2 PE=1 SV=2	sp|P48735|IDHP_HUMAN	51 kDa	21	23
Rab GDP dissociation inhibitor beta OS=Homo sapiens GN=GDI2 PE=1 SV=2	sp|P50395|GDIB_HUMAN	51 kDa	21	18
Heterogeneous nuclear ribonucleoprotein H2 OS=Homo sapiens GN=HNRNPH2 PE=1 SV=1	sp|P55795|HNRH2_HUMAN	49 kDa	21	0
40S ribosomal protein S3a OS=Homo sapiens GN=RPS3A PE=1 SV=2	sp|P61247|RS3A_HUMAN	30 kDa	21	11
60S ribosomal protein L18a OS=Homo sapiens GN=RPL18A PE=1 SV=2	sp|Q02543|RL18A_HUMAN	21 kDa	21	5
Polyadenylate-binding protein 1 OS=Homo sapiens GN=PABPC1 PE=1 SV=2	sp|P11940|PABP1_HUMAN	71 kDa	20	15
ADP/ATP translocase 1 OS=Homo sapiens GN=SLC25A4 PE=1 SV=4	sp|P12235|ADT1_HUMAN	33 kDa	20	14
ADP/ATP translocase 3 OS=Homo sapiens GN=SLC25A6 PE=1 SV=4	sp|P12236|ADT3_HUMAN	33 kDa	20	15
Probable ATP-dependent RNA helicase DDX5 OS=Homo sapiens GN=DDX5 PE=1 SV=1	sp|P17844|DDX5_HUMAN	69 kDa	20	10
Peroxiredoxin-6 OS=Homo sapiens GN=PRDX6 PE=1 SV=3	sp|P30041|PRDX6_HUMAN	25 kDa	20	13
Heterogeneous nuclear ribonucleoprotein F OS=Homo sapiens GN=HNRNPF PE=1 SV=3	sp|P52597|HNRPF_HUMAN	46 kDa	20	13
Eukaryotic initiation factor 4A-I OS=Homo sapiens GN=EIF4A1 PE=1 SV=1	sp|P60842|IF4A1_HUMAN	46 kDa	20	18
Cytoskeleton-associated protein 4 OS=Homo sapiens GN=CKAP4 PE=1 SV=2	sp|Q07065|CKAP4_HUMAN	66 kDa	20	20
Serine/arginine-rich splicing factor 1 OS=Homo sapiens GN=SRSF1 PE=1 SV=2	sp|Q07955|SRSF1_HUMAN	28 kDa	20	7
Retrotransposon-derived protein PEG10 OS=Homo sapiens GN=PEG10 PE=1 SV=2	sp|Q86TG7|PEG10_HUMAN	80 kDa	20	4
Probable ATP-dependent RNA helicase DDX17 OS=Homo sapiens GN=DDX17 PE=1 SV=1	sp|Q92841|DDX17_HUMAN	72 kDa	20	6
Retinal dehydrogenase 1 OS=Homo sapiens GN=ALDH1A1 PE=1 SV=2	sp|P00352|AL1A1_HUMAN	55 kDa	19	16
Alpha-actinin-1 OS=Homo sapiens GN=ACTN1 PE=1 SV=2	sp|P12814|ACTN1_HUMAN	103 kDa	19	28
Histone H2A.x OS=Homo sapiens GN=H2AFX PE=1 SV=2	sp|P16104|H2AX_HUMAN	15 kDa	19	0
40S ribosomal protein S4, Y isoform 1 OS=Homo sapiens GN=RPS4Y1 PE=2 SV=2	sp|P22090|RS4Y1_HUMAN	29 kDa	19	0
14-3-3 protein epsilon OS=Homo sapiens GN=YWHAE PE=1 SV=1	sp|P62258|1433E_HUMAN	29 kDa	19	17
60S ribosomal protein L8 OS=Homo sapiens GN=RPL8 PE=1 SV=2	sp|P62917|RL8_HUMAN	28 kDa	19	3
Spliceosome RNA helicase BAT1 OS=Homo sapiens GN=BAT1 PE=1 SV=1	sp|Q13838|UAP56_HUMAN	49 kDa	19	10
Calcium-binding mitochondrial carrier protein Aralar2 OS=Homo sapiens GN=SLC25A13 PE=1 SV=2	sp|Q9UJS0|CMC2_HUMAN	74 kDa	19	22
Alpha-fetoprotein OS=Homo sapiens GN=AFP PE=1 SV=1	sp|P02771|FETA_HUMAN	69 kDa	18	19
Heterogeneous nuclear ribonucleoproteins C1/C2 OS=Homo sapiens GN=HNRNPC PE=1	sp|P07910|HNRPC_HUMAN	34 kDa	18	13

SV=4				
40S ribosomal protein S2 OS=Homo sapiens GN=RPS2 PE=1 SV=2	sp|P15880|RS2_HUMAN	31 kDa	18	12
40S ribosomal protein S12 OS=Homo sapiens GN=RPS12 PE=1 SV=3	sp|P25398|RS12_HUMAN	15 kDa	18	9
Bifunctional purine biosynthesis protein PURH OS=Homo sapiens GN=ATIC PE=1 SV=3	sp|P31939|PUR9_HUMAN	65 kDa	18	21
60S ribosomal protein L26 OS=Homo sapiens GN=RPL26 PE=1 SV=1	sp|P61254|RL26_HUMAN	17 kDa	18	4
14-3-3 protein gamma OS=Homo sapiens GN=YWHAG PE=1 SV=2	sp|P61981|1433G_HUMAN	28 kDa	18	15
Peptidyl-prolyl cis-trans isomerase A OS=Homo sapiens GN=PPIA PE=1 SV=2	sp|P62937|PPIA_HUMAN	18 kDa	18	21
14-3-3 protein zeta/delta OS=Homo sapiens GN=YWHAZ PE=1 SV=1	sp|P63104|1433Z_HUMAN	28 kDa	18	12
Vigilin OS=Homo sapiens GN=HDLBP PE=1 SV=2	sp|Q00341|VIGLN_HUMAN	141 kDa	18	13
26S proteasome non-ATPase regulatory subunit 2 OS=Homo sapiens GN=PSMD2 PE=1 SV=3	sp|Q13200|PSMD2_HUMAN	100 kDa	18	13
Hypoxia up-regulated protein 1 OS=Homo sapiens GN=HYOU1 PE=1 SV=1	sp|Q9Y4L1|HYOU1_HUMAN	111 kDa	18	28
Tax_Id=9606 Gene_Symbol=ALB Isoform 1 of Serum albumin precursor	IPI:CON_00745872.2|SWISS-PROT:P02768-1 (+2)	69 kDa	17	29
Histone H1.2 OS=Homo sapiens GN=HIST1H1C PE=1 SV=2	sp|P16403|H12_HUMAN	21 kDa	17	17
Phosphoglycerate mutase 1 OS=Homo sapiens GN=PGAM1 PE=1 SV=2	sp|P18669|PGAM1_HUMAN	29 kDa	17	17
Polypyrimidine tract-binding protein 1 OS=Homo sapiens GN=PTBP1 PE=1 SV=1	sp|P26599|PTBP1_HUMAN	57 kDa	17	15
60S ribosomal protein L10 OS=Homo sapiens GN=RPL10 PE=1 SV=4	sp|P27635|RL10_HUMAN	25 kDa	17	7
14-3-3 protein beta/alpha OS=Homo sapiens GN=YWHAB PE=1 SV=3	sp|P31946|1433B_HUMAN	28 kDa	17	22
Malate dehydrogenase, mitochondrial OS=Homo sapiens GN=MDH2 PE=1 SV=3	sp|P40926|MDHM_HUMAN	36 kDa	17	25
40S ribosomal protein S9 OS=Homo sapiens GN=RPS9 PE=1 SV=3	sp|P46781|RS9_HUMAN	23 kDa	17	8
T-complex protein 1 subunit theta OS=Homo sapiens GN=CCT8 PE=1 SV=4	sp|P50990|TCPQ_HUMAN	60 kDa	17	25
40S ribosomal protein S8 OS=Homo sapiens GN=RPS8 PE=1 SV=2	sp|P62241|RS8_HUMAN	24 kDa	17	11
Heat shock protein 75 kDa, mitochondrial OS=Homo sapiens GN=TRAP1 PE=1 SV=3	sp|Q12931|TRAP1_HUMAN	80 kDa	17	18
Prohibitin-2 OS=Homo sapiens GN=PHB2 PE=1 SV=2	sp|Q99623|PHB2_HUMAN	33 kDa	17	24
Proteasome activator complex subunit 2 OS=Homo sapiens GN=PSME2 PE=1 SV=4	sp|Q9UL46|PSME2_HUMAN	27 kDa	17	14
Histone H1.4 OS=Homo sapiens GN=HIST1H1E PE=1 SV=2	sp|P10412|H14_HUMAN	22 kDa	16	16
X-ray repair cross-complementing protein 6 OS=Homo sapiens GN=XRCC6 PE=1 SV=2	sp|P12956|XRCC6_HUMAN	70 kDa	16	18
NAD(P)H dehydrogenase [quinone] 1 OS=Homo sapiens GN=NQO1 PE=1 SV=1	sp|P15559|NQO1_HUMAN	31 kDa	16	11
60S ribosomal protein L17 OS=Homo sapiens GN=RPL17 PE=1 SV=3	sp|P18621|RL17_HUMAN	21 kDa	16	4
60S ribosomal protein L13 OS=Homo sapiens GN=RPL13 PE=1 SV=4	sp|P26373|RL13_HUMAN	24 kDa	16	3
Dolichyl-diphosphooligosaccharide--protein glycosyltransferase 48 kDa subunit OS=Homo sapiens GN=DDOST PE=1 SV=4	sp|P39656|OST48_HUMAN	51 kDa	16	17
60S ribosomal protein L13a OS=Homo sapiens GN=RPL13A PE=1 SV=2	sp|P40429|RL13A_HUMAN	24 kDa	16	8
40S ribosomal protein S5 OS=Homo sapiens GN=RPS5 PE=1 SV=4	sp|P46782|RS5_HUMAN	23 kDa	16	9
6-phosphogluconate dehydrogenase,	sp|P52209|6PGD_HUMAN	53 kDa	16	15

decarboxylating OS=Homo sapiens GN=PGD PE=1 SV=3				
60S ribosomal protein L15 OS=Homo sapiens GN=RPL15 PE=1 SV=2	sp|P61313|RL15_HUMAN	24 kDa	16	7
40S ribosomal protein S13 OS=Homo sapiens GN=RPS13 PE=1 SV=2	sp|P62277|RS13_HUMAN	17 kDa	16	5
Nuclease-sensitive element-binding protein 1 OS=Homo sapiens GN=YBX1 PE=1 SV=3	sp|P67809|YBOX1_HUMAN	36 kDa	16	11
4-aminobutyrate aminotransferase, mitochondrial OS=Homo sapiens GN=ABAT PE=1 SV=3	sp|P80404|GABT_HUMAN	56 kDa	16	24
Transcription intermediary factor 1-beta OS=Homo sapiens GN=TRIM28 PE=1 SV=5	sp|Q13263|TIF1B_HUMAN	89 kDa	16	9
Heterogeneous nuclear ribonucleoprotein D0 OS=Homo sapiens GN=HNRNPD PE=1 SV=1	sp|Q14103|HNRPD_HUMAN	38 kDa	16	18
Importin subunit beta-1 OS=Homo sapiens GN=KPNB1 PE=1 SV=2	sp|Q14974|IMB1_HUMAN	97 kDa	16	13
Echinoderm microtubule-associated protein-like 4 OS=Homo sapiens GN=EML4 PE=1 SV=3	sp|Q9HC35|EMAL4_HUMAN	109 kDa	16	21
(Bos taurus) Bovine serum albumin precursor	IPI:CON_00708398.1|SWISS-PROT:P02769	69 kDa	15	40
ATP-dependent RNA helicase DDX39 OS=Homo sapiens GN=DDX39 PE=1 SV=2	sp|O00148|DDX39_HUMAN	49 kDa	15	0
Complement C3 OS=Homo sapiens GN=C3 PE=1 SV=2	sp|P01024|CO3_HUMAN	187 kDa	15	15
4F2 cell-surface antigen heavy chain OS=Homo sapiens GN=SLC3A2 PE=1 SV=3	sp|P08195|4F2_HUMAN	68 kDa	15	18
Cytochrome b-c1 complex subunit 2, mitochondrial OS=Homo sapiens GN=UQCRC2 PE=1 SV=3	sp|P22695|QCR2_HUMAN	48 kDa	15	17
14-3-3 protein theta OS=Homo sapiens GN=YWHAQ PE=1 SV=1	sp|P27348|1433T_HUMAN	28 kDa	15	15
Pyrroline-5-carboxylate reductase 1, mitochondrial OS=Homo sapiens GN=PYCR1 PE=1 SV=2	sp|P32322|P5CR1_HUMAN	33 kDa	15	18
T-complex protein 1 subunit delta OS=Homo sapiens GN=CCT4 PE=1 SV=4	sp|P50991|TCPD_HUMAN	58 kDa	15	12
Glypican-3 OS=Homo sapiens GN=GPC3 PE=1 SV=1	sp|P51654|GPC3_HUMAN	66 kDa	15	13
Arginyl-tRNA synthetase, cytoplasmic OS=Homo sapiens GN=RARS PE=1 SV=2	sp|P54136|SYRC_HUMAN	75 kDa	15	8
Microsomal triglyceride transfer protein large subunit OS=Homo sapiens GN=MTTP PE=1 SV=1	sp|P55157|MTP_HUMAN	99 kDa	15	16
10 kDa heat shock protein, mitochondrial OS=Homo sapiens GN=HSPE1 PE=1 SV=2	sp|P61604|CH10_HUMAN	11 kDa	15	19
40S ribosomal protein S16 OS=Homo sapiens GN=RPS16 PE=1 SV=2	sp|P62249|RS16_HUMAN	16 kDa	15	9
40S ribosomal protein S14 OS=Homo sapiens GN=RPS14 PE=1 SV=3	sp|P62263|RS14_HUMAN	16 kDa	15	8
Mannosyl-oligosaccharide glucosidase OS=Homo sapiens GN=MOGS PE=1 SV=5	sp|Q13724|MOGS_HUMAN	92 kDa	15	9
Poly(rC)-binding protein 1 OS=Homo sapiens GN=PCBP1 PE=1 SV=2	sp|Q15365|PCBP1_HUMAN	37 kDa	15	12
UPF0027 protein C22orf28 OS=Homo sapiens GN=C22orf28 PE=1 SV=1	sp|Q9Y3I0|CV028_HUMAN	55 kDa	15	0
Coatomer subunit gamma OS=Homo sapiens GN=COPG PE=1 SV=1	sp|Q9Y678|COPG_HUMAN	98 kDa	15	9
Chloride intracellular channel protein 1 OS=Homo sapiens GN=CLIC1 PE=1 SV=4	sp|O00299|CLIC1_HUMAN	27 kDa	14	13
Aldehyde dehydrogenase, mitochondrial OS=Homo sapiens GN=ALDH2 PE=1 SV=2	sp|P05091|ALDH2_HUMAN	56 kDa	14	17
Nucleophosmin OS=Homo sapiens GN=NPM1 PE=1 SV=2	sp|P06748|NPM_HUMAN	33 kDa	14	10
Annexin A5 OS=Homo sapiens GN=ANXA5 PE=1 SV=2	sp|P08758|ANXA5_HUMAN	36 kDa	14	20

Villin-1 OS=Homo sapiens GN=VIL1 PE=1 SV=4	sp|P09327|VILI_HUMAN	93 kDa	14	16
Adenosylhomocysteinase OS=Homo sapiens GN=AHCY PE=1 SV=4	sp|P23526|SAHH_HUMAN	48 kDa	14	14
Acetyl-CoA acetyltransferase, mitochondrial OS=Homo sapiens GN=ACAT1 PE=1 SV=1	sp|P24752|THIL_HUMAN	45 kDa	14	21
Elongation factor 1-gamma OS=Homo sapiens GN=EEF1G PE=1 SV=3	sp|P26641|EF1G_HUMAN	50 kDa	14	14
Delta-1-pyrroline-5-carboxylate dehydrogenase, mitochondrial OS=Homo sapiens GN=ALDH4A1 PE=1 SV=3	sp|P30038|AL4A1_HUMAN	62 kDa	14	14
Prohibitin OS=Homo sapiens GN=PHB PE=1 SV=1	sp|P35232|PHB_HUMAN	30 kDa	14	23
RNA-binding protein FUS OS=Homo sapiens GN=FUS PE=1 SV=1	sp|P35637|FUS_HUMAN	53 kDa	14	7
Glutaminyl-tRNA synthetase OS=Homo sapiens GN=QARS PE=1 SV=1	sp|P47897|SYQ_HUMAN	88 kDa	14	7
Peroxisomal multifunctional enzyme type 2 OS=Homo sapiens GN=HSD17B4 PE=1 SV=3	sp|P51659|DHB4_HUMAN	80 kDa	14	25
40S ribosomal protein S15a OS=Homo sapiens GN=RPS15A PE=1 SV=2	sp|P62244|RS15A_HUMAN	15 kDa	14	4
Ubiquitin-40S ribosomal protein S27a OS=Homo sapiens GN=RPS27A PE=1 SV=2	sp|P62979|RS27A_HUMAN	18 kDa	14	7
Interleukin enhancer-binding factor 3 OS=Homo sapiens GN=ILF3 PE=1 SV=3	sp|Q12906|ILF3_HUMAN	95 kDa	14	13
Delta(3,5)-Delta(2,4)-dienoyl-CoA isomerase, mitochondrial OS=Homo sapiens GN=ECH1 PE=1 SV=2	sp|Q13011|ECH1_HUMAN	36 kDa	14	19
Dihydropyrimidinase-related protein 2 OS=Homo sapiens GN=DPYSL2 PE=1 SV=1	sp|Q16555|DPYL2_HUMAN	62 kDa	14	13
Staphylococcal nuclease domain-containing protein 1 OS=Homo sapiens GN=SND1 PE=1 SV=1	sp|Q7KZF4|SND1_HUMAN	102 kDa	14	23
Leucine-rich repeat-containing protein 59 OS=Homo sapiens GN=LRRC59 PE=1 SV=1	sp|Q96AG4|LRC59_HUMAN	35 kDa	14	11
Adipocyte plasma membrane-associated protein OS=Homo sapiens GN=APMAP PE=1 SV=2	sp|Q9HDC9|APMAP_HUMAN	46 kDa	14	20
Putative pre-mRNA-splicing factor ATP-dependent RNA helicase DHX15 OS=Homo sapiens GN=DHX15 PE=1 SV=2	sp|O43143|DHX15_HUMAN	91 kDa	13	2
D-3-phosphoglycerate dehydrogenase OS=Homo sapiens GN=PHGDH PE=1 SV=4	sp|O43175|SERA_HUMAN	57 kDa	13	11
High mobility group protein B1 OS=Homo sapiens GN=HMGB1 PE=1 SV=3	sp|P09429|HMGB1_HUMAN	25 kDa	13	11
Annexin A4 OS=Homo sapiens GN=ANXA4 PE=1 SV=4	sp|P09525|ANXA4_HUMAN	36 kDa	13	21
Sarcoplasmic/endoplasmic reticulum calcium ATPase 2 OS=Homo sapiens GN=ATP2A2 PE=1 SV=1	sp|P16615|AT2A2_HUMAN	115 kDa	13	8
Peptidyl-prolyl cis-trans isomerase B OS=Homo sapiens GN=PPIB PE=1 SV=2	sp|P23284|PPIB_HUMAN	24 kDa	13	23
Phosphatidylethanolamine-binding protein 1 OS=Homo sapiens GN=PEBP1 PE=1 SV=3	sp|P30086|PEBP1_HUMAN	21 kDa	13	14
Cytochrome b-c1 complex subunit 1, mitochondrial OS=Homo sapiens GN=UQCRC1 PE=1 SV=3	sp|P31930|QCR1_HUMAN	53 kDa	13	16
Catenin beta-1 OS=Homo sapiens GN=CTNNB1 PE=1 SV=1	sp|P35222|CTNB1_HUMAN	85 kDa	13	15
ATP synthase subunit gamma, mitochondrial OS=Homo sapiens GN=ATP5C1 PE=1 SV=1	sp|P36542|ATPG_HUMAN	33 kDa	13	14
Isoleucyl-tRNA synthetase, cytoplasmic OS=Homo sapiens GN=IARS PE=1 SV=2	sp|P41252|SYIC_HUMAN	145 kDa	13	2
3-ketoacyl-CoA thiolase, mitochondrial OS=Homo sapiens GN=ACAA2 PE=1 SV=2	sp|P42765|THIM_HUMAN	42 kDa	13	12

Voltage-dependent anion-selective channel protein 2 OS=Homo sapiens GN=VDAC2 PE=1 SV=2	sp|P45880|VDAC2_HUMAN	32 kDa	13	18
Short/branched chain specific acyl-CoA dehydrogenase, mitochondrial OS=Homo sapiens GN=ACADSB PE=1 SV=1	sp|P45954|ACDSB_HUMAN	47 kDa	13	17
ATP synthase subunit O, mitochondrial OS=Homo sapiens GN=ATP5O PE=1 SV=1	sp|P48047|ATPO_HUMAN	23 kDa	13	13
Serpin H1 OS=Homo sapiens GN=SERPINH1 PE=1 SV=2	sp|P50454|SERPH_HUMAN	46 kDa	13	18
60S ribosomal protein L14 OS=Homo sapiens GN=RPL14 PE=1 SV=4	sp|P50914|RL14_HUMAN	23 kDa	13	3
GTP-binding nuclear protein Ran OS=Homo sapiens GN=RAN PE=1 SV=3	sp|P62826|RAN_HUMAN	24 kDa	13	9
60S ribosomal protein L18 OS=Homo sapiens GN=RPL18 PE=1 SV=2	sp|Q07020|RL18_HUMAN	22 kDa	13	7
Acetyl-CoA acetyltransferase, cytosolic OS=Homo sapiens GN=ACAT2 PE=1 SV=2	sp|Q9BWD1|THIC_HUMAN	41 kDa	13	6
Heterogeneous nuclear ribonucleoprotein Q OS=Homo sapiens GN=SYNCRIP PE=1 SV=2	sp|O60506|HNRPQ_HUMAN	70 kDa	12	12
Citrate synthase, mitochondrial OS=Homo sapiens GN=CS PE=1 SV=2	sp|O75390|CISY_HUMAN	52 kDa	12	16
Superoxide dismutase [Cu-Zn] OS=Homo sapiens GN=SOD1 PE=1 SV=2	sp|P00441|SODC_HUMAN	16 kDa	12	7
60S acidic ribosomal protein P0 OS=Homo sapiens GN=RPLP0 PE=1 SV=1	sp|P05388|RLA0_HUMAN	34 kDa	12	16
Cathepsin B OS=Homo sapiens GN=CTSB PE=1 SV=3	sp|P07858|CATB_HUMAN	38 kDa	12	14
Solute carrier family 2, facilitated glucose transporter member 1 OS=Homo sapiens GN=SLC2A1 PE=1 SV=2	sp|P11166|GTR1_HUMAN	54 kDa	12	20
Multifunctional protein ADE2 OS=Homo sapiens GN=PAICS PE=1 SV=3	sp|P22234|PUR6_HUMAN	47 kDa	12	9
Ubiquitin-like modifier-activating enzyme 1 OS=Homo sapiens GN=UBA1 PE=1 SV=3	sp|P22314|UBA1_HUMAN	118 kDa	12	13
Cofilin-1 OS=Homo sapiens GN=CFL1 PE=1 SV=3	sp|P23528|COF1_HUMAN	19 kDa	12	10
Valyl-tRNA synthetase OS=Homo sapiens GN=VARS PE=1 SV=4	sp|P26640|SYVC_HUMAN	140 kDa	12	6
Thioredoxin-dependent peroxide reductase, mitochondrial OS=Homo sapiens GN=PRDX3 PE=1 SV=3	sp|P30048|PRDX3_HUMAN	28 kDa	12	17
60S ribosomal protein L9 OS=Homo sapiens GN=RPL9 PE=1 SV=1	sp|P32969|RL9_HUMAN	22 kDa	12	4
60S ribosomal protein L27 OS=Homo sapiens GN=RPL27 PE=1 SV=2	sp|P61353|RL27_HUMAN	16 kDa	12	3
40S ribosomal protein S18 OS=Homo sapiens GN=RPS18 PE=1 SV=3	sp|P62269|RS18_HUMAN	18 kDa	12	9
40S ribosomal protein S15 OS=Homo sapiens GN=RPS15 PE=1 SV=2	sp|P62841|RS15_HUMAN	17 kDa	12	0
60S ribosomal protein L32 OS=Homo sapiens GN=RPL32 PE=1 SV=2	sp|P62910|RL32_HUMAN	16 kDa	12	2
Serine/arginine-rich splicing factor 6 OS=Homo sapiens GN=SRSF6 PE=1 SV=2	sp|Q13247|SRSF6_HUMAN	40 kDa	12	3
Protein transport protein Sec23A OS=Homo sapiens GN=SEC23A PE=1 SV=2	sp|Q15436|SC23A_HUMAN	86 kDa	12	11
Serine/arginine-rich splicing factor 7 OS=Homo sapiens GN=SRSF7 PE=1 SV=1	sp|Q16629|SRSF7_HUMAN	27 kDa	12	2
Pre-mRNA-processing-splicing factor 8 OS=Homo sapiens GN=PRPF8 PE=1 SV=2	sp|Q6P2Q9|PRP8_HUMAN	274 kDa	12	0
ATP-dependent RNA helicase DDX1 OS=Homo sapiens GN=DDX1 PE=1 SV=2	sp|Q92499|DDX1_HUMAN	82 kDa	12	0
Translational activator GCN1 OS=Homo sapiens GN=GCN1L1 PE=1 SV=6	sp|Q92616|GCN1L_HUMAN	293 kDa	12	4
Putative helicase MOV-10 OS=Homo sapiens	sp|Q9HCE1|MOV10_HUMAN	114 kDa	12	0

GN=MOV10 PE=1 SV=2				
26S proteasome non-ATPase regulatory subunit 3 OS=Homo sapiens GN=PSMD3 PE=1 SV=2	sp|O43242|PSMD3_HUMAN	61 kDa	11	8
Asparaginyl-tRNA synthetase, cytoplasmic OS=Homo sapiens GN=NARS PE=1 SV=1	sp|O43776|SYNC_HUMAN	63 kDa	11	3
Myosin-Ib OS=Homo sapiens GN=MYO1B PE=1 SV=3	sp|O43795|MYO1B_HUMAN	132 kDa	11	0
Alpha-2-macroglobulin OS=Homo sapiens GN=A2M PE=1 SV=3	sp|P01023|A2MG_HUMAN	163 kDa	11	13
Glycogen phosphorylase, liver form OS=Homo sapiens GN=PYGL PE=1 SV=4	sp|P06737|PYGL_HUMAN	97 kDa	11	4
Cathepsin D OS=Homo sapiens GN=CTSD PE=1 SV=1	sp|P07339|CATD_HUMAN	45 kDa	11	15
Profilin-1 OS=Homo sapiens GN=PFN1 PE=1 SV=2	sp|P07737|PROF1_HUMAN	15 kDa	11	11
Pyruvate dehydrogenase E1 component subunit alpha, somatic form, mitochondrial OS=Homo sapiens GN=PDHA1 PE=1 SV=3	sp|P08559|ODPA_HUMAN	43 kDa	11	8
40S ribosomal protein SA OS=Homo sapiens GN=RPSA PE=1 SV=4	sp|P08865|RSSA_HUMAN	33 kDa	11	7
Ribonuclease inhibitor OS=Homo sapiens GN=RNH1 PE=1 SV=2	sp|P13489|RINI_HUMAN	50 kDa	11	2
Electron transfer flavoprotein subunit alpha, mitochondrial OS=Homo sapiens GN=ETFA PE=1 SV=1	sp|P13804|ETFA_HUMAN	35 kDa	11	18
Voltage-dependent anion-selective channel protein 1 OS=Homo sapiens GN=VDAC1 PE=1 SV=2	sp|P21796|VDAC1_HUMAN	31 kDa	11	29
NADH-ubiquinone oxidoreductase 75 kDa subunit, mitochondrial OS=Homo sapiens GN=NDUFS1 PE=1 SV=3	sp|P28331|NDUS1_HUMAN	79 kDa	11	19
Elongation factor 1-delta OS=Homo sapiens GN=EEF1D PE=1 SV=5	sp|P29692|EF1D_HUMAN	31 kDa	11	7
60S ribosomal protein L12 OS=Homo sapiens GN=RPL12 PE=1 SV=1	sp|P30050|RL12_HUMAN	18 kDa	11	8
Stress-induced-phosphoprotein 1 OS=Homo sapiens GN=STIP1 PE=1 SV=1	sp|P31948|STIP1_HUMAN	63 kDa	11	12
Serine hydroxymethyltransferase, mitochondrial OS=Homo sapiens GN=SHMT2 PE=1 SV=3	sp|P34897|GLYM_HUMAN	56 kDa	11	20
Eukaryotic initiation factor 4A-III OS=Homo sapiens GN=EIF4A3 PE=1 SV=4	sp|P38919|IF4A3_HUMAN	47 kDa	11	9
Sulfotransferase 1A1 OS=Homo sapiens GN=SULT1A1 PE=1 SV=3	sp|P50225|ST1A1_HUMAN	34 kDa	11	8
Coatomer subunit beta OS=Homo sapiens GN=COPB1 PE=1 SV=3	sp|P53618|COPB_HUMAN	107 kDa	11	9
60S ribosomal protein L10a OS=Homo sapiens GN=RPL10A PE=1 SV=2	sp|P62906|RL10A_HUMAN	25 kDa	11	6
Eukaryotic translation initiation factor 5A-1 OS=Homo sapiens GN=EIF5A PE=1 SV=2	sp|P63241|IF5A1_HUMAN	17 kDa	11	8
Serine/arginine-rich splicing factor 3 OS=Homo sapiens GN=SRSF3 PE=1 SV=1	sp|P84103|SRSF3_HUMAN	19 kDa	11	6
Proteasome activator complex subunit 1 OS=Homo sapiens GN=PSME1 PE=1 SV=1	sp|Q06323|PSME1_HUMAN	29 kDa	11	10
Peroxiredoxin-4 OS=Homo sapiens GN=PRDX4 PE=1 SV=1	sp|Q13162|PRDX4_HUMAN	31 kDa	11	17
Non-POU domain-containing octamer-binding protein OS=Homo sapiens GN=NONO PE=1 SV=4	sp|Q15233|NONO_HUMAN	54 kDa	11	4
L-xylulose reductase OS=Homo sapiens GN=DCXR PE=1 SV=2	sp|Q7Z4W1|DCXR_HUMAN	26 kDa	11	18
Alanine aminotransferase 2 OS=Homo sapiens GN=GPT2 PE=1 SV=1	sp|Q8TD30|ALAT2_HUMAN	58 kDa	11	11
Pentatricopeptide repeat-containing protein 3,	sp|Q96EY7|PTCD3_HUMAN	79 kDa	11	7

mitochondrial OS=Homo sapiens GN=PTCD3 PE=1 SV=3				
ERO1-like protein alpha OS=Homo sapiens GN=ERO1L PE=1 SV=2	sp|Q96HE7|ERO1A_HUMAN	54 kDa	11	18
Protein DJ-1 OS=Homo sapiens GN=PARK7 PE=1 SV=2	sp|Q99497|PARK7_HUMAN	20 kDa	11	7
FACT complex subunit SPT16 OS=Homo sapiens GN=SUPT16H PE=1 SV=1	sp|Q9Y5B9|SP16H_HUMAN	120 kDa	11	4
Tax_Id=9606 Gene_Symbol=KRT19 Keratin, type I cytoskeletal 19	IPI:CON_IPI00479145.2|SWISS-PROT:P08727 (+1)	44 kDa	10	15
Heterogeneous nuclear ribonucleoprotein D-like OS=Homo sapiens GN=HNRPDL PE=1 SV=3	sp|O14979|HNRDL_HUMAN	46 kDa	10	6
Catenin delta-1 OS=Homo sapiens GN=CTNND1 PE=1 SV=1	sp|O60716|CTND1_HUMAN	108 kDa	10	3
Double-stranded RNA-binding protein Staufen homolog 1 OS=Homo sapiens GN=STAU1 PE=1 SV=2	sp|O95793|STAU1_HUMAN	63 kDa	10	0
Glutathione reductase, mitochondrial OS=Homo sapiens GN=GSR PE=1 SV=2	sp|P00390|GSHR_HUMAN	56 kDa	10	12
Lupus La protein OS=Homo sapiens GN=SSB PE=1 SV=2	sp|P05455|LA_HUMAN	47 kDa	10	12
U1 small nuclear ribonucleoprotein 70 kDa OS=Homo sapiens GN=SNRNP70 PE=1 SV=2	sp|P08621|RU17_HUMAN	52 kDa	10	2
Pyruvate carboxylase, mitochondrial OS=Homo sapiens GN=PC PE=1 SV=2	sp|P11498|PYC_HUMAN	130 kDa	10	8
6-phosphofructokinase, liver type OS=Homo sapiens GN=PFKL PE=1 SV=6	sp|P17858|K6PL_HUMAN	85 kDa	10	3
Protein-glutamine gamma-glutamyltransferase 2 OS=Homo sapiens GN=TGM2 PE=1 SV=2	sp|P21980|TGM2_HUMAN	77 kDa	10	0
Mitogen-activated protein kinase 1 OS=Homo sapiens GN=MAPK1 PE=1 SV=3	sp|P28482|MK01_HUMAN	41 kDa	10	7
Succinate dehydrogenase [ubiquinone] flavoprotein subunit, mitochondrial OS=Homo sapiens GN=SDHA PE=1 SV=2	sp|P31040|DHSA_HUMAN	73 kDa	10	14
Peroxiredoxin-2 OS=Homo sapiens GN=PRDX2 PE=1 SV=5	sp|P32119|PRDX2_HUMAN	22 kDa	10	9
Transaldolase OS=Homo sapiens GN=TALDO1 PE=1 SV=2	sp|P37837|TALDO_HUMAN	38 kDa	10	11
Electron transfer flavoprotein subunit beta OS=Homo sapiens GN=ETFB PE=1 SV=3	sp|P38117|ETFB_HUMAN	28 kDa	10	13
40S ribosomal protein S19 OS=Homo sapiens GN=RPS19 PE=1 SV=2	sp|P39019|RS19_HUMAN	16 kDa	10	6
60S ribosomal protein L35 OS=Homo sapiens GN=RPL35 PE=1 SV=2	sp|P42766|RL35_HUMAN	15 kDa	10	2
Transmembrane emp24 domain-containing protein 10 OS=Homo sapiens GN=TMED10 PE=1 SV=2	sp|P49755|TMEDA_HUMAN	25 kDa	10	16
Ribosomal protein S6 kinase alpha-3 OS=Homo sapiens GN=RPS6KA3 PE=1 SV=1	sp|P51812|KS6A3_HUMAN	84 kDa	10	5
Eukaryotic translation initiation factor 3 subunit B OS=Homo sapiens GN=EIF3B PE=1 SV=3	sp|P55884|EIF3B_HUMAN	92 kDa	10	0
Protein transport protein Sec61 subunit alpha isoform 1 OS=Homo sapiens GN=SEC61A1 PE=1 SV=2	sp|P61619|S61A1_HUMAN	52 kDa	10	10
Serine/threonine-protein phosphatase PP1-alpha catalytic subunit OS=Homo sapiens GN=PPP1CA PE=1 SV=1	sp|P62136|PP1A_HUMAN	38 kDa	10	4
60S ribosomal protein L19 OS=Homo sapiens GN=RPL19 PE=1 SV=1	sp|P84098|RL19_HUMAN	23 kDa	10	7
Mitochondrial 2-oxoglutarate/malate carrier protein OS=Homo sapiens GN=SLC25A11 PE=1 SV=3	sp|Q02978|M2OM_HUMAN	34 kDa	10	6
Complement component 1 Q subcomponent-binding protein, mitochondrial OS=Homo	sp|Q07021|C1QBP_HUMAN	31 kDa	10	10

sapiens GN=C1QBP PE=1 SV=1				
FACT complex subunit SSRP1 OS=Homo sapiens GN=SSRP1 PE=1 SV=1	sp|Q08945|SSRP1_HUMAN	81 kDa	10	3
Lysyl-tRNA synthetase OS=Homo sapiens GN=KARS PE=1 SV=3	sp|Q15046|SYK_HUMAN	68 kDa	10	9
Estradiol 17-beta-dehydrogenase 11 OS=Homo sapiens GN=HSD17B11 PE=1 SV=3	sp|Q8NBQ5|DHB11_HUMAN	33 kDa	10	7
Eukaryotic translation initiation factor 3 subunit C OS=Homo sapiens GN=EIF3C PE=1 SV=1	sp|Q99613|EIF3C_HUMAN	105 kDa	10	6
3-hydroxyacyl-CoA dehydrogenase type-2 OS=Homo sapiens GN=HSD17B10 PE=1 SV=3	sp|Q99714|HCD2_HUMAN	27 kDa	10	8
Probable serine carboxypeptidase CPVL OS=Homo sapiens GN=CPVL PE=1 SV=2	sp|Q9H3G5|CPVL_HUMAN	54 kDa	10	10
Zinc finger CCHC domain-containing protein 3 OS=Homo sapiens GN=ZCCHC3 PE=1 SV=1	sp|Q9NUD5|ZCHC3_HUMAN	44 kDa	10	0
Mitochondrial carrier homolog 2 OS=Homo sapiens GN=MTCH2 PE=1 SV=1	sp|Q9Y6C9|MTCH2_HUMAN	33 kDa	10	13
Tax_Id=9606 Gene_Symbol=KRT10 Keratin, type I cytoskeletal 10	IPI:CON_00009865.2|SWISS-PROT:P13645 (+1)	60 kDa	9	9
Acetolactate synthase-like protein OS=Homo sapiens GN=ILVBL PE=1 SV=2	sp|A1L0T0|ILVBL_HUMAN	68 kDa	9	4
Monocarboxylate transporter 4 OS=Homo sapiens GN=SLC16A3 PE=1 SV=1	sp|O15427|MOT4_HUMAN	49 kDa	9	8
Calumenin OS=Homo sapiens GN=CALU PE=1 SV=2	sp|O43852|CALU_HUMAN	37 kDa	9	9
Glutaminase kidney isoform, mitochondrial OS=Homo sapiens GN=GLS PE=1 SV=1	sp|O94925|GLSK_HUMAN	73 kDa	9	18
Aspartate aminotransferase, mitochondrial OS=Homo sapiens GN=GOT2 PE=1 SV=3	sp|P00505|AATM_HUMAN	48 kDa	9	24
HLA class I histocompatibility antigen, A-2 alpha chain OS=Homo sapiens GN=HLA-A PE=1 SV=1	sp|P01892|1A02_HUMAN (+1)	41 kDa	9	13
Dihydrolipoyl dehydrogenase, mitochondrial OS=Homo sapiens GN=DLD PE=1 SV=2	sp|P09622|DLDH_HUMAN	54 kDa	9	19
Glucose-6-phosphate 1-dehydrogenase OS=Homo sapiens GN=G6PD PE=1 SV=4	sp|P11413|G6PD_HUMAN	59 kDa	9	9
C-1-tetrahydrofolate synthase, cytoplasmic OS=Homo sapiens GN=MTHFD1 PE=1 SV=3	sp|P11586|C1TC_HUMAN	102 kDa	9	4
Prolyl 4-hydroxylase subunit alpha-1 OS=Homo sapiens GN=P4HA1 PE=1 SV=2	sp|P13674|P4HA1_HUMAN	61 kDa	9	16
Glucosidase 2 subunit beta OS=Homo sapiens GN=PRKCSH PE=1 SV=2	sp|P14314|GLU2B_HUMAN	59 kDa	9	17
Nucleoside diphosphate kinase A OS=Homo sapiens GN=NME1 PE=1 SV=1	sp|P15531|NDKA_HUMAN	17 kDa	9	11
Histone H1.5 OS=Homo sapiens GN=HIST1H1B PE=1 SV=3	sp|P16401|H15_HUMAN	23 kDa	9	5
Nucleoside diphosphate kinase B OS=Homo sapiens GN=NME2 PE=1 SV=1	sp|P22392|NDKB_HUMAN	17 kDa	9	14
NADPH:adrenodoxin oxidoreductase, mitochondrial OS=Homo sapiens GN=FDXR PE=1 SV=3	sp|P22570|ADRO_HUMAN	54 kDa	9	13
Glycine dehydrogenase [decarboxylating], mitochondrial OS=Homo sapiens GN=GLDC PE=1 SV=2	sp|P23378|GCSP_HUMAN	113 kDa	9	7
60S ribosomal protein L22 OS=Homo sapiens GN=RPL22 PE=1 SV=2	sp|P35268|RL22_HUMAN	15 kDa	9	2
Coatomer subunit beta' OS=Homo sapiens GN=COPB2 PE=1 SV=2	sp|P35606|COPB2_HUMAN	102 kDa	9	12
Basigin OS=Homo sapiens GN=BSG PE=1 SV=2	sp|P35613|BASI_HUMAN	42 kDa	9	14
Lon protease homolog, mitochondrial OS=Homo sapiens GN=LONP1 PE=1 SV=2	sp|P36776|LONM_HUMAN	106 kDa	9	11
Glycyl-tRNA synthetase OS=Homo sapiens GN=GARS PE=1 SV=3	sp|P41250|SYG_HUMAN	83 kDa	9	2
60S ribosomal protein L27a OS=Homo sapiens GN=RPL27A PE=1 SV=2	sp|P46776|RL27A_HUMAN	17 kDa	9	2

Sulfotransferase 1A3/1A4 OS=Homo sapiens GN=SULT1A3 PE=1 SV=1	sp|P50224|ST1A3_HUMAN	34 kDa	9	0
ADP-ribosylation factor 3 OS=Homo sapiens GN=ARF3 PE=1 SV=2	sp|P61204|ARF3_HUMAN (+1)	21 kDa	9	13
Casein kinase II subunit alpha OS=Homo sapiens GN=CSNK2A1 PE=1 SV=1	sp|P68400|CSK21_HUMAN	45 kDa	9	3
60S ribosomal protein L24 OS=Homo sapiens GN=RPL24 PE=1 SV=1	sp|P83731|RL24_HUMAN	18 kDa	9	6
Phosphate carrier protein, mitochondrial OS=Homo sapiens GN=SLC25A3 PE=1 SV=2	sp|Q00325|MPCP_HUMAN	40 kDa	9	13
Adenylyl cyclase-associated protein 1 OS=Homo sapiens GN=CAP1 PE=1 SV=5	sp|Q01518|CAP1_HUMAN	52 kDa	9	19
Polyadenylate-binding protein 4 OS=Homo sapiens GN=PABPC4 PE=1 SV=1	sp|Q13310|PABP4_HUMAN	71 kDa	9	10
Peroxisomal acyl-coenzyme A oxidase 1 OS=Homo sapiens GN=ACOX1 PE=1 SV=3	sp|Q15067|ACOX1_HUMAN	74 kDa	9	12
Splicing factor 3B subunit 3 OS=Homo sapiens GN=SF3B3 PE=1 SV=4	sp|Q15393|SF3B3_HUMAN	136 kDa	9	4
HLA class I histocompatibility antigen, Cw-16 alpha chain OS=Homo sapiens GN=HLA-C PE=2 SV=1	sp|Q29960|1C16_HUMAN	41 kDa	9	0
Acyl-coenzyme A thioesterase 1 OS=Homo sapiens GN=ACOT1 PE=1 SV=1	sp|Q86TX2|ACOT1_HUMAN	46 kDa	9	12
Acidic leucine-rich nuclear phosphoprotein 32 family member B OS=Homo sapiens GN=ANP32B PE=1 SV=1	sp|Q92688|AN32B_HUMAN	29 kDa	9	6
Aconitate hydratase, mitochondrial OS=Homo sapiens GN=ACO2 PE=1 SV=2	sp|Q99798|ACON_HUMAN	85 kDa	9	15
Methylcrotonoyl-CoA carboxylase beta chain, mitochondrial OS=Homo sapiens GN=MCCC2 PE=1 SV=1	sp|Q9HCC0|MCCB_HUMAN	61 kDa	9	12
Tax_Id=9606 Gene_Symbol=KRT2 Keratin, type II cytoskeletal 2 epidermal	IPI:CON_00021304.1|SWISS-PROT:P35908 (+1)	66 kDa	8	7
Tax_Id=9606 Gene_Symbol=KRT1 Keratin, type II cytoskeletal 1	IPI:CON_00220327.3|SWISS-PROT:P04264 (+1)	66 kDa	8	31
Importin-5 OS=Homo sapiens GN=IPO5 PE=1 SV=4	sp|O00410|IPO5_HUMAN	124 kDa	8	13
Proteasome subunit alpha type-7 OS=Homo sapiens GN=PSMA7 PE=1 SV=1	sp|O14818|PSA7_HUMAN	28 kDa	8	5
Mitochondrial import receptor subunit TOM70 OS=Homo sapiens GN=TOMM70A PE=1 SV=1	sp|O94826|TOM70_HUMAN	67 kDa	8	6
Superoxide dismutase [Mn], mitochondrial OS=Homo sapiens GN=SOD2 PE=1 SV=2	sp|P04179|SODM_HUMAN	25 kDa	8	14
HLA class I histocompatibility antigen, A-24 alpha chain OS=Homo sapiens GN=HLA-A PE=1 SV=2	sp|P05534|1A24_HUMAN	41 kDa	8	7
Histone H2A.Z OS=Homo sapiens GN=H2AFZ PE=1 SV=2	sp|P0C0S5|H2AZ_HUMAN (+1)	14 kDa	8	4
Glycogen phosphorylase, brain form OS=Homo sapiens GN=PYGB PE=1 SV=5	sp|P11216|PYGB_HUMAN	97 kDa	8	4
Cation-independent mannose-6-phosphate receptor OS=Homo sapiens GN=IGF2R PE=1 SV=3	sp|P11717|MPRI_HUMAN	274 kDa	8	12
Dipeptidyl peptidase 4 OS=Homo sapiens GN=DPP4 PE=1 SV=2	sp|P27487|DPP4_HUMAN	88 kDa	8	16
Enoyl-CoA hydratase, mitochondrial OS=Homo sapiens GN=ECHS1 PE=1 SV=4	sp|P30084|ECHM_HUMAN	31 kDa	8	9
DnaJ homolog subfamily A member 1 OS=Homo sapiens GN=DNAJA1 PE=1 SV=2	sp|P31689|DNJA1_HUMAN	45 kDa	8	7
Kinesin-1 heavy chain OS=Homo sapiens GN=KIF5B PE=1 SV=1	sp|P33176|KINH_HUMAN	110 kDa	8	3
Acidic leucine-rich nuclear phosphoprotein 32 family member A OS=Homo sapiens GN=ANP32A PE=1 SV=1	sp|P39687|AN32A_HUMAN	29 kDa	8	3

Alanyl-tRNA synthetase, cytoplasmic OS=Homo sapiens GN=AARS PE=1 SV=2	sp|P49588|SYAC_HUMAN	107 kDa	8	3
Tricarboxylate transport protein, mitochondrial OS=Homo sapiens GN=SLC25A1 PE=1 SV=2	sp|P53007|TXTP_HUMAN	34 kDa	8	9
Monocarboxylate transporter 1 OS=Homo sapiens GN=SLC16A1 PE=1 SV=3	sp|P53985|MOT1_HUMAN	54 kDa	8	5
Adenylate kinase 2, mitochondrial OS=Homo sapiens GN=AK2 PE=1 SV=2	sp|P54819|KAD2_HUMAN	26 kDa	8	14
40S ribosomal protein S11 OS=Homo sapiens GN=RPS11 PE=1 SV=3	sp|P62280|RS11_HUMAN	18 kDa	8	9
60S ribosomal protein L23a OS=Homo sapiens GN=RPL23A PE=1 SV=1	sp|P62750|RL23A_HUMAN	18 kDa	8	3
40S ribosomal protein S25 OS=Homo sapiens GN=RPS25 PE=1 SV=1	sp|P62851|RS25_HUMAN	14 kDa	8	4
40S ribosomal protein S26 OS=Homo sapiens GN=RPS26 PE=1 SV=3	sp|P62854|RS26_HUMAN	13 kDa	8	3
60S ribosomal protein L11 OS=Homo sapiens GN=RPL11 PE=1 SV=2	sp|P62913|RL11_HUMAN	20 kDa	8	7
Sorbitol dehydrogenase OS=Homo sapiens GN=SORD PE=1 SV=4	sp|Q00796|DHSO_HUMAN	38 kDa	8	0
Procollagen-lysine,2-oxoglutarate 5-dioxygenase 1 OS=Homo sapiens GN=PLOD1 PE=1 SV=2	sp|Q02809|PLOD1_HUMAN	84 kDa	8	7
Ras GTPase-activating-like protein IQGAP2 OS=Homo sapiens GN=IQGAP2 PE=1 SV=4	sp|Q13576|IQGA2_HUMAN	181 kDa	8	3
Eukaryotic translation initiation factor 3 subunit A OS=Homo sapiens GN=EIF3A PE=1 SV=1	sp|Q14152|EIF3A_HUMAN	167 kDa	8	5
116 kDa U5 small nuclear ribonucleoprotein component OS=Homo sapiens GN=EFTUD2 PE=1 SV=1	sp|Q15029|U5S1_HUMAN	109 kDa	8	0
24-dehydrocholesterol reductase OS=Homo sapiens GN=DHCR24 PE=1 SV=2	sp|Q15392|DHC24_HUMAN	60 kDa	8	8
Estradiol 17-beta-dehydrogenase 12 OS=Homo sapiens GN=HSD17B12 PE=1 SV=2	sp|Q53GQ0|DHB12_HUMAN	34 kDa	8	12
Pumilio domain-containing protein C14orf21 OS=Homo sapiens GN=C14orf21 PE=1 SV=1	sp|Q86U38|CN021_HUMAN	69 kDa	8	2
THO complex subunit 4 OS=Homo sapiens GN=THOC4 PE=1 SV=3	sp|Q86V81|THOC4_HUMAN	27 kDa	8	2
ATP-binding cassette sub-family F member 1 OS=Homo sapiens GN=ABCF1 PE=1 SV=2	sp|Q8NE71|ABCF1_HUMAN	96 kDa	8	2
Sec1 family domain-containing protein 1 OS=Homo sapiens GN=SCFD1 PE=1 SV=4	sp|Q8WVM8|SCFD1_HUMAN	72 kDa	8	5
39S ribosomal protein L38, mitochondrial OS=Homo sapiens GN=MRPL38 PE=1 SV=2	sp|Q96DV4|RM38_HUMAN	45 kDa	8	2
Protein NipSnap homolog 1 OS=Homo sapiens GN=NIPSNAP1 PE=1 SV=1	sp|Q9BPW8|NIPS1_HUMAN	33 kDa	8	8
Mitochondrial dicarboxylate carrier OS=Homo sapiens GN=SLC25A10 PE=1 SV=2	sp|Q9UBX3|DIC_HUMAN	31 kDa	8	8
Prenylcysteine oxidase 1 OS=Homo sapiens GN=PCYOX1 PE=1 SV=3	sp|Q9UHG3|PCYOX_HUMAN	57 kDa	8	21
Insulin-like growth factor 2 mRNA-binding protein 2 OS=Homo sapiens GN=IGF2BP2 PE=1 SV=2	sp|Q9Y6M1|IF2B2_HUMAN	66 kDa	8	4
Exportin-1 OS=Homo sapiens GN=XPO1 PE=1 SV=1	sp|O14980|XPO1_HUMAN	123 kDa	7	8
GDP-mannose 4,6 dehydratase OS=Homo sapiens GN=GMDS PE=1 SV=1	sp|O60547|GMDS_HUMAN	42 kDa	7	4
General vesicular transport factor p115 OS=Homo sapiens GN=USO1 PE=1 SV=2	sp|O60763|USO1_HUMAN	108 kDa	7	4
WD repeat-containing protein 1 OS=Homo sapiens GN=WDR1 PE=1 SV=4	sp|O75083|WDR1_HUMAN	66 kDa	7	13
Core histone macro-H2A.1 OS=Homo sapiens GN=H2AFY PE=1 SV=4	sp|O75367|H2AY_HUMAN	40 kDa	7	3
U5 small nuclear ribonucleoprotein 200 kDa	sp|O75643|U520_HUMAN	245 kDa	7	0

helicase OS=Homo sapiens GN=SNRNP200 PE=1 SV=2				
Protein transport protein Sec31A OS=Homo sapiens GN=SEC31A PE=1 SV=3	sp|O94979|SC31A_HUMAN	133 kDa	7	5
Fibrinogen gamma chain OS=Homo sapiens GN=FGG PE=1 SV=3	sp|P02679|FIBG_HUMAN	52 kDa	7	9
Fatty acid-binding protein, liver OS=Homo sapiens GN=FABP1 PE=1 SV=1	sp|P07148|FABPL_HUMAN	14 kDa	7	7
Annexin A6 OS=Homo sapiens GN=ANXA6 PE=1 SV=3	sp|P08133|ANXA6_HUMAN	76 kDa	7	25
39S ribosomal protein L3, mitochondrial OS=Homo sapiens GN=MRPL3 PE=1 SV=1	sp|P09001|RM03_HUMAN	39 kDa	7	0
Pyruvate dehydrogenase E1 component subunit beta, mitochondrial OS=Homo sapiens GN=PDHB PE=1 SV=3	sp|P11177|ODPB_HUMAN	39 kDa	7	9
Proliferating cell nuclear antigen OS=Homo sapiens GN=PCNA PE=1 SV=1	sp|P12004|PCNA_HUMAN	29 kDa	7	10
Ezrin OS=Homo sapiens GN=EZR PE=1 SV=4	sp|P15311|EZRI_HUMAN	69 kDa	7	11
Aspartate aminotransferase, cytoplasmic OS=Homo sapiens GN=GOT1 PE=1 SV=3	sp|P17174|AATC_HUMAN	46 kDa	7	9
60S ribosomal protein L35a OS=Homo sapiens GN=RPL35A PE=1 SV=2	sp|P18077|RL35A_HUMAN	13 kDa	7	2
Inter-alpha-trypsin inhibitor heavy chain H2 OS=Homo sapiens GN=ITIH2 PE=1 SV=2	sp|P19823|ITIH2_HUMAN	106 kDa	7	5
DNA replication licensing factor MCM3 OS=Homo sapiens GN=MCM3 PE=1 SV=3	sp|P25205|MCM3_HUMAN	91 kDa	7	5
ATP-binding cassette sub-family D member 3 OS=Homo sapiens GN=ABCD3 PE=1 SV=1	sp|P28288|ABCD3_HUMAN	75 kDa	7	3
Endoplasmic reticulum resident protein 29 OS=Homo sapiens GN=ERP29 PE=1 SV=4	sp|P30040|ERP29_HUMAN	29 kDa	7	15
Glycerol kinase OS=Homo sapiens GN=GK PE=1 SV=3	sp|P32189|GLPK_HUMAN	61 kDa	7	8
Heterogeneous nuclear ribonucleoprotein G OS=Homo sapiens GN=RBMX PE=1 SV=3	sp|P38159|HNRPG_HUMAN	42 kDa	7	2
Eukaryotic translation initiation factor 2 subunit 3 OS=Homo sapiens GN=EIF2S3 PE=1 SV=3	sp|P41091|IF2G_HUMAN	51 kDa	7	5
Dolichyl-diphosphooligosaccharide--protein glycosyltransferase subunit STT3A OS=Homo sapiens GN=STT3A PE=1 SV=2	sp|P46977|STT3A_HUMAN	81 kDa	7	17
Nuclear autoantigenic sperm protein OS=Homo sapiens GN=NASP PE=1 SV=2	sp|P49321|NASP_HUMAN	85 kDa	7	5
Methionyl-tRNA synthetase, cytoplasmic OS=Homo sapiens GN=MARS PE=1 SV=2	sp|P56192|SYMC_HUMAN	101 kDa	7	4
Transforming protein RhoA OS=Homo sapiens GN=RHOA PE=1 SV=1	sp|P61586|RHOA_HUMAN	22 kDa	7	10
Cellular nucleic acid-binding protein OS=Homo sapiens GN=CNBP PE=1 SV=1	sp|P62633|CNBP_HUMAN	19 kDa	7	4
60S ribosomal protein L23 OS=Homo sapiens GN=RPL23 PE=1 SV=1	sp|P62829|RL23_HUMAN	15 kDa	7	3
Guanine nucleotide-binding protein G(I)/G(S)/G(T) subunit beta-1 OS=Homo sapiens GN=GNB1 PE=1 SV=3	sp|P62873|GBB1_HUMAN	37 kDa	7	5
28S ribosomal protein S9, mitochondrial OS=Homo sapiens GN=MRPS9 PE=1 SV=2	sp|P82933|RT09_HUMAN	46 kDa	7	0
Cytochrome c OS=Homo sapiens GN=CYCS PE=1 SV=2	sp|P99999|CYC_HUMAN	12 kDa	7	8
14-3-3 protein eta OS=Homo sapiens GN=YWHAH PE=1 SV=4	sp|Q04917|1433F_HUMAN	28 kDa	7	6
Bile salt sulfotransferase OS=Homo sapiens GN=SULT2A1 PE=1 SV=3	sp|Q06520|ST2A1_HUMAN	34 kDa	7	2
Quinone oxidoreductase OS=Homo sapiens GN=CRYZ PE=1 SV=1	sp|Q08257|QOR_HUMAN	35 kDa	7	13
Chromobox protein homolog 3 OS=Homo sapiens GN=CBX3 PE=1 SV=4	sp|Q13185|CBX3_HUMAN	21 kDa	7	6

Mitochondrial inner membrane protein OS=Homo sapiens GN=IMMT PE=1 SV=1	sp|Q16891|IMMT_HUMAN	84 kDa	7	16
Fibronectin type III domain-containing protein 3B OS=Homo sapiens GN=FNDC3B PE=1 SV=2	sp|Q53EP0|FND3B_HUMAN	133 kDa	7	0
Putative ATP-dependent RNA helicase DHX30 OS=Homo sapiens GN=DHX30 PE=1 SV=1	sp|Q7L2E3|DHX30_HUMAN	134 kDa	7	0
Ubiquitin thioesterase OTUB1 OS=Homo sapiens GN=OTUB1 PE=1 SV=2	sp|Q96FW1|OTUB1_HUMAN	31 kDa	7	3
Copine-1 OS=Homo sapiens GN=CPNE1 PE=1 SV=1	sp|Q99829|CPNE1_HUMAN	59 kDa	7	5
Sideroflexin-1 OS=Homo sapiens GN=SFXN1 PE=1 SV=4	sp|Q9H9B4|SFXN1_HUMAN	36 kDa	7	8
39S ribosomal protein L44, mitochondrial OS=Homo sapiens GN=MRPL44 PE=1 SV=1	sp|Q9H9J2|RM44_HUMAN	38 kDa	7	3
Obg-like ATPase 1 OS=Homo sapiens GN=OLA1 PE=1 SV=2	sp|Q9NTK5|OLA1_HUMAN	45 kDa	7	6
Cell growth-regulating nucleolar protein OS=Homo sapiens GN=LYAR PE=1 SV=2	sp|Q9NX58|LYAR_HUMAN	44 kDa	7	0
39S ribosomal protein L15, mitochondrial OS=Homo sapiens GN=MRPL15 PE=1 SV=1	sp|Q9P015|RM15_HUMAN	33 kDa	7	0
Long-chain-fatty-acid--CoA ligase 5 OS=Homo sapiens GN=ACSL5 PE=1 SV=1	sp|Q9ULC5|ACSL5_HUMAN	76 kDa	7	6
60S ribosomal protein L36 OS=Homo sapiens GN=RPL36 PE=1 SV=3	sp|Q9Y3U8|RL36_HUMAN	12 kDa	7	0
Surfeit locus protein 4 OS=Homo sapiens GN=SURF4 PE=1 SV=3	sp|O15260|SURF4_HUMAN	30 kDa	6	9
Band 4.1-like protein 2 OS=Homo sapiens GN=EPB41L2 PE=1 SV=1	sp|O43491|E41L2_HUMAN	113 kDa	6	2
Rho-associated protein kinase 2 OS=Homo sapiens GN=ROCK2 PE=1 SV=4	sp|O75116|ROCK2_HUMAN	161 kDa	6	0
Splicing factor 3B subunit 1 OS=Homo sapiens GN=SF3B1 PE=1 SV=3	sp|O75533|SF3B1_HUMAN	146 kDa	6	7
ATP synthase subunit d, mitochondrial OS=Homo sapiens GN=ATP5H PE=1 SV=3	sp|O75947|ATP5H_HUMAN	18 kDa	6	12
Ribosomal L1 domain-containing protein 1 OS=Homo sapiens GN=RSL1D1 PE=1 SV=3	sp|O76021|RL1D1_HUMAN	55 kDa	6	0
Angiotensinogen OS=Homo sapiens GN=AGT PE=1 SV=1	sp|P01019|ANGT_HUMAN	53 kDa	6	8
Transferrin receptor protein 1 OS=Homo sapiens GN=TFRC PE=1 SV=2	sp|P02786|TFR1_HUMAN	85 kDa	6	18
Apolipoprotein B-100 OS=Homo sapiens GN=APOB PE=1 SV=2	sp|P04114|APOB_HUMAN	516 kDa	6	19
40S ribosomal protein S17 OS=Homo sapiens GN=RPS17 PE=1 SV=2	sp|P08708|RS17_HUMAN	16 kDa	6	2
Dihydrolipoyllysine-residue acetyltransferase component of pyruvate dehydrogenase complex, mitochondrial OS=Homo sapiens GN=DLAT PE=1 SV=3	sp|P10515|ODP2_HUMAN	69 kDa	6	6
Inosine-5'-monophosphate dehydrogenase 2 OS=Homo sapiens GN=IMPDH2 PE=1 SV=2	sp|P12268|IMDH2_HUMAN	56 kDa	6	4
Aminopeptidase N OS=Homo sapiens GN=ANPEP PE=1 SV=4	sp|P15144|AMPN_HUMAN	110 kDa	6	11
26S protease regulatory subunit 6A OS=Homo sapiens GN=PSMC3 PE=1 SV=3	sp|P17980|PRS6A_HUMAN	49 kDa	6	7
ADP-ribosylation factor 4 OS=Homo sapiens GN=ARF4 PE=1 SV=3	sp|P18085|ARF4_HUMAN	21 kDa	6	8
Isovaleryl-CoA dehydrogenase, mitochondrial OS=Homo sapiens GN=IVD PE=1 SV=1	sp|P26440|IVD_HUMAN	46 kDa	6	6
DNA-(apurinic or apyrimidinic site) lyase OS=Homo sapiens GN=APEX1 PE=1 SV=2	sp|P27695|APEX1_HUMAN	36 kDa	6	5
Phosphoglucomutase-1 OS=Homo sapiens GN=PGM1 PE=1 SV=3	sp|P36871|PGM1_HUMAN	61 kDa	6	4
Squalene synthase OS=Homo sapiens GN=FDFT1 PE=1 SV=1	sp|P37268|FDFT_HUMAN	48 kDa	6	13

Malate dehydrogenase, cytoplasmic OS=Homo sapiens GN=MDH1 PE=1 SV=4	sp|P40925|MDHC_HUMAN	36 kDa	6	10
26S protease regulatory subunit 6B OS=Homo sapiens GN=PSMC4 PE=1 SV=2	sp|P43686|PRS6B_HUMAN	47 kDa	6	5
60S ribosomal protein L21 OS=Homo sapiens GN=RPL21 PE=1 SV=2	sp|P46778|RL21_HUMAN	19 kDa	6	2
Utrophin OS=Homo sapiens GN=UTRN PE=1 SV=2	sp|P46939|UTRO_HUMAN	394 kDa	6	0
F-actin-capping protein subunit beta OS=Homo sapiens GN=CAPZB PE=1 SV=4	sp|P47756|CAPZB_HUMAN	31 kDa	6	4
Protein ERGIC-53 OS=Homo sapiens GN=LMAN1 PE=1 SV=2	sp|P49257|LMAN1_HUMAN	58 kDa	6	14
Fragile X mental retardation syndrome-related protein 1 OS=Homo sapiens GN=FXR1 PE=1 SV=3	sp|P51114|FXR1_HUMAN	70 kDa	6	0
Ras-related protein Rab-5C OS=Homo sapiens GN=RAB5C PE=1 SV=2	sp|P51148|RAB5C_HUMAN	23 kDa	6	6
Fatty aldehyde dehydrogenase OS=Homo sapiens GN=ALDH3A2 PE=1 SV=1	sp|P51648|AL3A2_HUMAN	55 kDa	6	8
Succinate-semialdehyde dehydrogenase, mitochondrial OS=Homo sapiens GN=ALDH5A1 PE=1 SV=2	sp|P51649|SSDH_HUMAN	57 kDa	6	7
Rho GDP-dissociation inhibitor 1 OS=Homo sapiens GN=ARHGDIA PE=1 SV=3	sp|P52565|GDIR1_HUMAN	23 kDa	6	5
Puromycin-sensitive aminopeptidase OS=Homo sapiens GN=NPEPPS PE=1 SV=2	sp|P55786|PSA_HUMAN	103 kDa	6	5
40S ribosomal protein S20 OS=Homo sapiens GN=RPS20 PE=1 SV=1	sp|P60866|RS20_HUMAN	13 kDa	6	4
Actin-related protein 3 OS=Homo sapiens GN=ACTR3 PE=1 SV=3	sp|P61158|ARP3_HUMAN	47 kDa	6	3
26S protease regulatory subunit 10B OS=Homo sapiens GN=PSMC6 PE=1 SV=1	sp|P62333|PRS10_HUMAN	44 kDa	6	4
60S ribosomal protein L30 OS=Homo sapiens GN=RPL30 PE=1 SV=2	sp|P62888|RL30_HUMAN	13 kDa	6	5
60S ribosomal protein L31 OS=Homo sapiens GN=RPL31 PE=1 SV=1	sp|P62899|RL31_HUMAN	14 kDa	6	0
Transformer-2 protein homolog beta OS=Homo sapiens GN=TRA2B PE=1 SV=1	sp|P62995|TRA2B_HUMAN	34 kDa	6	0
28S ribosomal protein S25, mitochondrial OS=Homo sapiens GN=MRPS25 PE=1 SV=1	sp|P82663|RT25_HUMAN	20 kDa	6	0
Splicing factor U2AF 35 kDa subunit OS=Homo sapiens GN=U2AF1 PE=1 SV=3	sp|Q01081|U2AF1_HUMAN	28 kDa	6	2
Serine/arginine-rich splicing factor 2 OS=Homo sapiens GN=SRSF2 PE=1 SV=4	sp|Q01130|SRSF2_HUMAN	25 kDa	6	2
Galectin-3-binding protein OS=Homo sapiens GN=LGALS3BP PE=1 SV=1	sp|Q08380|LG3BP_HUMAN	65 kDa	6	5
39S ribosomal protein L28, mitochondrial OS=Homo sapiens GN=MRPL28 PE=1 SV=4	sp|Q13084|RM28_HUMAN	30 kDa	6	0
Histone deacetylase 1 OS=Homo sapiens GN=HDAC1 PE=1 SV=1	sp|Q13547|HDAC1_HUMAN	55 kDa	6	0
E3 ubiquitin/ISG15 ligase TRIM25 OS=Homo sapiens GN=TRIM25 PE=1 SV=2	sp|Q14258|TRI25_HUMAN	71 kDa	6	0
DNA damage-binding protein 1 OS=Homo sapiens GN=DDB1 PE=1 SV=1	sp|Q16531|DDB1_HUMAN	127 kDa	6	14
Hydroxyacyl-coenzyme A dehydrogenase, mitochondrial OS=Homo sapiens GN=HADH PE=1 SV=3	sp|Q16836|HCDH_HUMAN	34 kDa	6	11
Bifunctional ATP-dependent dihydroxyacetone kinase/FAD-AMP lyase (cyclizing) OS=Homo sapiens GN=DAK PE=1 SV=2	sp|Q3LXA3|DHAK_HUMAN	59 kDa	6	2
Importin-4 OS=Homo sapiens GN=IPO4 PE=1 SV=2	sp|Q8TEX9|IPO4_HUMAN	119 kDa	6	5
Dimethyladenosine transferase 1, mitochondrial OS=Homo sapiens GN=TFB1M	sp|Q8WVM0|TFB1M_HUMAN	40 kDa	6	0

PE=1 SV=1				
Regulator of nonsense transcripts 1 OS=Homo sapiens GN=UPF1 PE=1 SV=2	sp|Q92900|RENT1_HUMAN	124 kDa	6	0
Ubiquitin carboxyl-terminal hydrolase 7 OS=Homo sapiens GN=USP7 PE=1 SV=2	sp|Q93009|UBP7_HUMAN	128 kDa	6	5
AP-2 complex subunit mu OS=Homo sapiens GN=AP2M1 PE=1 SV=2	sp|Q96CW1|AP2M1_HUMAN	50 kDa	6	0
Extended synaptotagmin-1 OS=Homo sapiens GN=ESYT1 PE=1 SV=1	sp|Q9BSJ8|ESYT1_HUMAN	123 kDa	6	4
Ras-related protein Rab-1B OS=Homo sapiens GN=RAB1B PE=1 SV=1	sp|Q9H0U4|RAB1B_HUMAN	22 kDa	6	11
Phenylalanyl-tRNA synthetase beta chain OS=Homo sapiens GN=FARSB PE=1 SV=3	sp|Q9NSD9|SYFB_HUMAN	66 kDa	6	0
ATPase family AAA domain-containing protein 3A OS=Homo sapiens GN=ATAD3A PE=1 SV=2	sp|Q9NVI7|ATD3A_HUMAN	71 kDa	6	2
Trans-2,3-enoyl-CoA reductase OS=Homo sapiens GN=TECR PE=1 SV=1	sp|Q9NZ01|TECR_HUMAN	36 kDa	6	6
Ataxin-10 OS=Homo sapiens GN=ATXN10 PE=1 SV=1	sp|Q9UBB4|ATX10_HUMAN	53 kDa	6	0
DnaJ homolog subfamily B member 11 OS=Homo sapiens GN=DNAJB11 PE=1 SV=1	sp|Q9UBS4|DJB11_HUMAN	41 kDa	6	5
Stomatin-like protein 2 OS=Homo sapiens GN=STOML2 PE=1 SV=1	sp|Q9UJZ1|STML2_HUMAN	39 kDa	6	13
Proliferation-associated protein 2G4 OS=Homo sapiens GN=PA2G4 PE=1 SV=3	sp|Q9UQ80|PA2G4_HUMAN	44 kDa	6	12
UPF0568 protein C14orf166 OS=Homo sapiens GN=C14orf166 PE=1 SV=1	sp|Q9Y224|CN166_HUMAN	28 kDa	6	2
Peptidyl-tRNA hydrolase 2, mitochondrial OS=Homo sapiens GN=PTRH2 PE=1 SV=1	sp|Q9Y3E5|PTH2_HUMAN	19 kDa	6	4
Phosphoserine aminotransferase OS=Homo sapiens GN=PSAT1 PE=1 SV=2	sp|Q9Y617|SERC_HUMAN	40 kDa	6	12
Trypsin - Sus scrofa (Pig).	IPI:CON_Trypsin|SWISS-PROT:P00761|TRYP_PIG	24 kDa	5	8
Procollagen-lysine,2-oxoglutarate 5-dioxygenase 2 OS=Homo sapiens GN=PLOD2 PE=1 SV=2	sp|O00469|PLOD2_HUMAN	85 kDa	5	10
Cytochrome b5 type B OS=Homo sapiens GN=CYB5B PE=1 SV=2	sp|O43169|CYB5B_HUMAN	16 kDa	5	9
Cleavage and polyadenylation specificity factor subunit 5 OS=Homo sapiens GN=NUDT21 PE=1 SV=1	sp|O43809|CPSF5_HUMAN	26 kDa	5	4
Signal recognition particle 72 kDa protein OS=Homo sapiens GN=SRP72 PE=1 SV=3	sp|O76094|SRP72_HUMAN	75 kDa	5	0
Apoptosis-inducing factor 1, mitochondrial OS=Homo sapiens GN=AIFM1 PE=1 SV=1	sp|O95831|AIFM1_HUMAN	67 kDa	5	13
Mitochondrial import receptor subunit TOM40 homolog OS=Homo sapiens GN=TOMM40 PE=1 SV=1	sp|O96008|TOM40_HUMAN	38 kDa	5	7
NADH-cytochrome b5 reductase 3 OS=Homo sapiens GN=CYB5R3 PE=1 SV=3	sp|P00387|NB5R3_HUMAN	34 kDa	5	14
60S acidic ribosomal protein P2 OS=Homo sapiens GN=RPLP2 PE=1 SV=1	sp|P05387|RLA2_HUMAN	12 kDa	5	3
Epoxide hydrolase 1 OS=Homo sapiens GN=EPHX1 PE=1 SV=1	sp|P07099|HYEP_HUMAN	53 kDa	5	14
Calpain-1 catalytic subunit OS=Homo sapiens GN=CAPN1 PE=1 SV=1	sp|P07384|CAN1_HUMAN	82 kDa	5	0
Adenine phosphoribosyltransferase OS=Homo sapiens GN=APRT PE=1 SV=2	sp|P07741|APT_HUMAN	20 kDa	5	4
Poly [ADP-ribose] polymerase 1 OS=Homo sapiens GN=PARP1 PE=1 SV=4	sp|P09874|PARP1_HUMAN	113 kDa	5	4
Lysosomal alpha-glucosidase OS=Homo sapiens GN=GAA PE=1 SV=4	sp|P10253|LYAG_HUMAN	105 kDa	5	7
Microsomal glutathione S-transferase 1 OS=Homo sapiens GN=MGST1 PE=1 SV=1	sp|P10620|MGST1_HUMAN	18 kDa	5	7
cAMP-dependent protein kinase type I-alpha	sp|P10644|KAP0_HUMAN	43 kDa	5	4

regulatory subunit OS=Homo sapiens GN=PRKAR1A PE=1 SV=1				
Alcohol dehydrogenase class-3 OS=Homo sapiens GN=ADH5 PE=1 SV=4	sp|P11766|ADHX_HUMAN	40 kDa	5	5
Small nuclear ribonucleoprotein-associated proteins B and B' OS=Homo sapiens GN=SNRPB PE=1 SV=2	sp|P14678|RSMB_HUMAN (+1)	25 kDa	5	3
Junction plakoglobin OS=Homo sapiens GN=JUP PE=1 SV=3	sp|P14923|PLAK_HUMAN	82 kDa	5	0
Trifunctional purine biosynthetic protein adenosine-3 OS=Homo sapiens GN=GART PE=1 SV=1	sp|P22102|PUR2_HUMAN	108 kDa	5	3
Elongation factor 1-beta OS=Homo sapiens GN=EEF1B2 PE=1 SV=3	sp|P24534|EF1B_HUMAN	25 kDa	5	3
ATP synthase subunit b, mitochondrial OS=Homo sapiens GN=ATP5F1 PE=1 SV=2	sp|P24539|AT5F1_HUMAN	29 kDa	5	16
Proteasome subunit alpha type-1 OS=Homo sapiens GN=PSMA1 PE=1 SV=1	sp|P25786|PSA1_HUMAN	30 kDa	5	8
Proteasome subunit alpha type-3 OS=Homo sapiens GN=PSMA3 PE=1 SV=2	sp|P25788|PSA3_HUMAN	28 kDa	5	8
Splicing factor U2AF 65 kDa subunit OS=Homo sapiens GN=U2AF2 PE=1 SV=4	sp|P26368|U2AF2_HUMAN	54 kDa	5	2
Adenylate kinase isoenzyme 4, mitochondrial OS=Homo sapiens GN=AK4 PE=1 SV=1	sp|P27144|KAD4_HUMAN	25 kDa	5	8
Proteasome subunit alpha type-5 OS=Homo sapiens GN=PSMA5 PE=1 SV=3	sp|P28066|PSA5_HUMAN	26 kDa	5	5
Probable global transcription activator SNF2L1 OS=Homo sapiens GN=SMARCA1 PE=1 SV=2	sp|P28370|SMCA1_HUMAN	123 kDa	5	0
Cytosol aminopeptidase OS=Homo sapiens GN=LAP3 PE=1 SV=3	sp|P28838|AMPL_HUMAN	56 kDa	5	15
Serine/threonine-protein phosphatase 2A 65 kDa regulatory subunit A alpha isoform OS=Homo sapiens GN=PPP2R1A PE=1 SV=4	sp|P30153|2AAA_HUMAN	65 kDa	5	9
ER lumen protein retaining receptor 2 OS=Homo sapiens GN=KDELR2 PE=1 SV=1	sp|P33947|ERD22_HUMAN	24 kDa	5	8
Heat shock 70 kDa protein 4 OS=Homo sapiens GN=HSPA4 PE=1 SV=4	sp|P34932|HSP74_HUMAN	94 kDa	5	5
Very long-chain specific acyl-CoA dehydrogenase, mitochondrial OS=Homo sapiens GN=ACADVL PE=1 SV=1	sp|P49748|ACADV_HUMAN	70 kDa	5	13
Eukaryotic translation initiation factor 6 OS=Homo sapiens GN=EIF6 PE=1 SV=1	sp|P56537|IF6_HUMAN	27 kDa	5	3
Transmembrane protein 33 OS=Homo sapiens GN=TMEM33 PE=1 SV=2	sp|P57088|TMM33_HUMAN	28 kDa	5	2
Myosin light polypeptide 6 OS=Homo sapiens GN=MYL6 PE=1 SV=2	sp|P60660|MYL6_HUMAN	17 kDa	5	0
Ubiquitin-conjugating enzyme E2 N OS=Homo sapiens GN=UBE2N PE=1 SV=1	sp|P61088|UBE2N_HUMAN	17 kDa	5	3
26S protease regulatory subunit 4 OS=Homo sapiens GN=PSMC1 PE=1 SV=1	sp|P62191|PRS4_HUMAN	49 kDa	5	7
40S ribosomal protein S23 OS=Homo sapiens GN=RPS23 PE=1 SV=3	sp|P62266|RS23_HUMAN	16 kDa	5	3
40S ribosomal protein S24 OS=Homo sapiens GN=RPS24 PE=1 SV=1	sp|P62847|RS24_HUMAN	15 kDa	5	3
Tropomyosin alpha-4 chain OS=Homo sapiens GN=TPM4 PE=1 SV=3	sp|P67936|TPM4_HUMAN	29 kDa	5	9
Glutathione S-transferase omega-1 OS=Homo sapiens GN=GSTO1 PE=1 SV=2	sp|P78417|GSTO1_HUMAN	28 kDa	5	8
28S ribosomal protein S34, mitochondrial OS=Homo sapiens GN=MRPS34 PE=1 SV=2	sp|P82930|RT34_HUMAN	26 kDa	5	2
Methylmalonate-semialdehyde dehydrogenase [acylating], mitochondrial OS=Homo sapiens GN=ALDH6A1 PE=1 SV=2	sp|Q02252|MMSA_HUMAN	58 kDa	5	0
Histone-binding protein RBBP4 OS=Homo	sp|Q09028|RBBP4_HUMAN	48 kDa	5	4

sapiens GN=RBBP4 PE=1 SV=3				
AP-1 complex subunit beta-1 OS=Homo sapiens GN=AP1B1 PE=1 SV=2	sp|Q10567|AP1B1_HUMAN	105 kDa	5	8
Interleukin enhancer-binding factor 2 OS=Homo sapiens GN=ILF2 PE=1 SV=2	sp|Q12905|ILF2_HUMAN	43 kDa	5	11
Serine/arginine-rich splicing factor 9 OS=Homo sapiens GN=SRSF9 PE=1 SV=1	sp|Q13242|SRSF9_HUMAN	26 kDa	5	0
Eukaryotic translation initiation factor 3 subunit I OS=Homo sapiens GN=EIF3I PE=1 SV=1	sp|Q13347|EIF3I_HUMAN	37 kDa	5	3
Nascent polypeptide-associated complex subunit alpha OS=Homo sapiens GN=NACA PE=1 SV=1	sp|Q13765|NACA_HUMAN	23 kDa	5	6
Caprin-1 OS=Homo sapiens GN=CAPRIN1 PE=1 SV=2	sp|Q14444|CAPR1_HUMAN	78 kDa	5	0
DNA replication licensing factor MCM6 OS=Homo sapiens GN=MCM6 PE=1 SV=1	sp|Q14566|MCM6_HUMAN	93 kDa	5	0
Poly(rC)-binding protein 2 OS=Homo sapiens GN=PCBP2 PE=1 SV=1	sp|Q15366|PCBP2_HUMAN	39 kDa	5	0
ELAV-like protein 1 OS=Homo sapiens GN=ELAVL1 PE=1 SV=2	sp|Q15717|ELAV1_HUMAN	36 kDa	5	0
Hsp90 co-chaperone Cdc37 OS=Homo sapiens GN=CDC37 PE=1 SV=1	sp|Q16543|CDC37_HUMAN	44 kDa	5	2
Histone-binding protein RBBP7 OS=Homo sapiens GN=RBBP7 PE=1 SV=1	sp|Q16576|RBBP7_HUMAN	48 kDa	5	0
Fascin OS=Homo sapiens GN=FSCN1 PE=1 SV=3	sp|Q16658|FSCN1_HUMAN	55 kDa	5	5
Endoplasmic reticulum metallopeptidase 1 OS=Homo sapiens GN=ERMP1 PE=1 SV=2	sp|Q7Z2K6|ERMP1_HUMAN	100 kDa	5	10
Cullin-associated NEDD8-dissociated protein 1 OS=Homo sapiens GN=CAND1 PE=1 SV=2	sp|Q86VP6|CAND1_HUMAN	136 kDa	5	7
Dolichyl-diphosphooligosaccharide--protein glycosyltransferase subunit STT3B OS=Homo sapiens GN=STT3B PE=1 SV=1	sp|Q8TCJ2|STT3B_HUMAN	94 kDa	5	7
Far upstream element-binding protein 2 OS=Homo sapiens GN=KHSRP PE=1 SV=4	sp|Q92945|FUBP2_HUMAN	73 kDa	5	4
Transportin-1 OS=Homo sapiens GN=TNPO1 PE=1 SV=2	sp|Q92973|TNPO1_HUMAN	102 kDa	5	0
Serine/threonine-protein phosphatase PGAM5, mitochondrial OS=Homo sapiens GN=PGAM5 PE=1 SV=2	sp|Q96HS1|PGAM5_HUMAN	32 kDa	5	0
Serine/threonine-protein kinase SRPK1 OS=Homo sapiens GN=SRPK1 PE=1 SV=2	sp|Q96SB4|SRPK1_HUMAN	74 kDa	5	0
Synaptic vesicle membrane protein VAT-1 homolog OS=Homo sapiens GN=VAT1 PE=1 SV=2	sp|Q99536|VAT1_HUMAN	42 kDa	5	5
Translational activator of cytochrome c oxidase 1 OS=Homo sapiens GN=TACO1 PE=1 SV=1	sp|Q9BSH4|TACO1_HUMAN	32 kDa	5	2
Transmembrane emp24 domain-containing protein 9 OS=Homo sapiens GN=TMED9 PE=1 SV=2	sp|Q9BVK6|TMED9_HUMAN	27 kDa	5	9
39S ribosomal protein L4, mitochondrial OS=Homo sapiens GN=MRPL4 PE=1 SV=1	sp|Q9BYD3|RM04_HUMAN	35 kDa	5	0
28S ribosomal protein S26, mitochondrial OS=Homo sapiens GN=MRPS26 PE=1 SV=1	sp|Q9BYN8|RT26_HUMAN	24 kDa	5	0
28S ribosomal protein S30, mitochondrial OS=Homo sapiens GN=MRPS30 PE=1 SV=2	sp|Q9NP92|RT30_HUMAN	50 kDa	5	0
Isoleucyl-tRNA synthetase, mitochondrial OS=Homo sapiens GN=IARS2 PE=1 SV=2	sp|Q9NSE4|SYIM_HUMAN	114 kDa	5	15
Protein RCC2 OS=Homo sapiens GN=RCC2 PE=1 SV=2	sp|Q9P258|RCC2_HUMAN	56 kDa	5	3
Signal recognition particle 68 kDa protein OS=Homo sapiens GN=SRP68 PE=1 SV=2	sp|Q9UHB9|SRP68_HUMAN	71 kDa	5	3
Pre-mRNA-processing factor 19 OS=Homo sapiens GN=PRPF19 PE=1 SV=1	sp|Q9UMS4|PRP19_HUMAN	55 kDa	5	0
RuvB-like 2 OS=Homo sapiens GN=RUVBL2	sp|Q9Y230|RUVB2_HUMAN	51 kDa	5	0

PE=1 SV=3				
Cofilin-2 OS=Homo sapiens GN=CFL2 PE=1 SV=1	sp|Q9Y281|COF2_HUMAN	19 kDa	5	4
Transducin beta-like protein 2 OS=Homo sapiens GN=TBL2 PE=1 SV=1	sp|Q9Y4P3|TBL2_HUMAN	50 kDa	5	0
Insulin-like growth factor 2 mRNA-binding protein 3 OS=Homo sapiens GN=IGF2BP3 PE=1 SV=2	sp|O00425|IF2B3_HUMAN	64 kDa	4	0
Coatomer subunit epsilon OS=Homo sapiens GN=COPE PE=1 SV=3	sp|O14579|COPE_HUMAN	34 kDa	4	4
Protein arginine N-methyltransferase 5 OS=Homo sapiens GN=PRMT5 PE=1 SV=4	sp|O14744|ANM5_HUMAN	73 kDa	4	0
Na(+)/H(+) exchange regulatory cofactor NHE-RF1 OS=Homo sapiens GN=SLC9A3R1 PE=1 SV=4	sp|O14745|NHRF1_HUMAN	39 kDa	4	5
Membrane-associated progesterone receptor component 2 OS=Homo sapiens GN=PGRMC2 PE=1 SV=1	sp|O15173|PGRC2_HUMAN	24 kDa	4	6
Laminin subunit alpha-5 OS=Homo sapiens GN=LAMA5 PE=1 SV=8	sp|O15230|LAMA5_HUMAN	400 kDa	4	0
Mitotic checkpoint protein BUB3 OS=Homo sapiens GN=BUB3 PE=1 SV=1	sp|O43684|BUB3_HUMAN	37 kDa	4	2
AP-1 complex subunit gamma-1 OS=Homo sapiens GN=AP1G1 PE=1 SV=5	sp|O43747|AP1G1_HUMAN	91 kDa	4	3
Perilipin-3 OS=Homo sapiens GN=PLIN3 PE=1 SV=3	sp|O60664|PLIN3_HUMAN	47 kDa	4	3
Mitochondrial-processing peptidase subunit beta OS=Homo sapiens GN=PMPCB PE=1 SV=2	sp|O75439|MPPB_HUMAN	54 kDa	4	5
NADH dehydrogenase [ubiquinone] iron-sulfur protein 3, mitochondrial OS=Homo sapiens GN=NDUFS3 PE=1 SV=1	sp|O75489|NDUS3_HUMAN	30 kDa	4	7
Luc7-like protein 3 OS=Homo sapiens GN=LUC7L3 PE=1 SV=2	sp|O95232|LC7L3_HUMAN	51 kDa	4	0
Sphingosine-1-phosphate lyase 1 OS=Homo sapiens GN=SGPL1 PE=1 SV=3	sp|O95470|SGPL1_HUMAN	64 kDa	4	0
Cytochrome c oxidase subunit 2 OS=Homo sapiens GN=MT-CO2 PE=1 SV=1	sp|P00403|COX2_HUMAN	26 kDa	4	5
Alpha-1-antitrypsin OS=Homo sapiens GN=SERPINA1 PE=1 SV=3	sp|P01009|A1AT_HUMAN	47 kDa	4	7
Apolipoprotein E OS=Homo sapiens GN=APOE PE=1 SV=1	sp|P02649|APOE_HUMAN	36 kDa	4	7
Sodium/potassium-transporting ATPase subunit beta-1 OS=Homo sapiens GN=ATP1B1 PE=1 SV=1	sp|P05026|AT1B1_HUMAN	35 kDa	4	6
60S acidic ribosomal protein P1 OS=Homo sapiens GN=RPLP1 PE=1 SV=1	sp|P05386|RLA1_HUMAN	12 kDa	4	0
Asialoglycoprotein receptor 1 OS=Homo sapiens GN=ASGR1 PE=1 SV=2	sp|P07306|ASGR1_HUMAN	33 kDa	4	10
Fumarate hydratase, mitochondrial OS=Homo sapiens GN=FH PE=1 SV=3	sp|P07954|FUMH_HUMAN	55 kDa	4	11
U1 small nuclear ribonucleoprotein A OS=Homo sapiens GN=SNRPA PE=1 SV=3	sp|P09012|SNRPA_HUMAN	31 kDa	4	3
Thioredoxin OS=Homo sapiens GN=TXN PE=1 SV=3	sp|P10599|THIO_HUMAN	12 kDa	4	3
Lysosomal protective protein OS=Homo sapiens GN=CTSA PE=1 SV=2	sp|P10619|PPGB_HUMAN	54 kDa	4	7
Solute carrier family 2, facilitated glucose transporter member 3 OS=Homo sapiens GN=SLC2A3 PE=1 SV=1	sp|P11169|GTR3_HUMAN	54 kDa	4	8
DNA topoisomerase 2-alpha OS=Homo sapiens GN=TOP2A PE=1 SV=3	sp|P11388|TOP2A_HUMAN	174 kDa	4	0
Macrophage migration inhibitory factor OS=Homo sapiens GN=MIF PE=1 SV=4	sp|P14174|MIF_HUMAN	12 kDa	4	0
Desmoplakin OS=Homo sapiens GN=DSP PE=1 SV=3	sp|P15924|DESP_HUMAN	332 kDa	4	0

Glutathione S-transferase Mu 3 OS=Homo sapiens GN=GSTM3 PE=1 SV=3	sp|P21266|GSTM3_HUMAN	27 kDa	4	2
Cytoplasmic aconitate hydratase OS=Homo sapiens GN=ACO1 PE=1 SV=3	sp|P21399|ACOC_HUMAN	98 kDa	4	3
Proteasome subunit alpha type-2 OS=Homo sapiens GN=PSMA2 PE=1 SV=2	sp|P25787|PSA2_HUMAN	26 kDa	4	6
Proteasome subunit alpha type-4 OS=Homo sapiens GN=PSMA4 PE=1 SV=1	sp|P25789|PSA4_HUMAN	29 kDa	4	5
High mobility group protein B2 OS=Homo sapiens GN=HMGB2 PE=1 SV=2	sp|P26583|HMGB2_HUMAN	24 kDa	4	5
UMP-CMP kinase OS=Homo sapiens GN=CMPK1 PE=1 SV=3	sp|P30085|KCY_HUMAN	22 kDa	4	2
DNA replication licensing factor MCM7 OS=Homo sapiens GN=MCM7 PE=1 SV=4	sp|P33993|MCM7_HUMAN	81 kDa	4	0
26S protease regulatory subunit 7 OS=Homo sapiens GN=PSMC2 PE=1 SV=3	sp|P35998|PRS7_HUMAN	49 kDa	4	2
Dihydrolipoyllysine-residue succinyltransferase component of 2-oxoglutarate dehydrogenase complex, mitochondrial OS=Homo sapiens GN=DLST PE=1 SV=4	sp|P36957|ODO2_HUMAN	49 kDa	4	6
3,2-trans-enoyl-CoA isomerase, mitochondrial OS=Homo sapiens GN=DCI PE=1 SV=1	sp|P42126|D3D2_HUMAN	33 kDa	4	6
Translocon-associated protein subunit alpha OS=Homo sapiens GN=SSR1 PE=1 SV=3	sp|P43307|SSRA_HUMAN	32 kDa	4	5
Vesicle-fusing ATPase OS=Homo sapiens GN=NSF PE=1 SV=3	sp|P46459|NSF_HUMAN	83 kDa	4	2
60S ribosomal protein L28 OS=Homo sapiens GN=RPL28 PE=1 SV=3	sp|P46779|RL28_HUMAN	16 kDa	4	4
40S ribosomal protein S10 OS=Homo sapiens GN=RPS10 PE=1 SV=1	sp|P46783|RS10_HUMAN	19 kDa	4	2
Coatomer subunit delta OS=Homo sapiens GN=ARCN1 PE=1 SV=1	sp|P48444|COPD_HUMAN	57 kDa	4	0
Alpha-aminoadipic semialdehyde dehydrogenase OS=Homo sapiens GN=ALDH7A1 PE=1 SV=5	sp|P49419|AL7A1_HUMAN	58 kDa	4	7
F-actin-capping protein subunit alpha-1 OS=Homo sapiens GN=CAPZA1 PE=1 SV=3	sp|P52907|CAZA1_HUMAN	33 kDa	4	4
Proteasome subunit alpha type-6 OS=Homo sapiens GN=PSMA6 PE=1 SV=1	sp|P60900|PSA6_HUMAN	27 kDa	4	6
Ras-related protein Rab-10 OS=Homo sapiens GN=RAB10 PE=1 SV=1	sp|P61026|RAB10_HUMAN	23 kDa	4	6
Calmodulin OS=Homo sapiens GN=CALM1 PE=1 SV=2	sp|P62158|CALM_HUMAN	17 kDa	4	0
26S protease regulatory subunit 8 OS=Homo sapiens GN=PSMC5 PE=1 SV=1	sp|P62195|PRS8_HUMAN	46 kDa	4	7
Small nuclear ribonucleoprotein Sm D1 OS=Homo sapiens GN=SNRPD1 PE=1 SV=1	sp|P62314|SMD1_HUMAN	13 kDa	4	0
Small nuclear ribonucleoprotein Sm D3 OS=Homo sapiens GN=SNRPD3 PE=1 SV=1	sp|P62318|SMD3_HUMAN	14 kDa	4	2
Ras-related protein Rab-11A OS=Homo sapiens GN=RAB11A PE=1 SV=3	sp|P62491|RB11A_HUMAN	24 kDa	4	5
Eukaryotic peptide chain release factor subunit 1 OS=Homo sapiens GN=ETF1 PE=1 SV=3	sp|P62495|ERF1_HUMAN	49 kDa	4	4
Peptidyl-prolyl cis-trans isomerase FKBP1A OS=Homo sapiens GN=FKBP1A PE=1 SV=2	sp|P62942|FKB1A_HUMAN	12 kDa	4	4
Dynein light chain 1, cytoplasmic OS=Homo sapiens GN=DYNLL1 PE=1 SV=1	sp|P63167|DYL1_HUMAN	10 kDa	4	0
28S ribosomal protein S22, mitochondrial OS=Homo sapiens GN=MRPS22 PE=1 SV=1	sp|P82650|RT22_HUMAN	41 kDa	4	2
28S ribosomal protein S5, mitochondrial OS=Homo sapiens GN=MRPS5 PE=1 SV=2	sp|P82675|RT05_HUMAN	48 kDa	4	0
Enhancer of rudimentary homolog OS=Homo sapiens GN=ERH PE=1 SV=1	sp|P84090|ERH_HUMAN	12 kDa	4	0
Protein SET OS=Homo sapiens GN=SET PE=1	sp|Q01105|SET_HUMAN	33 kDa	4	3

SV=3				
Lactoylglutathione lyase OS=Homo sapiens GN=GLO1 PE=1 SV=4	sp|Q04760|LGUL_HUMAN	21 kDa	4	2
Aminoacyl tRNA synthase complex-interacting multifunctional protein 2 OS=Homo sapiens GN=AIMP2 PE=1 SV=2	sp|Q13155|AIMP2_HUMAN	35 kDa	4	5
Malectin OS=Homo sapiens GN=MLEC PE=1 SV=1	sp|Q14165|MLEC_HUMAN	32 kDa	4	9
Nuclear mitotic apparatus protein 1 OS=Homo sapiens GN=NUMA1 PE=1 SV=2	sp|Q14980|NUMA1_HUMAN	238 kDa	4	0
Signal peptidase complex subunit 2 OS=Homo sapiens GN=SPCS2 PE=1 SV=3	sp|Q15005|SPCS2_HUMAN	25 kDa	4	4
Squamous cell carcinoma antigen recognized by T-cells 3 OS=Homo sapiens GN=SART3 PE=1 SV=1	sp|Q15020|SART3_HUMAN	110 kDa	4	0
Early endosome antigen 1 OS=Homo sapiens GN=EEA1 PE=1 SV=2	sp|Q15075|EEA1_HUMAN	162 kDa	4	0
Nicotinate-nucleotide pyrophosphorylase [carboxylating] OS=Homo sapiens GN=QPRT PE=1 SV=3	sp|Q15274|NADC_HUMAN	31 kDa	4	6
Cleavage and polyadenylation specificity factor subunit 6 OS=Homo sapiens GN=CPSF6 PE=1 SV=2	sp|Q16630|CPSF6_HUMAN	59 kDa	4	2
NADH dehydrogenase [ubiquinone] 1 alpha subcomplex subunit 9, mitochondrial OS=Homo sapiens GN=NDUFA9 PE=1 SV=2	sp|Q16795|NDUA9_HUMAN	43 kDa	4	12
Heterochromatin protein 1-binding protein 3 OS=Homo sapiens GN=HP1BP3 PE=1 SV=1	sp|Q5SSJ5|HP1B3_HUMAN	61 kDa	4	0
39S ribosomal protein L2, mitochondrial OS=Homo sapiens GN=MRPL2 PE=1 SV=2	sp|Q5T653|RM02_HUMAN	33 kDa	4	0
Hydroxysteroid dehydrogenase-like protein 2 OS=Homo sapiens GN=HSDL2 PE=1 SV=1	sp|Q6YN16|HSDL2_HUMAN	45 kDa	4	7
Inhibitor of nuclear factor kappa-B kinase-interacting protein OS=Homo sapiens GN=IKBIP PE=1 SV=1	sp|Q70UQ0|IKIP_HUMAN	39 kDa	4	6
40S ribosomal protein S27-like OS=Homo sapiens GN=RPS27L PE=1 SV=3	sp|Q71UM5|RS27L_HUMAN	9 kDa	4	0
39S ribosomal protein L21, mitochondrial OS=Homo sapiens GN=MRPL21 PE=1 SV=2	sp|Q7Z2W9|RM21_HUMAN	23 kDa	4	0
Eukaryotic peptide chain release factor GTP-binding subunit ERF3B OS=Homo sapiens GN=GSPT2 PE=1 SV=2	sp|Q8IYD1|ERF3B_HUMAN	69 kDa	4	3
39S ribosomal protein L43, mitochondrial OS=Homo sapiens GN=MRPL43 PE=1 SV=1	sp|Q8N983|RM43_HUMAN	23 kDa	4	0
Procollagen galactosyltransferase 1 OS=Homo sapiens GN=GLT25D1 PE=1 SV=1	sp|Q8NBJ5|GT251_HUMAN	72 kDa	4	6
Probable saccharopine dehydrogenase OS=Homo sapiens GN=SCCPDH PE=1 SV=1	sp|Q8NBX0|SCPDH_HUMAN	47 kDa	4	7
Programmed cell death 6-interacting protein OS=Homo sapiens GN=PDCD6IP PE=1 SV=1	sp|Q8WUM4|PDC6I_HUMAN	96 kDa	4	0
Zinc transporter SLC39A7 OS=Homo sapiens GN=SLC39A7 PE=1 SV=2	sp|Q92504|S39A7_HUMAN	50 kDa	4	3
Histone H1x OS=Homo sapiens GN=H1FX PE=1 SV=1	sp|Q92522|H1X_HUMAN	22 kDa	4	0
Heat shock protein 105 kDa OS=Homo sapiens GN=HSPH1 PE=1 SV=1	sp|Q92598|HS105_HUMAN	97 kDa	4	5
Gamma-glutamyl hydrolase OS=Homo sapiens GN=GGH PE=1 SV=2	sp|Q92820|GGH_HUMAN	36 kDa	4	8
UPF0556 protein C19orf10 OS=Homo sapiens GN=C19orf10 PE=1 SV=1	sp|Q969H8|CS010_HUMAN	19 kDa	4	4
GPI transamidase component PIG-T OS=Homo sapiens GN=PIGT PE=1 SV=1	sp|Q969N2|PIGT_HUMAN	66 kDa	4	0
Sodium-coupled neutral amino acid transporter 2 OS=Homo sapiens GN=SLC38A2 PE=1 SV=2	sp|Q96QD8|S38A2_HUMAN	56 kDa	4	12

Vacuolar protein sorting-associated protein 35 OS=Homo sapiens GN=VPS35 PE=1 SV=2	sp|Q96QK1|VPS35_HUMAN	92 kDa	4	2
26S proteasome non-ATPase regulatory subunit 1 OS=Homo sapiens GN=PSMD1 PE=1 SV=2	sp|Q99460|PSMD1_HUMAN	106 kDa	4	6
Protein arginine N-methyltransferase 1 OS=Homo sapiens GN=PRMT1 PE=1 SV=2	sp|Q99873|ANM1_HUMAN	42 kDa	4	8
Heterogeneous nuclear ribonucleoprotein U-like protein 1 OS=Homo sapiens GN=HNRNPUL1 PE=1 SV=2	sp|Q9BUJ2|HNRL1_HUMAN	96 kDa	4	0
Serrate RNA effector molecule homolog OS=Homo sapiens GN=SRRT PE=1 SV=1	sp|Q9BXP5|SRRT_HUMAN	101 kDa	4	0
AP-1 complex subunit mu-1 OS=Homo sapiens GN=AP1M1 PE=1 SV=3	sp|Q9BXS5|AP1M1_HUMAN	49 kDa	4	0
39S ribosomal protein L13, mitochondrial OS=Homo sapiens GN=MRPL13 PE=1 SV=1	sp|Q9BYD1|RM13_HUMAN	21 kDa	4	0
39S ribosomal protein L37, mitochondrial OS=Homo sapiens GN=MRPL37 PE=1 SV=2	sp|Q9BZE1|RM37_HUMAN	48 kDa	4	2
39S ribosomal protein L18, mitochondrial OS=Homo sapiens GN=MRPL18 PE=1 SV=1	sp|Q9H0U6|RM18_HUMAN	21 kDa	4	0
Golgi phosphoprotein 3 OS=Homo sapiens GN=GOLPH3 PE=1 SV=1	sp|Q9H4A6|GOLP3_HUMAN	34 kDa	4	2
GrpE protein homolog 1, mitochondrial OS=Homo sapiens GN=GRPEL1 PE=1 SV=2	sp|Q9HAV7|GRPE1_HUMAN	24 kDa	4	6
Sialic acid synthase OS=Homo sapiens GN=NANS PE=1 SV=2	sp|Q9NR45|SIAS_HUMAN	40 kDa	4	5
7-dehydrocholesterol reductase OS=Homo sapiens GN=DHCR7 PE=1 SV=1	sp|Q9UBM7|DHCR7_HUMAN	54 kDa	4	6
Glyoxylate reductase/hydroxypyruvate reductase OS=Homo sapiens GN=GRHPR PE=1 SV=1	sp|Q9UBQ7|GRHPR_HUMAN	36 kDa	4	0
F-box only protein 2 OS=Homo sapiens GN=FBXO2 PE=1 SV=2	sp|Q9UK22|FBX2_HUMAN	33 kDa	4	2
RNA-binding protein Raly OS=Homo sapiens GN=RALY PE=1 SV=1	sp|Q9UKM9|RALY_HUMAN	32 kDa	4	4
Protein canopy homolog 2 OS=Homo sapiens GN=CNPY2 PE=1 SV=1	sp|Q9Y2B0|CNPY2_HUMAN	21 kDa	4	6
Thyroid hormone receptor-associated protein 3 OS=Homo sapiens GN=THRAP3 PE=1 SV=2	sp|Q9Y2W1|TR150_HUMAN	109 kDa	4	0
AFG3-like protein 2 OS=Homo sapiens GN=AFG3L2 PE=1 SV=2	sp|Q9Y4W6|AFG32_HUMAN	89 kDa	4	3
(Bos taurus) Alpha-2-HS-glycoprotein precursor	IPI:CON_00707101.1|SWISS-PROT:P12763	38 kDa	3	10
Myosin-Ic OS=Homo sapiens GN=MYO1C PE=1 SV=4	sp|O00159|MYO1C_HUMAN	122 kDa	3	0
26S proteasome non-ATPase regulatory subunit 12 OS=Homo sapiens GN=PSMD12 PE=1 SV=3	sp|O00232|PSD12_HUMAN	53 kDa	3	7
26S proteasome non-ATPase regulatory subunit 14 OS=Homo sapiens GN=PSMD14 PE=1 SV=1	sp|O00487|PSDE_HUMAN	35 kDa	3	0
Ribonuclease T2 OS=Homo sapiens GN=RNASET2 PE=1 SV=2	sp|O00584|RNT2_HUMAN	29 kDa	3	3
Tripeptidyl-peptidase 1 OS=Homo sapiens GN=TPP1 PE=1 SV=2	sp|O14773|TPP1_HUMAN	61 kDa	3	3
Eukaryotic translation initiation factor 3 subunit D OS=Homo sapiens GN=EIF3D PE=1 SV=1	sp|O15371|EIF3D_HUMAN	64 kDa	3	5
Eukaryotic translation initiation factor 3 subunit H OS=Homo sapiens GN=EIF3H PE=1 SV=1	sp|O15372|EIF3H_HUMAN	40 kDa	3	0
Bifunctional 3'-phosphoadenosine 5'-phosphosulfate synthase 1 OS=Homo sapiens GN=PAPSS1 PE=1 SV=2	sp|O43252|PAPS1_HUMAN	71 kDa	3	0
Aldo-keto reductase family 1 member B10 OS=Homo sapiens GN=AKR1B10 PE=1 SV=2	sp|O60218|AK1BA_HUMAN	36 kDa	3	6
Importin subunit alpha-7 OS=Homo sapiens GN=KPNA6 PE=1 SV=1	sp|O60684|IMA7_HUMAN	60 kDa	3	2
Dolichol-phosphate mannosyltransferase OS=Homo sapiens GN=DPM1 PE=1 SV=1	sp|O60762|DPM1_HUMAN	30 kDa	3	0

DnaJ homolog subfamily A member 2 OS=Homo sapiens GN=DNAJA2 PE=1 SV=1	sp|O60884|DNJA2_HUMAN	46 kDa	3	0
Copine-3 OS=Homo sapiens GN=CPNE3 PE=1 SV=1	sp|O75131|CPNE3_HUMAN	60 kDa	3	0
NADH dehydrogenase [ubiquinone] iron-sulfur protein 2, mitochondrial OS=Homo sapiens GN=NDUFS2 PE=1 SV=2	sp|O75306|NDUS2_HUMAN	53 kDa	3	6
Serine/arginine-rich splicing factor 10 OS=Homo sapiens GN=SRSF10 PE=1 SV=1	sp|O75494|SRS10_HUMAN	31 kDa	3	0
Cold shock domain-containing protein E1 OS=Homo sapiens GN=CSDE1 PE=1 SV=2	sp|O75534|CSDE1_HUMAN	89 kDa	3	0
Interferon-inducible double stranded RNA-dependent protein kinase activator A OS=Homo sapiens GN=PRKRA PE=1 SV=1	sp|O75569|PRKRA_HUMAN	34 kDa	3	0
Phosphoacetylglucosamine mutase OS=Homo sapiens GN=PGM3 PE=1 SV=1	sp|O95394|AGM1_HUMAN	60 kDa	3	0
Thioredoxin domain-containing protein 12 OS=Homo sapiens GN=TXNDC12 PE=1 SV=1	sp|O95881|TXD12_HUMAN	19 kDa	3	2
Formimidoyltransferase-cyclodeaminase OS=Homo sapiens GN=FTCD PE=1 SV=2	sp|O95954|FTCD_HUMAN	59 kDa	3	0
Alpha-2-HS-glycoprotein OS=Homo sapiens GN=AHSG PE=1 SV=1	sp|P02765|FETUA_HUMAN	39 kDa	3	5
Guanine nucleotide-binding protein G(i) subunit alpha-2 OS=Homo sapiens GN=GNAI2 PE=1 SV=3	sp|P04899|GNAI2_HUMAN	40 kDa	3	3
Eukaryotic translation initiation factor 2 subunit 1 OS=Homo sapiens GN=EIF2S1 PE=1 SV=3	sp|P05198|IF2A_HUMAN	36 kDa	3	2
Integrin beta-1 OS=Homo sapiens GN=ITGB1 PE=1 SV=2	sp|P05556|ITB1_HUMAN	88 kDa	3	10
Cyclin-dependent kinase 1 OS=Homo sapiens GN=CDK1 PE=1 SV=2	sp|P06493|CDK1_HUMAN	34 kDa	3	0
Acyl-CoA-binding protein OS=Homo sapiens GN=DBI PE=1 SV=2	sp|P07108|ACBP_HUMAN	10 kDa	3	2
Laminin subunit beta-1 OS=Homo sapiens GN=LAMB1 PE=1 SV=2	sp|P07942|LAMB1_HUMAN	198 kDa	3	0
Galectin-1 OS=Homo sapiens GN=LGALS1 PE=1 SV=2	sp|P09382|LEG1_HUMAN	15 kDa	3	4
Dihydropteridine reductase OS=Homo sapiens GN=QDPR PE=1 SV=2	sp|P09417|DHPR_HUMAN	26 kDa	3	6
Complement C4-A OS=Homo sapiens GN=C4A PE=1 SV=1	sp|P0C0L4|CO4A_HUMAN (+1)	193 kDa	3	0
S-formylglutathione hydrolase OS=Homo sapiens GN=ESD PE=1 SV=2	sp|P10768|ESTD_HUMAN	31 kDa	3	3
Medium-chain specific acyl-CoA dehydrogenase, mitochondrial OS=Homo sapiens GN=ACADM PE=1 SV=1	sp|P11310|ACADM_HUMAN	47 kDa	3	6
DNA topoisomerase 1 OS=Homo sapiens GN=TOP1 PE=1 SV=2	sp|P11387|TOP1_HUMAN	91 kDa	3	3
Nucleoprotein TPR OS=Homo sapiens GN=TPR PE=1 SV=3	sp|P12270|TPR_HUMAN	267 kDa	3	0
Creatine kinase B-type OS=Homo sapiens GN=CKB PE=1 SV=1	sp|P12277|KCRB_HUMAN	43 kDa	3	3
Proto-oncogene tyrosine-protein kinase Src OS=Homo sapiens GN=SRC PE=1 SV=3	sp|P12931|SRC_HUMAN	60 kDa	3	3
Translationally-controlled tumor protein OS=Homo sapiens GN=TPT1 PE=1 SV=1	sp|P13693|TCTP_HUMAN	20 kDa	3	5
Alcohol dehydrogenase [NADP+] OS=Homo sapiens GN=AKR1A1 PE=1 SV=3	sp|P14550|AK1A1_HUMAN	37 kDa	3	3
Proteasome subunit beta type-1 OS=Homo sapiens GN=PSMB1 PE=1 SV=2	sp|P20618|PSB1_HUMAN	26 kDa	3	6
Cytochrome c oxidase subunit 5A, mitochondrial OS=Homo sapiens GN=COX5A PE=1 SV=2	sp|P20674|COX5A_HUMAN	17 kDa	3	0
V-type proton ATPase subunit B, brain isoform	sp|P21281|VATB2_HUMAN	57 kDa	3	4

OS=Homo sapiens GN=ATP6V1B2 PE=1 SV=3				
Catechol O-methyltransferase OS=Homo sapiens GN=COMT PE=1 SV=2	sp|P21964|COMT_HUMAN	30 kDa	3	2
Probable ATP-dependent RNA helicase DDX6 OS=Homo sapiens GN=DDX6 PE=1 SV=2	sp|P26196|DDX6_HUMAN	54 kDa	3	3
Peptidyl-prolyl cis-trans isomerase F, mitochondrial OS=Homo sapiens GN=PPIF PE=1 SV=1	sp|P30405|PPIF_HUMAN	22 kDa	3	9
Glycylpeptide N-tetradecanoyltransferase 1 OS=Homo sapiens GN=NMT1 PE=1 SV=2	sp|P30419|NMT1_HUMAN	57 kDa	3	0
Alpha-2-macroglobulin receptor-associated protein OS=Homo sapiens GN=LRPAP1 PE=1 SV=1	sp|P30533|AMRP_HUMAN	41 kDa	3	5
3-hydroxyisobutyrate dehydrogenase, mitochondrial OS=Homo sapiens GN=HIBADH PE=1 SV=2	sp|P31937|3HIDH_HUMAN	35 kDa	3	8
DNA replication licensing factor MCM5 OS=Homo sapiens GN=MCM5 PE=1 SV=5	sp|P33992|MCM5_HUMAN	82 kDa	3	0
Signal recognition particle 14 kDa protein OS=Homo sapiens GN=SRP14 PE=1 SV=2	sp|P37108|SRP14_HUMAN	15 kDa	3	2
ADP-ribosylation factor-like protein 1 OS=Homo sapiens GN=ARL1 PE=1 SV=1	sp|P40616|ARL1_HUMAN	20 kDa	3	0
Lysosomal Pro-X carboxypeptidase OS=Homo sapiens GN=PRCP PE=1 SV=1	sp|P42785|PCP_HUMAN	56 kDa	3	4
60S ribosomal protein L29 OS=Homo sapiens GN=RPL29 PE=1 SV=2	sp|P47914|RL29_HUMAN	18 kDa	3	3
Dimethylaniline monooxygenase [N-oxide-forming] 5 OS=Homo sapiens GN=FMO5 PE=2 SV=2	sp|P49326|FMO5_HUMAN	60 kDa	3	0
Proteasome subunit beta type-3 OS=Homo sapiens GN=PSMB3 PE=1 SV=2	sp|P49720|PSB3_HUMAN	23 kDa	3	5
Histidine triad nucleotide-binding protein 1 OS=Homo sapiens GN=HINT1 PE=1 SV=2	sp|P49773|HINT1_HUMAN	14 kDa	3	0
Basal cell adhesion molecule OS=Homo sapiens GN=BCAM PE=1 SV=2	sp|P50895|BCAM_HUMAN	67 kDa	3	5
Galactokinase OS=Homo sapiens GN=GALK1 PE=1 SV=1	sp|P51570|GALK1_HUMAN	42 kDa	3	0
Translocon-associated protein subunit delta OS=Homo sapiens GN=SSR4 PE=1 SV=1	sp|P51571|SSRD_HUMAN	19 kDa	3	4
B-cell receptor-associated protein 31 OS=Homo sapiens GN=BCAP31 PE=1 SV=3	sp|P51572|BAP31_HUMAN	28 kDa	3	9
26S proteasome non-ATPase regulatory subunit 7 OS=Homo sapiens GN=PSMD7 PE=1 SV=2	sp|P51665|PSD7_HUMAN	37 kDa	3	3
Importin subunit alpha-2 OS=Homo sapiens GN=KPNA2 PE=1 SV=1	sp|P52292|IMA2_HUMAN	58 kDa	3	0
39S ribosomal protein L12, mitochondrial OS=Homo sapiens GN=MRPL12 PE=1 SV=2	sp|P52815|RM12_HUMAN	21 kDa	3	4
Biliverdin reductase A OS=Homo sapiens GN=BLVRA PE=1 SV=2	sp|P53004|BIEA_HUMAN	33 kDa	3	2
Dipeptidyl peptidase 1 OS=Homo sapiens GN=CTSC PE=1 SV=2	sp|P53634|CATC_HUMAN	52 kDa	3	0
Protein transport protein Sec24C OS=Homo sapiens GN=SEC24C PE=1 SV=3	sp|P53992|SC24C_HUMAN	118 kDa	3	0
Activated RNA polymerase II transcriptional coactivator p15 OS=Homo sapiens GN=SUB1 PE=1 SV=3	sp|P53999|TCP4_HUMAN	14 kDa	3	2
Sodium/potassium-transporting ATPase subunit beta-3 OS=Homo sapiens GN=ATP1B3 PE=1 SV=1	sp|P54709|AT1B3_HUMAN	32 kDa	3	6
Nucleosome assembly protein 1-like 1 OS=Homo sapiens GN=NAP1L1 PE=1 SV=1	sp|P55209|NP1L1_HUMAN	45 kDa	3	4
NADH dehydrogenase [ubiquinone] 1 alpha subcomplex subunit 6 OS=Homo sapiens GN=NDUFA6 PE=1 SV=3	sp|P56556|NDUA6_HUMAN	18 kDa	3	2

Cell division control protein 42 homolog OS=Homo sapiens GN=CDC42 PE=1 SV=2	sp|P60953|CDC42_HUMAN	21 kDa	3	5
Destrin OS=Homo sapiens GN=DSTN PE=1 SV=3	sp|P60981|DEST_HUMAN	19 kDa	3	3
Ras-related protein Rab-2A OS=Homo sapiens GN=RAB2A PE=1 SV=1	sp|P61019|RAB2A_HUMAN	24 kDa	3	4
Actin-related protein 2 OS=Homo sapiens GN=ACTR2 PE=1 SV=1	sp|P61160|ARP2_HUMAN	45 kDa	3	3
60S ribosomal protein L37a OS=Homo sapiens GN=RPL37A PE=1 SV=2	sp|P61513|RL37A_HUMAN	10 kDa	3	0
Epididymal secretory protein E1 OS=Homo sapiens GN=NPC2 PE=1 SV=1	sp|P61916|NPC2_HUMAN	17 kDa	3	3
Small nuclear ribonucleoprotein F OS=Homo sapiens GN=SNRPF PE=1 SV=1	sp|P62306|RUXF_HUMAN	10 kDa	3	0
Ras-related C3 botulinum toxin substrate 1 OS=Homo sapiens GN=RAC1 PE=1 SV=1	sp|P63000|RAC1_HUMAN	21 kDa	3	6
S-phase kinase-associated protein 1 OS=Homo sapiens GN=SKP1 PE=1 SV=2	sp|P63208|SKP1_HUMAN	19 kDa	3	2
Casein kinase II subunit beta OS=Homo sapiens GN=CSNK2B PE=1 SV=1	sp|P67870|CSK2B_HUMAN	25 kDa	3	4
Platelet-activating factor acetylhydrolase IB subunit beta OS=Homo sapiens GN=PAFAH1B2 PE=1 SV=1	sp|P68402|PA1B2_HUMAN	26 kDa	3	0
28S ribosomal protein S35, mitochondrial OS=Homo sapiens GN=MRPS35 PE=1 SV=1	sp|P82673|RT35_HUMAN	37 kDa	3	0
28S ribosomal protein S6, mitochondrial OS=Homo sapiens GN=MRPS6 PE=1 SV=3	sp|P82932|RT06_HUMAN	14 kDa	3	0
Hydroxymethylglutaryl-CoA synthase, cytoplasmic OS=Homo sapiens GN=HMGCS1 PE=1 SV=2	sp|Q01581|HMCS1_HUMAN	57 kDa	3	0
Peptidyl-prolyl cis-trans isomerase FKBP4 OS=Homo sapiens GN=FKBP4 PE=1 SV=3	sp|Q02790|FKBP4_HUMAN	52 kDa	3	9
Eukaryotic translation initiation factor 4 gamma 1 OS=Homo sapiens GN=EIF4G1 PE=1 SV=4	sp|Q04637|IF4G1_HUMAN	175 kDa	3	4
Mitochondrial-processing peptidase subunit alpha OS=Homo sapiens GN=PMPCA PE=1 SV=2	sp|Q10713|MPPA_HUMAN	58 kDa	3	7
Aspartyl/asparaginyl beta-hydroxylase OS=Homo sapiens GN=ASPH PE=1 SV=3	sp|Q12797|ASPH_HUMAN	86 kDa	3	5
TAR DNA-binding protein 43 OS=Homo sapiens GN=TARDBP PE=1 SV=1	sp|Q13148|TADBP_HUMAN	45 kDa	3	2
Heterogeneous nuclear ribonucleoprotein A0 OS=Homo sapiens GN=HNRNPA0 PE=1 SV=1	sp|Q13151|ROA0_HUMAN	31 kDa	3	0
39S ribosomal protein L49, mitochondrial OS=Homo sapiens GN=MRPL49 PE=1 SV=1	sp|Q13405|RM49_HUMAN	19 kDa	3	0
RNA-binding protein 39 OS=Homo sapiens GN=RBM39 PE=1 SV=2	sp|Q14498|RBM39_HUMAN	59 kDa	3	0
Phosphoribosyl pyrophosphate synthase-associated protein 1 OS=Homo sapiens GN=PRPSAP1 PE=1 SV=2	sp|Q14558|KPRA_HUMAN	39 kDa	3	0
Clathrin interactor 1 OS=Homo sapiens GN=CLINT1 PE=1 SV=1	sp|Q14677|EPN4_HUMAN	68 kDa	3	0
Structural maintenance of chromosomes protein 1A OS=Homo sapiens GN=SMC1A PE=1 SV=2	sp|Q14683|SMC1A_HUMAN	143 kDa	3	0
Zinc transporter ZIP14 OS=Homo sapiens GN=SLC39A14 PE=1 SV=3	sp|Q15043|S39AE_HUMAN	54 kDa	3	4
3-beta-hydroxysteroid-Delta(8),Delta(7)-isomerase OS=Homo sapiens GN=EBP PE=1 SV=3	sp|Q15125|EBP_HUMAN	26 kDa	3	4
Serum paraoxonase/arylesterase 2 OS=Homo sapiens GN=PON2 PE=1 SV=2	sp|Q15165|PON2_HUMAN	39 kDa	3	5
Prostaglandin E synthase 3 OS=Homo sapiens GN=PTGES3 PE=1 SV=1	sp|Q15185|TEBP_HUMAN	19 kDa	3	0
Thiosulfate sulfurtransferase OS=Homo sapiens GN=TST PE=1 SV=4	sp|Q16762|THTR_HUMAN	33 kDa	3	2

UTP--glucose-1-phosphate uridylyltransferase OS=Homo sapiens GN=UGP2 PE=1 SV=5	sp|Q16851|UGPA_HUMAN	57 kDa	3	3
Pre-rRNA-processing protein TSR1 homolog OS=Homo sapiens GN=TSR1 PE=1 SV=1	sp|Q2NL82|TSR1_HUMAN	92 kDa	3	0
Basic leucine zipper and W2 domain-containing protein 1 OS=Homo sapiens GN=BZW1 PE=1 SV=1	sp|Q7L1Q6|BZW1_HUMAN	48 kDa	3	8
39S ribosomal protein L10, mitochondrial OS=Homo sapiens GN=MRPL10 PE=1 SV=3	sp|Q7Z7H8|RM10_HUMAN	29 kDa	3	0
Aldehyde dehydrogenase family 16 member A1 OS=Homo sapiens GN=ALDH16A1 PE=1 SV=2	sp|Q8IZ83|A16A1_HUMAN	85 kDa	3	0
Beta-catenin-like protein 1 OS=Homo sapiens GN=CTNNBL1 PE=1 SV=1	sp|Q8WYA6|CTBL1_HUMAN	65 kDa	3	0
28S ribosomal protein S31, mitochondrial OS=Homo sapiens GN=MRPS31 PE=1 SV=3	sp|Q92665|RT31_HUMAN	45 kDa	3	0
Golgi apparatus protein 1 OS=Homo sapiens GN=GLG1 PE=1 SV=2	sp|Q92896|GSLG1_HUMAN	135 kDa	3	7
Coiled-coil domain-containing protein 47 OS=Homo sapiens GN=CCDC47 PE=1 SV=1	sp|Q96A33|CCD47_HUMAN	56 kDa	3	5
Acyl-CoA synthetase family member 2, mitochondrial OS=Homo sapiens GN=ACSF2 PE=1 SV=2	sp|Q96CM8|ACSF2_HUMAN	68 kDa	3	5
DAZ-associated protein 1 OS=Homo sapiens GN=DAZAP1 PE=1 SV=1	sp|Q96EP5|DAZP1_HUMAN	43 kDa	3	2
Receptor expression-enhancing protein 6 OS=Homo sapiens GN=REEP6 PE=1 SV=1	sp|Q96HR9|REEP6_HUMAN	21 kDa	3	5
Cytosolic non-specific dipeptidase OS=Homo sapiens GN=CNDP2 PE=1 SV=2	sp|Q96KP4|CNDP2_HUMAN	53 kDa	3	0
Heterogeneous nuclear ribonucleoprotein A/B OS=Homo sapiens GN=HNRNPAB PE=1 SV=2	sp|Q99729|ROAA_HUMAN	36 kDa	3	6
Acidic leucine-rich nuclear phosphoprotein 32 family member E OS=Homo sapiens GN=ANP32E PE=1 SV=1	sp|Q9BTT0|AN32E_HUMAN	31 kDa	3	2
SRA stem-loop-interacting RNA-binding protein, mitochondrial OS=Homo sapiens GN=SLIRP PE=1 SV=1	sp|Q9GZT3|SLIRP_HUMAN	12 kDa	3	0
Acyl-CoA synthetase short-chain family member 3, mitochondrial OS=Homo sapiens GN=ACSS3 PE=2 SV=1	sp|Q9H6R3|ACSS3_HUMAN	75 kDa	3	10
Methyltransferase-like protein 7A OS=Homo sapiens GN=METTL7A PE=1 SV=1	sp|Q9H8H3|MET7A_HUMAN	28 kDa	3	3
Exportin-5 OS=Homo sapiens GN=XPO5 PE=1 SV=1	sp|Q9HAV4|XPO5_HUMAN	136 kDa	3	4
Calcyclin-binding protein OS=Homo sapiens GN=CACYBP PE=1 SV=2	sp|Q9HB71|CYBP_HUMAN	26 kDa	3	8
3-hydroxyacyl-CoA dehydratase 3 OS=Homo sapiens GN=PTPLAD1 PE=1 SV=2	sp|Q9P035|HACD3_HUMAN	43 kDa	3	3
Vesicle-associated membrane protein-associated protein A OS=Homo sapiens GN=VAPA PE=1 SV=3	sp|Q9P0L0|VAPA_HUMAN	28 kDa	3	6
Leucyl-tRNA synthetase, cytoplasmic OS=Homo sapiens GN=LARS PE=1 SV=2	sp|Q9P2J5|SYLC_HUMAN	134 kDa	3	0
Succinyl-CoA ligase [ADP-forming] subunit beta, mitochondrial OS=Homo sapiens GN=SUCLA2 PE=1 SV=3	sp|Q9P2R7|SUCB1_HUMAN	50 kDa	3	5
SUMO-activating enzyme subunit 1 OS=Homo sapiens GN=SAE1 PE=1 SV=1	sp|Q9UBE0|SAE1_HUMAN	38 kDa	3	4
Tight junction protein ZO-2 OS=Homo sapiens GN=TJP2 PE=1 SV=2	sp|Q9UDY2|ZO2_HUMAN	134 kDa	3	0
Translocation protein SEC63 homolog OS=Homo sapiens GN=SEC63 PE=1 SV=2	sp|Q9UGP8|SEC63_HUMAN	88 kDa	3	2
Cysteine and histidine-rich domain-containing protein 1 OS=Homo sapiens GN=CHORDC1 PE=1 SV=2	sp|Q9UHD1|CHRD1_HUMAN	37 kDa	3	3

Septin-9 OS=Homo sapiens GN=SEPT9 PE=1 SV=2	sp|Q9UHD8|SEPT9_HUMAN	65 kDa	3	2
GTP:AMP phosphotransferase, mitochondrial OS=Homo sapiens GN=AK3 PE=1 SV=4	sp|Q9UIJ7|KAD3_HUMAN	26 kDa	3	10
Transmembrane and coiled-coil domain-containing protein 1 OS=Homo sapiens GN=TMCO1 PE=1 SV=1	sp|Q9UM00|TMCO1_HUMAN	21 kDa	3	2
Eukaryotic translation initiation factor 3 subunit L OS=Homo sapiens GN=EIF3L PE=1 SV=1	sp|Q9Y262|EIF3L_HUMAN	67 kDa	3	6
Nuclear migration protein nudC OS=Homo sapiens GN=NUDC PE=1 SV=1	sp|Q9Y266|NUDC_HUMAN	38 kDa	3	3
Voltage-dependent anion-selective channel protein 3 OS=Homo sapiens GN=VDAC3 PE=1 SV=1	sp|Q9Y277|VDAC3_HUMAN	31 kDa	3	13
Phenylalanyl-tRNA synthetase alpha chain OS=Homo sapiens GN=FARSA PE=1 SV=3	sp|Q9Y285|SYFA_HUMAN	58 kDa	3	2
28S ribosomal protein S17, mitochondrial OS=Homo sapiens GN=MRPS17 PE=1 SV=1	sp|Q9Y2R5|RT17_HUMAN	15 kDa	3	0
Transmembrane emp24 domain-containing protein 7 OS=Homo sapiens GN=TMED7 PE=1 SV=2	sp|Q9Y3B3|TMED7_HUMAN	25 kDa	3	3
28S ribosomal protein S16, mitochondrial OS=Homo sapiens GN=MRPS16 PE=1 SV=1	sp|Q9Y3D3|RT16_HUMAN	15 kDa	3	0
Talin-1 OS=Homo sapiens GN=TLN1 PE=1 SV=3	sp|Q9Y490|TLN1_HUMAN	270 kDa	3	4
Signal recognition particle receptor subunit beta OS=Homo sapiens GN=SRPRB PE=1 SV=3	sp|Q9Y5M8|SRPRB_HUMAN	30 kDa	3	4
28S ribosomal protein S18b, mitochondrial OS=Homo sapiens GN=MRPS18B PE=1 SV=1	sp|Q9Y676|RT18B_HUMAN	29 kDa	3	0
Chloride intracellular channel protein 4 OS=Homo sapiens GN=CLIC4 PE=1 SV=4	sp|Q9Y696|CLIC4_HUMAN	29 kDa	3	0
GTP-binding protein SAR1b OS=Homo sapiens GN=SAR1B PE=1 SV=1	sp|Q9Y6B6|SAR1B_HUMAN	22 kDa	3	3
Cytosolic acyl coenzyme A thioester hydrolase OS=Homo sapiens GN=ACOT7 PE=1 SV=3	sp|O00154|BACH_HUMAN	42 kDa	2	0
26S proteasome non-ATPase regulatory subunit 11 OS=Homo sapiens GN=PSMD11 PE=1 SV=3	sp|O00231|PSD11_HUMAN	47 kDa	2	2
Eukaryotic translation initiation factor 3 subunit F OS=Homo sapiens GN=EIF3F PE=1 SV=1	sp|O00303|EIF3F_HUMAN	38 kDa	2	3
NADH dehydrogenase [ubiquinone] 1 alpha subcomplex subunit 4 OS=Homo sapiens GN=NDUFA4 PE=1 SV=1	sp|O00483|NDUA4_HUMAN	9 kDa	2	0
Pescadillo homolog OS=Homo sapiens GN=PES1 PE=1 SV=1	sp|O00541|PESC_HUMAN	68 kDa	2	0
Eukaryotic translation initiation factor 1A, Y-chromosomal OS=Homo sapiens GN=EIF1AY PE=1 SV=4	sp|O14602|IF1AY_HUMAN (+1)	16 kDa	2	0
Microsomal glutathione S-transferase 3 OS=Homo sapiens GN=MGST3 PE=1 SV=1	sp|O14880|MGST3_HUMAN	17 kDa	2	0
Very long-chain acyl-CoA synthetase OS=Homo sapiens GN=SLC27A2 PE=1 SV=2	sp|O14975|S27A2_HUMAN	70 kDa	2	2
Actin-related protein 2/3 complex subunit 1B OS=Homo sapiens GN=ARPC1B PE=1 SV=3	sp|O15143|ARC1B_HUMAN	41 kDa	2	0
Serine palmitoyltransferase 1 OS=Homo sapiens GN=SPTLC1 PE=1 SV=1	sp|O15269|SPTC1_HUMAN	53 kDa	2	3
Phosphomannomutase 2 OS=Homo sapiens GN=PMM2 PE=1 SV=1	sp|O15305|PMM2_HUMAN	28 kDa	2	0
Eukaryotic translation elongation factor 1 epsilon-1 OS=Homo sapiens GN=EEF1E1 PE=1 SV=1	sp|O43324|MCA3_HUMAN	20 kDa	2	0
Mitochondrial import inner membrane translocase subunit TIM44 OS=Homo sapiens GN=TIMM44 PE=1 SV=2	sp|O43615|TIM44_HUMAN	51 kDa	2	2
Isocitrate dehydrogenase [NAD] subunit beta, mitochondrial OS=Homo sapiens GN=IDH3B	sp|O43837|IDH3B_HUMAN	42 kDa	2	3

PE=1 SV=2				
H/ACA ribonucleoprotein complex subunit 4 OS=Homo sapiens GN=DKC1 PE=1 SV=3	sp|O60832|DKC1_HUMAN	58 kDa	2	0
Tubulin-specific chaperone A OS=Homo sapiens GN=TBCA PE=1 SV=3	sp|O75347|TBCA_HUMAN	13 kDa	2	3
Vesicle-trafficking protein SEC22b OS=Homo sapiens GN=SEC22B PE=1 SV=4	sp|O75396|SC22B_HUMAN	25 kDa	2	3
Pre-mRNA-processing factor 40 homolog A OS=Homo sapiens GN=PRPF40A PE=1 SV=2	sp|O75400|PR40A_HUMAN	109 kDa	2	0
Erlin-2 OS=Homo sapiens GN=ERLIN2 PE=1 SV=1	sp|O94905|ERLN2_HUMAN	38 kDa	2	6
Importin-7 OS=Homo sapiens GN=IPO7 PE=1 SV=1	sp|O95373|IPO7_HUMAN	120 kDa	2	3
Activator of 90 kDa heat shock protein ATPase homolog 1 OS=Homo sapiens GN=AHSA1 PE=1 SV=1	sp|O95433|AHSA1_HUMAN	38 kDa	2	3
Protein transport protein Sec24A OS=Homo sapiens GN=SEC24A PE=1 SV=2	sp|O95486|SC24A_HUMAN	120 kDa	2	0
BAG family molecular chaperone regulator 2 OS=Homo sapiens GN=BAG2 PE=1 SV=1	sp|O95816|BAG2_HUMAN	24 kDa	2	0
Actin-like protein 6A OS=Homo sapiens GN=ACTL6A PE=1 SV=1	sp|O96019|ACL6A_HUMAN	47 kDa	2	0
Hypoxanthine-guanine phosphoribosyltransferase OS=Homo sapiens GN=HPRT1 PE=1 SV=2	sp|P00492|HPRT_HUMAN	25 kDa	2	2
Catalase OS=Homo sapiens GN=CAT PE=1 SV=3	sp|P04040|CATA_HUMAN	60 kDa	2	13
Intercellular adhesion molecule 1 OS=Homo sapiens GN=ICAM1 PE=1 SV=2	sp|P05362|ICAM1_HUMAN	58 kDa	2	8
Eukaryotic translation initiation factor 4E OS=Homo sapiens GN=EIF4E PE=1 SV=2	sp|P06730|IF4E_HUMAN	25 kDa	2	2
Cytochrome c1, heme protein, mitochondrial OS=Homo sapiens GN=CYC1 PE=1 SV=3	sp|P08574|CY1_HUMAN	35 kDa	2	3
Cytochrome c oxidase subunit 4 isoform 1, mitochondrial OS=Homo sapiens GN=COX4I1 PE=1 SV=1	sp|P13073|COX41_HUMAN	20 kDa	2	7
Farnesyl pyrophosphate synthase OS=Homo sapiens GN=FDPS PE=1 SV=4	sp|P14324|FPPS_HUMAN	48 kDa	2	5
Aldose reductase OS=Homo sapiens GN=AKR1B1 PE=1 SV=3	sp|P15121|ALDR_HUMAN	36 kDa	2	4
Short-chain specific acyl-CoA dehydrogenase, mitochondrial OS=Homo sapiens GN=ACADS PE=1 SV=1	sp|P16219|ACADS_HUMAN	44 kDa	2	0
Beta-galactosidase OS=Homo sapiens GN=GLB1 PE=1 SV=2	sp|P16278|BGAL_HUMAN	76 kDa	2	7
CTP synthase 1 OS=Homo sapiens GN=CTPS PE=1 SV=2	sp|P17812|PYRG1_HUMAN	67 kDa	2	0
Succinate dehydrogenase [ubiquinone] iron-sulfur subunit, mitochondrial OS=Homo sapiens GN=SDHB PE=1 SV=3	sp|P21912|DHSB_HUMAN	32 kDa	2	4
Protein-L-isoaspartate(D-aspartate) O-methyltransferase OS=Homo sapiens GN=PCMT1 PE=1 SV=4	sp|P22061|PIMT_HUMAN	25 kDa	2	0
Ectonucleotide pyrophosphatase/phosphodiesterase family member 1 OS=Homo sapiens GN=ENPP1 PE=1 SV=2	sp|P22413|ENPP1_HUMAN	105 kDa	2	4
Low molecular weight phosphotyrosine protein phosphatase OS=Homo sapiens GN=ACP1 PE=1 SV=3	sp|P24666|PPAC_HUMAN	18 kDa	2	3
3-mercaptopyruvate sulfurtransferase OS=Homo sapiens GN=MPST PE=1 SV=3	sp|P25325|THTM_HUMAN	33 kDa	2	4
DnaJ homolog subfamily B member 1 OS=Homo sapiens GN=DNAJB1 PE=1 SV=4	sp|P25685|DNJB1_HUMAN	38 kDa	2	5
Threonyl-tRNA synthetase, cytoplasmic	sp|P26639|SYTC_HUMAN	83 kDa	2	2

OS=Homo sapiens GN=TARS PE=1 SV=3				
CAD protein OS=Homo sapiens GN=CAD PE=1 SV=3	sp|P27708|PYR1_HUMAN	243 kDa	2	0
Proteasome subunit beta type-6 OS=Homo sapiens GN=PSMB6 PE=1 SV=4	sp|P28072|PSB6_HUMAN	25 kDa	2	4
Proteasome subunit beta type-5 OS=Homo sapiens GN=PSMB5 PE=1 SV=3	sp|P28074|PSB5_HUMAN	28 kDa	2	7
Peroxiredoxin-5, mitochondrial OS=Homo sapiens GN=PRDX5 PE=1 SV=4	sp|P30044|PRDX5_HUMAN	22 kDa	2	6
Adenylosuccinate lyase OS=Homo sapiens GN=ADSL PE=1 SV=2	sp|P30566|PUR8_HUMAN	55 kDa	2	0
Glutathione S-transferase theta-1 OS=Homo sapiens GN=GSTT1 PE=1 SV=4	sp|P30711|GSTT1_HUMAN	27 kDa	2	0
Heterogeneous nuclear ribonucleoprotein H3 OS=Homo sapiens GN=HNRNPH3 PE=1 SV=2	sp|P31942|HNRH3_HUMAN	37 kDa	2	0
Estradiol 17-beta-dehydrogenase 2 OS=Homo sapiens GN=HSD17B2 PE=1 SV=1	sp|P37059|DHB2_HUMAN	43 kDa	2	0
Lanosterol synthase OS=Homo sapiens GN=LSS PE=1 SV=1	sp|P48449|ERG7_HUMAN	83 kDa	2	0
60S ribosomal protein L34 OS=Homo sapiens GN=RPL34 PE=1 SV=3	sp|P49207|RL34_HUMAN	13 kDa	2	0
Proteasome subunit beta type-2 OS=Homo sapiens GN=PSMB2 PE=1 SV=1	sp|P49721|PSB2_HUMAN	23 kDa	2	4
RNA-binding protein 25 OS=Homo sapiens GN=RBM25 PE=1 SV=3	sp|P49756|RBM25_HUMAN	100 kDa	2	0
NADH dehydrogenase [ubiquinone] flavoprotein 1, mitochondrial OS=Homo sapiens GN=NDUFV1 PE=1 SV=4	sp|P49821|NDUV1_HUMAN	51 kDa	2	5
Histamine N-methyltransferase OS=Homo sapiens GN=HNMT PE=1 SV=1	sp|P50135|HNMT_HUMAN	33 kDa	2	3
Isocitrate dehydrogenase [NAD] subunit alpha, mitochondrial OS=Homo sapiens GN=IDH3A PE=1 SV=1	sp|P50213|IDH3A_HUMAN	40 kDa	2	10
Hsc70-interacting protein OS=Homo sapiens GN=ST13 PE=1 SV=2	sp|P50502|F10A1_HUMAN	41 kDa	2	4
Palmitoyl-protein thioesterase 1 OS=Homo sapiens GN=PPT1 PE=1 SV=1	sp|P50897|PPT1_HUMAN	34 kDa	2	4
Ras-related protein Rab-7a OS=Homo sapiens GN=RAB7A PE=1 SV=1	sp|P51149|RAB7A_HUMAN	23 kDa	2	9
Hepatoma-derived growth factor OS=Homo sapiens GN=HDGF PE=1 SV=1	sp|P51858|HDGF_HUMAN	27 kDa	2	2
NADH dehydrogenase [ubiquinone] 1 alpha subcomplex subunit 8 OS=Homo sapiens GN=NDUFA8 PE=1 SV=3	sp|P51970|NDUA8_HUMAN	20 kDa	2	3
DNA mismatch repair protein Msh6 OS=Homo sapiens GN=MSH6 PE=1 SV=2	sp|P52701|MSH6_HUMAN	153 kDa	2	0
Hexokinase-2 OS=Homo sapiens GN=HK2 PE=1 SV=2	sp|P52789|HXK2_HUMAN	102 kDa	2	4
Succinyl-CoA ligase [GDP-forming] subunit alpha, mitochondrial OS=Homo sapiens GN=SUCLG1 PE=1 SV=4	sp|P53597|SUCA_HUMAN	36 kDa	2	5
Tyrosyl-tRNA synthetase, cytoplasmic OS=Homo sapiens GN=YARS PE=1 SV=4	sp|P54577|SYYC_HUMAN	59 kDa	2	0
Eukaryotic translation initiation factor 5 OS=Homo sapiens GN=EIF5 PE=1 SV=2	sp|P55010|IF5_HUMAN	49 kDa	2	3
26S proteasome non-ATPase regulatory subunit 4 OS=Homo sapiens GN=PSMD4 PE=1 SV=1	sp|P55036|PSMD4_HUMAN	41 kDa	2	2
Mesencephalic astrocyte-derived neurotrophic factor OS=Homo sapiens GN=MANF PE=1 SV=2	sp|P55145|MANF_HUMAN	20 kDa	2	6
Double-stranded RNA-specific adenosine deaminase OS=Homo sapiens GN=ADAR PE=1 SV=4	sp|P55265|DSRAD_HUMAN	136 kDa	2	0
Protein SEC13 homolog OS=Homo sapiens GN=SEC13 PE=1 SV=3	sp|P55735|SEC13_HUMAN	36 kDa	2	3

Small ubiquitin-related modifier 3 OS=Homo sapiens GN=SUMO3 PE=1 SV=2	sp|P55854|SUMO3_HUMAN (+1)	12 kDa	2	0
ATP synthase subunit f, mitochondrial OS=Homo sapiens GN=ATP5J2 PE=1 SV=3	sp|P56134|ATPK_HUMAN	11 kDa	2	2
Actin-related protein 2/3 complex subunit 4 OS=Homo sapiens GN=ARPC4 PE=1 SV=3	sp|P59998|ARPC4_HUMAN	20 kDa	2	0
Eukaryotic translation initiation factor 3 subunit E OS=Homo sapiens GN=EIF3E PE=1 SV=1	sp|P60228|EIF3E_HUMAN	52 kDa	2	9
Signal peptidase complex subunit 3 OS=Homo sapiens GN=SPCS3 PE=1 SV=1	sp|P61009|SPCS3_HUMAN	20 kDa	2	3
Alpha-centractin OS=Homo sapiens GN=ACTR1A PE=1 SV=1	sp|P61163|ACTZ_HUMAN	43 kDa	2	3
ATP-binding cassette sub-family E member 1 OS=Homo sapiens GN=ABCE1 PE=1 SV=1	sp|P61221|ABCE1_HUMAN	67 kDa	2	4
Ras-related protein Rap-1b OS=Homo sapiens GN=RAP1B PE=1 SV=1	sp|P61224|RAP1B_HUMAN	21 kDa	2	2
Lysozyme C OS=Homo sapiens GN=LYZ PE=1 SV=1	sp|P61626|LYSC_HUMAN	17 kDa	2	2
Dolichyl-diphosphooligosaccharide--protein glycosyltransferase subunit DAD1 OS=Homo sapiens GN=DAD1 PE=1 SV=3	sp|P61803|DAD1_HUMAN	12 kDa	2	3
Coatomer subunit zeta-1 OS=Homo sapiens GN=COPZ1 PE=1 SV=1	sp|P61923|COPZ1_HUMAN	20 kDa	2	2
Small nuclear ribonucleoprotein E OS=Homo sapiens GN=SNRPE PE=1 SV=1	sp|P62304|RUXE_HUMAN	11 kDa	2	0
Small nuclear ribonucleoprotein Sm D2 OS=Homo sapiens GN=SNRPD2 PE=1 SV=1	sp|P62316|SMD2_HUMAN	14 kDa	2	2
Serine/threonine-protein phosphatase 2A 55 kDa regulatory subunit B alpha isoform OS=Homo sapiens GN=PPP2R2A PE=1 SV=1	sp|P63151|2ABA_HUMAN	52 kDa	2	0
General transcription factor II-I OS=Homo sapiens GN=GTF2I PE=1 SV=2	sp|P78347|GTF2I_HUMAN	112 kDa	2	4
60S ribosomal protein L36a OS=Homo sapiens GN=RPL36A PE=1 SV=2	sp|P83881|RL36A_HUMAN (+1)	12 kDa	2	0
Receptor expression-enhancing protein 5 OS=Homo sapiens GN=REEP5 PE=1 SV=3	sp|Q00765|REEP5_HUMAN	21 kDa	2	3
Aminoacylase-1 OS=Homo sapiens GN=ACY1 PE=1 SV=1	sp|Q03154|ACY1_HUMAN	46 kDa	2	0
Single-stranded DNA-binding protein, mitochondrial OS=Homo sapiens GN=SSBP1 PE=1 SV=1	sp|Q04837|SSBP_HUMAN	17 kDa	2	5
Tight junction protein ZO-1 OS=Homo sapiens GN=TJP1 PE=1 SV=3	sp|Q07157|ZO1_HUMAN	195 kDa	2	0
KH domain-containing, RNA-binding, signal transduction-associated protein 1 OS=Homo sapiens GN=KHDRBS1 PE=1 SV=1	sp|Q07666|KHDR1_HUMAN	48 kDa	2	3
Peroxisomal bifunctional enzyme OS=Homo sapiens GN=EHHADH PE=1 SV=3	sp|Q08426|ECHP_HUMAN	79 kDa	2	0
tRNA (cytosine-5-)-methyltransferase NSUN2 OS=Homo sapiens GN=NSUN2 PE=1 SV=2	sp|Q08J23|NSUN2_HUMAN	86 kDa	2	0
G-rich sequence factor 1 OS=Homo sapiens GN=GRSF1 PE=1 SV=3	sp|Q12849|GRSF1_HUMAN	53 kDa	2	2
Aminoacyl tRNA synthase complex-interacting multifunctional protein 1 OS=Homo sapiens GN=AIMP1 PE=1 SV=2	sp|Q12904|AIMP1_HUMAN	34 kDa	2	3
Vesicular integral-membrane protein VIP36 OS=Homo sapiens GN=LMAN2 PE=1 SV=1	sp|Q12907|LMAN2_HUMAN	40 kDa	2	5
Ubiquitin-conjugating enzyme E2 variant 1 OS=Homo sapiens GN=UBE2V1 PE=1 SV=2	sp|Q13404|UB2V1_HUMAN	16 kDa	2	5
Cullin-1 OS=Homo sapiens GN=CUL1 PE=1 SV=2	sp|Q13616|CUL1_HUMAN	90 kDa	2	0
LDLR chaperone MESD OS=Homo sapiens GN=MESDC2 PE=1 SV=2	sp|Q14696|MESD_HUMAN	26 kDa	2	5
26S proteasome non-ATPase regulatory subunit 6 OS=Homo sapiens GN=PSMD6 PE=1 SV=1	sp|Q15008|PSMD6_HUMAN	46 kDa	2	3

Septin-2 OS=Homo sapiens GN=SEPT2 PE=1 SV=1	sp|Q15019|SEPT2_HUMAN	41 kDa	2	4
Inorganic pyrophosphatase OS=Homo sapiens GN=PPA1 PE=1 SV=2	sp|Q15181|IPYR_HUMAN	33 kDa	2	0
Thyroid receptor-interacting protein 11 OS=Homo sapiens GN=TRIP11 PE=1 SV=3	sp|Q15643|TRIPB_HUMAN	228 kDa	2	3
NADH dehydrogenase [ubiquinone] 1 alpha subcomplex subunit 5 OS=Homo sapiens GN=NDUFA5 PE=1 SV=3	sp|Q16718|NDUA5_HUMAN	13 kDa	2	0
Heterogeneous nuclear ribonucleoprotein U-like protein 2 OS=Homo sapiens GN=HNRNPUL2 PE=1 SV=1	sp|Q1KMD3|HNRL2_HUMAN	85 kDa	2	0
Prolyl 3-hydroxylase 1 OS=Homo sapiens GN=LEPRE1 PE=1 SV=2	sp|Q32P28|P3H1_HUMAN	83 kDa	2	2
Tetratricopeptide repeat protein 38 OS=Homo sapiens GN=TTC38 PE=1 SV=1	sp|Q5R3I4|TTC38_HUMAN	53 kDa	2	3
Transmembrane protein 214 OS=Homo sapiens GN=TMEM214 PE=1 SV=2	sp|Q6NUQ4|TM214_HUMAN	77 kDa	2	2
Fumarylacetoacetate hydrolase domain-containing protein 1 OS=Homo sapiens GN=FAHD1 PE=1 SV=2	sp|Q6P587|FAHD1_HUMAN	25 kDa	2	2
LAG1 longevity assurance homolog 6 OS=Homo sapiens GN=LASS6 PE=1 SV=1	sp|Q6ZMG9|LASS6_HUMAN	45 kDa	2	0
Mitochondrial ribonuclease P protein 1 OS=Homo sapiens GN=RG9MTD1 PE=1 SV=2	sp|Q7L0Y3|MRRP1_HUMAN	47 kDa	2	2
Eukaryotic translation initiation factor 3 subunit M OS=Homo sapiens GN=EIF3M PE=1 SV=1	sp|Q7L2H7|EIF3M_HUMAN	43 kDa	2	2
Heparan sulfate 2-O-sulfotransferase 1 OS=Homo sapiens GN=HS2ST1 PE=1 SV=1	sp|Q7LGA3|HS2ST_HUMAN	42 kDa	2	0
Kinectin OS=Homo sapiens GN=KTN1 PE=1 SV=1	sp|Q86UP2|KTN1_HUMAN	156 kDa	2	8
Leucine-rich repeat-containing protein 47 OS=Homo sapiens GN=LRRC47 PE=1 SV=1	sp|Q8N1G4|LRC47_HUMAN	63 kDa	2	0
Cleavage and polyadenylation specificity factor subunit 7 OS=Homo sapiens GN=CPSF7 PE=1 SV=1	sp|Q8N684|CPSF7_HUMAN	52 kDa	2	0
Lysophosphatidylcholine acyltransferase 1 OS=Homo sapiens GN=LPCAT1 PE=1 SV=2	sp|Q8NF37|PCAT1_HUMAN	59 kDa	2	0
Minor histocompatibility antigen H13 OS=Homo sapiens GN=HM13 PE=1 SV=1	sp|Q8TCT9|HM13_HUMAN	41 kDa	2	8
Proteasome inhibitor PI31 subunit OS=Homo sapiens GN=PSMF1 PE=1 SV=2	sp|Q92530|PSMF1_HUMAN	30 kDa	2	0
Transmembrane 9 superfamily member 4 OS=Homo sapiens GN=TM9SF4 PE=1 SV=2	sp|Q92544|TM9S4_HUMAN	75 kDa	2	7
28S ribosomal protein S27, mitochondrial OS=Homo sapiens GN=MRPS27 PE=1 SV=3	sp|Q92552|RT27_HUMAN	48 kDa	2	4
Glutaryl-CoA dehydrogenase, mitochondrial OS=Homo sapiens GN=GCDH PE=1 SV=1	sp|Q92947|GCDH_HUMAN	48 kDa	2	0
Homogentisate 1,2-dioxygenase OS=Homo sapiens GN=HGD PE=1 SV=2	sp|Q93099|HGD_HUMAN	50 kDa	2	3
Nicalin OS=Homo sapiens GN=NCLN PE=1 SV=2	sp|Q969V3|NCLN_HUMAN	63 kDa	2	2
Protein TBRG4 OS=Homo sapiens GN=TBRG4 PE=1 SV=1	sp|Q969Z0|TBRG4_HUMAN	71 kDa	2	5
39S ribosomal protein L24, mitochondrial OS=Homo sapiens GN=MRPL24 PE=1 SV=1	sp|Q96A35|RM24_HUMAN	25 kDa	2	0
Isochorismatase domain-containing protein 2, mitochondrial OS=Homo sapiens GN=ISOC2 PE=1 SV=1	sp|Q96AB3|ISOC2_HUMAN	22 kDa	2	5
Far upstream element-binding protein 1 OS=Homo sapiens GN=FUBP1 PE=1 SV=3	sp|Q96AE4|FUBP1_HUMAN	68 kDa	2	9
28S ribosomal protein S24, mitochondrial OS=Homo sapiens GN=MRPS24 PE=1 SV=1	sp|Q96EL2|RT24_HUMAN	19 kDa	2	0
Abhydrolase domain-containing protein 14B OS=Homo sapiens GN=ABHD14B PE=1 SV=1	sp|Q96IU4|ABHEB_HUMAN	22 kDa	2	2
Transmembrane protein C20orf108 OS=Homo	sp|Q96KR6|CT108_HUMAN	20 kDa	2	0

sapiens GN=C20orf108 PE=1 SV=2				
Importin-9 OS=Homo sapiens GN=IPO9 PE=1 SV=3	sp|Q96P70|IPO9_HUMAN	116 kDa	2	0
Microtubule-actin cross-linking factor 1, isoform 4 OS=Homo sapiens GN=MACF1 PE=1 SV=2	sp|Q96PK2|MACF4_HUMAN (+1)	670 kDa	2	0
RNA-binding protein 14 OS=Homo sapiens GN=RBM14 PE=1 SV=2	sp|Q96PK6|RBM14_HUMAN	69 kDa	2	0
Elongation factor G, mitochondrial OS=Homo sapiens GN=GFM1 PE=1 SV=2	sp|Q96RP9|EFGM_HUMAN	83 kDa	2	0
Methylcrotonoyl-CoA carboxylase subunit alpha, mitochondrial OS=Homo sapiens GN=MCCC1 PE=1 SV=3	sp|Q96RQ3|MCCA_HUMAN	80 kDa	2	0
Ribonucleases P/MRP protein subunit POP1 OS=Homo sapiens GN=POP1 PE=1 SV=2	sp|Q99575|POP1_HUMAN	115 kDa	2	0
Equilibrative nucleoside transporter 1 OS=Homo sapiens GN=SLC29A1 PE=1 SV=3	sp|Q99808|S29A1_HUMAN	50 kDa	2	0
Myb-binding protein 1A OS=Homo sapiens GN=MYBBP1A PE=1 SV=2	sp|Q9BQG0|MBB1A_HUMAN	149 kDa	2	0
Thioredoxin domain-containing protein 17 OS=Homo sapiens GN=TXNDC17 PE=1 SV=1	sp|Q9BRA2|TXD17_HUMAN	14 kDa	2	0
Calcineurin-like phosphoesterase domain-containing protein 1 OS=Homo sapiens GN=CPPED1 PE=1 SV=3	sp|Q9BRF8|CPPED_HUMAN	36 kDa	2	3
Endoplasmic reticulum resident protein 44 OS=Homo sapiens GN=ERP44 PE=1 SV=1	sp|Q9BS26|ERP44_HUMAN	47 kDa	2	6
Probable ATP-dependent RNA helicase DDX23 OS=Homo sapiens GN=DDX23 PE=1 SV=3	sp|Q9BUQ8|DDX23_HUMAN	96 kDa	2	0
Guanine nucleotide-binding protein-like 3 OS=Homo sapiens GN=GNL3 PE=1 SV=2	sp|Q9BVP2|GNL3_HUMAN	62 kDa	2	0
Peroxisomal trans-2-enoyl-CoA reductase OS=Homo sapiens GN=PECR PE=1 SV=2	sp|Q9BY49|PECR_HUMAN	33 kDa	2	0
39S ribosomal protein L20, mitochondrial OS=Homo sapiens GN=MRPL20 PE=1 SV=1	sp|Q9BYC9|RM20_HUMAN	17 kDa	2	0
Protein dpy-30 homolog OS=Homo sapiens GN=DPY30 PE=1 SV=1	sp|Q9C005|DPY30_HUMAN	11 kDa	2	0
Epidermal growth factor receptor kinase substrate 8-like protein 2 OS=Homo sapiens GN=EPS8L2 PE=1 SV=2	sp|Q9H6S3|ES8L2_HUMAN	81 kDa	2	0
Golgi reassembly-stacking protein 2 OS=Homo sapiens GN=GORASP2 PE=1 SV=3	sp|Q9H8Y8|GORS2_HUMAN	47 kDa	2	5
Transmembrane 9 superfamily member 3 OS=Homo sapiens GN=TM9SF3 PE=1 SV=2	sp|Q9HD45|TM9S3_HUMAN	68 kDa	2	5
Seryl-tRNA synthetase, mitochondrial OS=Homo sapiens GN=SARS2 PE=1 SV=1	sp|Q9NP81|SYSM_HUMAN	58 kDa	2	0
Reticulon-4 OS=Homo sapiens GN=RTN4 PE=1 SV=2	sp|Q9NQC3|RTN4_HUMAN	130 kDa	2	5
14 kDa phosphohistidine phosphatase OS=Homo sapiens GN=PHPT1 PE=1 SV=1	sp|Q9NRX4|PHP14_HUMAN	14 kDa	2	0
Mitochondrial import receptor subunit TOM22 homolog OS=Homo sapiens GN=TOMM22 PE=1 SV=3	sp|Q9NS69|TOM22_HUMAN	16 kDa	2	4
Abhydrolase domain-containing protein 10, mitochondrial OS=Homo sapiens GN=ABHD10 PE=1 SV=1	sp|Q9NUJ1|ABHDA_HUMAN	34 kDa	2	2
SPATS2-like protein OS=Homo sapiens GN=SPATS2L PE=1 SV=2	sp|Q9NUQ6|SPS2L_HUMAN	62 kDa	2	0
Septin-11 OS=Homo sapiens GN=SEPT11 PE=1 SV=3	sp|Q9NVA2|SEP11_HUMAN	49 kDa	2	2
39S ribosomal protein L22, mitochondrial OS=Homo sapiens GN=MRPL22 PE=1 SV=1	sp|Q9NWU5|RM22_HUMAN	24 kDa	2	0
39S ribosomal protein L16, mitochondrial OS=Homo sapiens GN=MRPL16 PE=1 SV=1	sp|Q9NX20|RM16_HUMAN	28 kDa	2	0
39S ribosomal protein L39, mitochondrial	sp|Q9NYK5|RM39_HUMAN	39 kDa	2	0

OS=Homo sapiens GN=MRPL39 PE=1 SV=3				
Endoplasmic reticulum aminopeptidase 1 OS=Homo sapiens GN=ERAP1 PE=1 SV=3	sp|Q9NZ08|ERAP1_HUMAN	107 kDa	2	5
Peroxisomal sarcosine oxidase OS=Homo sapiens GN=PIPOX PE=2 SV=2	sp|Q9P0Z9|SOX_HUMAN	44 kDa	2	2
SUMO-activating enzyme subunit 2 OS=Homo sapiens GN=UBA2 PE=1 SV=2	sp|Q9UBT2|SAE2_HUMAN	71 kDa	2	4
Alpha-aminoadipic semialdehyde synthase, mitochondrial OS=Homo sapiens GN=AASS PE=1 SV=1	sp|Q9UDR5|AASS_HUMAN	102 kDa	2	4
NADH dehydrogenase [ubiquinone] 1 alpha subcomplex subunit 12 OS=Homo sapiens GN=NDUFA12 PE=1 SV=1	sp|Q9UI09|NDUAC_HUMAN	17 kDa	2	3
Translocon-associated protein subunit gamma OS=Homo sapiens GN=SSR3 PE=1 SV=1	sp|Q9UNL2|SSRG_HUMAN	21 kDa	2	0
26S proteasome non-ATPase regulatory subunit 13 OS=Homo sapiens GN=PSMD13 PE=1 SV=2	sp|Q9UNM6|PSD13_HUMAN	43 kDa	2	7
Endoribonuclease Dicer OS=Homo sapiens GN=DICER1 PE=1 SV=3	sp|Q9UPY3|DICER_HUMAN	219 kDa	2	0
Structural maintenance of chromosomes protein 3 OS=Homo sapiens GN=SMC3 PE=1 SV=2	sp|Q9UQE7|SMC3_HUMAN	142 kDa	2	0
Developmentally-regulated GTP-binding protein 1 OS=Homo sapiens GN=DRG1 PE=1 SV=1	sp|Q9Y295|DRG1_HUMAN	41 kDa	2	2
28S ribosomal protein S7, mitochondrial OS=Homo sapiens GN=MRPS7 PE=1 SV=2	sp|Q9Y2R9|RT07_HUMAN	28 kDa	2	0
Suppressor of G2 allele of SKP1 homolog OS=Homo sapiens GN=SUGT1 PE=1 SV=3	sp|Q9Y2Z0|SUGT1_HUMAN	41 kDa	2	0
28S ribosomal protein S2, mitochondrial OS=Homo sapiens GN=MRPS2 PE=1 SV=1	sp|Q9Y399|RT02_HUMAN	33 kDa	2	2
Protein dopey-2 OS=Homo sapiens GN=DOPEY2 PE=1 SV=5	sp|Q9Y3R5|DOP2_HUMAN	258 kDa	2	0
SAM domain and HD domain-containing protein 1 OS=Homo sapiens GN=SAMHD1 PE=1 SV=2	sp|Q9Y3Z3|SAMH1_HUMAN	72 kDa	2	0
Tax_Id=9606 Gene_Symbol=KRT5 Keratin, type II cytoskeletal 5	IPI:CON_00009867.3|SWISS-PROT:P13647 (+1)	62 kDa	0	7
Tax_Id=9606 Gene_Symbol=KRT16 Keratin, type I cytoskeletal 16	IPI:CON_00217963.3|SWISS-PROT:P08779 (+2)	51 kDa	0	10
Tax_Id=9606 Gene_Symbol=KRT6C Keratin, type II cytoskeletal 6C	IPI:CON_00299145.9|SWISS-PROT:P48668 (+3)	60 kDa	0	7
Tax_Id=9606 Gene_Symbol=KRT14 Keratin, type I cytoskeletal 14	IPI:CON_00384444.5|SWISS-PROT:P02533 (+1)	52 kDa	0	11
Tax_Id=10090 Gene_Symbol=Krt4 Keratin, type II cytoskeletal 4	IPI:CON_00420312.4|SWISS-PROT:P07744	56 kDa	0	3
(Bos taurus) Alpha-1-antiproteinase precursor	IPI:CON_00695489.1|SWISS-PROT:P34955	46 kDa	0	2
(Bos taurus) similar to apolipoprotein B, partial	IPI:CON_00708008.1|ENSEMBL:ENSBTAP00000032840	92 kDa	0	3
(Bos taurus) similar to apolipoprotein B, partial	IPI:CON_00711422.1|ENSEMBL:ENSBTAP00000011213	410 kDa	0	4
(Bos taurus) Vitronectin	IPI:CON_00712934.1|TREMBL:Q3ZBS7	54 kDa	0	2
(Bos taurus) similar to HBG protein	IPI:CON_00713928.4|TREMBL:Q3SX09	22 kDa	0	2
Putative annexin A2-like protein OS=Homo sapiens GN=ANXA2P2 PE=5 SV=2	sp|A6NMY6|AXA2L_HUMAN (+1)	39 kDa	0	2
PDZ and LIM domain protein 1 OS=Homo sapiens GN=PDLIM1 PE=1 SV=4	sp|O00151|PDLI1_HUMAN	36 kDa	0	2
NADH dehydrogenase [ubiquinone] iron-sulfur protein 8, mitochondrial OS=Homo sapiens GN=NDUFS8 PE=1 SV=1	sp|O00217|NDUS8_HUMAN	24 kDa	0	4
Membrane-associated progesterone receptor component 1 OS=Homo sapiens GN=PGRMC1 PE=1 SV=3	sp|O00264|PGRC1_HUMAN	22 kDa	0	5
Golgi integral membrane protein 4 OS=Homo sapiens GN=GOLIM4 PE=1 SV=1	sp|O00461|GOLI4_HUMAN	82 kDa	0	3

Carboxylesterase 2 OS=Homo sapiens GN=CES2 PE=1 SV=1	sp|O00748|EST2_HUMAN	62 kDa	0	2
Lysosomal alpha-mannosidase OS=Homo sapiens GN=MAN2B1 PE=1 SV=3	sp|O00754|MA2B1_HUMAN	114 kDa	0	3
Protein RER1 OS=Homo sapiens GN=RER1 PE=1 SV=1	sp|O15258|RER1_HUMAN	23 kDa	0	2
Prolyl 4-hydroxylase subunit alpha-2 OS=Homo sapiens GN=P4HA2 PE=1 SV=1	sp|O15460|P4HA2_HUMAN	61 kDa	0	4
Thioredoxin-like protein 1 OS=Homo sapiens GN=TXNL1 PE=1 SV=3	sp|O43396|TXNL1_HUMAN	32 kDa	0	2
Trans-Golgi network integral membrane protein 2 OS=Homo sapiens GN=TGOLN2 PE=1 SV=2	sp|O43493|TGON2_HUMAN	51 kDa	0	5
Synaptogyrin-2 OS=Homo sapiens GN=SYNGR2 PE=1 SV=1	sp|O43760|SNG2_HUMAN	25 kDa	0	2
Procollagen-lysine,2-oxoglutarate 5-dioxygenase 3 OS=Homo sapiens GN=PLOD3 PE=1 SV=1	sp|O60568|PLOD3_HUMAN	85 kDa	0	3
Protein NipSnap homolog 2 OS=Homo sapiens GN=GBAS PE=1 SV=1	sp|O75323|NIPS2_HUMAN	34 kDa	0	3
Programmed cell death protein 6 OS=Homo sapiens GN=PDCD6 PE=1 SV=1	sp|O75340|PDCD6_HUMAN	22 kDa	0	2
Mannose-P-dolichol utilization defect 1 protein OS=Homo sapiens GN=MPDU1 PE=1 SV=2	sp|O75352|MPU1_HUMAN	27 kDa	0	3
Metaxin-2 OS=Homo sapiens GN=MTX2 PE=1 SV=1	sp|O75431|MTX2_HUMAN	30 kDa	0	2
Erlin-1 OS=Homo sapiens GN=ERLIN1 PE=1 SV=1	sp|O75477|ERLN1_HUMAN	39 kDa	0	6
Peroxisomal 3,2-trans-enoyl-CoA isomerase OS=Homo sapiens GN=PECI PE=1 SV=4	sp|O75521|PECI_HUMAN	44 kDa	0	3
CAAX prenyl protease 1 homolog OS=Homo sapiens GN=ZMPSTE24 PE=1 SV=2	sp|O75844|FACE1_HUMAN	55 kDa	0	7
Protein SCO1 homolog, mitochondrial OS=Homo sapiens GN=SCO1 PE=1 SV=1	sp|O75880|SCO1_HUMAN	34 kDa	0	3
ATP synthase subunit g, mitochondrial OS=Homo sapiens GN=ATP5L PE=1 SV=3	sp|O75964|ATP5L_HUMAN	11 kDa	0	4
Wolframin OS=Homo sapiens GN=WFS1 PE=1 SV=2	sp|O76024|WFS1_HUMAN	100 kDa	0	2
Retinal dehydrogenase 2 OS=Homo sapiens GN=ALDH1A2 PE=1 SV=3	sp|O94788|AL1A2_HUMAN	57 kDa	0	2
LETM1 and EF-hand domain-containing protein 1, mitochondrial OS=Homo sapiens GN=LETM1 PE=1 SV=1	sp|O95202|LETM1_HUMAN	83 kDa	0	5
NADH dehydrogenase [ubiquinone] 1 alpha subcomplex subunit 10, mitochondrial OS=Homo sapiens GN=NDUFA10 PE=1 SV=1	sp|O95299|NDUAA_HUMAN	41 kDa	0	4
Brain protein 44 OS=Homo sapiens GN=BRP44 PE=1 SV=1	sp|O95563|BR44_HUMAN	14 kDa	0	2
Phosphatidate cytidylyltransferase 2 OS=Homo sapiens GN=CDS2 PE=1 SV=1	sp|O95674|CDS2_HUMAN	51 kDa	0	2
3'(2'),5'-bisphosphate nucleotidase 1 OS=Homo sapiens GN=BPNT1 PE=1 SV=1	sp|O95861|BPNT1_HUMAN	33 kDa	0	2
NADH dehydrogenase [ubiquinone] 1 beta subcomplex subunit 10 OS=Homo sapiens GN=NDUFB10 PE=1 SV=3	sp|O96000|NDUBA_HUMAN	21 kDa	0	3
Cleft lip and palate transmembrane protein 1 OS=Homo sapiens GN=CLPTM1 PE=1 SV=1	sp|O96005|CLPT1_HUMAN	76 kDa	0	2
Prelamin-A/C OS=Homo sapiens GN=LMNA PE=1 SV=1	sp|P02545|LMNA_HUMAN	74 kDa	0	2
Fibrinogen alpha chain OS=Homo sapiens GN=FGA PE=1 SV=2	sp|P02671|FIBA_HUMAN	95 kDa	0	2
Cystatin-B OS=Homo sapiens GN=CSTB PE=1 SV=2	sp|P04080|CYTB_HUMAN	11 kDa	0	2
Ornithine aminotransferase, mitochondrial OS=Homo sapiens GN=OAT PE=1 SV=1	sp|P04181|OAT_HUMAN	49 kDa	0	9

Propionyl-CoA carboxylase beta chain, mitochondrial OS=Homo sapiens GN=PCCB PE=1 SV=3	sp|P05166|PCCB_HUMAN	58 kDa	0	2
Beta-hexosaminidase subunit alpha OS=Homo sapiens GN=HEXA PE=1 SV=2	sp|P06865|HEXA_HUMAN	61 kDa	0	5
Histone H1.0 OS=Homo sapiens GN=H1F0 PE=1 SV=3	sp|P07305|H10_HUMAN	21 kDa	0	5
Asialoglycoprotein receptor 2 OS=Homo sapiens GN=ASGR2 PE=1 SV=2	sp|P07307|ASGR2_HUMAN	35 kDa	0	5
Proactivator polypeptide OS=Homo sapiens GN=PSAP PE=1 SV=2	sp|P07602|SAP_HUMAN	58 kDa	0	2
Beta-hexosaminidase subunit beta OS=Homo sapiens GN=HEXB PE=1 SV=3	sp|P07686|HEXB_HUMAN	63 kDa	0	7
Multidrug resistance protein 1 OS=Homo sapiens GN=ABCB1 PE=1 SV=3	sp|P08183|MDR1_HUMAN	141 kDa	0	2
Heme oxygenase 1 OS=Homo sapiens GN=HMOX1 PE=1 SV=1	sp|P09601|HMOX1_HUMAN	33 kDa	0	8
Cathepsin H OS=Homo sapiens GN=CTSH PE=1 SV=4	sp|P09668|CATH_HUMAN	37 kDa	0	2
Leukotriene A-4 hydrolase OS=Homo sapiens GN=LTA4H PE=1 SV=2	sp|P09960|LKHA4_HUMAN	69 kDa	0	2
Ras-related protein Ral-A OS=Homo sapiens GN=RALA PE=1 SV=1	sp|P11233|RALA_HUMAN	24 kDa	0	3
Lysosome-associated membrane glycoprotein 1 OS=Homo sapiens GN=LAMP1 PE=1 SV=3	sp|P11279|LAMP1_HUMAN	45 kDa	0	2
Lysosome-associated membrane glycoprotein 2 OS=Homo sapiens GN=LAMP2 PE=1 SV=2	sp|P13473|LAMP2_HUMAN	45 kDa	0	2
CD59 glycoprotein OS=Homo sapiens GN=CD59 PE=1 SV=1	sp|P13987|CD59_HUMAN	14 kDa	0	2
Bifunctional methylenetetrahydrofolate dehydrogenase/cyclohydrolase, mitochondrial OS=Homo sapiens GN=MTHFD2 PE=1 SV=2	sp|P13995|MTDC_HUMAN	38 kDa	0	2
N-acetylglucosamine-6-sulfatase OS=Homo sapiens GN=GNS PE=1 SV=3	sp|P15586|GNS_HUMAN	62 kDa	0	2
Arylsulfatase B OS=Homo sapiens GN=ARSB PE=1 SV=1	sp|P15848|ARSB_HUMAN	60 kDa	0	3
Epithelial cell adhesion molecule OS=Homo sapiens GN=EPCAM PE=1 SV=2	sp|P16422|EPCAM_HUMAN	35 kDa	0	2
Integrin alpha-2 OS=Homo sapiens GN=ITGA2 PE=1 SV=1	sp|P17301|ITA2_HUMAN	129 kDa	0	7
Tyrosine-protein phosphatase non-receptor type 1 OS=Homo sapiens GN=PTPN1 PE=1 SV=1	sp|P18031|PTN1_HUMAN	50 kDa	0	3
NADH dehydrogenase [ubiquinone] flavoprotein 2, mitochondrial OS=Homo sapiens GN=NDUFV2 PE=1 SV=2	sp|P19404|NDUV2_HUMAN	27 kDa	0	4
Annexin A7 OS=Homo sapiens GN=ANXA7 PE=1 SV=3	sp|P20073|ANXA7_HUMAN	53 kDa	0	3
Ras-related protein Rab-6A OS=Homo sapiens GN=RAB6A PE=1 SV=3	sp|P20340|RAB6A_HUMAN	24 kDa	0	4
Cation-dependent mannose-6-phosphate receptor OS=Homo sapiens GN=M6PR PE=1 SV=1	sp|P20645|MPRD_HUMAN	31 kDa	0	3
Histone H2A type 1-D OS=Homo sapiens GN=HIST1H2AD PE=1 SV=2	sp|P20671|H2A1D_HUMAN	14 kDa	0	14
Lamin-B1 OS=Homo sapiens GN=LMNB1 PE=1 SV=2	sp|P20700|LMNB1_HUMAN	66 kDa	0	3
Non-specific lipid-transfer protein OS=Homo sapiens GN=SCP2 PE=1 SV=2	sp|P22307|NLTP_HUMAN	59 kDa	0	3
ER lumen protein retaining receptor 1 OS=Homo sapiens GN=KDELR1 PE=1 SV=1	sp|P24390|ERD21_HUMAN	25 kDa	0	5
Erythrocyte band 7 integral membrane protein OS=Homo sapiens GN=STOM PE=1 SV=3	sp|P27105|STOM_HUMAN	32 kDa	0	4
Amine oxidase [flavin-containing] B OS=Homo sapiens GN=MAOB PE=1 SV=3	sp|P27338|AOFB_HUMAN	59 kDa	0	6

Proteasome subunit beta type-4 OS=Homo sapiens GN=PSMB4 PE=1 SV=4	sp|P28070|PSB4_HUMAN	29 kDa	0	3
ES1 protein homolog, mitochondrial OS=Homo sapiens GN=C21orf33 PE=1 SV=3	sp|P30042|ES1_HUMAN	28 kDa	0	3
ATP synthase subunit delta, mitochondrial OS=Homo sapiens GN=ATP5D PE=1 SV=2	sp|P30049|ATPD_HUMAN	17 kDa	0	2
S-adenosylmethionine synthase isoform type-2 OS=Homo sapiens GN=MAT2A PE=1 SV=1	sp|P31153|METK2_HUMAN	44 kDa	0	2
Deoxyuridine 5'-triphosphate nucleotidohydrolase, mitochondrial OS=Homo sapiens GN=DUT PE=1 SV=3	sp|P33316|DUT_HUMAN	27 kDa	0	3
Mannosyl-oligosaccharide 1,2-alpha-mannosidase IA OS=Homo sapiens GN=MAN1A1 PE=1 SV=3	sp|P33908|MA1A1_HUMAN	73 kDa	0	4
Serpin B6 OS=Homo sapiens GN=SERPINB6 PE=1 SV=3	sp|P35237|SPB6_HUMAN	43 kDa	0	2
Sepiapterin reductase OS=Homo sapiens GN=SPR PE=1 SV=1	sp|P35270|SPRE_HUMAN	28 kDa	0	5
Keratin, type I cytoskeletal 9 OS=Homo sapiens GN=KRT9 PE=1 SV=3	sp|P35527|K1C9_HUMAN	62 kDa	0	25
Coproporphyrinogen-III oxidase, mitochondrial OS=Homo sapiens GN=CPOX PE=1 SV=3	sp|P36551|HEM6_HUMAN	50 kDa	0	5
V-type proton ATPase catalytic subunit A OS=Homo sapiens GN=ATP6V1A PE=1 SV=2	sp|P38606|VATA_HUMAN	68 kDa	0	3
Signal transducer and activator of transcription 3 OS=Homo sapiens GN=STAT3 PE=1 SV=2	sp|P40763|STAT3_HUMAN	88 kDa	0	3
DNA mismatch repair protein Msh2 OS=Homo sapiens GN=MSH2 PE=1 SV=1	sp|P43246|MSH2_HUMAN	105 kDa	0	3
Ubiquitin carboxyl-terminal hydrolase 5 OS=Homo sapiens GN=USP5 PE=1 SV=2	sp|P45974|UBP5_HUMAN	96 kDa	0	2
Ran GTPase-activating protein 1 OS=Homo sapiens GN=RANGAP1 PE=1 SV=1	sp|P46060|RAGP1_HUMAN	64 kDa	0	2
Glutathione synthetase OS=Homo sapiens GN=GSS PE=1 SV=1	sp|P48637|GSHB_HUMAN	52 kDa	0	2
Seryl-tRNA synthetase, cytoplasmic OS=Homo sapiens GN=SARS PE=1 SV=3	sp|P49591|SYSC_HUMAN	59 kDa	0	2
DNA replication licensing factor MCM2 OS=Homo sapiens GN=MCM2 PE=1 SV=4	sp|P49736|MCM2_HUMAN	102 kDa	0	2
28S ribosomal protein S29, mitochondrial OS=Homo sapiens GN=DAP3 PE=1 SV=1	sp|P51398|RT29_HUMAN	46 kDa	0	4
Alpha-soluble NSF attachment protein OS=Homo sapiens GN=NAPA PE=1 SV=3	sp|P54920|SNAA_HUMAN	33 kDa	0	2
Afadin OS=Homo sapiens GN=MLLT4 PE=1 SV=3	sp|P55196|AFAD_HUMAN	207 kDa	0	2
Protein transport protein Sec61 subunit beta OS=Homo sapiens GN=SEC61B PE=1 SV=2	sp|P60468|SC61B_HUMAN	10 kDa	0	2
Ras-related protein Rab-8A OS=Homo sapiens GN=RAB8A PE=1 SV=1	sp|P61006|RAB8A_HUMAN	24 kDa	0	6
Ras-related protein Rab-14 OS=Homo sapiens GN=RAB14 PE=1 SV=4	sp|P61106|RAB14_HUMAN	24 kDa	0	6
Proteasome activator complex subunit 3 OS=Homo sapiens GN=PSME3 PE=1 SV=1	sp|P61289|PSME3_HUMAN	30 kDa	0	3
Beta-2-microglobulin OS=Homo sapiens GN=B2M PE=1 SV=1	sp|P61769|B2MG_HUMAN	14 kDa	0	4
Serine/threonine-protein phosphatase 2A catalytic subunit beta isoform OS=Homo sapiens GN=PPP2CB PE=1 SV=1	sp|P62714|PP2AB_HUMAN (+1)	36 kDa	0	4
Signal peptidase complex catalytic subunit SEC11A OS=Homo sapiens GN=SEC11A PE=1 SV=1	sp|P67812|SC11A_HUMAN	21 kDa	0	2
Ubiquitin-conjugating enzyme E2 L3 OS=Homo sapiens GN=UBE2L3 PE=1 SV=1	sp|P68036|UB2L3_HUMAN	18 kDa	0	2
Nodal modulator 3 OS=Homo sapiens GN=NOMO3 PE=2 SV=2	sp|P69849|NOMO3_HUMAN (+1)	134 kDa	0	7
Nucleobindin-2 OS=Homo sapiens GN=NUCB2	sp|P80303|NUCB2_HUMAN	50 kDa	0	3

PE=1 SV=2				
Transcription factor A, mitochondrial OS=Homo sapiens GN=TFAM PE=1 SV=1	sp|Q00059|TFAM_HUMAN	29 kDa	0	4
Large neutral amino acids transporter small subunit 1 OS=Homo sapiens GN=SLC7A5 PE=1 SV=2	sp|Q01650|LAT1_HUMAN	55 kDa	0	5
2-oxoglutarate dehydrogenase, mitochondrial OS=Homo sapiens GN=OGDH PE=1 SV=3	sp|Q02218|ODO1_HUMAN	116 kDa	0	2
Sterol 26-hydroxylase, mitochondrial OS=Homo sapiens GN=CYP27A1 PE=1 SV=1	sp|Q02318|CP27A_HUMAN	60 kDa	0	5
Nucleobindin-1 OS=Homo sapiens GN=NUCB1 PE=1 SV=4	sp|Q02818|NUCB1_HUMAN	54 kDa	0	4
Peptidyl-prolyl cis-trans isomerase D OS=Homo sapiens GN=PPID PE=1 SV=3	sp|Q08752|PPID_HUMAN	41 kDa	0	2
Nuclear cap-binding protein subunit 1 OS=Homo sapiens GN=NCBP1 PE=1 SV=1	sp|Q09161|NCBP1_HUMAN	92 kDa	0	2
Polypeptide N-acetylgalactosaminyltransferase 2 OS=Homo sapiens GN=GALNT2 PE=1 SV=1	sp|Q10471|GALT2_HUMAN	65 kDa	0	3
DnaJ homolog subfamily C member 3 OS=Homo sapiens GN=DNAJC3 PE=1 SV=1	sp|Q13217|DNJC3_HUMAN	58 kDa	0	2
Ras GTPase-activating protein-binding protein 1 OS=Homo sapiens GN=G3BP1 PE=1 SV=1	sp|Q13283|G3BP1_HUMAN	52 kDa	0	5
Acid ceramidase OS=Homo sapiens GN=ASAH1 PE=1 SV=5	sp|Q13510|ASAH1_HUMAN	45 kDa	0	2
Cullin-4A OS=Homo sapiens GN=CUL4A PE=1 SV=3	sp|Q13619|CUL4A_HUMAN (+1)	88 kDa	0	2
Lamin-B receptor OS=Homo sapiens GN=LBR PE=1 SV=2	sp|Q14739|LBR_HUMAN	71 kDa	0	5
Chromodomain-helicase-DNA-binding protein 4 OS=Homo sapiens GN=CHD4 PE=1 SV=2	sp|Q14839|CHD4_HUMAN	218 kDa	0	3
Tetratricopeptide repeat protein 35 OS=Homo sapiens GN=TTC35 PE=1 SV=1	sp|Q15006|TTC35_HUMAN	35 kDa	0	2
Mitochondrial inner membrane protein OXA1L OS=Homo sapiens GN=OXA1L PE=1 SV=3	sp|Q15070|OXA1L_HUMAN	49 kDa	0	2
Ras-related protein Rab-35 OS=Homo sapiens GN=RAB35 PE=1 SV=1	sp|Q15286|RAB35_HUMAN	23 kDa	0	5
Transmembrane emp24 domain-containing protein 2 OS=Homo sapiens GN=TMED2 PE=1 SV=1	sp|Q15363|TMED2_HUMAN	23 kDa	0	4
Nuclear receptor coactivator 2 OS=Homo sapiens GN=NCOA2 PE=1 SV=2	sp|Q15596|NCOA2_HUMAN	159 kDa	0	2
Translin OS=Homo sapiens GN=TSN PE=1 SV=1	sp|Q15631|TSN_HUMAN	26 kDa	0	5
Splicing factor 1 OS=Homo sapiens GN=SF1 PE=1 SV=4	sp|Q15637|SF01_HUMAN	68 kDa	0	2
Microtubule-associated protein RP/EB family member 1 OS=Homo sapiens GN=MAPRE1 PE=1 SV=3	sp|Q15691|MARE1_HUMAN	30 kDa	0	4
Neutral amino acid transporter B(0) OS=Homo sapiens GN=SLC1A5 PE=1 SV=2	sp|Q15758|AAAT_HUMAN	57 kDa	0	4
Alpha-mannosidase 2 OS=Homo sapiens GN=MAN2A1 PE=1 SV=2	sp|Q16706|MA2A1_HUMAN	131 kDa	0	3
Lanosterol 14-alpha demethylase OS=Homo sapiens GN=CYP51A1 PE=1 SV=3	sp|Q16850|CP51A_HUMAN	57 kDa	0	3
Mitochondrial import inner membrane translocase subunit TIM50 OS=Homo sapiens GN=TIMM50 PE=1 SV=2	sp|Q3ZCQ8|TIM50_HUMAN	40 kDa	0	3
Coiled-coil domain-containing protein 58 OS=Homo sapiens GN=CCDC58 PE=1 SV=1	sp|Q4VC31|CCD58_HUMAN	17 kDa	0	2
Torsin-1A-interacting protein 1 OS=Homo sapiens GN=TOR1AIP1 PE=1 SV=2	sp|Q5JTV8|TOIP1_HUMAN	66 kDa	0	4
3-hydroxyisobutyryl-CoA hydrolase, mitochondrial OS=Homo sapiens GN=HIBCH PE=1 SV=2	sp|Q6NVY1|HIBCH_HUMAN	43 kDa	0	5
UPF0598 protein C8orf82 OS=Homo sapiens	sp|Q6P1X6|CH082_HUMAN	24 kDa	0	2

GN=C8orf82 PE=1 SV=2				
FAST kinase domain-containing protein 5 OS=Homo sapiens GN=FASTKD5 PE=1 SV=1	sp|Q7L8L6|FAKD5_HUMAN	87 kDa	0	2
Transmembrane emp24 domain-containing protein 4 OS=Homo sapiens GN=TMED4 PE=1 SV=1	sp|Q7Z7H5|TMED4_HUMAN	26 kDa	0	5
Protein KIAA1967 OS=Homo sapiens GN=KIAA1967 PE=1 SV=2	sp|Q8N163|K1967_HUMAN	103 kDa	0	3
Immunoglobulin superfamily member 1 OS=Homo sapiens GN=IGSF1 PE=1 SV=3	sp|Q8N6C5|IGSF1_HUMAN	149 kDa	0	2
Uncharacterized protein KIAA0090 OS=Homo sapiens GN=KIAA0090 PE=1 SV=1	sp|Q8N766|K0090_HUMAN	112 kDa	0	2
Aflatoxin B1 aldehyde reductase member 4 OS=Homo sapiens GN=AKR7L PE=2 SV=6	sp|Q8NHP1|ARK74_HUMAN	37 kDa	0	2
Adenosine 3'-phospho 5'-phosphosulfate transporter 1 OS=Homo sapiens GN=SLC35B2 PE=1 SV=1	sp|Q8TB61|S35B2_HUMAN	48 kDa	0	3
Polyribonucleotide nucleotidyltransferase 1, mitochondrial OS=Homo sapiens GN=PNPT1 PE=1 SV=2	sp|Q8TCS8|PNPT1_HUMAN	86 kDa	0	3
UBX domain-containing protein 4 OS=Homo sapiens GN=UBXN4 PE=1 SV=2	sp|Q92575|UBXN4_HUMAN	57 kDa	0	2
GPI-anchor transamidase OS=Homo sapiens GN=PIGK PE=1 SV=2	sp|Q92643|GPI8_HUMAN	45 kDa	0	2
Protein FAM162A OS=Homo sapiens GN=FAM162A PE=1 SV=2	sp|Q96A26|F162A_HUMAN	17 kDa	0	3
Peptidyl-prolyl cis-trans isomerase FKBP10 OS=Homo sapiens GN=FKBP10 PE=1 SV=1	sp|Q96AY3|FKB10_HUMAN	64 kDa	0	6
Aldose 1-epimerase OS=Homo sapiens GN=GALM PE=1 SV=1	sp|Q96C23|GALM_HUMAN	38 kDa	0	4
LAG1 longevity assurance homolog 2 OS=Homo sapiens GN=LASS2 PE=1 SV=1	sp|Q96G23|LASS2_HUMAN	45 kDa	0	2
Transmembrane protein 49 OS=Homo sapiens GN=TMEM49 PE=2 SV=1	sp|Q96GC9|TMM49_HUMAN	46 kDa	0	3
DDRGK domain-containing protein 1 OS=Homo sapiens GN=DDRGK1 PE=1 SV=2	sp|Q96HY6|DDRGK_HUMAN	36 kDa	0	3
Probable asparaginyl-tRNA synthetase, mitochondrial OS=Homo sapiens GN=NARS2 PE=1 SV=3	sp|Q96I59|SYNM_HUMAN	54 kDa	0	4
Succinyl-CoA ligase [GDP-forming] subunit beta, mitochondrial OS=Homo sapiens GN=SUCLG2 PE=1 SV=2	sp|Q96I99|SUCB2_HUMAN	47 kDa	0	6
CDK5 regulatory subunit-associated protein 3 OS=Homo sapiens GN=CDK5RAP3 PE=1 SV=2	sp|Q96JB5|CK5P3_HUMAN	57 kDa	0	3
GPI transamidase component PIG-S OS=Homo sapiens GN=PIGS PE=1 SV=3	sp|Q96S52|PIGS_HUMAN	62 kDa	0	2
Sortilin OS=Homo sapiens GN=SORT1 PE=1 SV=3	sp|Q99523|SORT_HUMAN	92 kDa	0	4
Perilipin-2 OS=Homo sapiens GN=PLIN2 PE=1 SV=2	sp|Q99541|PLIN2_HUMAN	48 kDa	0	7
Nucleosome assembly protein 1-like 4 OS=Homo sapiens GN=NAP1L4 PE=1 SV=1	sp|Q99733|NP1L4_HUMAN	43 kDa	0	5
Microsomal glutathione S-transferase 2 OS=Homo sapiens GN=MGST2 PE=1 SV=1	sp|Q99735|MGST2_HUMAN	17 kDa	0	2
45 kDa calcium-binding protein OS=Homo sapiens GN=SDF4 PE=1 SV=1	sp|Q9BRK5|CAB45_HUMAN	42 kDa	0	2
UPF0765 protein C10orf58 OS=Homo sapiens GN=C10orf58 PE=1 SV=3	sp|Q9BRX8|CJ058_HUMAN	26 kDa	0	3
Agmatinase, mitochondrial OS=Homo sapiens GN=AGMAT PE=1 SV=2	sp|Q9BSE5|SPEB_HUMAN	38 kDa	0	7
Cell adhesion molecule 1 OS=Homo sapiens GN=CADM1 PE=1 SV=2	sp|Q9BY67|CADM1_HUMAN	49 kDa	0	3
39S ribosomal protein L1, mitochondrial OS=Homo sapiens GN=MRPL1 PE=1 SV=2	sp|Q9BYD6|RM01_HUMAN	37 kDa	0	3

5'-3' exoribonuclease 2 OS=Homo sapiens GN=XRN2 PE=1 SV=1	sp|Q9H0D6|XRN2_HUMAN	109 kDa	0	2
Inorganic pyrophosphatase 2, mitochondrial OS=Homo sapiens GN=PPA2 PE=1 SV=2	sp|Q9H2U2|IPYR2_HUMAN	38 kDa	0	4
39S ribosomal protein L46, mitochondrial OS=Homo sapiens GN=MRPL46 PE=1 SV=1	sp|Q9H2W6|RM46_HUMAN	32 kDa	0	2
Transmembrane protein C9orf5 OS=Homo sapiens GN=C9orf5 PE=1 SV=2	sp|Q9H330|CI005_HUMAN	101 kDa	0	2
DnaJ homolog subfamily C member 5 OS=Homo sapiens GN=DNAJC5 PE=1 SV=1	sp|Q9H3Z4|DNJC5_HUMAN	22 kDa	0	3
GDP-fucose protein O-fucosyltransferase 1 OS=Homo sapiens GN=POFUT1 PE=1 SV=1	sp|Q9H488|OFUT1_HUMAN	44 kDa	0	5
Acyl-CoA dehydrogenase family member 9, mitochondrial OS=Homo sapiens GN=ACAD9 PE=1 SV=1	sp|Q9H845|ACAD9_HUMAN	69 kDa	0	5
Probable cysteinyl-tRNA synthetase, mitochondrial OS=Homo sapiens GN=CARS2 PE=1 SV=1	sp|Q9HA77|SYCM_HUMAN	62 kDa	0	2
Thioredoxin reductase 2, mitochondrial OS=Homo sapiens GN=TXNRD2 PE=1 SV=3	sp|Q9NNW7|TRXR2_HUMAN	57 kDa	0	3
Acyl-coenzyme A thioesterase 13 OS=Homo sapiens GN=ACOT13 PE=1 SV=1	sp|Q9NPJ3|ACO13_HUMAN	15 kDa	0	2
PDZ and LIM domain protein 7 OS=Homo sapiens GN=PDLIM7 PE=1 SV=1	sp|Q9NR12|PDLI7_HUMAN	50 kDa	0	2
Enoyl-CoA hydratase domain-containing protein 1 OS=Homo sapiens GN=ECHDC1 PE=1 SV=2	sp|Q9NTX5|ECHD1_HUMAN	34 kDa	0	2
Mitochondrial carrier homolog 1 OS=Homo sapiens GN=MTCH1 PE=1 SV=1	sp|Q9NZJ7|MTCH1_HUMAN	42 kDa	0	6
NADH dehydrogenase [ubiquinone] 1 alpha subcomplex subunit 13 OS=Homo sapiens GN=NDUFA13 PE=1 SV=3	sp|Q9P0J0|NDUAD_HUMAN	17 kDa	0	5
Transmembrane protein 14C OS=Homo sapiens GN=TMEM14C PE=1 SV=1	sp|Q9P0S9|TM14C_HUMAN	12 kDa	0	3
Transmembrane protein 2 OS=Homo sapiens GN=TMEM2 PE=1 SV=1	sp|Q9UHN6|TMEM2_HUMAN	154 kDa	0	3
Poly(U)-binding-splicing factor PUF60 OS=Homo sapiens GN=PUF60 PE=1 SV=1	sp|Q9UHX1|PUF60_HUMAN	60 kDa	0	2
Importin-11 OS=Homo sapiens GN=IPO11 PE=1 SV=1	sp|Q9UI26|IPO11_HUMAN	113 kDa	0	2
Nuclear pore complex protein Nup50 OS=Homo sapiens GN=NUP50 PE=1 SV=2	sp|Q9UKX7|NUP50_HUMAN	50 kDa	0	2
Coronin-1C OS=Homo sapiens GN=CORO1C PE=1 SV=1	sp|Q9ULV4|COR1C_HUMAN	53 kDa	0	2
HIG1 domain family member 1A OS=Homo sapiens GN=HIGD1A PE=1 SV=1	sp|Q9Y241|HIG1A_HUMAN	10 kDa	0	3
Glutathione S-transferase kappa 1 OS=Homo sapiens GN=GSTK1 PE=1 SV=3	sp|Q9Y2Q3|GSTK1_HUMAN	25 kDa	0	2
28S ribosomal protein S28, mitochondrial OS=Homo sapiens GN=MRPS28 PE=1 SV=1	sp|Q9Y2Q9|RT28_HUMAN	21 kDa	0	2
Transmembrane emp24 domain-containing protein 5 OS=Homo sapiens GN=TMED5 PE=1 SV=1	sp|Q9Y3A6|TMED5_HUMAN	26 kDa	0	2
Mitochondrial fission 1 protein OS=Homo sapiens GN=FIS1 PE=1 SV=2	sp|Q9Y3D6|FIS1_HUMAN	17 kDa	0	2
Junctional adhesion molecule A OS=Homo sapiens GN=F11R PE=1 SV=1	sp|Q9Y624|JAM1_HUMAN	33 kDa	0	3
NADH dehydrogenase [ubiquinone] 1 beta subcomplex subunit 9 OS=Homo sapiens GN=NDUFB9 PE=1 SV=3	sp|Q9Y6M9|NDUB9_HUMAN	22 kDa	0	5

APPENDIX C

OPTIMIZED GEOMETRIES OF THE 8 CP-PAHS (NEUTRAL AND ANION)

USING B3LYP/6-311G(D,P)

C1. CP-PAH **1** *Neutral* Optimized Geometry

Center Number	Atomic Number	Atomic Type	Coordinates (Angstroms) X	Y	Z
1	6	0	-0.069397	1.465803	0.000063
2	6	0	-0.346327	2.867075	0.000142
3	1	0	0.470943	3.579012	0.000187
4	6	0	-1.648806	3.317810	0.000159
5	1	0	-1.839189	4.384874	0.000221
6	6	0	-2.765574	2.428077	0.000096
7	1	0	-3.772306	2.831110	0.000117
8	6	0	-2.530681	1.075280	0.000020
9	6	0	-1.191824	0.606714	0.000003
10	6	0	-1.187078	-0.809232	-0.000100
11	6	0	0.069392	-1.465563	-0.000143
12	6	0	1.191819	-0.606475	-0.000071
13	6	0	1.187072	0.809471	0.000026
14	6	0	0.346323	-2.866835	-0.000251
15	1	0	-0.470947	-3.578773	-0.000309
16	6	0	1.648801	-3.317570	-0.000283
17	1	0	1.839183	-4.384634	-0.000362
18	6	0	2.765569	-2.427836	-0.000212
19	1	0	3.772302	-2.830871	-0.000232
20	6	0	2.530676	-1.075040	-0.000100
21	6	0	-3.395167	-0.129056	-0.000045
22	6	0	-2.569060	-1.239290	-0.000151
23	1	0	-2.912447	-2.263826	-0.000236
24	6	0	2.569054	1.239530	0.000033
25	1	0	2.912437	2.264067	0.000083
26	6	0	3.395162	0.129298	0.000023
27	6	0	4.798843	0.106372	0.000047
28	6	0	6.013226	0.055850	0.000055
29	6	0	-4.798848	-0.106122	-0.000039
30	6	0	-6.013233	-0.055639	-0.000039
31	6	0	7.430750	0.007763	0.000067
32	6	0	8.196004	1.186893	0.000083
33	1	0	7.691716	2.145690	0.000084
34	6	0	9.585737	1.147654	0.000093
35	1	0	10.139697	2.076310	0.000100
36	6	0	10.246963	-0.086670	0.000091
37	6	0	9.496383	-1.273072	0.000075
38	1	0	10.024086	-2.219156	0.000073
39	6	0	8.115536	-1.227630	0.000063
40	1	0	7.547234	-2.149850	0.000051

41	6	0	-7.430763	-0.007744	-0.000034
42	6	0	-8.195865	-1.186972	-0.000110
43	1	0	-7.691455	-2.145704	-0.000178
44	6	0	-9.585603	-1.147910	-0.000104
45	1	0	-10.139450	-2.076635	-0.000170
46	6	0	-10.246985	0.086329	-0.000017
47	6	0	-9.496560	1.272828	0.000060
48	1	0	-10.024385	2.218844	0.000128
49	6	0	-8.115707	1.227562	0.000051
50	1	0	-7.547524	2.149856	0.000113
51	8	0	11.595262	-0.240133	0.000094
52	8	0	-11.595303	0.239605	-0.000012
53	6	0	-12.418868	-0.928187	0.000068
54	1	0	-12.246797	-1.533980	-0.894464
55	1	0	-13.444330	-0.564995	0.000183
56	1	0	-12.246600	-1.533996	0.894550
57	6	0	12.419013	0.927529	0.000180
58	1	0	13.444419	0.564178	0.000230
59	1	0	12.246886	1.533330	0.894696
60	1	0	12.246993	1.533386	-0.894319

C2. CP-PAH **1** *Anion* Optimized Geometry

Center Number	Atomic Number	Atomic Type	Coordinates (Angstroms) X	Y	Z
1	6	0	-0.066654	1.478632	0.000083
2	6	0	-0.328084	2.869862	0.000154
3	1	0	0.495772	3.575936	0.000194
4	6	0	-1.640363	3.344721	0.000175
5	1	0	-1.809772	4.416719	0.000231
6	6	0	-2.753317	2.481408	0.000126
7	1	0	-3.758439	2.890734	0.000149
8	6	0	-2.531145	1.106514	0.000055
9	6	0	-1.195652	0.627365	0.000032
10	6	0	-1.201078	-0.801755	-0.000056
11	6	0	0.066654	-1.478603	-0.000091
12	6	0	1.195652	-0.627336	-0.000034
13	6	0	1.201078	0.801784	0.000047
14	6	0	0.328083	-2.869833	-0.000175
15	1	0	-0.495773	-3.575906	-0.000222
16	6	0	1.640362	-3.344692	-0.000197
17	1	0	1.809771	-4.416689	-0.000258
18	6	0	2.753316	-2.481379	-0.000137
19	1	0	3.758438	-2.890704	-0.000148
20	6	0	2.531144	-1.106485	-0.000053
21	6	0	-3.396066	-0.074333	-0.000001
22	6	0	-2.563055	-1.209371	-0.000095

23	1	0	-2.924339	-2.229298	-0.000164
24	6	0	2.563054	1.209400	0.000061
25	1	0	2.924339	2.229327	0.000109
26	6	0	3.396065	0.074362	0.000048
27	6	0	4.798656	0.057445	0.000080
28	6	0	6.016662	0.021419	0.000082
29	6	0	-4.798657	-0.057414	0.000012
30	6	0	-6.016663	-0.021391	0.000009
31	6	0	7.435232	-0.010593	0.000061
32	6	0	8.193790	1.174082	0.000088
33	1	0	7.681354	2.128828	0.000123
34	6	0	9.585816	1.149684	0.000070
35	1	0	10.128001	2.085688	0.000091
36	6	0	10.261841	-0.074620	0.000025
37	6	0	9.522879	-1.266335	-0.000001
38	1	0	10.059046	-2.208167	-0.000035
39	6	0	8.139900	-1.236043	0.000017
40	1	0	7.583738	-2.165937	-0.000004
41	6	0	-7.435234	0.010598	-0.000011
42	6	0	-8.193771	-1.174090	-0.000135
43	1	0	-7.681320	-2.128827	-0.000220
44	6	0	-9.585798	-1.149716	-0.000149
45	1	0	-10.127966	-2.085729	-0.000247
46	6	0	-10.261843	0.074576	-0.000040
47	6	0	-9.522901	1.266304	0.000084
48	1	0	-10.059084	2.208127	0.000169
49	6	0	-8.139922	1.236035	0.000098
50	1	0	-7.583776	2.165938	0.000196
51	8	0	11.618766	-0.213962	0.000002
52	8	0	-11.618771	0.213896	-0.000045
53	6	0	-12.421456	-0.964759	-0.000136
54	1	0	-12.240793	-1.570273	-0.894018
55	1	0	-13.453986	-0.620686	-0.000105
56	1	0	-12.240786	-1.570415	0.893648
57	6	0	12.421472	0.964679	0.000029
58	1	0	13.453996	0.620587	0.000009
59	1	0	12.240825	1.570241	0.893881
60	1	0	12.240807	1.570292	-0.893785

C3. CP-PAH **2** *Neutral* Optimized Geometry

Center Number	Atomic Number	Atomic Type	Coordinates (Angstroms) X	Y	Z
1	6	0	-2.798055	4.040837	-0.000030
2	6	0	-1.457498	3.734581	-0.000024
3	6	0	-1.033302	2.364719	-0.000019
4	6	0	-3.819071	3.033624	-0.000034

5	6	0	0.281251	1.882624	-0.000017
6	6	0	-0.548452	-0.496808	-0.000017
7	6	0	0.548445	0.496837	-0.000017
8	6	0	-0.281259	-1.882596	-0.000014
9	1	0	1.113751	2.577103	-0.000019
10	1	0	-3.104145	5.080603	-0.000033
11	1	0	-0.717074	4.526863	-0.000024
12	1	0	-4.861570	3.332623	-0.000033
13	1	0	-1.113761	-2.577072	-0.000012
14	6	0	1.033294	-2.364691	-0.000017
15	6	0	1.457492	-3.734554	-0.000015
16	6	0	2.798048	-4.040809	-0.000018
17	1	0	0.717067	-4.526835	-0.000010
18	6	0	3.819066	-3.033595	-0.000028
19	1	0	3.104140	-5.080574	-0.000017
20	1	0	4.861564	-3.332595	-0.000035
21	6	0	2.059105	-1.401419	-0.000018
22	6	0	1.872677	-0.018078	-0.000012
23	6	0	3.444920	-1.715071	-0.000029
24	6	0	-2.059112	1.401448	-0.000018
25	6	0	-1.872683	0.018106	-0.000017
26	6	0	-3.444925	1.715100	-0.000025
27	6	0	4.154600	-0.415300	-0.000045
28	6	0	-4.154602	0.415329	-0.000012
29	6	0	5.551726	-0.260609	-0.000047
30	6	0	6.761819	-0.151954	-0.000048
31	6	0	-5.551727	0.260631	-0.000002
32	6	0	-6.761819	0.151966	0.000008
33	6	0	-8.174158	0.011552	0.000014
34	6	0	-8.775214	-1.258811	0.000021
35	6	0	-9.017649	1.144062	0.000013
36	6	0	-10.158015	-1.405535	0.000028
37	1	0	-8.147474	-2.141785	0.000021
38	6	0	-10.392566	1.004864	0.000020
39	1	0	-8.577611	2.133952	0.000008
40	1	0	-10.582083	-2.400192	0.000033
41	1	0	-11.041655	1.872237	0.000020
42	6	0	8.174159	-0.011558	-0.000020
43	6	0	8.775233	1.258796	-0.000002
44	6	0	9.017635	-1.144080	-0.000009
45	6	0	10.158037	1.405501	0.000026
46	1	0	8.147507	2.141780	-0.000010
47	6	0	10.392554	-1.004902	0.000019
48	1	0	8.577583	-2.133963	-0.000023
49	6	0	10.978236	0.270824	0.000038
50	1	0	10.582119	2.400152	0.000038
51	1	0	11.041631	-1.872283	0.000027
52	6	0	3.197600	0.583060	-0.000009
53	1	0	3.416075	1.641277	-0.000088
54	6	0	-3.197604	-0.583031	-0.000007
55	1	0	-3.416081	-1.641248	0.000032
56	6	0	-10.978230	-0.270869	0.000028

57	8	0	12.335555	0.298641	0.000064
58	8	0	-12.335549	-0.298706	0.000035
59	6	0	-12.995908	-1.565527	0.000054
60	1	0	-12.745096	-2.143517	0.894531
61	1	0	-14.060689	-1.342304	0.000068
62	1	0	-12.745121	-2.143531	-0.894420
63	6	0	12.995932	1.565453	0.000102
64	1	0	12.745110	2.143443	0.894575
65	1	0	14.060710	1.342214	0.000136
66	1	0	12.745172	2.143463	-0.894376

C4. CP-PAH **2** *Anion* Optimized Geometry

Center Number	Atomic Number	Atomic Type	Coordinates (Angstroms) X	Y	Z
1	6	0	2.793598	-4.073032	-0.000017
2	6	0	1.440444	-3.744095	-0.000020
3	6	0	1.034971	-2.383128	-0.000017
4	6	0	3.812727	-3.092416	-0.000012
5	6	0	-0.289651	-1.874194	-0.000020
6	6	0	0.552929	0.499426	-0.000011
7	6	0	-0.552934	-0.499391	-0.000016
8	6	0	0.289646	1.874228	-0.000012
9	1	0	-1.126127	-2.565791	-0.000025
10	1	0	3.079365	-5.119848	-0.000019
11	1	0	0.693151	-4.531435	-0.000024
12	1	0	4.854234	-3.397348	-0.000009
13	1	0	1.126122	2.565825	-0.000010
14	6	0	-1.034977	2.383162	-0.000016
15	6	0	-1.440449	3.744130	-0.000019
16	6	0	-2.793603	4.073066	-0.000025
17	1	0	-0.693157	4.531470	-0.000018
18	6	0	-3.812733	3.092450	-0.000027
19	1	0	-3.079371	5.119883	-0.000026
20	1	0	-4.854239	3.397382	-0.000026
21	6	0	-2.066504	1.429240	-0.000019
22	6	0	-1.883246	0.031791	-0.000020
23	6	0	-3.446861	1.751744	-0.000021
24	6	0	2.066498	-1.429206	-0.000012
25	6	0	1.883241	-0.031756	-0.000009
26	6	0	3.446856	-1.751709	-0.000009
27	6	0	-4.158425	0.470334	-0.000009
28	6	0	4.158419	-0.470299	-0.000004
29	6	0	-5.554546	0.309469	-0.000001
30	6	0	-6.765641	0.186835	0.000006
31	6	0	5.554541	-0.309435	0.000001
32	6	0	6.765636	-0.186804	0.000004

33	6	0	8.176750	-0.029274	0.000008
34	6	0	8.767569	1.246778	0.000011
35	6	0	9.038465	-1.149061	0.000010
36	6	0	10.150072	1.410020	0.000015
37	1	0	8.130794	2.123510	0.000010
38	6	0	10.413034	-0.993166	0.000013
39	1	0	8.611855	-2.145056	0.000008
40	1	0	10.561031	2.410471	0.000016
41	1	0	11.071274	-1.854080	0.000014
42	6	0	-8.176751	0.029274	0.000013
43	6	0	-8.767544	-1.246790	0.000007
44	6	0	-9.038490	1.149043	0.000027
45	6	0	-10.150043	-1.410062	0.000014
46	1	0	-8.130750	-2.123509	-0.000004
47	6	0	-10.413056	0.993119	0.000034
48	1	0	-8.611901	2.145047	0.000032
49	6	0	-10.984543	-0.287579	0.000028
50	1	0	-10.560981	-2.410521	0.000009
51	1	0	-11.071314	1.854018	0.000045
52	6	0	-3.195296	-0.547726	-0.000033
53	1	0	-3.429740	-1.603778	-0.000041
54	6	0	3.195291	0.547760	-0.000006
55	1	0	3.429735	1.603813	-0.000004
56	6	0	10.984548	0.287520	0.000016
57	8	0	-12.347051	-0.332232	0.000036
58	8	0	12.347057	0.332143	0.000019
59	6	0	12.985465	1.607518	0.000024
60	1	0	12.726067	2.183675	0.893926
61	1	0	14.054526	1.403624	0.000028
62	1	0	12.726074	2.183679	-0.893877
63	6	0	-12.985432	-1.607620	0.000034
64	1	0	-12.726018	-2.183779	0.893930
65	1	0	-14.054497	-1.403749	0.000043
66	1	0	-12.726032	-2.183769	-0.893873

C5. CP-PAH **3** *Neutral* Optimized Geometry

Center Number	Atomic Number	Atomic Type	Coordinates (Angstroms) X	Y	Z
1	6	0	-0.107926	1.459933	-0.000043
2	6	0	-0.421349	2.855615	-0.000030
3	1	0	0.375798	3.590012	0.000047
4	6	0	-1.734906	3.265755	-0.000121
5	1	0	-1.957600	4.326852	-0.000103
6	6	0	-2.829081	2.343858	-0.000243
7	1	0	-3.840346	2.735518	-0.000341
8	6	0	-2.570780	0.993363	-0.000254

9	6	0	-1.210135	0.571607	-0.000147
10	6	0	-1.160408	-0.836551	-0.000185
11	6	0	0.107927	-1.459900	-0.000110
12	6	0	1.210135	-0.571574	-0.000007
13	6	0	1.160409	0.836585	0.000031
14	6	0	0.421350	-2.855582	-0.000130
15	1	0	-0.375796	-3.589979	-0.000213
16	6	0	1.734908	-3.265722	-0.000035
17	1	0	1.957601	-4.326820	-0.000050
18	6	0	2.829081	-2.343825	0.000090
19	1	0	3.840349	-2.735479	0.000180
20	6	0	2.570778	-0.993331	0.000096
21	6	0	-3.414221	-0.230344	-0.000302
22	6	0	-2.549416	-1.298129	-0.000319
23	1	0	-2.844329	-2.339288	-0.000423
24	6	0	2.549420	1.298161	0.000125
25	1	0	2.844335	2.339319	0.000195
26	6	0	3.414222	0.230374	0.000181
27	14	0	-5.294738	-0.334311	0.000123
28	14	0	5.294741	0.334288	0.000039
29	6	0	-5.806742	-2.150793	-0.005307
30	1	0	-5.433664	-2.677695	0.877738
31	1	0	-6.897947	-2.234433	-0.004783
32	1	0	-5.434898	-2.671825	-0.892342
33	6	0	-5.981743	0.523232	-1.538601
34	1	0	-7.075245	0.472708	-1.551253
35	1	0	-5.696558	1.578636	-1.574479
36	1	0	-5.612182	0.047030	-2.451449
37	6	0	-5.980468	0.513754	1.544675
38	1	0	-5.695661	1.569052	1.586490
39	1	0	-7.073933	0.462687	1.558197
40	1	0	-5.609708	0.032285	2.454269
41	6	0	5.806806	2.150758	0.002945
42	1	0	6.898014	2.234363	0.002703
43	1	0	5.434061	2.676305	-0.881046
44	1	0	5.434660	2.673172	0.889041
45	6	0	5.981364	-0.521062	1.540157
46	1	0	5.696211	-1.576429	1.577426
47	1	0	7.074861	-0.470470	1.553035
48	1	0	5.611530	-0.043598	2.452235
49	6	0	5.980775	-0.516054	-1.543121
50	1	0	7.074248	-0.465128	-1.556447
51	1	0	5.695869	-1.571380	-1.583492
52	1	0	5.610293	-0.035858	-2.453500

C6. CP-PAH **3** *Anion* Optimized Geometry

Center Number	Atomic Number	Atomic Type	Coordinates (Angstroms) X	Y	Z
1	6	0	0.128009	-1.472059	0.000004
2	6	0	0.447609	-2.851889	0.000013
3	1	0	-0.345325	-3.593060	0.000049
4	6	0	1.780266	-3.268228	-0.000027
5	1	0	1.996596	-4.332331	-0.000014
6	6	0	2.855848	-2.358477	-0.000064
7	1	0	3.872692	-2.739626	-0.000069
8	6	0	2.587402	-0.986611	-0.000059
9	6	0	1.223912	-0.573924	-0.000034
10	6	0	1.163667	0.847395	-0.000052
11	6	0	-0.128009	1.472059	-0.000012
12	6	0	-1.223912	0.573924	0.000027
13	6	0	-1.163667	-0.847395	0.000044
14	6	0	-0.447609	2.851889	-0.000024
15	1	0	0.345325	3.593060	-0.000061
16	6	0	-1.780266	3.268228	0.000014
17	1	0	-1.996596	4.332331	0.000000
18	6	0	-2.855848	2.358477	0.000051
19	1	0	-3.872692	2.739626	0.000059
20	6	0	-2.587402	0.986611	0.000049
21	6	0	3.412096	0.224798	-0.000040
22	6	0	2.523058	1.306376	-0.000146
23	1	0	2.821942	2.348085	-0.000197
24	6	0	-2.523058	-1.306376	0.000133
25	1	0	-2.821942	-2.348085	0.000181
26	6	0	-3.412096	-0.224798	0.000038
27	14	0	5.271390	0.341471	0.000020
28	14	0	-5.271390	-0.341472	-0.000010
29	6	0	5.800153	2.160132	-0.000021
30	1	0	5.426758	2.685862	0.883932
31	1	0	6.891865	2.243060	0.000044
32	1	0	5.426865	2.685804	-0.884053
33	6	0	6.012942	-0.497947	-1.532197
34	1	0	7.107076	-0.447724	-1.521061
35	1	0	5.727219	-1.552930	-1.585201
36	1	0	5.662174	-0.014991	-2.449421
37	6	0	6.012847	-0.497827	1.532352
38	1	0	5.727152	-1.552813	1.585416
39	1	0	7.106981	-0.447572	1.521297
40	1	0	5.661995	-0.014809	2.449511
41	6	0	-5.800153	-2.160132	0.000014
42	1	0	-6.891865	-2.243060	-0.000031
43	1	0	-5.426773	-2.685852	-0.883952
44	1	0	-5.426849	-2.685815	0.884033
45	6	0	-6.012934	0.497927	1.532223
46	1	0	-5.727214	1.552909	1.585238

47	1	0	-7.107068	0.447699	1.521095
48	1	0	-5.662156	0.014960	2.449437
49	6	0	-6.012856	0.497847	-1.532326
50	1	0	-7.106990	0.447596	-1.521262
51	1	0	-5.727157	1.552833	-1.585379
52	1	0	-5.662013	0.014841	-2.449495

C7. CP-PAH **4** *Neutral* Optimized Geometry

Center Number	Atomic Number	Atomic Type	Coordinates (Angstroms) X	Y	Z
1	6	0	-3.373104	3.567592	0.000307
2	6	0	-2.003102	3.472060	0.000312
3	6	0	-1.377186	2.180445	0.000237
4	6	0	-4.230798	2.415291	0.000206
5	6	0	-0.006858	1.903255	0.000261
6	6	0	-0.468573	-0.572116	0.000154
7	6	0	0.468573	0.572115	0.000189
8	6	0	0.006858	-1.903255	0.000209
9	1	0	0.711322	2.715571	0.000328
10	1	0	-3.835623	4.548133	0.000400
11	1	0	-1.391710	4.367815	0.000385
12	1	0	-5.304406	2.569135	0.000282
13	1	0	-0.711322	-2.715571	0.000218
14	6	0	1.377186	-2.180446	0.000235
15	6	0	2.003102	-3.472061	0.000291
16	6	0	3.373104	-3.567593	0.000329
17	1	0	1.391710	-4.367816	0.000314
18	6	0	4.230798	-2.415291	0.000286
19	1	0	3.835623	-4.548134	0.000412
20	1	0	5.304406	-2.569135	0.000409
21	6	0	2.247831	-1.072336	0.000205
22	6	0	1.851965	0.260445	0.000216
23	6	0	3.672407	-1.161129	0.000179
24	6	0	-2.247832	1.072336	0.000144
25	6	0	-1.851965	-0.260445	0.000134
26	6	0	-3.672407	1.161129	0.000088
27	6	0	4.190515	0.229748	0.000214
28	6	0	-4.190515	-0.229749	0.000082
29	6	0	3.088176	1.051896	0.000234
30	1	0	3.121837	2.133516	0.000253
31	6	0	-3.088176	-1.051896	0.000107
32	1	0	-3.121837	-2.133516	0.000099
33	14	0	5.985258	0.797276	-0.000261
34	14	0	-5.985258	-0.797275	-0.000239
35	6	0	6.028295	2.684117	0.000233

36	1	0	5.535717	3.098002	-0.884399
37	1	0	5.536621	3.097463	0.885621
38	1	0	7.063685	3.038637	-0.000188
39	6	0	6.864888	0.141663	1.539735
40	1	0	6.855917	-0.951630	1.573503
41	1	0	7.910112	0.466874	1.555276
42	1	0	6.385032	0.506773	2.452444
43	6	0	6.863463	0.142360	-1.541375
44	1	0	7.909013	0.466497	-1.557259
45	1	0	6.853282	-0.950886	-1.576246
46	1	0	6.383409	0.508866	-2.453426
47	6	0	-6.028297	-2.684117	-0.000923
48	1	0	-5.536012	-3.097437	-0.885981
49	1	0	-5.536331	-3.098027	0.884039
50	1	0	-7.063688	-3.038636	-0.001218
51	6	0	-6.864390	-0.142608	1.540441
52	1	0	-6.855120	0.950659	1.575007
53	1	0	-7.909692	-0.467568	1.555997
54	1	0	-6.384398	-0.508502	2.452764
55	6	0	-6.863958	-0.141414	-1.540670
56	1	0	-7.909428	-0.465809	-1.556550
57	1	0	-6.854084	0.951860	-1.574739
58	1	0	-6.384028	-0.507127	-2.453105

C8. CP-PAH **4** *Anion* Optimized Geometry

Center Number	Atomic Number	Atomic Type	Coordinates (Angstroms) X	Y	Z
1	6	0	-3.419843	-3.560308	-0.000660
2	6	0	-2.031007	-3.459750	-0.000669
3	6	0	-1.408656	-2.182824	-0.000475
4	6	0	-4.264453	-2.424857	-0.000455
5	6	0	-0.019704	-1.897029	-0.000470
6	6	0	-0.466167	0.581430	-0.000095
7	6	0	0.466167	-0.581430	-0.000270
8	6	0	0.019704	1.897030	0.000032
9	1	0	0.693228	-2.715941	-0.000623
10	1	0	-3.874680	-4.545933	-0.000802
11	1	0	-1.422682	-4.359183	-0.000824
12	1	0	-5.340536	-2.568468	-0.000437
13	1	0	-0.693228	2.715941	0.000139
14	6	0	1.408656	2.182824	0.000029
15	6	0	2.031007	3.459750	0.000172
16	6	0	3.419843	3.560308	0.000172
17	1	0	1.422682	4.359184	0.000289
18	6	0	4.264453	2.424857	0.000048

19	1	0	3.874680	4.545933	0.000311
20	1	0	5.340536	2.568468	0.000134
21	6	0	2.272335	1.072166	-0.000119
22	6	0	1.861414	-0.270442	-0.000289
23	6	0	3.693263	1.153716	-0.000083
24	6	0	-2.272335	-1.072166	-0.000283
25	6	0	-1.861414	0.270442	-0.000110
26	6	0	-3.693263	-1.153716	-0.000258
27	6	0	4.198650	-0.225416	-0.000038
28	6	0	-4.198650	0.225416	0.000021
29	6	0	3.076893	-1.053759	-0.000545
30	1	0	3.113868	-2.136522	-0.000760
31	6	0	-3.076893	1.053759	-0.000034
32	1	0	-3.113868	2.136522	0.000083
33	14	0	5.974756	-0.798435	0.000289
34	14	0	-5.974756	0.798435	0.000271
35	6	0	6.030264	-2.690217	0.000164
36	1	0	5.536421	-3.104832	0.884053
37	1	0	5.536892	-3.104702	-0.884049
38	1	0	7.065931	-3.044981	0.000413
39	6	0	6.893181	-0.163096	-1.532250
40	1	0	6.891720	0.930393	-1.571713
41	1	0	7.936565	-0.496089	-1.534457
42	1	0	6.420625	-0.526674	-2.449802
43	6	0	6.892547	-0.163279	1.533283
44	1	0	7.936048	-0.495902	1.535688
45	1	0	6.890682	0.930198	1.573078
46	1	0	6.419853	-0.527300	2.450589
47	6	0	-6.030264	2.690217	0.000498
48	1	0	-5.536545	3.104663	0.884536
49	1	0	-5.536769	3.104871	-0.883567
50	1	0	-7.065931	3.044981	0.000671
51	6	0	-6.893025	0.163366	-1.532473
52	1	0	-6.891471	-0.930115	-1.572167
53	1	0	-7.936435	0.496274	-1.534686
54	1	0	-6.420429	0.527175	-2.449914
55	6	0	-6.892704	0.163009	1.533059
56	1	0	-7.936176	0.495720	1.535461
57	1	0	-6.890936	-0.930476	1.572621
58	1	0	-6.420046	0.526795	2.450478

C9. CP-PAH **5** *Neutral* Optimized Geometry

Center Number	Atomic Number	Atomic Type	Coordinates (Angstroms) X	Y	Z
1	6	0	-8.899931	-1.937536	-0.118724

2	6	0	-7.480431	-1.926865	-0.118028
3	6	0	-6.775241	-0.726644	-0.118036
4	6	0	-7.495958	0.470162	-0.118761
5	6	0	-8.893524	0.462590	-0.119438
6	6	0	-9.606615	-0.741824	-0.119412
7	1	0	-5.691148	-0.720501	-0.117506
8	1	0	-6.965666	1.415441	-0.118791
9	1	0	-9.433349	1.402532	-0.119993
10	1	0	-10.690913	-0.732553	-0.119950
11	6	0	-8.120531	-4.155174	-0.117609
12	6	0	-9.329207	-3.339235	-0.118525
13	6	0	-10.644201	-5.340954	-0.118548
14	6	0	-9.435532	-6.156867	-0.117599
15	6	0	-11.284326	-7.569185	-0.118378
16	6	0	-9.864814	-7.558506	-0.117676
17	6	0	-11.989524	-8.769394	-0.118529
18	6	0	-9.158164	-8.754235	-0.117141
19	6	0	-11.268807	-9.966207	-0.117977
20	1	0	-13.073613	-8.775541	-0.119071
21	6	0	-9.871247	-9.958647	-0.117294
22	1	0	-8.073861	-8.763527	-0.116576
23	1	0	-11.799113	-10.911480	-0.118081
24	1	0	-9.331396	-10.898574	-0.116863
25	6	0	-7.009428	-3.315170	-0.117383
26	6	0	-11.755320	-6.180928	-0.118860
27	6	0	-13.107416	-5.790307	-0.119644
28	6	0	-14.273871	-5.475649	-0.120360
29	1	0	-15.299774	-5.193546	-0.121082
30	6	0	-5.657337	-3.705785	-0.116555
31	6	0	-4.490881	-4.020423	-0.115806
32	1	0	-3.464967	-4.302486	-0.115178
33	6	0	-8.199019	-5.580911	-0.117089
34	1	0	-7.289941	-6.172381	-0.116405
35	6	0	-10.565733	-3.915235	-0.118955
36	1	0	-11.474797	-3.323752	-0.119620

C10. CP-PAH **5** *Anion* Optimized Geometry

Center Number	Atomic Number	Atomic Type	Coordinates (Angstroms) X	Y	Z
1	6	0	-2.693003	-0.888969	0.000010
2	6	0	-3.392414	0.359351	0.000048
3	6	0	-4.793964	0.375502	0.000059
4	6	0	-5.486573	-0.831867	0.000032
5	6	0	-4.800340	-2.057474	-0.000005
6	6	0	-3.405548	-2.088788	-0.000016

7	1	0	-5.331179	1.318530	0.000088
8	1	0	-6.571681	-0.827837	0.000041
9	1	0	-5.360655	-2.986237	-0.000025
10	1	0	-2.883489	-3.040735	-0.000045
11	6	0	-1.124592	0.842822	0.000041
12	6	0	-1.267097	-0.597514	0.000006
13	6	0	1.124590	-0.842825	-0.000022
14	6	0	1.267095	0.597512	0.000013
15	6	0	3.392412	-0.359353	-0.000030
16	6	0	2.693001	0.888967	0.000008
17	6	0	4.793962	-0.375504	-0.000044
18	6	0	3.405545	2.088786	0.000031
19	6	0	5.486571	0.831865	-0.000020
20	1	0	5.331177	-1.318532	-0.000072
21	6	0	4.800337	2.057471	0.000017
22	1	0	2.883486	3.040733	0.000059
23	1	0	6.571679	0.827835	-0.000031
24	1	0	5.360652	2.986235	0.000034
25	6	0	-2.422503	1.434503	0.000074
26	6	0	2.422501	-1.434506	-0.000047
27	6	0	2.719810	-2.805005	-0.000082
28	6	0	2.984971	-3.989614	-0.000132
29	1	0	3.214360	-5.027255	-0.000296
30	6	0	-2.719810	2.805003	0.000123
31	6	0	-2.984972	3.989612	0.000048
32	1	0	-3.214383	5.027248	-0.000638
33	6	0	0.158983	1.427224	0.000045
34	1	0	0.266019	2.507937	0.000072
35	6	0	-0.158985	-1.427226	-0.000025
36	1	0	-0.266022	-2.507940	-0.000052

C11. CP-PAH **6** *Neutral* Optimized Geometry

Center Number	Atomic Number	Atomic Type	Coordinates (Angstroms) X	Y	Z
1	6	0	-3.968695	-0.000048	0.000379
2	6	0	-3.293751	1.225030	0.000228
3	6	0	-1.888286	1.263224	-0.000157
4	6	0	-1.229698	-0.000012	-0.000461
5	6	0	-1.888253	-1.263267	-0.000158
6	6	0	-3.293728	-1.225101	0.000231
7	6	0	-1.101778	2.496758	-0.000037
8	6	0	0.171340	-0.000005	-0.000723
9	6	0	0.889875	1.170102	-0.000524
10	6	0	0.277059	2.455772	-0.000180
11	6	0	2.289807	1.216700	-0.000068

12	6	0	3.015885	0.000049	0.000081
13	6	0	2.289858	-1.216658	-0.000214
14	6	0	0.889919	-1.170087	-0.000629
15	6	0	0.277121	-2.455774	-0.000194
16	6	0	-1.101724	-2.496763	-0.000001
17	1	0	-1.644259	-3.437113	0.000387
18	1	0	-1.644355	3.437083	0.000260
19	1	0	-5.052484	-0.000050	0.000688
20	1	0	-3.862800	2.148567	0.000466
21	1	0	-3.862742	-2.148662	0.000476
22	1	0	4.101279	0.000075	0.000581
23	6	0	2.586886	2.667683	0.000602
24	6	0	1.420714	3.388379	0.000210
25	6	0	2.586963	-2.667619	0.000326
26	6	0	1.420789	-3.388344	0.000381
27	1	0	1.351906	4.467493	0.000210
28	1	0	3.579766	3.098396	0.000884
29	1	0	3.579845	-3.098431	0.000755
30	1	0	1.352030	-4.467471	0.000736

C12 CP-PAH **6** *Anion* Optimized Geometry

Center Number	Atomic Number	Atomic Type	Coordinates (Angstroms) X	Y	Z
1	6	0	3.984998	-0.000047	-0.000197
2	6	0	3.318963	1.228725	-0.000130
3	6	0	1.895002	1.273524	0.000000
4	6	0	1.234011	-0.000016	0.000088
5	6	0	1.894973	-1.273572	-0.000040
6	6	0	3.318935	-1.228804	-0.000164
7	6	0	1.117478	2.488210	-0.000045
8	6	0	-0.172083	-0.000001	0.000197
9	6	0	-0.892739	1.175705	0.000169
10	6	0	-0.290083	2.449980	0.000002
11	6	0	-2.312773	1.221158	-0.000002
12	6	0	-3.031275	0.000031	-0.000160
13	6	0	-2.312800	-1.221112	-0.000055
14	6	0	-0.892766	-1.175690	0.000137
15	6	0	-0.290138	-2.449979	-0.000051
16	6	0	1.117423	-2.488240	-0.000111
17	1	0	1.656039	-3.432326	-0.000268
18	1	0	1.656115	3.432284	-0.000202
19	1	0	5.071226	-0.000059	-0.000297
20	1	0	3.889447	2.152223	-0.000197
21	1	0	3.889400	-2.152315	-0.000254
22	1	0	-4.119093	0.000043	-0.000334

23	6	0	-2.608429	2.650597	-0.000098
24	6	0	-1.423169	3.374670	-0.000309
25	6	0	-2.608488	-2.650544	-0.000263
26	6	0	-1.423244	-3.374643	-0.000322
27	1	0	-1.358564	4.455978	-0.000529
28	1	0	-3.599060	3.089530	-0.000174
29	1	0	-3.599129	-3.089455	-0.000412
30	1	0	-1.358663	-4.455953	-0.000513

C13. CP-PAH **7** *Neutral* Optimized Geometry

Center Number	Atomic Number	Atomic Type	Coordinates (Angstroms) X	Y	Z
1	6	0	-3.557459	-1.643587	-0.913332
2	6	0	-2.145553	-1.642926	-0.801591
3	6	0	-1.438475	-0.600335	-0.230173
4	6	0	-2.228393	0.580070	0.044783
5	6	0	-3.610888	0.579422	-0.064640
6	6	0	-4.346566	-0.601847	-0.459871
7	6	0	-3.995112	-2.990535	-0.923813
8	6	0	-2.853675	-3.822252	-0.818684
9	6	0	-1.710546	-2.989423	-0.743208
10	1	0	-1.741154	1.467345	0.435626
11	1	0	-4.154303	1.466242	0.244750
12	6	0	-0.117150	-0.957986	0.238006
13	6	0	-2.896922	-5.089491	-0.265514
14	6	0	-0.542182	-3.373916	-0.110127
15	6	0	0.308918	-2.276540	0.295126
16	6	0	-0.500759	-4.767355	0.276454
17	6	0	-1.619975	-5.582826	0.202461
18	6	0	-5.724572	-0.960770	-0.204415
19	6	0	-5.248117	-3.376142	-0.482022
20	6	0	-6.153311	-2.279631	-0.215210
21	6	0	-4.231012	-5.584250	-0.004035
22	6	0	-5.348712	-4.769737	-0.106996
23	1	0	0.530709	-0.187472	0.643011
24	1	0	1.274355	-2.488650	0.742830
25	1	0	0.402790	-5.169310	0.723076
26	1	0	-1.550256	-6.592408	0.594037
27	1	0	-4.360289	-6.593783	0.372279
28	1	0	-6.310823	-5.172463	0.192293
29	1	0	-7.176854	-2.492763	0.075344
30	1	0	-6.428525	-0.190849	0.094065

C14. CP-PAH **7** *Anion* Optimized Geometry

Center Number	Atomic Number	Atomic Type	Coordinates (Angstroms) X	Y	Z
1	6	0	-3.553177	-1.637673	-0.875290
2	6	0	-2.156995	-1.637346	-0.765149
3	6	0	-1.417675	-0.580367	-0.218901
4	6	0	-2.227779	0.613760	0.012153
5	6	0	-3.606676	0.613214	-0.096030
6	6	0	-4.369614	-0.580753	-0.451335
7	6	0	-3.989652	-2.992370	-0.873686
8	6	0	-2.856268	-3.826065	-0.787796
9	6	0	-1.724448	-2.991952	-0.696235
10	1	0	-1.744213	1.522107	0.362740
11	1	0	-4.139614	1.521230	0.174848
12	6	0	-0.122702	-0.935185	0.246705
13	6	0	-2.897357	-5.130717	-0.263877
14	6	0	-0.532215	-3.373838	-0.087803
15	6	0	0.316053	-2.285094	0.300792
16	6	0	-0.489843	-4.791470	0.255824
17	6	0	-1.619073	-5.609913	0.188303
18	6	0	-5.721106	-0.936994	-0.193631
19	6	0	-5.261329	-3.375715	-0.458365
20	6	0	-6.161542	-2.286638	-0.208334
21	6	0	-4.228808	-5.610497	-0.015045
22	6	0	-5.356220	-4.792327	-0.124572
23	1	0	0.526307	-0.172985	0.669824
24	1	0	1.277195	-2.490790	0.763209
25	1	0	0.418553	-5.207309	0.682792
26	1	0	-1.532496	-6.625852	0.566232
27	1	0	-4.372226	-6.626026	0.346376
28	1	0	-6.319529	-5.208175	0.157298
29	1	0	-7.183179	-2.493175	0.097464
30	1	0	-6.429186	-0.175250	0.121996

C15. CP-PAH **8** *Neutral* Optimized Geometry

Center Number	Atomic Number	Atomic Type	Coordinates (Angstroms) X	Y	Z
1	6	0	-5.020066	-1.619866	-0.072122
2	6	0	-3.653183	-1.641698	0.012685
3	6	0	-2.910548	-0.415946	-0.018705
4	6	0	-3.574965	0.853132	-0.138475
5	6	0	-5.025188	0.870245	-0.227631

6	6	0	-5.670397	-0.360367	-0.190391
7	1	0	-3.118666	-2.579380	0.104038
8	6	0	-1.460326	-0.433070	0.070617
9	6	0	-2.832336	2.078880	-0.170065
10	6	0	-1.465451	2.057051	-0.085468
11	6	0	-0.815099	0.797527	0.032986
12	1	0	-3.366862	3.016549	-0.261540
13	6	0	-0.402391	3.069639	-0.084204
14	6	0	0.583855	0.988513	0.106110
15	6	0	-0.605714	-1.565525	0.193436
16	6	0	1.390347	-0.126516	0.225015
17	6	0	0.768649	-1.400811	0.266884
18	6	0	0.801979	2.442283	0.028407
19	6	0	-5.879854	2.002721	-0.349717
20	6	0	-7.069389	-0.551347	-0.263178
21	6	0	-7.254238	1.838048	-0.422743
22	6	0	-7.875933	0.563727	-0.381266
23	6	0	-6.083145	-2.632438	-0.073472
24	6	0	-7.287544	-2.005097	-0.185705
25	1	0	-0.561562	4.136464	-0.160732
26	1	0	1.769597	2.924763	0.057194
27	1	0	2.470475	-0.051715	0.286048
28	1	0	1.394812	-2.280962	0.360049
29	1	0	-1.010679	-2.568889	0.231543
30	1	0	-5.923927	-3.699247	0.002997
31	1	0	-8.255111	-2.487716	-0.214247
32	1	0	-8.956079	0.488946	-0.441995
33	1	0	-7.880444	2.718241	-0.515167
34	1	0	-5.474913	3.006120	-0.387139

C16. CP-PAH **8** *Anion* Optimized Geometry

Center Number	Atomic Number	Atomic Type	Coordinates (Angstroms) X	Y	Z
1	6	0	-1.689674	0.915180	-0.000077
2	6	0	-2.503808	-0.219606	-0.000140
3	6	0	-3.925939	-0.206692	-0.000172
4	6	0	-0.241098	0.692714	-0.000053
5	6	0	0.241085	-0.692737	-0.000082
6	6	0	-2.037030	-1.564795	-0.00017
7	6	0	2.037017	1.564772	0.000022

8	6	0	3.925926	0.206669	0.000051
9	6	0	2.503795	0.219583	-0.000001
10	6	0	1.689662	-0.915203	-0.000046
11	6	0	4.342327	1.597724	0.000107
12	1	0	5.367629	1.945129	0.000151
13	6	0	3.213250	2.401642	0.000090
14	1	0	3.210965	3.484725	0.000122
15	6	0	-4.342339	-1.597747	-0.000236
16	1	0	-5.367641	-1.945152	-0.000277
17	6	0	-3.213263	-2.401665	-0.000238
18	1	0	-3.210978	-3.484748	-0.000281
19	6	0	-0.657727	-1.775316	-0.000144
20	1	0	-0.262903	-2.786110	-0.000172
21	6	0	-4.567733	1.035230	-0.000142
22	1	0	-5.650164	1.119321	-0.000166
23	6	0	-3.774473	2.195337	-0.000080
24	1	0	-4.264525	3.164014	-0.000053
25	6	0	-2.375607	2.155566	-0.000046
26	1	0	-1.831695	3.092995	0.000004
27	6	0	0.657714	1.775293	-0.000001
28	1	0	0.262890	2.786087	0.000023
29	6	0	4.567720	-1.035253	0.000049
30	1	0	5.650151	-1.119343	0.000089
31	6	0	3.774461	-2.195360	0.000003
32	1	0	4.264513	-3.164037	0.000005
33	6	0	2.375595	-2.155589	-0.000042
34	1	0	1.831683	-3.093018	-0.000073

APPENDIX D

VIBRATIONAL FREQUENCIES OF THE 8 CP-PAHS (NEUTRAL AND ANION)

USING B3LYP/6-311G(D,P)

D1. CP-PAH **1** *Neutral* Vibrational Frequencies in cm^{-1}

	1	2	3
Frequencies --	7.3084	12.9605	21.3788
	4	5	6
Frequencies --	22.7444	24.5972	25.6983
	7	8	9
Frequencies --	48.6756	72.8025	84.8889
	10	11	12
Frequencies --	88.6350	99.0997	104.8697
	13	14	15
Frequencies --	115.3252	135.2899	145.0533
	16	17	18
Frequencies --	179.3379	195.4245	201.7487
	19	20	21
Frequencies --	223.9951	224.5786	239.4531
	22	23	24
Frequencies --	247.4236	252.5521	254.8520
	25	26	27
Frequencies --	259.0434	269.1023	315.8009
	28	29	30
Frequencies --	337.2221	337.7710	388.3257
	31	32	33
Frequencies --	391.4721	411.6828	418.9175
	34	35	36
Frequencies --	419.5276	420.8281	430.1821
	37	38	39
Frequencies --	452.7691	474.7018	483.6421
	40	41	42
Frequencies --	485.9063	504.1914	520.4462
	43	44	45
Frequencies --	534.2081	535.4657	549.5861

	46	47	48
Frequencies --	555.6610	556.0936	558.4599
	49	50	51
Frequencies --	592.5191	604.7139	617.7438
	52	53	54
Frequencies --	625.1294	651.0289	652.8591
	55	56	57
Frequencies --	653.6971	664.5395	672.5002
	58	59	60
Frequencies --	678.4083	680.0332	688.0882
	61	62	63
Frequencies --	733.2784	733.2792	751.2437
	64	65	66
Frequencies --	757.8521	767.8573	769.8742
	67	68	69
Frequencies --	807.3415	814.5863	821.7872
	70	71	72
Frequencies --	821.8469	822.2788	838.5499
	73	74	75
Frequencies --	845.8891	845.9083	850.2948
	76	77	78
Frequencies --	854.0504	856.7624	863.2397
	79	80	81
Frequencies --	940.6176	941.4929	958.6241
	82	83	84
Frequencies --	959.4420	959.4451	972.8343
	85	86	87
Frequencies --	972.8346	985.0992	995.1740
	88	89	90
Frequencies --	995.1904	1021.3167	1021.6693
	91	92	93
Frequencies --	1043.0085	1044.1080	1044.8282
	94	95	96
Frequencies --	1056.4990	1070.5132	1119.1624

	97	98	99
Frequencies --	1132.0293	1132.0633	1147.5893
	100	101	102
Frequencies --	1148.5494	1169.6791	1169.6792
	103	104	105
Frequencies --	1187.8758	1191.2007	1195.0698
	106	107	108
Frequencies --	1202.9260	1203.5735	1205.3556
	109	110	111
Frequencies --	1213.1092	1252.4781	1254.0166
	112	113	114
Frequencies --	1270.8478	1274.6262	1275.5076
	115	116	117
Frequencies --	1290.8173	1311.3821	1315.1351
	118	119	120
Frequencies --	1319.7109	1331.3559	1331.4110
	121	122	123
Frequencies --	1333.6504	1342.3891	1405.6409
	124	125	126
Frequencies --	1405.9605	1442.2302	1447.6250
	127	128	129
Frequencies --	1447.6374	1451.5760	1457.3387
	130	131	132
Frequencies --	1475.3888	1476.4866	1477.0704
	133	134	135
Frequencies --	1486.6906	1486.6923	1493.1545
	136	137	138
Frequencies --	1497.6843	1497.9661	1502.8170
	139	140	141
Frequencies --	1517.4538	1549.3907	1552.4224
	142	143	144
Frequencies --	1557.0884	1585.7902	1588.9794
	145	146	147
Frequencies --	1589.0428	1614.9458	1642.1666

	148	149	150
Frequencies --	1642.6660	1649.1021	1654.7984
	151	152	153
Frequencies --	2261.5323	2262.5486	3017.9866
	154	155	156
Frequencies --	3018.0364	3082.4086	3082.4168
	157	158	159
Frequencies --	3145.2559	3145.2583	3172.1357
	160	161	162
Frequencies --	3172.2013	3182.0779	3182.1065
	163	164	165
Frequencies --	3183.1021	3183.1048	3186.8206
	166	167	168
Frequencies --	3186.8239	3192.8569	3193.1692
	169	170	171
Frequencies --	3197.8720	3197.8992	3211.5443
	172	173	174
Frequencies --	3211.5752	3224.6481	3225.0545

D2. CP-PAH **1** *Anion* Vibrational Frequencies in cm^{-1}

	1	2	3
Frequencies --	5.7555	11.8276	12.7661
	4	5	6
Frequencies --	15.6257	24.1079	26.5741
	7	8	9
Frequencies --	48.4451	72.5667	86.9966
	10	11	12
Frequencies --	87.5013	96.7728	104.1619
	13	14	15
Frequencies --	110.2639	134.7943	142.6898
	16	17	18
Frequencies --	181.4976	191.8746	198.6151

	19	20	21
Frequencies --	225.6946	228.5748	240.8499
	22	23	24
Frequencies --	252.2521	252.4226	254.6010
	25	26	27
Frequencies --	258.9071	269.0195	319.8741
	28	29	30
Frequencies --	339.2325	340.4595	387.1896
	31	32	33
Frequencies --	392.6342	402.3648	408.1454
	34	35	36
Frequencies --	418.9123	420.6957	420.8991
	37	38	39
Frequencies --	450.6746	472.3760	484.2277
	40	41	42
Frequencies --	497.0364	519.1817	521.8921
	43	44	45
Frequencies --	534.2018	535.4369	545.1561
	46	47	48
Frequencies --	548.4805	552.0239	554.0163
	49	50	51
Frequencies --	590.8996	598.3180	619.1138
	52	53	54
Frequencies --	623.2342	642.6241	654.1221
	55	56	57
Frequencies --	654.4585	661.8800	665.5724
	58	59	60
Frequencies --	673.2446	674.5394	677.2910
	61	62	63
Frequencies --	729.0195	729.0208	750.3133
	64	65	66
Frequencies --	751.4761	751.8232	764.8012
	67	68	69
Frequencies --	781.9085	808.6630	813.3040

	70	71	72
Frequencies --	819.0550	819.0578	823.3481
	73	74	75
Frequencies --	830.8751	835.2322	840.9078
	76	77	78
Frequencies --	840.9448	851.3798	864.6850
	79	80	81
Frequencies --	884.8487	885.6229	950.9900
	82	83	84
Frequencies --	951.6238	951.6949	951.8994
	85	86	87
Frequencies --	952.0147	966.7743	966.7753
	88	89	90
Frequencies --	1001.7154	1020.3266	1020.5328
	91	92	93
Frequencies --	1047.6678	1048.8401	1054.8074
	94	95	96
Frequencies --	1065.1159	1074.8426	1120.9223
	97	98	99
Frequencies --	1127.3424	1127.3571	1145.8437
	100	101	102
Frequencies --	1146.7121	1170.3649	1170.3653
	103	104	105
Frequencies --	1178.6049	1185.0660	1190.0987
	106	107	108
Frequencies --	1190.9517	1202.9683	1202.9756
	109	110	111
Frequencies --	1218.1482	1223.6710	1255.1283
	112	113	114
Frequencies --	1264.3440	1265.3832	1269.7947
	115	116	117
Frequencies --	1295.7306	1297.3863	1309.6073
	118	119	120
Frequencies --	1311.9673	1323.6601	1328.4907

	121	122	123
Frequencies --	1328.6208	1342.1553	1382.7143
	124	125	126
Frequencies --	1398.8084	1403.3057	1408.0927
	127	128	129
Frequencies --	1442.1101	1442.3201	1464.5488
	130	131	132
Frequencies --	1470.1848	1472.8473	1476.0571
	133	134	135
Frequencies --	1482.0065	1483.9262	1485.4874
	136	137	138
Frequencies --	1485.4875	1493.9485	1499.7169
	139	140	141
Frequencies --	1499.8179	1540.2572	1543.7929
	142	143	144
Frequencies --	1544.3256	1553.8451	1587.7572
	145	146	147
Frequencies --	1587.7724	1597.6886	1602.8452
	148	149	150
Frequencies --	1606.3779	1643.1910	1643.2086
	151	152	153
Frequencies --	2236.6659	2237.0221	3010.6795
	154	155	156
Frequencies --	3010.7354	3071.7023	3071.7062
	157	158	159
Frequencies --	3137.6742	3137.6774	3149.8593
	160	161	162
Frequencies --	3149.9036	3162.8956	3162.9018
	163	164	165
Frequencies --	3174.2407	3174.6997	3176.9928
	166	167	168
Frequencies --	3176.9958	3182.0054	3182.0132
	169	170	171
Frequencies --	3192.3860	3192.4101	3202.2582

	172	173	174
Frequencies --	3202.7173	3206.4938	3206.5271

D3. CP-PAH **2** *Neutral* Vibrational Frequencies in cm^{-1}

	1	2	3
Frequencies --	6.4866	10.7918	18.6322
	4	5	6
Frequencies --	20.1722	22.0441	23.8993
	7	8	9
Frequencies --	43.1574	58.0450	69.3266
	10	11	12
Frequencies --	80.6023	88.8958	98.9878
	13	14	15
Frequencies --	110.7529	124.7089	128.1714
	16	17	18
Frequencies --	145.7123	146.9551	182.6972
	19	20	21
Frequencies --	192.7445	218.2149	219.4450
	22	23	24
Frequencies --	223.0780	227.5197	243.8311
	25	26	27
Frequencies --	248.7845	251.1276	270.4347
	28	29	30
Frequencies --	273.4520	295.5283	315.3247
	31	32	33
Frequencies --	333.4221	340.8723	378.9388
	34	35	36
Frequencies --	391.6315	392.5409	420.2329
	37	38	39
Frequencies --	421.2759	430.7749	441.2546
	40	41	42
Frequencies --	457.9431	471.2513	493.0795

	43	44	45
Frequencies --	505.2904	512.7543	514.6125
	46	47	48
Frequencies --	518.1146	525.2419	528.4125
	49	50	51
Frequencies --	543.2821	553.8613	556.1680
	52	53	54
Frequencies --	558.9031	559.4575	582.4926
	55	56	57
Frequencies --	611.8465	621.7832	622.5416
	58	59	60
Frequencies --	629.2063	639.4281	652.6835
	61	62	63
Frequencies --	654.7389	658.5388	668.2871
	64	65	66
Frequencies --	678.3882	711.4240	712.4880
	67	68	69
Frequencies --	729.1870	732.6601	733.6291
	70	71	72
Frequencies --	733.6297	765.2575	774.6466
	73	74	75
Frequencies --	783.7130	786.5121	801.7447
	76	77	78
Frequencies --	810.1470	818.9161	822.0084
	79	80	81
Frequencies --	822.0110	841.8613	845.9561
	82	83	84
Frequencies --	845.9703	852.1386	852.2547
	85	86	87
Frequencies --	862.6165	886.6197	897.4711
	88	89	90
Frequencies --	919.1827	944.4746	944.4941
	91	92	93
Frequencies --	959.4068	959.4091	973.0082

	94	95	96
Frequencies --	973.0105	979.3037	995.6866
	97	98	99
Frequencies --	995.7337	1013.9444	1021.2044
	100	101	102
Frequencies --	1021.5306	1034.3298	1041.9508
	103	104	105
Frequencies --	1044.8185	1044.8843	1058.3839
	106	107	108
Frequencies --	1091.1063	1130.9288	1130.9361
	109	110	111
Frequencies --	1134.8912	1142.1622	1169.0158
	112	113	114
Frequencies --	1169.0160	1179.2090	1189.7658
	115	116	117
Frequencies --	1193.9674	1197.0765	1200.3924
	118	119	120
Frequencies --	1202.0358	1202.0790	1227.3248
	121	122	123
Frequencies --	1230.2431	1249.6044	1271.0991
	124	125	126
Frequencies --	1273.9551	1274.4618	1280.0997
	127	128	129
Frequencies --	1283.5440	1314.1403	1314.5409
	130	131	132
Frequencies --	1329.6138	1329.6343	1330.8485
	133	134	135
Frequencies --	1335.2996	1349.9383	1362.8136
	136	137	138
Frequencies --	1389.7969	1393.1421	1423.8360
	139	140	141
Frequencies --	1424.6016	1439.9502	1446.5693
	142	143	144
Frequencies --	1446.7122	1465.6393	1476.0833

	145	146	147
Frequencies --	1476.1223	1480.5717	1480.8746
	148	149	150
Frequencies --	1485.9124	1485.9129	1495.6197
	151	152	153
Frequencies --	1495.6388	1509.9371	1513.8653
	154	155	156
Frequencies --	1522.4712	1553.4277	1553.8500
	157	158	159
Frequencies --	1577.6250	1589.2959	1589.3043
	160	161	162
Frequencies --	1593.2213	1609.2021	1639.9470
	163	164	165
Frequencies --	1642.7837	1643.6611	1655.0173
	166	167	168
Frequencies --	1660.0266	2267.2772	2267.2850
	169	170	171
Frequencies --	3016.4187	3016.4412	3080.1654
	172	173	174
Frequencies --	3080.1699	3144.3809	3144.3838
	175	176	177
Frequencies --	3170.1115	3170.1527	3178.5836
	178	179	180
Frequencies --	3178.6027	3181.9929	3182.0552
	181	182	183
Frequencies --	3182.3919	3182.3989	3185.3708
	184	185	186
Frequencies --	3185.3723	3190.7231	3190.8980
	187	188	189
Frequencies --	3197.2342	3197.2474	3212.4837
	190	191	192
Frequencies --	3212.4940	3224.4177	3224.5718

D4. CP-PAH **2** *Anion* Vibrational Frequencies in cm^{-1}

	1	2	3
Frequencies --	6.7750	11.7433	16.1648
	4	5	6
Frequencies --	17.6719	22.1537	24.6398
	7	8	9
Frequencies --	42.3560	59.7001	70.0824
	10	11	12
Frequencies --	80.7439	86.8981	99.0267
	13	14	15
Frequencies --	107.3054	120.5720	129.5130
	16	17	18
Frequencies --	148.1256	152.9697	181.5468
	19	20	21
Frequencies --	191.3491	215.8189	218.2730
	22	23	24
Frequencies --	223.7200	231.1757	247.0752
	25	26	27
Frequencies --	250.1351	252.3507	265.9123
	28	29	30
Frequencies --	286.1763	293.9030	315.3602
	31	32	33
Frequencies --	330.7338	341.8212	385.3608
	34	35	36
Frequencies --	393.6550	397.5646	413.6210
	37	38	39
Frequencies --	422.4980	423.1516	439.7670
	40	41	42
Frequencies --	456.0683	467.3257	498.8375
	43	44	45
Frequencies --	502.6053	513.9491	514.2971
	46	47	48
Frequencies --	523.3963	528.6076	534.9372
	49	50	51
Frequencies --	542.0654	550.8599	553.1384

	52	53	54
Frequencies --	555.9128	557.3674	582.8367
	55	56	57
Frequencies --	614.5775	617.3363	618.4715
	58	59	60
Frequencies --	620.2849	640.1919	646.6538
	61	62	63
Frequencies --	652.9152	658.8351	666.6592
	64	65	66
Frequencies --	668.1854	708.6513	712.0577
	67	68	69
Frequencies --	721.5761	731.1392	731.1397
	70	71	72
Frequencies --	733.2133	748.9947	761.3833
	73	74	75
Frequencies --	771.6348	781.5285	789.5310
	76	77	78
Frequencies --	798.8033	819.6832	820.7981
	79	80	81
Frequencies --	820.8131	823.3918	824.5246
	82	83	84
Frequencies --	839.1183	841.9752	842.8347
	85	86	87
Frequencies --	842.8512	846.8274	863.3622
	88	89	90
Frequencies --	892.7734	892.8861	912.9458
	91	92	93
Frequencies --	953.8259	953.8274	954.6025
	94	95	96
Frequencies --	954.7188	968.4510	968.4518
	97	98	99
Frequencies --	977.2523	1018.8078	1020.9440
	100	101	102
Frequencies --	1022.2649	1048.7379	1048.7539

	103	104	105
Frequencies --	1050.9651	1051.6580	1054.7761
	106	107	108
Frequencies --	1097.9825	1128.9615	1128.9645
	109	110	111
Frequencies --	1132.8536	1136.3370	1169.0703
	112	113	114
Frequencies --	1169.0703	1171.3895	1183.4190
	115	116	117
Frequencies --	1188.8386	1192.8131	1193.5501
	118	119	120
Frequencies --	1201.8242	1201.8398	1210.0605
	121	122	123
Frequencies --	1232.5782	1245.1174	1260.6314
	124	125	126
Frequencies --	1266.6145	1269.1197	1274.5160
	127	128	129
Frequencies --	1281.0422	1308.4782	1309.5133
	130	131	132
Frequencies --	1320.0359	1323.5391	1324.7382
	133	134	135
Frequencies --	1328.9677	1329.0564	1359.5776
	136	137	138
Frequencies --	1379.3669	1399.3445	1415.5394
	139	140	141
Frequencies --	1415.9648	1424.8906	1442.5485
	142	143	144
Frequencies --	1443.0783	1445.5407	1453.7285
	145	146	147
Frequencies --	1472.6768	1474.8735	1479.6115
	148	149	150
Frequencies --	1484.7159	1484.7165	1486.6696
	151	152	153
Frequencies --	1490.5441	1497.6785	1497.7572

	154	155	156
Frequencies --	1506.0555	1534.8510	1543.6605

D5. CP-PAH **3** *Neutral* Vibrational Frequencies in cm^{-1}

	1	2	3
Frequencies --	19.2969	21.7584	26.8017
	4	5	6
Frequencies --	55.1366	60.1898	79.5518
	7	8	9
Frequencies --	82.8207	110.1732	144.3715
	10	11	12
Frequencies --	144.3950	151.1497	157.0446
	13	14	15
Frequencies --	162.7166	166.2518	168.0833
	16	17	18
Frequencies --	168.6374	172.5844	182.8450
	19	20	21
Frequencies --	188.6786	189.4140	213.1916
	22	23	24
Frequencies --	218.2494	226.2206	230.3446
	25	26	27
Frequencies --	242.3218	243.7163	266.8815
	28	29	30
Frequencies --	275.8078	302.8979	380.9864
	31	32	33
Frequencies --	381.9698	384.4263	408.1529
	34	35	36
Frequencies --	478.5986	485.6233	518.0954
	37	38	39
Frequencies --	518.2454	556.8729	598.0692
	40	41	42
Frequencies --	600.2015	612.8474	613.1983
	43	44	45
Frequencies --	641.1882	650.0940	671.2562

	46	47	48
Frequencies --	681.2617	685.7073	687.8026
	49	50	51
Frequencies --	688.3588	691.5288	691.8309
	52	53	54
Frequencies --	697.6274	698.0834	699.3659
	55	56	57
Frequencies --	754.7924	769.1391	774.7581
	58	59	60
Frequencies --	775.4867	777.1160	778.9545
	61	62	63
Frequencies --	797.8954	811.8774	823.3882
	64	65	66
Frequencies --	843.2120	859.9794	860.4969
	67	68	69
Frequencies --	861.4252	863.3638	865.2170
	70	71	72
Frequencies --	870.0984	876.4802	880.2720
	73	74	75
Frequencies --	928.9109	934.1996	935.4665
	76	77	78
Frequencies --	954.7120	992.1776	992.2096
	79	80	81
Frequencies --	1011.3639	1046.3476	1058.1342
	82	83	84
Frequencies --	1087.0212	1143.1001	1145.3681
	85	86	87
Frequencies --	1189.1762	1200.8231	1210.0155
	88	89	90
Frequencies --	1262.0942	1264.7578	1265.1443
	91	92	93
Frequencies --	1285.3892	1285.4005	1286.5282
	94	95	96
Frequencies --	1287.2614	1291.1361	1294.0097

	97	98	99
Frequencies --	1294.7620	1327.3517	1400.3796
	100	101	102
Frequencies --	1403.8064	1424.4383	1448.2956
	103	104	105
Frequencies --	1450.0917	1450.0939	1452.2452
	106	107	108
Frequencies --	1452.2700	1453.4647	1453.5193
	109	110	111
Frequencies --	1456.6022	1460.0334	1460.0369
	112	113	114
Frequencies --	1461.1605	1461.1641	1466.9156
	115	116	117
Frequencies --	1466.9225	1477.1830	1487.0768
	118	119	120
Frequencies --	1487.2745	1508.4829	1545.6304
	121	122	123
Frequencies --	1590.7941	1617.9725	1645.5777
	124	125	126
Frequencies --	1649.7559	3019.0400	3019.0479
	127	128	129
Frequencies --	3019.8917	3019.9201	3021.9985
	130	131	132
Frequencies --	3022.0211	3087.9154	3087.9232
	133	134	135
Frequencies --	3088.9188	3088.9242	3090.6061
	136	137	138
Frequencies --	3090.6417	3093.8822	3093.8982
	139	140	141
Frequencies --	3094.3763	3094.3981	3094.6185
	142	143	144
Frequencies --	3094.6286	3167.1821	3167.2668
	145	146	147
Frequencies --	3177.6421	3177.6680	3190.1750

	148	149	150
Frequencies --	3190.5692	3204.2605	3204.7145

D6. CP-PAH **3** *Anion* Vibrational Frequencies in cm^{-1}

	1	2	3
Frequencies --	29.6184	36.4164	36.8673
	4	5	6
Frequencies --	56.7694	61.5083	81.4251
	7	8	9
Frequencies --	90.4815	112.8222	143.7958
	10	11	12
Frequencies --	144.7722	152.3939	156.6857
	13	14	15
Frequencies --	162.8982	162.9550	168.4045
	16	17	18
Frequencies --	173.6661	175.9156	187.0875
	19	20	21
Frequencies --	188.9088	191.8428	213.3008
	22	23	24
Frequencies --	221.7248	230.8678	233.3626
	25	26	27
Frequencies --	244.6430	249.8016	269.5060
	28	29	30
Frequencies --	276.2513	304.4915	367.0885
	31	32	33
Frequencies --	377.1351	387.3031	389.8294
	34	35	36
Frequencies --	479.5298	515.6549	523.5483
	37	38	39
Frequencies --	531.6090	560.7045	594.4024
	40	41	42
Frequencies --	599.2292	610.5855	610.7116
	43	44	45
Frequencies --	640.3508	642.8973	659.7911

	46	47	48
Frequencies --	675.9807	676.4666	676.5512
	49	50	51
Frequencies --	681.5516	682.2904	682.8933
	52	53	54
Frequencies --	689.0482	693.3335	693.3425
	55	56	57
Frequencies --	743.7698	747.2267	766.3708
	58	59	60
Frequencies --	769.0183	770.0362	771.8818
	61	62	63
Frequencies --	787.2537	801.0243	808.0251
	64	65	66
Frequencies --	831.8806	841.2612	841.6559
	67	68	69
Frequencies --	854.4850	854.5080	857.3194
	70	71	72
Frequencies --	857.7816	859.4120	868.6861
	73	74	75
Frequencies --	869.9275	871.4659	924.2085
	76	77	78
Frequencies --	936.9392	938.0582	979.4465
	79	80	81
Frequencies --	1023.8675	1058.9426	1069.9129
	82	83	84
Frequencies --	1085.0823	1138.9148	1147.4782
	85	86	87
Frequencies --	1177.9333	1187.7510	1216.3016
	88	89	90
Frequencies --	1228.9202	1258.8861	1263.1372
	94	95	96
Frequencies --	1280.4720	1287.3083	1287.6856
	97	98	99
Frequencies --	1301.0798	1332.2675	1377.4699

	100	101	102
Frequencies --	1381.3669	1391.2547	1402.5659
	103	104	105
Frequencies --	1430.0982	1433.8598	1450.3601
	106	107	108
Frequencies --	1450.3612	1454.0884	1454.6560
	109	110	111
Frequencies --	1454.7374	1454.7597	1454.8654
	112	113	114
Frequencies --	1460.5455	1460.5485	1460.6599

D7. CP-PAH **4** *Neutral* Vibrational Frequencies in cm^{-1}

	1	2	3
Frequencies --	4.2545	12.3336	26.8087
	4	5	6
Frequencies --	49.5148	56.0166	58.8342
	7	8	9
Frequencies --	81.1322	87.6978	133.2492
	10	11	12
Frequencies --	135.9910	139.6957	145.7663
	13	14	15
Frequencies --	148.0754	161.6240	162.0658
	16	17	18
Frequencies --	163.8218	175.9612	177.0913
	19	20	21
Frequencies --	181.6177	188.9640	191.8214
	22	23	24
Frequencies --	203.7364	215.0494	219.6939
	25	26	27
Frequencies --	219.7881	236.2096	242.0490
	28	29	30
Frequencies --	257.1282	277.8017	286.7180

	31	32	33
Frequencies --	287.8101	310.0638	351.5496
	34	35	36
Frequencies --	357.1514	407.1241	417.8027
	37	38	39
Frequencies --	488.6359	500.5900	502.8149
	40	41	42
Frequencies --	515.3303	538.0339	541.1548
	43	44	45
Frequencies --	541.4253	581.6429	611.5807
	46	47	48
Frequencies --	614.3233	615.1242	623.9577
	49	50	51
Frequencies --	642.6144	651.0000	681.4195
	52	53	54
Frequencies --	686.9573	689.1759	690.8470
	55	56	57
Frequencies --	692.3363	692.5906	700.6886
	58	59	60
Frequencies --	700.9391	700.9425	702.7080
	61	62	63
Frequencies --	731.8192	762.7535	771.9846
	64	65	66
Frequencies --	774.0442	776.0512	780.7120
	67	68	69
Frequencies --	782.3417	787.7448	803.9930
	70	71	72
Frequencies --	806.7265	811.4113	861.3504
	73	74	75
Frequencies --	861.6607	862.1206	862.6558
	76	77	78
Frequencies --	866.8328	867.4759	876.6820
	79	80	81
Frequencies --	879.7423	887.3485	897.0949

	82	83	84
Frequencies --	902.6657	930.7818	937.5759
	85	86	87
Frequencies --	937.6945	989.2499	990.5991
	88	89	90
Frequencies --	990.6464	1032.6189	1042.2739
	91	92	93
Frequencies --	1048.5284	1071.1953	1110.2437
	94	95	96
Frequencies --	1130.2891	1186.4687	1193.3464
	97	98	99
Frequencies --	1199.0519	1227.0030	1228.2336
	100	101	102
Frequencies --	1252.5859	1265.8271	1277.1862
	103	104	105
Frequencies --	1286.3020	1286.3045	1288.0478
	106	107	108
Frequencies --	1288.9149	1291.5071	1296.5220
	109	110	111
Frequencies --	1296.8305	1353.7111	1359.5655
	112	113	114
Frequencies --	1384.9306	1385.0553	1411.0344
	115	116	117
Frequencies --	1411.2322	1436.7244	1450.6749
	118	119	120
Frequencies --	1450.6779	1452.5489	1452.5575
	121	122	123
Frequencies --	1453.2825	1453.2848	1457.9845
	124	125	126
Frequencies --	1461.8466	1462.1919	1462.6118
	127	128	129
Frequencies --	1462.6159	1466.8952	1466.9556
	130	131	132
Frequencies --	1478.6288	1483.8291	1499.0332

	133	134	135
Frequencies --	1499.2352	1522.6487	1574.9520
	136	137	138
Frequencies --	1593.7201	1609.2444	1644.7038
	139	140	141
Frequencies --	1648.5732	1655.3576	3019.0515
	142	143	144
Frequencies --	3019.0546	3020.0322	3020.0481
	145	146	147
Frequencies --	3022.3674	3022.3780	3087.6663
	148	149	150
Frequencies --	3087.6704	3088.7711	3088.7773
	151	152	153
Frequencies --	3090.9545	3090.9731	3093.9030
	154	155	156
Frequencies --	3093.9075	3094.3682	3094.3723
	157	158	159
Frequencies --	3095.1133	3095.1212	3165.7720
	160	161	162
Frequencies --	3165.8202	3173.7224	3173.7241
	163	164	165
Frequencies --	3178.5942	3178.6302	3187.6622
	166	167	168
Frequencies --	3187.9081	3204.2083	3204.3417

D8. CP-PAH **4** *Anion* Vibrational Frequencies in cm^{-1}

	1	2	3
Frequencies --	22.0327	25.8283	26.0764
	4	5	6
Frequencies --	46.7948	52.2693	56.0180
	7	8	9
Frequencies --	73.9398	85.6155	130.8511
	10	11	12
Frequencies --	139.3629	143.4303	147.3899

	13	14	15
Frequencies --	147.6596	161.2659	167.0842
	16	17	18
Frequencies --	168.8028	168.8812	169.1612
	19	20	21
Frequencies --	176.8581	187.0924	188.5899
	22	23	24
Frequencies --	205.4947	215.3980	218.4252
	25	26	27
Frequencies --	219.2113	236.6954	246.9890
	28	29	30
Frequencies --	255.5688	283.4129	285.6714
	31	32	33
Frequencies --	291.5089	307.4438	345.9197
	34	35	36
Frequencies --	359.4533	388.7781	420.3549
	37	38	39
Frequencies --	486.6166	503.3895	517.6699
	40	41	42
Frequencies --	533.0784	538.1148	540.2224
	43	44	45
Frequencies --	544.8954	580.3501	609.2200
	46	47	48
Frequencies --	612.8250	613.7471	616.8881
	49	50	51
Frequencies --	643.9936	644.6216	674.1689
	52	53	54
Frequencies --	679.2959	679.5491	682.4670
	55	56	57
Frequencies --	685.0905	686.4441	694.8522
	58	59	60
Frequencies --	694.8564	698.3862	701.7805
	61	62	63
Frequencies --	724.9509	748.2434	763.4742

	64	65	66
Frequencies --	765.9760	767.6205	774.5251
	67	68	69
Frequencies --	774.6748	778.5779	791.1821
	70	71	72
Frequencies --	799.5455	819.6538	834.9957
	73	74	75
Frequencies --	841.3898	846.7245	846.7406
	76	77	78
Frequencies --	855.2823	855.7702	858.5535
	79	80	81
Frequencies --	858.5648	860.4234	862.7065
	82	83	84
Frequencies --	885.6112	885.7623	897.5291
	85	86	87
Frequencies --	929.6415	946.4882	946.6068
	88	89	90
Frequencies --	995.8952	1044.8891	1053.6518
	91	92	93
Frequencies --	1054.7817	1081.6816	1111.1555
	94	95	96
Frequencies --	1129.8762	1179.7255	1185.5474
	97	98	99
Frequencies --	1191.1693	1212.3803	1231.2566
	100	101	102
Frequencies --	1246.8585	1256.0116	1279.1716
	103	104	105
Frequencies --	1279.1738	1279.3029	1281.6611
	106	107	108
Frequencies --	1281.8818	1289.1008	1290.3984
	109	110	111
Frequencies --	1293.6789	1324.9332	1348.5521
	112	113	114
Frequencies --	1368.2527	1394.0576	1395.8893

	115	116	117
Frequencies --	1405.7629	1410.6418	1434.5462
	118	119	120
Frequencies --	1450.6459	1450.6466	1450.6552
	121	122	123
Frequencies --	1454.6157	1454.6291	1454.7930
	124	125	126
Frequencies --	1455.0797	1456.0046	1460.5599
	127	128	129
Frequencies --	1460.7340	1461.2993	1461.3014
	130	131	132
Frequencies --	1467.8210	1468.9565	1470.2714
	133	134	135
Frequencies --	1479.2887	1505.3739	1529.6762
	136	137	138
Frequencies --	1549.1743	1594.4768	1595.4574
	139	140	141
Frequencies --	1607.5556	1623.9788	3013.7018
	142	143	144
Frequencies --	3013.7034	3014.7229	3014.7677
	145	146	147
Frequencies --	3018.2508	3018.2738	3081.3743
	148	149	150
Frequencies --	3081.3805	3082.4568	3082.4780
	151	152	153
Frequencies --	3085.7029	3085.7367	3088.9349

D9. CP-PAH **5** *Neutral* Vibrational Frequencies in cm^{-1}

	1	2	3
Frequencies --	41.3726	48.3057	87.5214
	4	5	6
Frequencies --	103.2800	104.1253	112.6202

	7	8	9
Frequencies --	124.5288	140.8688	178.9179
	10	11	12
Frequencies --	196.8559	238.2900	297.1851
	13	14	15
Frequencies --	301.0260	342.8381	366.8429
	16	17	18
Frequencies --	395.7027	404.3211	416.7197
	19	20	21
Frequencies --	433.3599	455.6604	486.1664
	22	23	24
Frequencies --	493.9730	494.2643	497.9804
	25	26	27
Frequencies --	523.9021	571.6752	585.2827
	28	29	30
Frequencies --	613.9911	626.8301	630.2758
	31	32	33
Frequencies --	645.2837	647.4599	669.6126
	34	35	36
Frequencies --	691.2653	697.5999	697.6567
	37	38	39
Frequencies --	713.3278	717.4353	735.3099
	40	41	42
Frequencies --	748.1206	771.3362	775.8130
	43	44	45
Frequencies --	776.1730	784.7239	829.1114
	46	47	48
Frequencies --	885.4318	886.5314	924.0473
	49	50	51
Frequencies --	932.2550	940.5327	945.4945
	52	53	54
Frequencies --	957.2371	957.2710	995.8380
	55	56	57
Frequencies --	995.8715	1010.7318	1040.4465

	58	59	60
Frequencies --	1041.8368	1057.5033	1064.7704
	61	62	63
Frequencies --	1121.6204	1129.9903	1173.9079
	64	65	66
Frequencies --	1177.3972	1208.9072	1218.0013
	67	68	69
Frequencies --	1232.1925	1242.5347	1264.1037
	70	71	72
Frequencies --	1318.2953	1318.8308	1339.7420
	73	74	75
Frequencies --	1359.6518	1375.5342	1380.4750
	76	77	78
Frequencies --	1426.2912	1464.7441	1475.2577
	79	80	81
Frequencies --	1494.3519	1499.1699	1539.1137
	82	83	84
Frequencies --	1560.2364	1591.1810	1613.1990
	85	86	87
Frequencies --	1617.7914	1628.9943	1635.7199
	88	89	90
Frequencies --	1647.3753	2175.0728	2177.5661
	91	92	93
Frequencies --	3167.9365	3167.9565	3175.1762
	94	95	96
Frequencies --	3175.1993	3179.1405	3180.0377
	97	98	99
Frequencies --	3183.5413	3183.5573	3193.2505
	100	101	102
Frequencies --	3193.5058	3457.7187	3458.1124

D10. CP-PAH **5** *Anion* Vibrational Frequencies in cm^{-1}

	1	2	3
Frequencies --	40.4620	50.2177	88.3912

	4	5	6
Frequencies --	102.8116	105.5924	111.4180
	7	8	9
Frequencies --	123.3182	142.9476	186.0726
	10	11	12
Frequencies --	196.6890	242.5762	299.1916
	13	14	15
Frequencies --	303.6074	357.4546	371.4776
	16	17	18
Frequencies --	405.2346	418.9885	423.0036
	19	20	21
Frequencies --	436.1055	451.6472	457.6398
	22	23	24
Frequencies --	461.8973	488.2989	496.3553
	25	26	27
Frequencies --	496.7157	497.0683	523.1605
	28	29	30
Frequencies --	574.6926	579.6879	599.7659
	31	32	33
Frequencies --	608.0966	631.7408	671.2327
	34	35	36
Frequencies --	680.4505	680.4730	687.4466
	37	38	39
Frequencies --	704.4326	724.8854	734.3092
	40	41	42
Frequencies --	738.2867	757.1271	765.3591
	43	44	45
Frequencies --	770.1800	773.7424	830.2772
	46	47	48
Frequencies --	864.0521	864.1749	894.3669
	49	50	51
Frequencies --	894.9439	935.4290	935.4453
	52	53	54
Frequencies --	940.5784	947.4288	969.2428

	55	56	57
Frequencies --	969.2905	1012.0222	1036.0749
	58	59	60
Frequencies --	1036.3486	1052.5929	1058.6387
	61	62	63
Frequencies --	1116.6884	1130.9674	1161.1905
	64	65	66
Frequencies --	1161.3020	1205.4126	1227.2982
	67	68	69
Frequencies --	1227.8030	1247.8389	1257.0190
	70	71	72
Frequencies --	1309.6556	1329.3298	1337.8677
	73	74	75
Frequencies --	1352.3256	1359.2094	1374.1154
	76	77	78
Frequencies --	1402.2858	1458.6639	1460.5810
	79	80	81
Frequencies --	1480.0312	1493.9708	1494.2174
	82	83	84
Frequencies --	1511.9994	1531.6218	1588.9986
	85	86	87
Frequencies --	1591.8534	1612.0301	1622.7712
	88	89	90
Frequencies --	1626.4046	2125.2432	2127.3296
	91	92	93
Frequencies --	3148.7302	3148.8088	3153.7594
	94	95	96
Frequencies --	3154.3680	3155.7040	3156.8358
	97	98	99
Frequencies --	3166.7133	3166.7276	3178.3201
	100	101	102
Frequencies --	3178.7217	3462.3683	3462.9715

D11. CP-PAH **6** *Neutral* Vibrational Frequencies in cm^{-1}

	1	2	3
Frequencies --	63.7599	133.3330	138.3186
	4	5	6
Frequencies --	255.7250	258.7116	276.1986
	7	8	9
Frequencies --	332.6161	338.8375	373.6129
	10	11	12
Frequencies --	388.3596	416.5414	419.9194
	13	14	15
Frequencies --	452.6736	482.9959	508.9442
	16	17	18
Frequencies --	513.6285	588.3395	600.1874
	19	20	21
Frequencies --	605.3466	616.4203	656.8872
	22	23	24
Frequencies --	662.8501	679.6499	705.9008
	25	26	27
Frequencies --	708.8564	722.3495	760.3401
	28	29	30
Frequencies --	775.3133	794.2297	794.9081
	31	32	33
Frequencies --	806.1811	808.4889	811.9475
	34	35	36
Frequencies --	884.9784	907.8396	911.0984
	37	38	39
Frequencies --	919.2243	933.4280	936.4949
	40	41	42
Frequencies --	943.1863	950.5380	1000.8305
	43	44	45
Frequencies --	1017.9987	1051.5761	1062.4929
	46	47	48
Frequencies --	1079.7599	1090.4280	1109.7562

	49	50	51
Frequencies --	1162.3537	1171.9169	1190.8708
	52	53	54
Frequencies --	1198.0721	1225.4838	1242.6657
	55	56	57
Frequencies --	1266.6364	1306.2775	1321.7129
	58	59	60
Frequencies --	1336.2607	1363.8132	1367.0499
	61	62	63
Frequencies --	1399.9973	1420.5317	1466.3658
	64	65	66
Frequencies --	1470.6165	1497.6604	1501.9137
	67	68	69
Frequencies --	1506.8361	1519.5238	1538.1926
	70	71	72
Frequencies --	1575.1213	1610.9699	1617.1413
	73	74	75
Frequencies --	1702.0069	1712.9580	3165.8731
	76	77	78
Frequencies --	3165.9684	3168.4846	3168.8665
	79	80	81
Frequencies --	3174.8102	3190.8240	3201.3274
	82	83	84
Frequencies --	3201.7578	3221.5598	3221.8880

D12. CP-PAH **6** *Anion* Vibrational Frequencies in cm^{-1}

	1	2	3
Frequencies --	66.1290	131.0997	135.2949
	4	5	6
Frequencies --	243.2553	264.9110	265.0355
	7	8	9
Frequencies --	331.6775	332.0639	380.7285
	10	11	12
Frequencies --	384.7977	413.1935	416.2876

	13	14	15
Frequencies --	458.6430	482.0032	506.2119
	16	17	18
Frequencies --	510.0053	589.5816	595.0729
	19	20	21
Frequencies --	602.6668	613.8186	645.8041
	22	23	24
Frequencies --	651.2257	677.8578	695.1324
	25	26	27
Frequencies --	703.8673	710.7447	725.4783
	28	29	30
Frequencies --	761.0016	764.0759	770.5659
	31	32	33
Frequencies --	791.2878	805.2024	809.7300
	34	35	36
Frequencies --	809.8393	835.8439	841.7065
	37	38	39
Frequencies --	870.5545	873.6532	896.9265
	40	41	42
Frequencies --	911.5400	923.8893	956.0011
	43	44	45
Frequencies --	1025.3346	1047.0492	1055.0174
	46	47	48
Frequencies --	1066.4628	1069.7966	1109.8766
	49	50	51
Frequencies --	1135.0603	1177.3810	1178.7480
	52	53	54
Frequencies --	1184.4840	1204.2195	1241.6610
	55	56	57
Frequencies --	1254.0965	1302.9384	1309.6228
	58	59	60
Frequencies --	1330.7830	1338.4617	1368.5316
	61	62	63
Frequencies --	1372.7939	1388.9128	1413.2249

	64	65	66
Frequencies --	1439.8350	1456.9119	1464.9589
	67	68	69
Frequencies --	1476.9467	1491.2336	1516.8225
	70	71	72
Frequencies --	1547.1554	1552.9887	1567.7539
	73	74	75
Frequencies --	1666.6574	1677.1593	3134.8974
	76	77	78
Frequencies --	3139.6115	3140.1076	3141.4556
	79	80	81
Frequencies --	3155.2571	3166.8006	3176.3760
	82	83	84
Frequencies --	3176.9381	3195.8793	3196.4882

D13. CP-PAH **7** *Neutral* Vibrational Frequencies in cm^{-1}

	1	2	3
Frequencies --	139.1965	140.0158	147.4415
	4	5	6
Frequencies --	279.5086	280.2133	311.6331
	7	8	9
Frequencies --	311.6825	410.4088	410.6425
	10	11	12
Frequencies --	439.0766	439.1844	454.6346
	13	14	15
Frequencies --	455.2531	543.9761	548.2568
	16	17	18
Frequencies --	548.9225	560.0826	604.6159
	19	20	21
Frequencies --	614.0090	614.3154	648.9833
	22	23	24
Frequencies --	649.3468	649.6542	674.1545

	25	26	27
Frequencies --	674.2684	759.7309	759.9017
	28	29	30
Frequencies --	772.9642	773.6463	813.4195
	31	32	33
Frequencies --	813.7562	837.0629	837.5436
	34	35	36
Frequencies --	858.4631	864.4655	864.5479
	37	38	39
Frequencies --	939.0423	972.5930	978.7032
	40	41	42
Frequencies --	979.3701	986.6851	987.5205
	43	44	45
Frequencies --	1046.3005	1087.6122	1087.7208
	46	47	48
Frequencies --	1158.7059	1159.0028	1159.4071
	49	50	51
Frequencies --	1160.2721	1183.9532	1184.1003
	52	53	54
Frequencies --	1213.8050	1214.2276	1239.1166
	55	56	57
Frequencies --	1255.8912	1332.7007	1332.9836
	58	59	60
Frequencies --	1374.8830	1375.2936	1423.6212
	61	62	63
Frequencies --	1423.8236	1439.8201	1440.1604
	64	65	66
Frequencies --	1459.4343	1468.3082	1468.7320
	67	68	69
Frequencies --	1480.9715	1481.0792	1510.0941
	70	71	72
Frequencies --	1649.8522	1650.3191	1650.7574
	73	74	75
Frequencies --	1651.3685	1651.3891	3161.2588

	76	77	78
Frequencies --	3161.4674	3161.6409	3161.8351
	79	80	81
Frequencies --	3162.0708	3176.7997	3176.8950
	82	83	84
Frequencies --	3177.2391	3177.3640	3178.4358

D14. CP-PAH **7** *Anion* Vibrational Frequencies in cm^{-1}

	1	2	3
Frequencies --	32.0234	138.2813	142.2537
	4	5	6
Frequencies --	214.8475	279.0384	284.6470
	7	8	9
Frequencies --	295.3977	307.1596	398.8570
	10	11	12
Frequencies --	406.5533	414.9715	434.1997
	13	14	15
Frequencies --	455.6894	474.3494	522.2940
	16	17	18
Frequencies --	547.3931	548.1102	557.6525
	19	20	21
Frequencies --	592.6472	603.8681	641.6015
	22	23	24
Frequencies --	642.0102	643.1315	643.9659
	25	26	27
Frequencies --	666.3054	686.2165	732.6423
	28	29	30
Frequencies --	744.7530	754.6477	776.7551
	31	32	33
Frequencies --	784.2049	791.8711	796.7334
	34	35	36
Frequencies --	806.0808	832.0180	848.8220
	37	38	39
Frequencies --	853.3982	878.9977	887.0502

	40	41	42
Frequencies --	928.0648	935.8758	940.2235
	43	44	45
Frequencies --	963.3303	1028.7872	1087.1839
	46	47	48
Frequencies --	1104.1675	1106.3412	1114.7062
	49	50	51
Frequencies --	1141.6690	1142.8107	1190.5981
	52	53	54
Frequencies --	1201.7546	1208.4458	1232.5295
	55	56	57
Frequencies --	1252.4505	1278.8493	1304.8592
	58	59	60
Frequencies --	1318.0911	1362.8463	1372.5466
	61	62	63
Frequencies --	1388.4933	1416.4374	1416.5098
	64	65	66
Frequencies --	1440.0374	1450.0813	1458.9109
	67	68	69
Frequencies --	1460.4361	1468.4843	1506.9612
	70	71	72
Frequencies --	1543.1345	1580.9653	1609.9501
	73	74	75
Frequencies --	1615.1395	1625.6590	3130.8209
	76	77	78
Frequencies --	3131.0605	3131.4171	3133.7997
	79	80	81
Frequencies --	3133.9587	3149.7445	3150.2641
	82	83	84
Frequencies --	3150.9170	3152.5122	3153.8929

D15. CP-PAH **8** *Neutral* Vibrational Frequencies in cm^{-1}

	1	2	3
Frequencies --	54.1286	60.3355	161.1545
	4	5	6
Frequencies --	165.8457	170.2152	202.1156
	7	8	9
Frequencies --	229.0759	261.7778	278.9497
	10	11	12
Frequencies --	319.1902	336.2783	369.5913
	13	14	15
Frequencies --	464.7411	468.1845	470.4921
	16	17	18
Frequencies --	477.5569	508.6213	531.2255
	19	20	21
Frequencies --	542.0700	571.1726	597.7345
	22	23	24
Frequencies --	601.0222	623.2565	623.7477
	25	26	27
Frequencies --	662.3406	669.1932	704.5194
	28	29	30
Frequencies --	708.7537	731.1414	735.5929
	31	32	33
Frequencies --	755.7412	778.3187	779.3091
	34	35	36
Frequencies --	784.0757	800.5573	826.3053
	37	38	39
Frequencies --	827.6228	850.4771	850.6912
	40	41	42
Frequencies --	908.5528	914.9173	925.2679
	43	44	45
Frequencies --	925.7928	940.1885	945.1349
	46	47	48
Frequencies --	946.3477	986.3865	986.5154

	49	50	51
Frequencies --	1012.8030	1052.4183	1052.7297
	52	53	54
Frequencies --	1060.4096	1085.1218	1100.6394
	55	56	57
Frequencies --	1108.5646	1147.2602	1181.9295
	58	59	60
Frequencies --	1195.7653	1217.8870	1222.9207
	61	62	63
Frequencies --	1234.3324	1247.0928	1254.9103
	64	65	66
Frequencies --	1301.5665	1322.1694	1342.0347
	67	68	69
Frequencies --	1353.4673	1381.3513	1402.0903
	70	71	72
Frequencies --	1415.2069	1424.6978	1431.0930
	73	74	75
Frequencies --	1480.2733	1484.9876	1490.9576
	76	77	78
Frequencies --	1514.3356	1528.5990	1533.4706
	79	80	81
Frequencies --	1585.5997	1635.6369	1640.9172
	82	83	84
Frequencies --	1647.0024	1649.9699	1658.7122
	85	86	87
Frequencies --	3169.5952	3169.6140	3181.2009
	88	89	90
Frequencies --	3181.3303	3187.9775	3188.1373
	91	92	93
Frequencies --	3199.1504	3199.5738	3205.9913
	94	95	96
Frequencies --	3206.0569	3224.8810	3225.0562

D16. CP-PAH **8** *Anion* Vibrational Frequencies in cm^{-1}

	1	2	3
Frequencies --	46.0013	59.4151	163.6559
	4	5	6
Frequencies --	166.5050	173.2234	207.2830
	7	8	9
Frequencies --	224.5523	259.6112	276.6552
	10	11	12
Frequencies --	323.1195	333.2445	364.8253
	13	14	15
Frequencies --	446.7627	468.9610	471.5872
	16	17	18
Frequencies --	497.8996	503.6533	535.6316
	19	20	21
Frequencies --	541.9030	566.4113	596.8646
	22	23	24
Frequencies --	598.8975	612.7554	619.7034
	25	26	27
Frequencies --	648.3055	654.5076	692.4505
	28	29	30
Frequencies --	708.8609	712.2955	726.9373
	31	32	33
Frequencies --	727.5781	751.7935	752.9539
	34	35	36
Frequencies --	773.1935	801.7910	804.6751
	37	38	39
Frequencies --	809.6129	845.3378	845.4337
	40	41	42
Frequencies --	859.0420	862.3175	868.8722
	43	44	45
Frequencies --	872.9165	891.1494	891.3260
	46	47	48
Frequencies --	942.6431	948.3421	949.0047

	49	50	51
Frequencies --	1013.8809	1051.5692	1052.2910
	52	53	54
Frequencies --	1060.7450	1063.4377	1089.4209
	55	56	57
Frequencies --	1106.4035	1141.9914	1181.9584
	58	59	60
Frequencies --	1184.2810	1217.9014	1219.9972
	61	62	63
Frequencies --	1234.3553	1251.4617	1265.7416
	64	65	66
Frequencies --	1294.3355	1316.0481	1342.4756
	67	68	69
Frequencies --	1345.0501	1362.1136	1366.0982
	70	71	72
Frequencies --	1388.6064	1388.7788	1417.3526
	73	74	75
Frequencies --	1455.1437	1462.2031	1479.5543
	76	77	78
Frequencies --	1488.0637	1495.4901	1514.5247
	79	80	81
Frequencies --	1536.4263	1570.3270	1595.6200
	82	83	84
Frequencies --	1597.2125	1617.6853	1632.0515
	85	86	87
Frequencies --	3146.2680	3146.3441	3158.0622
	88	89	90
Frequencies --	3158.4854	3163.4274	3163.6404
	91	92	93
Frequencies --	3179.1516	3179.7360	3182.5118
	94	95	96
Frequencies --	3182.5846	3202.1115	3202.4298

APPENDIX E

PREDICTED EXCITATION ENERGIES OF THE 8 CP-PAHS USING

B3LYP/TD-CAMB3LYP AND 6-311G (d,p) BASIS SET

E1. Excited State Energies with Oscillator Strength of CP-PAH 1

```
Excited State   1:    Singlet-A       1.8320 eV  676.78 nm  f=0.7787
     124 ->128        -0.17087
     127 ->128         0.67509

Excited State   2:    Singlet-A       2.6450 eV  468.75 nm  f=0.0000
     123 ->128         0.34532
     126 ->128         0.59874

Excited State   3:    Singlet-A       3.0034 eV  412.81 nm  f=0.3296
     122 ->128         0.11454
     124 ->128         0.29713
     125 ->128         0.60940
     127 ->128         0.10266

Excited State   4:    Singlet-A       3.4728 eV  357.02 nm  f=0.4998
     122 ->128         0.55255
     124 ->128         0.25093
     125 ->128        -0.26404
     125 ->131        -0.12427
     127 ->131        -0.13587

Excited State   5:    Singlet-A       3.6511 eV  339.58 nm  f=0.0000
     117 ->128         0.19531
     123 ->128         0.54325
     126 ->128        -0.27542
     127 ->129        -0.26028

Excited State   6:    Singlet-A       3.8472 eV  322.27 nm  f=0.0000
     123 ->128         0.18686
     124 ->129        -0.14604
     126 ->128        -0.20720
     127 ->129         0.59202
     127 ->132         0.13354

Excited State   7:    Singlet-A       4.0072 eV  309.40 nm  f=0.9007
     116 ->128         0.14614
     122 ->128        -0.28605
     124 ->128         0.45900
     125 ->128        -0.20265
     126 ->129         0.13709
     127 ->130         0.27801

Excited State   8:    Singlet-A       4.3556 eV  284.66 nm  f=0.0000
     118 ->129         0.22457
```

```
     119 ->128         0.64992

Excited State   9:    Singlet-A       4.3689 eV  283.79 nm  f=1.3789
     122 ->128         0.19175
     124 ->128        -0.25163
     126 ->129         0.16075
     126 ->132        -0.16541
     127 ->130         0.55463

Excited State  10:    Singlet-A       4.4488 eV  278.69 nm  f=0.0000
     118 ->128         0.64061
     118 ->130         0.10316
     119 ->129         0.24765

Excited State  11:    Singlet-A       4.6463 eV  266.84 nm  f=0.0943
     122 ->128         0.14954
     124 ->131        -0.12673
     126 ->129        -0.22154
     127 ->131         0.61948

Excited State  12:    Singlet-A       4.6789 eV  264.98 nm  f=0.0000
     124 ->129        -0.12566
     126 ->130        -0.36016
     127 ->132         0.51572

Excited State  13:    Singlet-A       4.7585 eV  260.56 nm  f=0.0335
     120 ->128        -0.30602
     120 ->130        -0.16678
     121 ->129         0.15924
     121 ->132        -0.12278
     123 ->134        -0.12172
     124 ->133         0.17431
     126 ->134         0.32009
     127 ->133         0.39459

Excited State  14:    Singlet-A       4.7623 eV  260.35 nm  f=0.0000
     120 ->129        -0.15311
     120 ->132         0.12314
     121 ->128         0.30575
     121 ->130         0.15925
     123 ->133        -0.11877
     124 ->134         0.15940
     126 ->133         0.32005
     127 ->134         0.39695

Excited State  15:    Singlet-A       5.0754 eV  244.29 nm  f=0.0000
     115 ->128        -0.20121
     117 ->128         0.38964
     121 ->128        -0.10870
     122 ->129         0.15462
     122 ->132         0.12124
     123 ->131         0.19706
```

```
     124 ->129         0.17826
     125 ->129         0.26022
     126 ->131         0.17396
     127 ->132         0.12968

Excited State  16:    Singlet-A       5.1925 eV  238.77 nm  f=0.0000
     117 ->128        -0.22396
     121 ->128         0.47079
     123 ->128         0.10703
     123 ->131         0.12721
     125 ->129         0.24055
     126 ->131         0.12319
     126 ->133        -0.14394
     127 ->134        -0.20336

Excited State  17:    Singlet-A       5.2171 eV  237.65 nm  f=0.0699
     120 ->128         0.60735
     126 ->134         0.17880
     127 ->133         0.26790

Excited State  18:    Singlet-A       5.2511 eV  236.11 nm  f=0.3346
     122 ->128         0.11913
     123 ->129         0.18983
     125 ->131         0.12713
     126 ->129         0.55375
     126 ->132         0.14502
     127 ->130        -0.17100
     127 ->131         0.20011

Excited State  19:    Singlet-A       5.2698 eV  235.27 nm  f=0.0000
     114 ->128        -0.11596
     117 ->128         0.42881
     121 ->128         0.36736
     123 ->128        -0.10286
     125 ->129        -0.24663
     126 ->133        -0.11390
     127 ->134        -0.14757

Excited State  20:    Singlet-A       5.4736 eV  226.51 nm  f=0.0000
     111 ->128         0.54663
     113 ->128         0.41637

Excited State  21:    Singlet-A       5.5066 eV  225.16 nm  f=0.0000
     115 ->128         0.15859
     117 ->128         0.13195
     122 ->129        -0.17511
     123 ->131        -0.18463
     125 ->129         0.45116
     125 ->132         0.13374
     126 ->130        -0.14739
     126 ->131        -0.28669
     127 ->132        -0.17383
```

```
Excited State  22:    Singlet-A       5.5224 eV  224.51 nm  f=0.0000
     116 ->137         0.11237
     117 ->140        -0.13683
     126 ->140         0.33987
     126 ->141        -0.10526
     127 ->137         0.49678
     127 ->139        -0.15115
     127 ->142        -0.15750

Excited State  23:    Singlet-A       5.5615 eV  222.93 nm  f=0.5868
     122 ->128         0.10928
     122 ->131        -0.11960
     123 ->129         0.22147
     124 ->131         0.15231
     125 ->130         0.34140
     125 ->131         0.40166
     126 ->129        -0.15111
     126 ->132         0.12589
     127 ->130         0.10927

Excited State  24:    Singlet-A       5.6619 eV  218.98 nm  f=0.1849
     123 ->129        -0.26558
     124 ->130         0.24823
     125 ->131         0.38562
     126 ->132        -0.31513
     127 ->136         0.17906
```

E2. Excited State Energies with Oscillator Strength of CP-PAH 2

```
Excited State   1:    Singlet-A       1.8074 eV  685.97 nm  f=0.6307
     136 ->141        -0.12141
     139 ->142        -0.11310
     140 ->141         0.68323

Excited State   2:    Singlet-A       2.4883 eV  498.27 nm  f=0.0000
     136 ->142         0.10361
     137 ->141        -0.23290
     139 ->141         0.59035
     140 ->142        -0.25199

Excited State   3:    Singlet-A       2.9386 eV  421.91 nm  f=0.0504
     136 ->141        -0.36762
     137 ->142         0.13067
     138 ->141         0.55811
     139 ->142        -0.13227

Excited State   4:    Singlet-A       3.0955 eV  400.53 nm  f=0.0000
     137 ->141        -0.15371
     138 ->142        -0.15757
```

```
     139 ->141         0.20536
     140 ->142         0.62242

Excited State   5:    Singlet-A       3.3472 eV  370.42 nm  f=0.5355
     135 ->141         0.51880
     136 ->141         0.28213
     138 ->141         0.25554
     140 ->143         0.11258
     140 ->144         0.18745

Excited State   6:    Singlet-A       3.5661 eV  347.67 nm  f=0.0000
     134 ->141        -0.25810
     136 ->142        -0.16437
     137 ->141         0.55791
     139 ->141         0.25550

Excited State   7:    Singlet-A       3.8792 eV  319.61 nm  f=1.6389
     129 ->141        -0.13860
     135 ->141        -0.23977
     136 ->141         0.35713
     137 ->142        -0.10971
     138 ->141         0.17108
     139 ->142        -0.34448
     139 ->145        -0.11618
     140 ->143        -0.30710

Excited State   8:    Singlet-A       4.0593 eV  305.43 nm  f=0.0383
     134 ->142        -0.12813
     135 ->141        -0.14771
     136 ->141         0.18523
     137 ->142        -0.17051
     138 ->141         0.26342
     139 ->142         0.48207
     140 ->141         0.15192
     140 ->144        -0.22346

Excited State   9:    Singlet-A       4.2525 eV  291.56 nm  f=1.7230
     135 ->141        -0.31533
     136 ->141         0.14083
     139 ->142        -0.10294
     139 ->145         0.17325
     140 ->143         0.50576
     140 ->144         0.20886

Excited State  10:    Singlet-A       4.3611 eV  284.29 nm  f=0.0000
     127 ->141        -0.14699
     132 ->141         0.10575
     134 ->141         0.42923
     136 ->142        -0.12175
     137 ->141         0.12143
     138 ->142        -0.26164
     139 ->143        -0.24715
```

```
     140 ->145        -0.26876

Excited State  11:    Singlet-A       4.4849 eV  276.45 nm  f=0.0000
     130 ->142         0.31477
     131 ->141         0.59774
     131 ->143        -0.11600

Excited State  12:    Singlet-A       4.4986 eV  275.61 nm  f=0.0000
     127 ->141        -0.13009
     128 ->141         0.12451
     134 ->141         0.28909
     135 ->142        -0.19546
     136 ->142        -0.29688
     138 ->142         0.35389
     139 ->141         0.15050
     139 ->143         0.16402
     140 ->145         0.20562

Excited State  13:    Singlet-A      4.5054 eV  275.19 nm  f=0.0000
     130 ->141         0.59252
     130 ->143        -0.12067
     131 ->142         0.32481

Excited State  14:    Singlet-A       4.6415 eV  267.12 nm  f=0.0000
     128 ->141        -0.12982
     134 ->141         0.24805
     135 ->142         0.14717
     136 ->142         0.20802
     137 ->141         0.22266
     137 ->144        -0.10254
     138 ->142        -0.23211
     139 ->143         0.25263
     140 ->145         0.35964

Excited State  15:    Singlet-A       4.6953 eV  264.06 nm  f=0.4981
     135 ->141        -0.14234
     136 ->141        -0.12264
     139 ->142         0.22650
     139 ->145        -0.20824
     140 ->143        -0.17026
     140 ->144         0.54072

Excited State  16:    Singlet-A       4.7746 eV  259.67 nm  f=0.0175
     132 ->142         0.13474
     132 ->145         0.15618
     133 ->141        -0.22184
     133 ->143         0.15987
     136 ->146         0.13974
     137 ->147         0.12677
     138 ->146         0.20856
     139 ->147         0.36231
     140 ->146         0.36575
```

```
Excited State  17:    Singlet-A       4.7770 eV  259.55 nm  f=0.0000
     132 ->141        -0.22409
     132 ->143         0.15677
     133 ->142         0.13701
     133 ->145         0.15716
     136 ->147         0.13919
     137 ->146         0.12716
     138 ->147         0.20948
     139 ->146         0.36244
     140 ->147         0.36639

Excited State  18:    Singlet-A       4.8187 eV  257.30 nm  f=0.0000
     128 ->141        -0.18134
     134 ->141         0.16287
     135 ->142         0.41672
     136 ->142         0.11896
     138 ->142         0.40106
     139 ->143        -0.11315
     140 ->145        -0.11699

Excited State  19:    Singlet-A       5.1381 eV  241.30 nm  f=0.1166
     129 ->141         0.13065
     134 ->142        -0.33529
     136 ->141         0.18527
     137 ->142         0.47380
     138 ->144         0.10223
     140 ->148         0.17426

Excited State  20:    Singlet-A       5.2382 eV  236.69 nm  f=0.2529
     134 ->142         0.10376
     136 ->141         0.12876
     137 ->142         0.21065
     138 ->143         0.34304
     139 ->145         0.31282
     140 ->143        -0.17273
     140 ->144         0.10084
     140 ->148        -0.32057

Excited State  21:    Singlet-A       5.2410 eV  236.57 nm  f=0.0000
     137 ->143        -0.10305
     137 ->144        -0.18385
     138 ->142         0.10080
     139 ->143         0.34560
     139 ->144         0.42165
     140 ->145        -0.26539
     140 ->149         0.18176

Excited State  22:    Singlet-A       5.2774 eV  234.93 nm  f=0.0000
     132 ->141         0.60665
     133 ->142        -0.13619
     134 ->141        -0.15540
```

```
     139 ->146         0.16161
     140 ->147         0.20008

Excited State  23:    Singlet-A       5.2800 eV  234.82 nm  f=0.1147
     132 ->142        -0.13756
     133 ->141         0.62080
     139 ->147         0.16252
     140 ->146         0.19923

Excited State  24:    Singlet-A       5.4265 eV  228.48 nm  f=0.0000
     128 ->141         0.29756
     129 ->142        -0.11399
     135 ->142        -0.14055
     136 ->142         0.41437
     137 ->141         0.16739
     137 ->143         0.13695
     138 ->145         0.14492
     139 ->144        -0.17819
     140 ->145        -0.19055
```

E3. Excited State Energies with Oscillator Strength of CP-PAH 3

```
Excited State   1:    Singlet-A       2.3709 eV  522.94 nm  f=0.1576
      96 ->100         0.11379
      98 ->100        -0.24309
      99 ->100         0.64527

Excited State   2:    Singlet-A       3.0062 eV  412.43 nm  f=0.0000
      97 ->100         0.69252

Excited State   3:    Singlet-A       3.0981 eV  400.19 nm  f=0.2006
      96 ->100        -0.11760
      98 ->100         0.63708
      99 ->100         0.26444

Excited State   4:    Singlet-A       3.6470 eV  339.96 nm  f=0.3505
      96 ->100         0.64034
      98 ->100         0.15899
      98 ->102         0.11702
      99 ->102         0.19667

Excited State   5:    Singlet-A       4.3971 eV  281.97 nm  f=0.0000
      89 ->100        -0.10186
      95 ->100         0.12467
      99 ->101         0.67013

Excited State   6:      Singlet-A      4.8988 eV  253.09 nm  f=0.0000
      90 ->101        -0.15186
      92 ->100        -0.12838
      94 ->100         0.66193
```

```
Excited State   7:      Singlet-A      4.9520 eV  250.37 nm  f=0.7118
      96 ->100        -0.17975
      97 ->101         0.11491
      99 ->102         0.66178

Excited State   8:    Singlet-A       5.1460 eV  240.93 nm  f=0.0000
      89 ->100        -0.26035
      95 ->100         0.37036
      96 ->101         0.23353
      97 ->102         0.31449
      98 ->101        -0.28637
      99 ->101        -0.17284

Excited State   9:    Singlet-A       5.2459 eV  236.34 nm  f=0.0020
      86 ->100         0.12182
      87 ->100        -0.24670
      90 ->100         0.59500
      93 ->100        -0.14000
      94 ->101        -0.18399

Excited State  10:    Singlet-A       5.3707 eV  230.85 nm  f=0.0000
      88 ->100         0.19570
      95 ->100         0.50503
      96 ->101        -0.14522
      97 ->102        -0.24508
      98 ->101         0.29978

Excited State  11:    Singlet-A       5.5382 eV  223.87 nm  f=0.9123
      96 ->100        -0.15524
      97 ->101        -0.28735
      98 ->102         0.59124

Excited State  12:    Singlet-A       5.6066 eV  221.14 nm  f=0.0015
      86 ->100        -0.35733
      87 ->100        -0.37841
      93 ->100         0.45169

Excited State  13:    Singlet-A       5.6957 eV  217.68 nm  f=0.0000
      88 ->100        -0.17281
      96 ->101         0.17129
      97 ->102         0.32719
      98 ->101         0.54268
      98 ->104         0.10407

Excited State  14:    Singlet-A       5.7019 eV  217.44 nm  f=0.0597
      96 ->102        -0.19832
      97 ->101         0.55037
      98 ->102         0.30466
      99 ->103        -0.17764

Excited State  15:    Singlet-A       5.7642 eV  215.09 nm  f=0.0064
      86 ->100        -0.24782
```

```
      87 ->100         0.51709
      90 ->100         0.26933
      93 ->100         0.22545
      94 ->101        -0.13023

Excited State  16:    Singlet-A       5.8841 eV  210.71 nm  f=0.0000
      84 ->100        -0.12093
      92 ->100         0.66265
      93 ->101         0.14173
      94 ->100         0.12181

Excited State  17:    Singlet-A       5.9305 eV  209.06 nm  f=0.1040
      91 ->100         0.67618
      95 ->101         0.12233

Excited State  18:    Singlet-A       6.0752 eV  204.08 nm  f=0.0000
      88 ->100         0.15822
      89 ->100         0.27362
      96 ->101        -0.40292
      97 ->102         0.43785
      97 ->103         0.10196

Excited State  19:    Singlet-A       6.0991 eV  203.28 nm  f=0.0000
      88 ->100         0.39334
      89 ->100         0.36810
      96 ->101         0.43228

Excited State  20:    Singlet-A       6.1242 eV  202.45 nm  f=0.0010
      86 ->100         0.51907
      92 ->101         0.10233
      93 ->100         0.43987

Excited State  21:    Singlet-A       6.1661 eV  201.07 nm  f=0.0000
      88 ->100         0.46248
      89 ->100        -0.42187
      91 ->101        -0.11654
      95 ->100        -0.24893

Excited State  22:    Singlet-A       6.1771 eV  200.72 nm  f=0.4281
      96 ->102        -0.30462
      97 ->104         0.10040
      98 ->103        -0.10060
      99 ->103         0.59660

Excited State  23:    Singlet-A       6.2825 eV  197.35 nm  f=0.7694
      96 ->102         0.54148
      97 ->101         0.27384
      98 ->103         0.12599
      99 ->103         0.27655

Excited State  24:    Singlet-A       6.4122 eV  193.36 nm  f=0.0000
      97 ->103         0.12989
```

```
      99 ->104         0.66971
```

E4. Excited State Energies with Oscillator Strength of CP-PAH 4

```
Excited State   1:      Singlet-A      2.1616 eV  573.56 nm  f=0.2055
     110 ->113         0.13262
     112 ->113         0.68476

Excited State   2:    Singlet-A       2.9036 eV  427.01 nm  f=0.0000
     110 ->114        -0.21630
     111 ->113         0.62777
     112 ->114        -0.21937

Excited State   3:    Singlet-A       3.0172 eV  410.92 nm  f=0.0949
     109 ->113         0.18134
     110 ->113         0.62473
     111 ->114        -0.20010
     112 ->113        -0.15796

Excited State   4:    Singlet-A       3.4375 eV  360.68 nm  f=0.0000
     108 ->113        -0.15517
     111 ->113         0.23028
     112 ->114         0.64116

Excited State   5:    Singlet-A       3.4918 eV  355.07 nm  f=0.3592
     109 ->113         0.60806
     110 ->113        -0.19920
     112 ->115        -0.26589

Excited State   6:    Singlet-A       4.1122 eV  301.50 nm  f=0.0000
     108 ->113         0.67051
     112 ->114         0.16271

Excited State   7:    Singlet-A       4.5047 eV  275.23 nm  f=1.2210
     108 ->114        -0.12173
     109 ->113         0.24365
     111 ->114        -0.23652
     112 ->115         0.58349

Excited State   8:    Singlet-A       4.6821 eV  264.80 nm  f=0.0000
     102 ->113         0.10368
     104 ->113         0.22313
     108 ->115         0.13647
     109 ->114         0.40252
     110 ->114         0.42718
     111 ->113         0.17213
     111 ->115        -0.13236
```

```
Excited State   9:    Singlet-A       4.8707 eV  254.55 nm  f=1.1234
     108 ->114         0.14299
     109 ->113         0.14007
     110 ->113         0.18037
     111 ->114         0.57164
     112 ->115         0.24927
     112 ->116         0.13735

Excited State  10:    Singlet-A       5.0778 eV  244.17 nm  f=0.0000
      98 ->113        -0.11072
      99 ->113         0.11266
     101 ->114        -0.24026
     103 ->113         0.58055
     105 ->113        -0.21862
     106 ->114         0.10060

Excited State  11:      Singlet-A      5.1145 eV  242.41 nm  f=0.0000
     104 ->113        -0.15969
     108 ->115        -0.13764
     109 ->114        -0.39498
     110 ->114         0.48843
     111 ->113         0.13289
     112 ->117        -0.12199

Excited State  12:      Singlet-A      5.1684 eV  239.89 nm  f=0.0023
      94 ->113        -0.10131
     101 ->113         0.54800
     103 ->114        -0.27077
     105 ->114         0.11874
     106 ->113        -0.27552

Excited State  13:      Singlet-A      5.3061 eV  233.66 nm  f=0.2110
     100 ->113         0.11649
     107 ->113         0.12984
     108 ->114         0.52313
     110 ->115         0.11222
     111 ->114        -0.19117
     112 ->116         0.32946
     112 ->119         0.12326

Excited State  14:      Singlet-A      5.5381 eV  223.87 nm  f=0.0000
     102 ->113        -0.12463
     104 ->113        -0.38986
     109 ->114         0.30323
     111 ->115         0.44061

Excited State  15:    Singlet-A       5.5677 eV  222.68 nm  f=0.2132
      95 ->113        -0.10775
     107 ->113        -0.11687
     108 ->114        -0.10836
     110 ->115         0.61441
     111 ->117         0.14647
```

```
     111 ->121         0.11408

Excited State  16:    Singlet-A       5.6018 eV  221.33 nm  f=0.0000
      96 ->114         0.14135
      98 ->113         0.36645
      99 ->113         0.40224
     103 ->113         0.15904
     105 ->113         0.36064
     106 ->114        -0.12764

Excited State  17:    Singlet-A       5.6686 eV  218.72 nm  f=0.0000
     102 ->113         0.12282
     104 ->113         0.42047
     109 ->114        -0.17331
     111 ->115         0.47689
     112 ->121         0.10256

Excited State  18:    Singlet-A       5.7203 eV  216.74 nm  f=0.0358
     100 ->113        -0.17760
     107 ->113        -0.30041
     108 ->114        -0.19587
     109 ->115         0.21285
     110 ->115        -0.13913
     112 ->116         0.48571

Excited State  19:    Singlet-A       5.7537 eV  215.49 nm  f=0.0000
      94 ->114         0.13740
      98 ->113        -0.39035
      99 ->113         0.50325
     101 ->114         0.10917
     103 ->113        -0.16873
     105 ->113        -0.10840

Excited State  20:    Singlet-A       5.8628 eV  211.48 nm  f=0.0057
      96 ->113        -0.22602
     101 ->113         0.27048
     103 ->114        -0.14645
     105 ->114        -0.17564
     106 ->113         0.54692

Excited State  21:    Singlet-A       5.8786 eV  210.91 nm  f=0.1080
     102 ->114         0.13830
     107 ->113         0.51554
     108 ->114        -0.20385
     109 ->115         0.31146
     112 ->116         0.16392

Excited State  22:    Singlet-A       5.9229 eV  209.33 nm  f=0.0000
      97 ->113         0.10532
     102 ->113         0.31333
     104 ->113        -0.15437
     107 ->114         0.13215
```

```
     108 ->115         0.13127
     109 ->114        -0.12353
     112 ->117         0.52924

 Excited State  23:   Singlet-A       5.9979 eV  206.71 nm  f=0.0000
     102 ->113         0.53597
     104 ->113        -0.13902
     107 ->114         0.16881
     112 ->117        -0.35658

Excited State  24:    Singlet-A       6.0497 eV  204.94 nm  f=0.0000
      98 ->113        -0.39649
      99 ->113        -0.15200
     103 ->113         0.13323
     105 ->113         0.49086
     106 ->114        -0.15693
```

E5. Excited State Energies with Oscillator Strength of CP-PAH 5

```
Excited State   1:    Singlet-A       2.0751 eV  597.48 nm  f=0.0000
      77 -> 79         0.70113

Excited State   2:    Singlet-A       2.1858 eV  567.22 nm  f=0.8921
      78 -> 79         0.69755

Excited State   3:    Singlet-A       3.7250 eV  332.85 nm  f=0.0000
      76 -> 79        -0.44766
      78 -> 80         0.52088

Excited State   4:    Singlet-A       3.8139 eV  325.09 nm  f=0.1686
      75 -> 79         0.68721

Excited State   5:    Singlet-A       3.9074 eV  317.30 nm  f=0.0000
      73 -> 79        -0.10934
      76 -> 79         0.51088
      78 -> 80         0.45137

Excited State   6:    Singlet-A       4.2345 eV  292.80 nm  f=0.4180
      74 -> 79         0.63004
      77 -> 80        -0.24804

Excited State   7:    Singlet-A       4.3689 eV  283.79 nm  f=0.0000
      71 -> 83        -0.13766
      72 -> 79         0.67882

Excited State   8:    Singlet-A       4.3893 eV  282.47 nm  f=0.0000
      71 -> 79         0.67816
      72 -> 83        -0.13892
```

```
Excited State   9:    Singlet-A       4.5057 eV  275.17 nm  f=0.0000
      70 -> 79        -0.11701
      73 -> 79         0.67280
      76 -> 79         0.10495

Excited State  10:    Singlet-A       4.5214 eV  274.22 nm  f=1.3711
      74 -> 79         0.26868
      75 -> 81        -0.10473
      77 -> 80         0.62544

Excited State  11:    Singlet-A       5.0869 eV  243.73 nm  f=0.0000
      70 -> 79         0.43265
      75 -> 80        -0.13699
      78 -> 82         0.48398

Excited State  12:    Singlet-A       5.1938 eV  238.72 nm  f=0.0000
      70 -> 79         0.42088
      73 -> 79         0.10143
      74 -> 80         0.11223
      75 -> 80         0.16666
      75 -> 82         0.10607
      77 -> 81        -0.26170
      78 -> 82        -0.38090

Excited State  13:    Singlet-A       5.2044 eV  238.23 nm  f=0.0547
      69 -> 79        -0.10612
      76 -> 80        -0.19962
      77 -> 82        -0.18470
      77 -> 83         0.10976
      78 -> 81         0.59178

Excited State  14:    Singlet-A       5.4284 eV  228.40 nm  f=0.0000
      62 -> 79         0.12821
      66 -> 79         0.20793
      68 -> 79         0.65425

Excited State  15:    Singlet-A       5.5337 eV  224.05 nm  f=0.0000
      70 -> 79        -0.17287
      75 -> 80         0.14031
      76 -> 84        -0.12659
      77 -> 81        -0.24172
      78 -> 83         0.55860

Excited State  16:    Singlet-A       5.5713 eV  222.54 nm  f=0.0960
      69 -> 79        -0.10984
      75 -> 81         0.12234
      77 -> 82        -0.40531
      78 -> 81        -0.25830
      78 -> 84         0.41031

Excited State  17:    Singlet-A       5.6180 eV  220.69 nm  f=0.0000
      70 -> 79         0.23709
```

```
      74 -> 80        -0.15027
      75 -> 80        -0.14904
      75 -> 82        -0.10534
      77 -> 81         0.37008
      77 -> 84        -0.14438
      78 -> 82        -0.20558
      78 -> 83         0.35252
      78 -> 87        -0.13426

Excited State  18:    Singlet-A       5.7408 eV  215.97 nm  f=0.0000
      73 -> 86        -0.21948
      74 -> 85        -0.14661
      77 -> 86         0.12727
      78 -> 85         0.61980

Excited State  19:    Singlet-A       5.7611 eV  215.21 nm  f=0.6231
      69 -> 79         0.34763
      72 -> 85        -0.10085
      73 -> 80         0.12043
      77 -> 82         0.29109
      78 -> 81         0.10572
      78 -> 84         0.44999

Excited State  20:    Singlet-A       5.8285 eV  212.72 nm  f=0.0000
      69 -> 86        -0.10100
      73 -> 85        -0.23815
      74 -> 86        -0.14802
      77 -> 85         0.14762
      78 -> 86         0.59608

Excited State  21:    Singlet-A       5.9482 eV  208.44 nm  f=0.0995
      69 -> 79         0.15490
      76 -> 80         0.48311
      77 -> 82        -0.21178
      77 -> 83        -0.31384
      78 -> 81         0.21876

Excited State  22:    Singlet-A       6.0136 eV  206.17 nm  f=0.0000
      58 -> 79         0.11807
      67 -> 79         0.66794

Excited State  23:    Singlet-A       6.0243 eV  205.81 nm  f=0.0000
      61 -> 79         0.18201
      66 -> 79         0.61836
      68 -> 79        -0.20241

Excited State  24:    Singlet-A       6.0652 eV  204.42 nm  f=0.1442
      69 -> 79         0.51713
      76 -> 80        -0.13287
      77 -> 82        -0.27249
      77 -> 83         0.16752
      78 -> 84        -0.21548
```

E6. Excited State Energies with Oscillator Strength of CP-PAH 6

```
Excited State   1:    Singlet-A       2.8648 eV  432.78 nm  f=0.0170
      63 -> 66        -0.13170
      64 -> 67        -0.10204
      65 -> 66         0.68056

Excited State   2:    Singlet-A       3.2485 eV  381.67 nm  f=0.0035
      62 -> 66         0.36921
      63 -> 67         0.11137
      64 -> 66         0.50750
      65 -> 67        -0.28740

Excited State   3:    Singlet-A       3.5696 eV  347.33 nm  f=0.0154
      62 -> 66        -0.38971
      64 -> 66         0.46082
      65 -> 67         0.33585

Excited State   4:    Singlet-A       3.7551 eV  330.17 nm  f=0.4312
      62 -> 67         0.19707
      63 -> 66         0.65719
      65 -> 66         0.13413

Excited State   5:    Singlet-A       4.0084 eV  309.31 nm  f=0.2518
      62 -> 66         0.41024
      63 -> 67        -0.19498
      65 -> 67         0.50041
      65 -> 68        -0.14887

Excited State   6:    Singlet-A       4.5933 eV  269.92 nm  f=0.1383
      63 -> 67         0.63160
      64 -> 66        -0.10695
      65 -> 67         0.14445
      65 -> 68        -0.13446
      65 -> 70         0.12591

Excited State   7:    Singlet-A       4.6705 eV  265.46 nm  f=0.1056
      62 -> 67         0.14864
      62 -> 68         0.10529
      64 -> 67         0.66116

Excited State   8:    Singlet-A       5.0246 eV  246.75 nm  f=0.4632
      62 -> 67         0.64279
      63 -> 66        -0.19691
      64 -> 67        -0.13457

Excited State   9:    Singlet-A       5.1091 eV  242.67 nm  f=0.2105
      61 -> 66        -0.28146
      62 -> 66         0.14220
      64 -> 69        -0.11808
      65 -> 67         0.13528
      65 -> 68         0.57226
```

```
      65 -> 70        -0.14785

Excited State  10:    Singlet-A       5.7262 eV  216.52 nm  f=0.0000
      58 -> 66         0.68601

Excited State  11:    Singlet-A       5.7664 eV  215.01 nm  f=0.0226
      61 -> 66         0.40850
      63 -> 68         0.49569
      64 -> 69         0.11910
      65 -> 68         0.18310

Excited State  12:    Singlet-A       5.8224 eV  212.94 nm  f=0.0000
      57 -> 66         0.68207

Excited State  13:    Singlet-A       5.8452 eV  212.11 nm  f=0.0732
      59 -> 66         0.38898
      61 -> 66         0.32305
      62 -> 69         0.20271
      63 -> 67         0.14451
      63 -> 68        -0.33906
      65 -> 68         0.12300
      65 -> 70        -0.14211

Excited State  14:    Singlet-A       5.9191 eV  209.46 nm  f=0.2830
      64 -> 68         0.64804
      65 -> 69        -0.15173

Excited State  15:    Singlet-A       6.0288 eV  205.65 nm  f=0.0011
      59 -> 66         0.34382
      60 -> 67         0.17235
      61 -> 66        -0.32232
      62 -> 69         0.14780
      63 -> 68         0.26203
      63 -> 70        -0.20283
      65 -> 68        -0.22248
      65 -> 70        -0.22362

Excited State  16:    Singlet-A       6.0315 eV  205.56 nm  f=0.5807
      60 -> 66         0.25440
      62 -> 68         0.58613
      63 -> 69         0.18203
      64 -> 67        -0.12744
      64 -> 70         0.10896

Excited State  17:    Singlet-A       6.0653 eV  204.41 nm  f=0.0211
      60 -> 66         0.56678
      62 -> 68        -0.23125
      64 -> 70        -0.12571
      65 -> 69         0.24896
      65 -> 74        -0.10538
```

```
Excited State  18:    Singlet-A       6.2625 eV  197.98 nm  f=0.0858
      60 -> 66        -0.25867
      64 -> 68         0.11198
      65 -> 69         0.61024

Excited State  19:    Singlet-A       6.3341 eV  195.74 nm  f=0.1163
      59 -> 66         0.27278
      61 -> 66        -0.12014
      64 -> 69         0.14565
      65 -> 68         0.12875
      65 -> 70         0.58768

Excited State  20:    Singlet-A       6.4611 eV  191.89 nm  f=0.1079
      59 -> 66        -0.31553
      60 -> 67         0.20968
      62 -> 69         0.29029
      63 -> 70        -0.23776
      64 -> 69         0.42371

Excited State  21:    Singlet-A       6.5875 eV  188.21 nm  f=0.3795
      62 -> 68        -0.23952
      62 -> 70         0.13858
      63 -> 69         0.58354
      64 -> 70         0.17132

Excited State  22:    Singlet-A       6.6299 eV  187.01 nm  f=0.0000
      50 -> 66        -0.11518
      56 -> 66         0.53653
      58 -> 67        -0.39326
      58 -> 68         0.10856

Excited State  23:    Singlet-A       6.6509 eV  186.42 nm  f=0.0003
      55 -> 66         0.30883
      57 -> 67         0.60015

Excited State  24:    Singlet-A       6.7485 eV  183.72 nm  f=0.7738
      59 -> 66         0.14603
      62 -> 69        -0.33615
      63 -> 70         0.24317
      64 -> 69         0.48130
      65 -> 70        -0.16776
```

E7. Excited State Energies with Oscillator Strength of CP-PAH 7

```
Excited State   1:    Singlet-A       3.9279 eV  315.65 nm  f=0.0000
      64 -> 66        -0.25013
      64 -> 67        -0.42409
      65 -> 66         0.43259
      65 -> 67        -0.24780
```

```
Excited State   2:    Singlet-A       3.9462 eV  314.18 nm  f=0.0000
      62 -> 67        -0.23972
      63 -> 66        -0.24497
      64 -> 67         0.41651
      65 -> 66         0.40589
      65 -> 67         0.10098

Excited State   3:    Singlet-A       3.9465 eV  314.16 nm  f=0.0000
      62 -> 66        -0.25028
      63 -> 67         0.24507
      64 -> 66        -0.40674
      65 -> 67         0.40955

Excited State   4:    Singlet-A       4.1916 eV  295.79 nm  f=0.0000
      62 -> 66        -0.42252
      63 -> 67         0.42504
      64 -> 66         0.25497
      65 -> 67        -0.24962

Excited State   5:   Singlet-A        4.1919 eV  295.77 nm  f=0.0000
      62 -> 67         0.42821
      63 -> 66         0.42570
      64 -> 67         0.24513
      65 -> 66         0.24899

Excited State   6:    Singlet-A       4.6086 eV  269.03 nm  f=0.0219
      64 -> 66         0.42800
      64 -> 67        -0.24898
      65 -> 66         0.24871
      65 -> 67         0.42825

Excited State   7:    Singlet-A       4.8310 eV  256.64 nm  f=0.6692
      62 -> 66         0.35880
      62 -> 67        -0.31274
      63 -> 66         0.31249
      63 -> 67         0.35914
      64 -> 68        -0.18174

Excited State   8:    Singlet-A       4.8311 eV  256.64 nm  f=0.6687
      62 -> 66         0.31251
      62 -> 67         0.35898
      63 -> 66        -0.35890
      63 -> 67         0.31268
      65 -> 68         0.18189

Excited State   9:    Singlet-A       5.6409 eV  219.80 nm  f=0.5520
      59 -> 66        -0.15635
      60 -> 67        -0.11382
      61 -> 66        -0.11395
      64 -> 68         0.60528
```

```
Excited State  10:    Singlet-A       5.6409 eV  219.79 nm  f=0.5521
      59 -> 67        -0.15626
      60 -> 66        -0.11382
      61 -> 67         0.11388
      65 -> 68         0.60534

Excited State  11:    Singlet-A       5.9842 eV  207.19 nm  f=0.0000
      62 -> 68        -0.26508
      62 -> 69         0.16183
      63 -> 68         0.58848
      64 -> 70        -0.12249
      65 -> 71         0.12249

Excited State  12:    Singlet-A       5.9843 eV  207.18 nm  f=0.0000
      62 -> 68         0.58843
      63 -> 68         0.26504
      63 -> 69        -0.16179
      64 -> 71        -0.12252
      65 -> 70        -0.12258

Excited State  13:    Singlet-A       6.2659 eV  197.87 nm  f=0.0160
      60 -> 66         0.32613
      60 -> 67        -0.12420
      61 -> 66        -0.12447
      61 -> 67        -0.32607
      62 -> 70        -0.27983
      63 -> 71         0.27857
      64 -> 69         0.17130
      65 -> 68         0.20525

Excited State  14:    Singlet-A       6.2660 eV  197.87 nm  f=0.0160
      60 -> 66         0.12434
      60 -> 67         0.32577
      61 -> 66         0.32630
      61 -> 67        -0.12425
      62 -> 71        -0.27764
      63 -> 70        -0.27880
      64 -> 68         0.20536
      65 -> 69        -0.17112

Excited State  15:    Singlet-A       6.4842 eV  191.21 nm  f=0.0876
      59 -> 66         0.28902
      62 -> 71        -0.15247
      63 -> 70        -0.15547
      64 -> 68         0.16604
      64 -> 70         0.16201
      64 -> 71         0.14826
      65 -> 69         0.43450
      65 -> 70        -0.15191
      65 -> 71         0.16477
```

```
Excited State  16:    Singlet-A       6.4845 eV  191.20 nm  f=0.0873
      59 -> 67        -0.28906
      62 -> 70         0.15848
      63 -> 71        -0.15567
      64 -> 69         0.43390
      64 -> 70         0.14343
      64 -> 71        -0.15753
      65 -> 68        -0.16596
      65 -> 70         0.16723
      65 -> 71         0.15379

Excited State  17:    Singlet-A       6.5030 eV  190.66 nm  f=0.0000
      62 -> 69         0.12296
      63 -> 69         0.13985
      64 -> 70         0.36854
      64 -> 71        -0.27558
      65 -> 70        -0.27093
      65 -> 71        -0.36406

Excited State  18:    Singlet-A       6.5031 eV  190.66 nm  f=0.0000
      62 -> 69         0.14002
      63 -> 69        -0.12305
      64 -> 70         0.27405
      64 -> 71         0.36749
      65 -> 70         0.36503
      65 -> 71        -0.27237

Excited State  19:    Singlet-A       6.5251 eV  190.01 nm  f=0.0321
      59 -> 68         0.13214
      62 -> 70         0.44505
      62 -> 71         0.12179
      63 -> 70        -0.12126
      63 -> 71         0.44529

Excited State  20:    Singlet-A       6.5844 eV  188.30 nm  f=0.0000
      57 -> 67        -0.27673
      58 -> 66        -0.27786
      60 -> 66         0.32431
      60 -> 67        -0.15363
      61 -> 66         0.15377
      61 -> 67         0.32427
      62 -> 69        -0.11963
      63 -> 69        -0.13699

Excited State  21:    Singlet-A       6.5845 eV  188.30 nm  f=0.0000
      57 -> 66         0.27730
      58 -> 67        -0.27759
      60 -> 66         0.15348
      60 -> 67         0.32428
      61 -> 66        -0.32415
      61 -> 67         0.15368
      62 -> 69        -0.13661
```

```
      63 -> 69         0.11938

Excited State  22:    Singlet-A       6.6223 eV  187.22 nm  f=0.0000
      62 -> 70         0.12971
      62 -> 71        -0.47460
      63 -> 70         0.47488
      63 -> 71         0.12949

Excited State  23:    Singlet-A       6.7434 eV  183.86 nm  f=0.2167
      57 -> 66        -0.16182
      57 -> 67         0.16976
      58 -> 66        -0.16949
      58 -> 67        -0.16257
      60 -> 67         0.17891
      61 -> 66         0.17823
      62 -> 71         0.13941
      63 -> 70         0.14109
      64 -> 70        -0.14776
      64 -> 71        -0.12243
      65 -> 69         0.41473
      65 -> 70         0.12084
      65 -> 71        -0.14863

Excited State  24:    Singlet-A       6.7435 eV  183.86 nm  f=0.2168
      57 -> 66        -0.16953
      57 -> 67        -0.16212
      58 -> 66         0.16254
      58 -> 67        -0.16980
      60 -> 66        -0.17826
      61 -> 67         0.17862
      62 -> 70        -0.14391
      63 -> 71         0.14179
      64 -> 69         0.41511
      64 -> 70        -0.11855
      64 -> 71         0.14663
      65 -> 70        -0.14645
      65 -> 71        -0.12126
```

E8. Excited State Energies with Oscillator Strength of CP-PAH 8

```
Excited State   1:    Singlet-A       3.1464 eV  394.06 nm  f=0.1528
      69 -> 73        -0.32831
      70 -> 74         0.18971
      71 -> 73         0.13634
      72 -> 73         0.57235

Excited State   2:    Singlet-A       3.4348 eV  360.97 nm  f=0.0000
      69 -> 74        -0.24402
```

```
      70 -> 73         0.63095
      72 -> 74         0.17885

Excited State   3:    Singlet-A       3.5601 eV  348.26 nm  f=0.5063
      69 -> 73         0.49303
      71 -> 73        -0.25715
      71 -> 75        -0.10912
      72 -> 73         0.37399
      72 -> 75        -0.12675

Excited State   4:    Singlet-A       3.7891 eV  327.21 nm  f=0.1711
      69 -> 73         0.28862
      69 -> 75         0.14058
      70 -> 74        -0.13862
      71 -> 73         0.59502

Excited State   5:    Singlet-A       4.3340 eV  286.08 nm  f=0.0000
      67 -> 73         0.17403
      70 -> 73        -0.19377
      71 -> 74         0.31708
      72 -> 74         0.55307

Excited State   6:    Singlet-A       4.5679 eV  271.42 nm  f=0.0000
      67 -> 73         0.11281
      68 -> 73        -0.30858
      69 -> 74        -0.18057
      69 -> 76        -0.10907
      70 -> 75        -0.24001
      71 -> 74         0.37122
      71 -> 76        -0.14428
      72 -> 74        -0.33759

Excited State   7:    Singlet-A       4.8514 eV  255.56 nm  f=0.5858
      71 -> 73        -0.12859
      72 -> 75         0.66042

Excited State   8:    Singlet-A       5.0900 eV  243.58 nm  f=0.0000
      67 -> 73         0.14619
      68 -> 73         0.55446
      69 -> 74        -0.26273
      70 -> 75        -0.15430
      71 -> 74         0.10368
      72 -> 74        -0.12239
      72 -> 76         0.16354

Excited State   9:    Singlet-A      5.1654 eV  240.03 nm  f=0.3391
      69 -> 73         0.19573
      70 -> 74         0.43669
      71 -> 75         0.49144

Excited State  10:    Singlet-A       5.1733 eV  239.66 nm  f=0.4179
      68 -> 74        -0.11797
```

```
      69 -> 75         0.43222
      70 -> 74        -0.30599
      70 -> 76         0.20719
      71 -> 73        -0.15772
      71 -> 75         0.31499

Excited State  11:    Singlet-A       5.2771 eV  234.95 nm  f=0.0000
      68 -> 73         0.12902
      69 -> 74         0.55083
      69 -> 76        -0.10908
      70 -> 73         0.22816
      70 -> 75        -0.23684
      71 -> 74         0.17400

Excited State  12:    Singlet-A       5.3340 eV  232.44 nm  f=0.0000
      68 -> 73         0.12374
      69 -> 76         0.10207
      70 -> 75         0.48003
      71 -> 74         0.43544
      72 -> 76        -0.10592

Excited State  13:    Singlet-A       5.4120 eV  229.09 nm  f=0.5378
      68 -> 74        -0.13597
      69 -> 73         0.10284
      69 -> 75         0.41179
      70 -> 74         0.36495
      71 -> 75        -0.33410
      72 -> 75         0.10390

Excited State  14:    Singlet-A       5.7048 eV  217.33 nm  f=0.0000
      67 -> 73         0.62708
      70 -> 75         0.21184
      71 -> 74        -0.12840

Excited State  15:    Singlet-A       5.9031 eV  210.03 nm  f=0.0000
      60 -> 74         0.10957
      63 -> 74         0.19032
      66 -> 73         0.66021

 Excited State  16:   Singlet-A       6.0330 eV  205.51 nm  f=0.0000
      68 -> 73        -0.17951
      68 -> 75        -0.32718
      70 -> 75         0.10284
      72 -> 76         0.56368

Excited State  17:    Singlet-A       6.2086 eV  199.70 nm  f=0.0001
      60 -> 73         0.11452
      63 -> 73         0.59493
      64 -> 74         0.12870
      66 -> 74         0.30992
```

```
Excited State  18:    Singlet-A       6.2703 eV  197.73 nm  f=0.0000
      60 -> 74        -0.12789
      63 -> 74         0.13723
      64 -> 73         0.66131

Excited State  19:    Singlet-A       6.2935 eV  197.00 nm  f=0.4341
      65 -> 73        -0.12139
      68 -> 74         0.59778
      69 -> 75         0.25342

Excited State  20:    Singlet-A       6.4681 eV  191.69 nm  f=0.0000
      67 -> 75        -0.15710
      68 -> 75         0.22814
      69 -> 76        -0.38643
      70 -> 77         0.20647
      71 -> 76         0.40659

Excited State  21:    Singlet-A       6.6400 eV  186.72 nm  f=0.0373
      61 -> 73        -0.17746
      67 -> 74         0.55785
      68 -> 74         0.15495
      71 -> 77        -0.17128
      72 -> 77        -0.17681
      72 -> 78         0.13374

Excited State  22:    Singlet-A       6.6618 eV  186.11 nm  f=0.0000
      68 -> 75         0.48927
      70 -> 75         0.12904
      71 -> 76        -0.31891
      72 -> 76         0.31281

Excited State  23:    Singlet-A       6.6839 eV  185.50 nm  f=0.6440
      68 -> 74         0.20772
      69 -> 75        -0.17801
      69 -> 77        -0.11397
      69 -> 78        -0.15149
      70 -> 76         0.45359
      72 -> 77         0.38325

Excited State  24:    Singlet-A       6.6905 eV  185.31 nm  f=0.0003
      60 -> 73         0.52991
      63 -> 73        -0.16654
      64 -> 74        -0.29889
      66 -> 74         0.25867
```

APPENDIX F

OPTIMIZED GEOMETRIES OF THE 7 MTPA DERIVATIVES (NEUTRAL AND ANION) USING B3LYP/6-31+G (D,P)

F1. MTPAa *Neutral* Optimized Geometry

Center Number	Atomic Number	Atomic Type	Coordinates (Angstroms) X	Y	Z
1	6	0	-3.181279	-0.513052	-0.312600
2	6	0	-4.133198	0.276433	0.238750
3	1	0	-3.490730	-1.371288	-0.907230
4	1	0	-3.820031	1.139158	0.825205
5	6	0	-5.585342	0.117098	0.141706
6	6	0	-6.424469	1.060532	0.769928
7	6	0	-6.221591	-0.937247	-0.549667
8	6	0	-7.812706	0.969114	0.715360
9	1	0	-5.974715	1.886336	1.316159
10	6	0	-7.606005	-1.038901	-0.611525
11	1	0	-5.627719	-1.697397	-1.048238
12	6	0	-8.432234	-0.086054	0.020831
13	1	0	-8.423748	1.718615	1.211884
14	1	0	-8.061072	-1.863724	-1.154258
15	6	0	-1.729706	-0.348261	-0.207573
16	6	0	-0.883889	-1.252824	-0.882154
17	6	0	-1.101383	0.672701	0.539471
18	6	0	0.503690	-1.146317	-0.830533
19	1	0	-1.326879	-2.050459	-1.473653
20	6	0	0.282320	0.779016	0.608076
21	1	0	-1.699799	1.389812	1.092983
22	6	0	1.114543	-0.126790	-0.080217
23	1	0	1.118076	-1.856071	-1.374539
24	1	0	0.729533	1.569121	1.202461
25	7	0	2.524468	-0.011596	-0.011072
26	6	0	3.338821	-1.178836	0.043531
27	6	0	4.497713	-1.282492	-0.741248
28	6	0	3.007472	-2.247079	0.893303
29	6	0	5.301336	-2.421997	-0.670301
30	1	0	4.772653	-0.467219	-1.402918
31	6	0	3.809943	-3.386994	0.942269
32	1	0	2.121773	-2.181221	1.517314
33	6	0	4.973240	-3.501002	0.164100
34	1	0	6.195818	-2.473972	-1.286439
35	1	0	3.532455	-4.197555	1.612087
36	6	0	3.139831	1.272936	-0.030740
37	6	0	4.196938	1.572857	0.845078
38	6	0	2.711892	2.263223	-0.927610
39	6	0	4.807382	2.826032	0.813739
40	1	0	4.540943	0.819786	1.547066

41	6	0	3.320546	3.520428	-0.936886
42	1	0	1.902875	2.048892	-1.618755
43	6	0	4.380453	3.829239	-0.072247
44	1	0	5.625314	3.030990	1.500557
45	1	0	2.970769	4.269217	-1.643448
46	7	0	-9.819737	-0.157163	-0.093121
47	1	0	-10.201028	-1.072334	-0.295320
48	1	0	-10.347945	0.326014	0.621953
49	6	0	5.033274	5.192348	-0.077880
50	1	0	4.774951	5.760652	0.824326
51	1	0	6.125537	5.112545	-0.105572
52	1	0	4.714729	5.781537	-0.942570
53	6	0	5.823302	-4.749923	0.206391
54	1	0	5.439471	-5.514088	-0.481666
55	1	0	6.856919	-4.539032	-0.083887
56	1	0	5.833372	-5.192139	1.207756

F2. MTPAa *Anion* Optimized Geometry

Center Number	Atomic Number	Atomic Type	Coordinates (Angstroms) X	Y	Z
1	6	0	3.132293	-0.334723	0.461505
2	6	0	4.107946	0.220649	-0.374660
3	1	0	3.466863	-0.911006	1.324602
4	1	0	3.781223	0.809460	-1.231564
5	6	0	5.534826	0.105186	-0.229745
6	6	0	6.411803	0.742488	-1.157012
7	6	0	6.183932	-0.629920	0.809554
8	6	0	7.796351	0.661662	-1.060780
9	1	0	5.977206	1.315300	-1.974621
10	6	0	7.573446	-0.710936	0.903354
11	1	0	5.588051	-1.150742	1.553484
12	6	0	8.411330	-0.072606	-0.025553
13	1	0	8.416005	1.172595	-1.795969
14	1	0	8.018105	-1.283915	1.715957
15	6	0	1.715137	-0.235054	0.324248
16	6	0	0.842832	-0.850688	1.282511
17	6	0	1.052194	0.465152	-0.744761
18	6	0	-0.537424	-0.771665	1.196212
19	1	0	1.288672	-1.390661	2.116655
20	6	0	-0.333024	0.524913	-0.834109
21	1	0	1.643133	0.952056	-1.515326
22	6	0	-1.161101	-0.081555	0.129232
23	1	0	-1.154662	-1.249363	1.953862
24	1	0	-0.792787	1.057768	-1.664239
25	7	0	-2.590815	-0.003396	0.035369
26	6	0	-3.340862	-1.199059	-0.057386

27	6	0	-4.600424	-1.334660	0.558677
28	6	0	-2.823554	-2.315489	-0.742671
29	6	0	-5.312204	-2.531923	0.473402
30	1	0	-5.023246	-0.498573	1.105969
31	6	0	-3.542688	-3.509011	-0.810209
32	1	0	-1.852696	-2.240171	-1.220967
33	6	0	-4.802554	-3.648722	-0.207028
34	1	0	-6.282660	-2.599538	0.960583
35	1	0	-3.114159	-4.348494	-1.353759
36	6	0	-3.213966	1.266410	0.050099
37	6	0	-4.360721	1.537349	-0.721824
38	6	0	-2.675333	2.319474	0.814844
39	6	0	-4.947344	2.803780	-0.709438
40	1	0	-4.794527	0.752627	-1.332994
41	6	0	-3.267123	3.582638	0.808633
42	1	0	-1.787863	2.140255	1.412675
43	6	0	-4.416288	3.857518	0.049903
44	1	0	-5.833087	2.976046	-1.317288
45	1	0	-2.826946	4.370091	1.416863
46	7	0	9.825685	-0.096658	0.113877
47	1	0	10.161467	-0.921239	0.600347
48	1	0	10.312619	-0.014325	-0.772492
49	6	0	-5.031913	5.238157	0.025958
50	1	0	-4.540781	5.884459	-0.713495
51	1	0	-6.094446	5.196718	-0.233716
52	1	0	-4.939884	5.733889	0.998232
53	6	0	-5.559898	-4.956178	-0.258258
54	1	0	-5.256705	-5.628249	0.555485
55	1	0	-6.638651	-4.796852	-0.162310
56	1	0	-5.378366	-5.486892	-1.198867

F3. MTPAo *Neutral* Optimized Geometry

Center Number	Atomic Number	Atomic Type	Coordinates (Angstroms) X	Y	Z
1	6	0	-2.778741	-0.571898	-0.355168
2	6	0	-3.744274	0.201573	0.193171
3	1	0	-3.072482	-1.432148	-0.954647
4	1	0	-3.449419	1.063809	0.789173
5	6	0	-5.194226	0.020391	0.080094
6	6	0	-6.049599	0.938722	0.714481
7	6	0	-5.804508	-1.034287	-0.638403
8	6	0	-7.442262	0.832172	0.648542
9	1	0	-5.617591	1.762824	1.276757
10	6	0	-7.184366	-1.154715	-0.714099
11	1	0	-5.193487	-1.773515	-1.146817
12	6	0	-8.018253	-0.221430	-0.071313
13	1	0	-8.054720	1.567873	1.155882

14	1	0	-7.640853	-1.968786	-1.268808
15	6	0	-1.330142	-0.388945	-0.239612
16	6	0	-0.468864	-1.292706	-0.894859
17	6	0	-0.720801	0.649478	0.498553
18	6	0	0.916767	-1.170456	-0.831778
19	1	0	-0.897653	-2.102937	-1.479611
20	6	0	0.660656	0.772604	0.577993
21	1	0	-1.332244	1.368185	1.035486
22	6	0	1.509443	-0.133722	-0.089908
23	1	0	1.543708	-1.880624	-1.360567
24	1	0	1.093260	1.576402	1.164607
25	7	0	2.916119	-0.001715	-0.009820
26	6	0	3.744887	-1.158916	0.054233
27	6	0	4.906734	-1.252667	-0.727034
28	6	0	3.425254	-2.224773	0.911238
29	6	0	5.725508	-2.380660	-0.645268
30	1	0	5.172382	-0.438499	-1.393862
31	6	0	4.242718	-3.353426	0.970901
32	1	0	2.537337	-2.165677	1.532797
33	6	0	5.409480	-3.457521	0.196471
34	1	0	6.622334	-2.425312	-1.258515
35	1	0	3.974456	-4.162520	1.646197
36	6	0	3.517760	1.289833	-0.026259
37	6	0	4.560275	1.603673	0.861845
38	6	0	3.091642	2.271529	-0.933129
39	6	0	5.158774	2.862638	0.832768
40	1	0	4.902413	0.856848	1.571370
41	6	0	3.687958	3.534670	-0.940216
42	1	0	2.294169	2.045956	-1.634058
43	6	0	4.733464	3.857563	-0.063317
44	1	0	5.965661	3.078788	1.529127
45	1	0	3.340152	4.276880	-1.654611
46	6	0	-10.259445	0.489710	0.422838
47	1	0	-10.126125	1.504264	0.030713
48	1	0	-11.262104	0.135349	0.183711
49	1	0	-10.121925	0.493683	1.509977
50	8	0	-9.362361	-0.427912	-0.206925
51	6	0	5.374194	5.226397	-0.067763
52	1	0	5.112173	5.790966	0.835642
53	1	0	6.467115	5.156062	-0.096957
54	1	0	5.049562	5.813826	-0.931336
55	6	0	6.276316	-4.694362	0.251063
56	1	0	5.900489	-5.471721	-0.426504
57	1	0	7.306090	-4.473160	-0.045004
58	1	0	6.295269	-5.124343	1.257619

F4. MTPAo *Anion* Optimized Geometry

Center Number	Atomic Number	Atomic Type	Coordinates (Angstroms) X	Y	Z
1	6	0	2.729752	-0.381043	0.532316
2	6	0	3.719110	0.175628	-0.286936
3	1	0	3.048760	-0.972403	1.390930
4	1	0	3.405905	0.778258	-1.139128
5	6	0	5.142098	0.045158	-0.131091
6	6	0	6.034675	0.684033	-1.039271
7	6	0	5.771325	-0.710899	0.909885
8	6	0	7.422675	0.589814	-0.935000
9	1	0	5.616020	1.273523	-1.852930
10	6	0	7.153968	-0.807729	1.018500
11	1	0	5.160870	-1.230792	1.642217
12	6	0	7.999461	-0.162345	0.102239
13	1	0	8.040167	1.104050	-1.663735
14	1	0	7.600624	-1.390490	1.820613
15	6	0	1.315118	-0.265363	0.380082
16	6	0	0.426144	-0.885939	1.319174
17	6	0	0.672203	0.455595	-0.686496
18	6	0	-0.952288	-0.793960	1.216418
19	1	0	0.856756	-1.441034	2.151295
20	6	0	-0.711138	0.527960	-0.793136
21	1	0	1.276824	0.948320	-1.442538
22	6	0	-1.556268	-0.084905	0.151111
23	1	0	-1.583170	-1.276500	1.959518
24	1	0	-1.155542	1.075770	-1.621768
25	7	0	-2.983807	0.004026	0.038702
26	6	0	-3.741364	-1.185564	-0.072254
27	6	0	-5.011098	-1.313775	0.524968
28	6	0	-3.223779	-2.301850	-0.756528
29	6	0	-5.731840	-2.503722	0.422042
30	1	0	-5.434376	-0.477004	1.070901
31	6	0	-3.952326	-3.489065	-0.841430
32	1	0	-2.245639	-2.232434	-1.220649
33	6	0	-5.221603	-3.621218	-0.257709
34	1	0	-6.709899	-2.565724	0.894607
35	1	0	-3.523213	-4.329185	-1.383417
36	6	0	-3.597821	1.278452	0.043749
37	6	0	-4.729361	1.557934	-0.747319
38	6	0	-3.065373	2.326634	0.819205
39	6	0	-5.307743	2.828097	-0.743048
40	1	0	-5.157977	0.776780	-1.366647
41	6	0	-3.648497	3.593841	0.804560
42	1	0	-2.189673	2.140729	1.432196
43	6	0	-4.782532	3.877319	0.026685
44	1	0	-6.181975	3.007047	-1.365456
45	1	0	-3.213627	4.377573	1.421317
46	6	0	10.245181	0.310525	-0.615212

47	1	0	10.122793	1.401277	-0.602155
48	1	0	11.254967	0.057558	-0.288025
49	1	0	10.093556	-0.055382	-1.638954
50	8	0	9.362132	-0.324240	0.300971
51	6	0	-5.388415	5.262057	-0.006681
52	1	0	-4.895346	5.898450	-0.753414
53	1	0	-6.452129	5.226277	-0.262517
54	1	0	-5.289337	5.765011	0.961078
55	6	0	-5.990326	-4.921251	-0.325819
56	1	0	-5.775903	-5.560273	0.541053
57	1	0	-7.071219	-4.747099	-0.339176
58	1	0	-5.728258	-5.493087	-1.221929

F5. MTPA *Neutral* Optimized Geometry

Center Number	Atomic Number	Atomic Type	Coordinates (Angstroms) X	Y	Z
1	6	0	-3.582217	-0.531164	-0.305188
2	6	0	-4.537378	0.260220	0.234758
3	1	0	-3.887731	-1.401280	-0.884018
4	1	0	-4.233886	1.132797	0.810577
5	6	0	-5.990764	0.081541	0.134615
6	6	0	-6.832316	1.024688	0.760625
7	6	0	-6.603765	-0.986316	-0.556568
8	6	0	-8.222726	0.911526	0.701188
9	1	0	-6.384651	1.856179	1.299366
10	6	0	-7.991657	-1.099453	-0.616108
11	1	0	-5.994559	-1.735937	-1.051840
12	6	0	-8.811637	-0.152274	0.011565
13	1	0	-8.844541	1.654084	1.193294
14	1	0	-8.437684	-1.931130	-1.154415
15	6	0	-2.131843	-0.358742	-0.205876
16	6	0	-1.284905	-1.284661	-0.848483
17	6	0	-1.507595	0.689512	0.505161
18	6	0	0.101870	-1.175311	-0.798016
19	1	0	-1.726075	-2.102755	-1.412621
20	6	0	-0.124934	0.801298	0.571344
21	1	0	-2.108236	1.425046	1.031294
22	6	0	0.710626	-0.128240	-0.082881
23	1	0	0.717446	-1.902733	-1.316264
24	1	0	0.319279	1.613012	1.137722
25	7	0	2.117081	-0.009179	-0.015622
26	6	0	2.938378	-1.173250	0.038280
27	6	0	4.085180	-1.277403	-0.763246
28	6	0	2.627421	-2.232044	0.906601
29	6	0	4.897798	-2.410429	-0.691275
30	1	0	4.343821	-0.467573	-1.438111
31	6	0	3.438475	-3.365871	0.956840

32	1	0	1.751661	-2.163684	1.544265
33	6	0	4.589881	-3.481124	0.161425
34	1	0	5.783234	-2.463878	-1.320125
35	1	0	3.177719	-4.169904	1.640982
36	6	0	2.732211	1.276945	-0.029697
37	6	0	3.774786	1.579078	0.861223
38	6	0	2.320902	2.261475	-0.940619
39	6	0	4.387753	2.831635	0.832795
40	1	0	4.106748	0.828664	1.571820
41	6	0	2.931145	3.517417	-0.947203
42	1	0	1.525036	2.042564	-1.645515
43	6	0	3.976232	3.829932	-0.065246
44	1	0	5.195496	3.039097	1.530682
45	1	0	2.596016	4.262051	-1.665159
46	6	0	4.623536	5.195559	-0.063378
47	1	0	4.249797	5.810081	0.765408
48	1	0	5.709885	5.123136	0.053275
49	1	0	4.416290	5.735316	-0.992043
50	6	0	5.449374	-4.723459	0.205384
51	1	0	5.068363	-5.492683	-0.478543
52	1	0	6.480270	-4.506199	-0.089801
53	1	0	5.466249	-5.161682	1.208310
54	1	0	-9.892512	-0.244841	-0.037316

F6. MTPA Anion Optimized Geometry

Center Number	Atomic Number	Atomic Type	Coordinates (Angstroms) X	Y	Z
1	6	0	-3.531018	-0.373677	-0.468325
2	6	0	-4.510914	0.188918	0.357449
3	1	0	-3.858446	-0.967134	-1.321813
4	1	0	-4.185885	0.790633	1.206027
5	6	0	-5.931484	0.067399	0.214951
6	6	0	-6.808749	0.716076	1.141702
7	6	0	-6.574346	-0.683621	-0.824110
8	6	0	-8.191400	0.626834	1.042704
9	1	0	-6.368773	1.298583	1.949757
10	6	0	-7.961145	-0.766608	-0.914764
11	1	0	-5.970171	-1.203905	-1.561840
12	6	0	-8.797390	-0.118020	0.010074
13	1	0	-8.811471	1.140583	1.774823
14	1	0	-8.402320	-1.348988	-1.721855
15	6	0	-2.113176	-0.260394	-0.328174
16	6	0	-1.237521	-0.888996	-1.271936
17	6	0	-1.460088	0.463897	0.726330
18	6	0	0.142698	-0.799411	-1.183734
19	1	0	-1.678088	-1.447943	-2.095912
20	6	0	-0.075519	0.534804	0.819092

21	1	0	-2.056375	0.962339	1.485058
22	6	0	0.757633	-0.085798	-0.130280
23	1	0	0.764914	-1.287496	-1.930251
24	1	0	0.378468	1.086441	1.639621
25	7	0	2.185957	0.001495	-0.033293
26	6	0	2.943602	-1.190488	0.057956
27	6	0	4.195941	-1.321403	-0.571778
28	6	0	2.441763	-2.303894	0.759053
29	6	0	4.917181	-2.513281	-0.485344
30	1	0	4.605990	-0.486462	-1.130458
31	6	0	3.169252	-3.492027	0.827069
32	1	0	1.476781	-2.231012	1.249613
33	6	0	4.422999	-3.627565	0.209758
34	1	0	5.882168	-2.578507	-0.983386
35	1	0	2.753203	-4.329998	1.382436
36	6	0	2.803092	1.274606	-0.046901
37	6	0	3.948484	1.548017	0.725823
38	6	0	2.262833	2.324934	-0.813384
39	6	0	4.532109	2.815514	0.713248
40	1	0	4.383583	0.764206	1.337233
41	6	0	2.851326	3.589958	-0.806682
42	1	0	1.377510	2.143389	-1.413718
43	6	0	3.998648	3.867726	-0.046982
44	1	0	5.417189	2.990124	1.321316
45	1	0	2.410018	4.375994	-1.415805
46	6	0	4.611350	5.249611	-0.021933
47	1	0	4.145286	5.881474	0.745641
48	1	0	5.682561	5.207477	0.199366
49	1	0	4.483387	5.760829	-0.981831
50	6	0	5.189992	-4.929187	0.265186
51	1	0	4.836602	-5.635946	-0.497113
52	1	0	6.258686	-4.769786	0.090986
53	1	0	5.074873	-5.420611	1.237276
54	1	0	-9.878309	-0.188298	-0.068525

F7. MTPAcl *Neutral* Optimized Geometry

Center Number	Atomic Number	Atomic Type	Coordinates (Angstroms) X	Y	Z
1	6	0	-2.804815	-0.482466	-0.286984
2	6	0	-3.750324	0.326777	0.243981
3	1	0	-3.120705	-1.357272	-0.853048
4	1	0	-3.437844	1.204146	0.806961
5	6	0	-5.203948	0.159949	0.147923
6	6	0	-6.038345	1.116908	0.760896
7	6	0	-5.829032	-0.910368	-0.527406
8	6	0	-7.429346	1.022431	0.708917
9	1	0	-5.589250	1.953474	1.289255

10	6	0	-7.215920	-1.019476	-0.588977
11	1	0	-5.232313	-1.674425	-1.014605
12	6	0	-8.007764	-0.049502	0.031283
13	1	0	-8.050520	1.771359	1.188096
14	1	0	-7.677435	-1.849617	-1.112728
15	6	0	-1.353257	-0.324371	-0.192955
16	6	0	-0.517642	-1.268044	-0.824597
17	6	0	-0.716688	0.726913	0.502615
18	6	0	0.870047	-1.172919	-0.778177
19	1	0	-0.968605	-2.088947	-1.376732
20	6	0	0.666881	0.825271	0.564277
21	1	0	-1.308338	1.475709	1.020106
22	6	0	1.491633	-0.122136	-0.078889
23	1	0	1.476581	-1.913884	-1.287642
24	1	0	1.120469	1.639946	1.118653
25	7	0	2.898247	-0.016584	-0.016535
26	6	0	3.710115	-1.187895	0.034874
27	6	0	4.849281	-1.303956	-0.775588
28	6	0	3.397948	-2.240225	0.910366
29	6	0	5.653512	-2.443088	-0.705698
30	1	0	5.108640	-0.498653	-1.455601
31	6	0	4.200397	-3.380237	0.958622
32	1	0	2.528267	-2.161946	1.555179
33	6	0	5.344106	-3.507748	0.153999
34	1	0	6.533415	-2.506103	-1.341359
35	1	0	3.939236	-4.179362	1.648307
36	6	0	3.526608	1.263653	-0.031471
37	6	0	4.568658	1.556987	0.862727
38	6	0	3.129110	2.249411	-0.946966
39	6	0	5.194418	2.803233	0.833623
40	1	0	4.890023	0.804888	1.576436
41	6	0	3.752081	3.499049	-0.954378
42	1	0	2.334115	2.036328	-1.654640
43	6	0	4.796526	3.803190	-0.068678
44	1	0	6.001510	3.004353	1.534081
45	1	0	3.427785	4.245136	-1.675760
46	6	0	5.457411	5.162255	-0.067672
47	1	0	5.084596	5.783313	0.756639
48	1	0	6.542219	5.079460	0.056034
49	1	0	5.261223	5.700752	-0.999465
50	6	0	6.194251	-4.756519	0.196137
51	1	0	5.802006	-5.525185	-0.482025
52	1	0	7.224497	-4.548366	-0.107710
53	1	0	6.215316	-5.191143	1.200531
54	17	0	-9.765177	-0.186491	-0.044943

F8. MTPAcl Anion Optimized Geometry

Center Number	Atomic Number	Atomic Type	Coordinates (Angstroms) X	Y	Z
1	6	0	-2.753828	-0.338340	-0.448918
2	6	0	-3.725882	0.232945	0.378941
3	1	0	-3.087240	-0.931103	-1.300376
4	1	0	-3.393485	0.831346	1.226694
5	6	0	-5.144911	0.123865	0.240700
6	6	0	-6.015522	0.776575	1.171325
7	6	0	-5.797861	-0.619231	-0.799697
8	6	0	-7.398533	0.704205	1.083403
9	1	0	-5.574050	1.353781	1.981349
10	6	0	-7.183729	-0.695432	-0.893764
11	1	0	-5.204674	-1.143104	-1.542741
12	6	0	-7.986845	-0.036477	0.043970
13	1	0	-8.020885	1.215611	1.811743
14	1	0	-7.641611	-1.267585	-1.695739
15	6	0	-1.333557	-0.234540	-0.311571
16	6	0	-0.466507	-0.873637	-1.254374
17	6	0	-0.674263	0.488644	0.737470
18	6	0	0.915014	-0.794180	-1.169480
19	1	0	-0.913263	-1.432681	-2.074752
20	6	0	0.711084	0.550184	0.827204
21	1	0	-1.265176	0.994787	1.495205
22	6	0	1.536728	-0.080972	-0.121285
23	1	0	1.531872	-1.290065	-1.915121
24	1	0	1.171036	1.101892	1.644146
25	7	0	2.965535	-0.003755	-0.027283
26	6	0	3.715320	-1.201413	0.057925
27	6	0	4.962080	-1.340297	-0.581078
28	6	0	3.211589	-2.310613	0.763616
29	6	0	5.676184	-2.536602	-0.499462
30	1	0	5.373111	-0.508121	-1.143142
31	6	0	3.931747	-3.503725	0.826368
32	1	0	2.251274	-2.231245	1.262323
33	6	0	5.179639	-3.647536	0.199640
34	1	0	6.637107	-2.608175	-1.004424
35	1	0	3.514607	-4.338699	1.385319
36	6	0	3.592442	1.264841	-0.046959
37	6	0	4.742304	1.529914	0.723420
38	6	0	3.060413	2.316642	-0.815017
39	6	0	5.337730	2.790668	0.705574
40	1	0	5.169991	0.743806	1.337157
41	6	0	3.661423	3.576992	-0.813387
42	1	0	2.171963	2.142335	-1.412866
43	6	0	4.812682	3.845741	-0.058507
44	1	0	6.225282	2.959106	1.311919
45	1	0	3.225968	4.365446	-1.423377
46	6	0	5.446553	5.218203	-0.042341

47	1	0	5.172592	5.776548	0.862340
48	1	0	6.539954	5.155418	-0.062699
49	1	0	5.125979	5.813522	-0.902858
50	6	0	5.938524	-4.954137	0.247838
51	1	0	5.613328	-5.636279	-0.548717
52	1	0	7.014146	-4.795984	0.120886
53	1	0	5.782146	-5.472446	1.199752
54	17	0	-9.757578	-0.134445	-0.078257

F9. MTPA-c *Neutral* Optimized Geometry

Center Number	Atomic Number	Atomic Type	Coordinates (Angstroms) X	Y	Z
1	6	0	-2.974153	-0.489880	-0.265754
2	6	0	-3.920987	0.336040	0.241938
3	1	0	-3.291199	-1.381538	-0.803784
4	1	0	-3.610758	1.228522	0.781040
5	6	0	-5.369304	0.161144	0.145878
6	6	0	-6.208200	1.127122	0.745451
7	6	0	-5.988245	-0.924036	-0.517185
8	6	0	-7.592800	1.025720	0.692063
9	1	0	-5.759288	1.971071	1.261101
10	6	0	-7.369389	-1.037570	-0.578400
11	1	0	-5.385459	-1.690006	-0.992627
12	6	0	-8.188062	-0.061810	0.026719
13	1	0	-8.215043	1.780932	1.160417
14	1	0	-7.823554	-1.878076	-1.092529
15	6	0	-1.525777	-0.330231	-0.178400
16	6	0	-0.691384	-1.300801	-0.771104
17	6	0	-0.887893	0.749047	0.472816
18	6	0	0.695361	-1.206593	-0.728161
19	1	0	-1.143718	-2.142845	-1.289079
20	6	0	0.494590	0.849333	0.528651
21	1	0	-1.478498	1.519513	0.958561
22	6	0	1.319406	-0.126384	-0.074400
23	1	0	1.300121	-1.969042	-1.206586
24	1	0	0.948415	1.686413	1.047742
25	7	0	2.722159	-0.019128	-0.018176
26	6	0	3.540822	-1.187675	0.028388
27	6	0	4.661091	-1.306293	-0.806380
28	6	0	3.256088	-2.228119	0.926870
29	6	0	5.475350	-2.438777	-0.738559
30	1	0	4.898428	-0.508618	-1.503282
31	6	0	4.067907	-3.361186	0.973590
32	1	0	2.401338	-2.145367	1.590859
33	6	0	5.193766	-3.491932	0.144126
34	1	0	6.340982	-2.505143	-1.393032
35	1	0	3.829266	-4.151683	1.681082

36	6	0	3.353006	1.261736	-0.031334
37	6	0	4.376007	1.559440	0.883044
38	6	0	2.977750	2.238224	-0.964513
39	6	0	5.005409	2.803431	0.856357
40	1	0	4.677862	0.812873	1.610995
41	6	0	3.604500	3.486504	-0.970095
42	1	0	2.197263	2.020201	-1.686738
43	6	0	4.630405	3.795293	-0.065198
44	1	0	5.796614	3.010155	1.573096
45	1	0	3.297603	4.227166	-1.704358
46	6	0	-9.612444	-0.177386	-0.036343
47	7	0	-10.773353	-0.272061	-0.088150
48	6	0	5.305269	5.147469	-0.068719
49	1	0	5.047407	5.721727	0.829587
50	1	0	6.396314	5.049180	-0.085019
51	1	0	5.005552	5.738881	-0.938439
52	6	0	6.054869	-4.733049	0.187899
53	1	0	5.621491	-5.536526	-0.421180
54	1	0	7.059275	-4.535200	-0.197698
55	1	0	6.150203	-5.116940	1.208678

F10. MTPA-c *Anion* Optimized Geometry

Center Number	Atomic Number	Atomic Type	Coordinates (Angstroms) X	Y	Z
1	6	0	-2.926545	-0.381210	-0.438346
2	6	0	-3.896850	0.224254	0.354172
3	1	0	-3.251393	-1.018529	-1.259402
4	1	0	-3.562382	0.859723	1.174031
5	6	0	-5.310403	0.116013	0.226081
6	6	0	-6.175837	0.812994	1.136388
7	6	0	-5.970778	-0.668469	-0.785944
8	6	0	-7.548863	0.743906	1.057513
9	1	0	-5.723012	1.419446	1.918359
10	6	0	-7.343254	-0.743201	-0.872829
11	1	0	-5.376563	-1.220858	-1.507479
12	6	0	-8.183960	-0.041598	0.043478
13	1	0	-8.161799	1.289470	1.769720
14	1	0	-7.800486	-1.346985	-1.652470
15	6	0	-1.498851	-0.261620	-0.298227
16	6	0	-0.636434	-0.952978	-1.197741
17	6	0	-0.851767	0.521334	0.703862
18	6	0	0.747033	-0.865683	-1.115096
19	1	0	-1.080714	-1.560770	-1.983251
20	6	0	0.533326	0.594693	0.794758
21	1	0	-1.446700	1.069635	1.427973
22	6	0	1.360834	-0.090834	-0.112711
23	1	0	1.366465	-1.402827	-1.828380

24	1	0	0.989069	1.195473	1.577699
25	7	0	2.786296	-0.003528	-0.019539
26	6	0	3.548359	-1.196276	0.057590
27	6	0	4.775224	-1.329002	-0.616982
28	6	0	3.080186	-2.296167	0.799946
29	6	0	5.507575	-2.514645	-0.535780
30	1	0	5.157074	-0.500831	-1.205036
31	6	0	3.816274	-3.479380	0.860655
32	1	0	2.136469	-2.218541	1.329980
33	6	0	5.046242	-3.618048	0.197884
34	1	0	6.453690	-2.583765	-1.067965
35	1	0	3.428200	-4.309043	1.447526
36	6	0	3.408727	1.268888	-0.042206
37	6	0	4.550733	1.537785	0.737590
38	6	0	2.886161	2.311382	-0.826844
39	6	0	5.148519	2.796678	0.713516
40	1	0	4.969606	0.755928	1.362822
41	6	0	3.488438	3.571828	-0.829968
42	1	0	2.005047	2.132982	-1.434404
43	6	0	4.632322	3.844937	-0.066885
44	1	0	6.029963	2.970028	1.327191
45	1	0	3.060227	4.355347	-1.451004
46	6	0	-9.587547	-0.121160	-0.048980
47	7	0	-10.759832	-0.186709	-0.125086
48	6	0	5.277408	5.212171	-0.065734
49	1	0	5.135772	5.721863	0.895679
50	1	0	6.357779	5.146518	-0.237560
51	1	0	4.850915	5.851678	-0.844210
52	6	0	5.823721	-4.913430	0.249477
53	1	0	5.448615	-5.634513	-0.488427
54	1	0	6.884592	-4.750333	0.036100
55	1	0	5.744357	-5.388410	1.233075

F11. MTPAcc *Neutral* Optimized Geometry

Center Number	Atomic Number	Atomic Type	Coordinates (Angstroms) X	Y	Z
1	7	0	4.398873	0.053597	0.005879
2	6	0	5.096510	-1.189842	0.101362
3	6	0	4.750296	-2.134253	1.079322
4	6	0	6.158157	-1.476262	-0.768950
5	6	0	5.442647	-3.342421	1.168101
6	1	0	3.942146	-1.919621	1.771550
7	6	0	6.853478	-2.681524	-0.659498
8	1	0	6.441084	-0.752184	-1.526625
9	6	0	6.506765	-3.642345	0.303034
10	1	0	5.159261	-4.057845	1.936241
11	1	0	7.675825	-2.880238	-1.342353

12	6	0	5.162345	1.260017	-0.060971
13	6	0	4.891747	2.225654	-1.043086
14	6	0	6.212717	1.486711	0.838456
15	6	0	5.649225	3.394538	-1.108223
16	1	0	4.090760	2.056417	-1.755987
17	6	0	6.974218	2.654476	0.753167
18	1	0	6.436755	0.746486	1.600222
19	6	0	6.705778	3.634196	-0.213855
20	1	0	5.424220	4.127062	-1.879643
21	1	0	7.786670	2.807213	1.459204
22	6	0	2.995106	0.090969	0.008693
23	6	0	2.293811	1.191640	0.542451
24	6	0	2.240637	-0.977663	-0.529212
25	6	0	0.904666	1.213071	0.538347
26	1	0	2.841690	2.025116	0.967278
27	6	0	0.854969	-0.947624	-0.521975
28	1	0	2.753380	-1.830279	-0.960059
29	6	0	0.140453	0.148235	0.014185
30	1	0	0.392482	2.071145	0.966342
31	1	0	0.321092	-1.787394	-0.955511
32	6	0	-1.312259	0.232577	0.054126
33	1	0	-1.692969	1.154735	0.489179
34	6	0	-2.201354	-0.698075	-0.380436
35	1	0	-1.828550	-1.623833	-0.813030
36	6	0	-3.652222	-0.596312	-0.327023
37	6	0	-4.429380	-1.668597	-0.823739
38	6	0	-4.348471	0.521486	0.199737
39	6	0	-5.813691	-1.628306	-0.794293
40	1	0	-3.928170	-2.540001	-1.235269
41	6	0	-5.730369	0.565191	0.231611
42	1	0	-3.796963	1.369296	0.591303
43	6	0	-6.508613	-0.512709	-0.265282
44	1	0	-6.380908	-2.469303	-1.183289
45	1	0	-6.210661	1.442505	0.645084
46	6	0	-7.948985	-0.573490	-0.278296
47	1	0	-8.349182	-1.486243	-0.709882
48	6	0	-8.914208	0.303598	0.153642
49	6	0	-8.649577	1.569897	0.758039
50	7	0	-8.448920	2.605748	1.253001
51	6	0	-10.357424	-0.007475	0.024507
52	8	0	-11.252353	0.737536	0.394291
53	8	0	-10.603813	-1.207043	-0.546633
54	1	0	-11.568657	-1.321551	-0.586800
55	6	0	7.236587	-4.962517	0.390091
56	1	0	6.766593	-5.716198	-0.254552
57	1	0	8.278517	-4.865004	0.070329
58	1	0	7.227050	-5.356337	1.411056
59	6	0	7.508723	4.912385	-0.283425
60	1	0	6.961103	5.748008	0.170243
61	1	0	8.459779	4.814658	0.247757
62	1	0	7.723644	5.192671	-1.319878

F12. MTPAcc Anion Optimized Geometry

Center Number	Atomic Number	Atomic Type	Coordinates (Angstroms) X	Y	Z
1	7	0	4.444051	0.051147	0.026464
2	6	0	5.127294	-1.192449	0.126122
3	6	0	4.706697	-2.173215	1.039691
4	6	0	6.239464	-1.469607	-0.686004
5	6	0	5.375066	-3.395167	1.125105
6	1	0	3.855708	-1.976008	1.683862
7	6	0	6.908807	-2.689387	-0.578714
8	1	0	6.581730	-0.725971	-1.398720
9	6	0	6.489189	-3.681590	0.320968
10	1	0	5.029364	-4.134621	1.843741
11	1	0	7.768768	-2.875462	-1.217847
12	6	0	5.183362	1.261676	-0.081835
13	6	0	4.783517	2.269555	-0.976406
14	6	0	6.329989	1.478538	0.698327
15	6	0	5.506473	3.457892	-1.073446
16	1	0	3.905167	2.118240	-1.595780
17	6	0	7.054238	2.666670	0.579276
18	1	0	6.657002	0.714079	1.395972
19	6	0	6.657185	3.684268	-0.300386
20	1	0	5.175439	4.219101	-1.776231
21	1	0	7.939921	2.806406	1.194519
22	6	0	3.024522	0.085425	0.056407
23	6	0	2.337258	1.072668	0.783643
24	6	0	2.264502	-0.868634	-0.648017
25	6	0	0.945937	1.103258	0.796593
26	1	0	2.897423	1.818633	1.338342
27	6	0	0.875430	-0.842085	-0.617275
28	1	0	2.772801	-1.634502	-1.225426
29	6	0	0.166397	0.147093	0.105879
30	1	0	0.442795	1.878783	1.369177
31	1	0	0.333967	-1.594128	-1.182816
32	6	0	-1.287595	0.230522	0.168443
33	1	0	-1.665824	1.085193	0.726757
34	6	0	-2.182541	-0.639835	-0.386604
35	1	0	-1.793646	-1.501871	-0.928004
36	6	0	-3.624823	-0.568857	-0.344325
37	6	0	-4.398571	-1.593431	-0.959976
38	6	0	-4.356487	0.479578	0.283579
39	6	0	-5.777449	-1.574637	-0.948761
40	1	0	-3.881827	-2.414876	-1.452394
41	6	0	-5.736037	0.508154	0.300136
42	1	0	-3.820354	1.291690	0.766743
43	6	0	-6.522828	-0.522063	-0.318175
44	1	0	-6.325861	-2.380165	-1.432125
45	1	0	-6.229715	1.336088	0.793694
46	6	0	-7.935860	-0.579143	-0.357887

47	1	0	-8.340926	-1.440527	-0.879672
48	6	0	-8.941866	0.290327	0.160528
49	6	0	-8.677634	1.476408	0.886737
50	7	0	-8.474658	2.461424	1.489794
51	6	0	-10.347770	0.020584	-0.019874
52	8	0	-11.290709	0.713863	0.391636
53	8	0	-10.617708	-1.129436	-0.724189
54	1	0	-11.585421	-1.190141	-0.771456
55	6	0	7.191881	-5.017293	0.400663
56	1	0	6.751641	-5.739834	-0.298656
57	1	0	8.252997	-4.926300	0.148481
58	1	0	7.115491	-5.448743	1.403692
59	6	0	7.420811	4.984842	-0.399167
60	1	0	6.912837	5.786850	0.151414
61	1	0	8.427970	4.887746	0.016798
62	1	0	7.512774	5.316555	-1.438908

F13. MTPAn *Neutral* Optimized Geometry

Center Number	Atomic Number	Atomic Type	Coordinates (Angstroms) X	Y	Z
1	6	0	-2.518207	-0.490642	-0.314572
2	6	0	-3.470306	0.303755	0.249573
3	1	0	-2.834675	-1.339517	-0.918381
4	1	0	-3.145468	1.159840	0.840034
5	6	0	-4.910968	0.157019	0.158968
6	6	0	-5.748830	1.109411	0.795926
7	6	0	-5.560262	-0.898010	-0.539592
8	6	0	-7.130917	1.032567	0.746729
9	1	0	-5.287563	1.929954	1.341343
10	6	0	-6.937861	-0.994759	-0.601015
11	1	0	-4.968189	-1.657391	-1.041859
12	6	0	-7.755163	-0.027529	0.041745
13	1	0	-7.749152	1.771801	1.240268
14	1	0	-7.413996	-1.806550	-1.136603
15	6	0	-1.070500	-0.333450	-0.209154
16	6	0	-0.225533	-1.222362	-0.910381
17	6	0	-0.434578	0.665817	0.564421
18	6	0	1.161815	-1.119450	-0.859993
19	1	0	-0.672278	-2.002648	-1.521936
20	6	0	0.949968	0.765022	0.632341
21	1	0	-1.029378	1.368673	1.139610
22	6	0	1.777078	-0.122873	-0.083100
23	1	0	1.773993	-1.815414	-1.424519
24	1	0	1.401968	1.536810	1.247366
25	7	0	3.190808	-0.013757	-0.015137
26	6	0	3.995000	-1.185273	0.055664
27	6	0	5.167135	-1.300751	-0.708697

28	6	0	3.638311	-2.252574	0.897006
29	6	0	5.957819	-2.448223	-0.625141
30	1	0	5.461797	-0.488223	-1.365184
31	6	0	4.428648	-3.400413	0.958507
32	1	0	2.741472	-2.179838	1.504009
33	6	0	5.604576	-3.525395	0.201505
34	1	0	6.862088	-2.508439	-1.226210
35	1	0	4.130398	-4.209386	1.621391
36	6	0	3.808226	1.267796	-0.047210
37	6	0	4.880212	1.570045	0.808976
38	6	0	3.364458	2.258878	-0.937688
39	6	0	5.489618	2.824355	0.765439
40	1	0	5.238497	0.818380	1.505241
41	6	0	3.972070	3.515339	-0.959184
42	1	0	2.543775	2.043335	-1.614507
43	6	0	5.046530	3.826688	-0.112058
44	1	0	6.320071	3.029499	1.436971
45	1	0	3.610121	4.262661	-1.661417
46	7	0	-9.141540	-0.121327	-0.019686
47	8	0	-9.690141	-1.099234	-0.666178
48	8	0	-9.869210	0.771361	0.570203
49	6	0	5.684962	5.196561	-0.123000
50	1	0	5.236407	5.849640	0.636670
51	1	0	6.756991	5.139713	0.090902
52	1	0	5.556368	5.688332	-1.092136
53	6	0	6.440786	-4.783255	0.255785
54	1	0	6.066481	-5.539348	-0.446399
55	1	0	7.483299	-4.581041	-0.008049
56	1	0	6.422373	-5.232016	1.254169

F14. MTPAn Anion Optimized Geometry

Center Number	Atomic Number	Atomic Type	Coordinates (Angstroms) X	Y	Z
1	6	0	-2.518207	-0.490642	-0.314572
2	6	0	-3.470306	0.303755	0.249573
3	1	0	-2.834675	-1.339517	-0.918381
4	1	0	-3.145468	1.159840	0.840034
5	6	0	-4.910968	0.157019	0.158968
6	6	0	-5.748830	1.109411	0.795926
7	6	0	-5.560262	-0.898010	-0.539592
8	6	0	-7.130917	1.032567	0.746729
9	1	0	-5.287563	1.929954	1.341343
10	6	0	-6.937861	-0.994759	-0.601015
11	1	0	-4.968189	-1.657391	-1.041859
12	6	0	-7.755163	-0.027529	0.041745
13	1	0	-7.749152	1.771801	1.240268

14	1	0	-7.413996	-1.806550	-1.136603
15	6	0	-1.070500	-0.333450	-0.209154
16	6	0	-0.225533	-1.222362	-0.910381
17	6	0	-0.434578	0.665817	0.564421
18	6	0	1.161815	-1.119450	-0.859993
19	1	0	-0.672278	-2.002648	-1.521936
20	6	0	0.949968	0.765022	0.632341
21	1	0	-1.029378	1.368673	1.139610
22	6	0	1.777078	-0.122873	-0.083100
23	1	0	1.773993	-1.815414	-1.424519
24	1	0	1.401968	1.536810	1.247366
25	7	0	3.190808	-0.013757	-0.015137
26	6	0	3.995000	-1.185273	0.055664
27	6	0	5.167135	-1.300751	-0.708697
28	6	0	3.638311	-2.252574	0.897006
29	6	0	5.957819	-2.448223	-0.625141
30	1	0	5.461797	-0.488223	-1.365184
31	6	0	4.428648	-3.400413	0.958507
32	1	0	2.741472	-2.179838	1.504009
33	6	0	5.604576	-3.525395	0.201505
34	1	0	6.862088	-2.508439	-1.226210
35	1	0	4.130398	-4.209386	1.621391
36	6	0	3.808226	1.267796	-0.047210
37	6	0	4.880212	1.570045	0.808976
38	6	0	3.364458	2.258878	-0.937688
39	6	0	5.489618	2.824355	0.765439
40	1	0	5.238497	0.818380	1.505241
41	6	0	3.972070	3.515339	-0.959184
42	1	0	2.543775	2.043335	-1.614507
43	6	0	5.046530	3.826688	-0.112058
44	1	0	6.320071	3.029499	1.436971
45	1	0	3.610121	4.262661	-1.661417
46	7	0	-9.141540	-0.121327	-0.019686
47	8	0	-9.690141	-1.099234	-0.666178
48	8	0	-9.869210	0.771361	0.570203
49	6	0	5.684962	5.196561	-0.123000
50	1	0	5.236407	5.849640	0.636670
51	1	0	6.756991	5.139713	0.090902
52	1	0	5.556368	5.688332	-1.092136
53	6	0	6.440786	-4.783255	0.255785
54	1	0	6.066481	-5.539348	-0.446399
55	1	0	7.483299	-4.581041	-0.008049
56	1	0	6.422373	-5.232016	1.254169

APPENDIX G

VIBRATIONAL FREQUENCIES OF THE 7 MTPA DERIVATIVES (NEUTRAL AND ANION) USING B3LYP/6-31+G (D,P)

G1. MTPAa *Neutral* Vibrational Frequencies in cm^{-1}

	1	2	3
Frequencies --	13.8279	18.4882	25.3014
	4	5	6
Frequencies --	28.8516	29.2705	37.0734
	7	8	9
Frequencies --	40.6012	49.3229	52.7783
	10	11	12
Frequencies --	62.0820	80.9124	86.5721
	13	14	15
Frequencies --	134.1322	145.2949	165.1560
	16	17	18
Frequencies --	175.6881	189.2558	218.4873
	19	20	21
Frequencies --	259.0032	286.4353	296.3857
	22	23	24
Frequencies --	314.8994	320.8721	335.3664
	25	26	27
Frequencies --	347.7704	356.9447	384.9457
	28	29	30
Frequencies --	386.9757	393.5709	419.3534
	31	32	33
Frequencies --	421.3205	423.7077	427.2661
	34	35	36
Frequencies --	462.9681	486.1648	494.5813
	37	38	39
Frequencies --	500.1145	515.6569	531.9463
	40	41	42
Frequencies --	540.1776	560.0767	575.5350

	43	44	45
Frequencies --	600.8851	647.9137	649.1019
	46	47	48
Frequencies --	654.1391	656.7394	669.6708
	49	50	51
Frequencies --	717.0010	721.9942	727.1408
	52	53	54
Frequencies --	736.8273	791.6015	800.5482
	55	56	57
Frequencies --	813.1341	821.5160	826.3037
	58	59	60
Frequencies --	829.3877	833.8282	834.7818
	61	62	63
Frequencies --	841.2387	842.9549	844.2775
	64	65	66
Frequencies --	849.5676	884.0471	886.9472
	67	68	69
Frequencies --	932.8842	935.4014	951.5763
	70	71	72
Frequencies --	959.4860	963.7812	964.4822
	73	74	75
Frequencies --	967.0494	976.5226	980.3271
	76	77	78
Frequencies --	980.9821	993.9487	1006.9668
	79	80	81
Frequencies --	1008.6647	1021.5091	1023.8371
	82	83	84
Frequencies --	1030.0764	1030.8723	1059.9612
	85	86	87
Frequencies --	1060.6224	1082.8971	1138.6137
	88	89	90
Frequencies --	1140.7056	1142.9546	1155.0104
	91	92	93
Frequencies --	1188.9008	1201.3230	1202.4016

	94	95	96
Frequencies --	1203.0285	1216.1602	1219.9971

	97	98	99
Frequencies --	1232.7580	1234.4431	1256.7204

	100	101	102
Frequencies --	1295.5521	1299.2773	1306.7080

	103	104	105
Frequencies --	1308.4831	1312.2734	1334.3508

	106	107	108
Frequencies --	1338.1751	1339.8169	1350.1821

	109	110	111
Frequencies --	1352.5569	1360.1280	1366.1279

	112	113	114
Frequencies --	1381.3016	1414.8780	1415.1792

	115	116	117
Frequencies --	1438.6511	1447.1937	1458.9233

	118	119	120
Frequencies --	1473.6314	1481.1210	1483.0233

	121	122	123
Frequencies --	1488.3399	1490.4560	1536.9439

	124	125	126
Frequencies --	1539.8736	1545.5411	1550.9954

	127	128	129
Frequencies --	1591.5291	1606.3546	1610.4342

	130	131	132
Frequencies --	1615.5001	1637.6986	1649.3242

	133	134	135
Frequencies --	1649.3908	1656.2470	1659.5777

	136	137	138
Frequencies --	1683.2374	3030.6258	3032.5057

	139	140	141
Frequencies --	3087.2252	3088.6899	3118.1648

	142	143	144
Frequencies --	3118.2952	3148.6369	3157.0571

	145	146	147
Frequencies --	3171.5066	3175.2114	3175.3716
	148	149	150
Frequencies --	3176.2313	3176.3244	3176.9026
	151	152	153
Frequencies --	3177.3080	3187.7624	3191.6667
	154	155	156
Frequencies --	3198.7021	3203.5552	3203.8096
	157	158	159
Frequencies --	3205.2395	3205.3902	3208.1717
	160	161	162
Frequencies --	3209.3842	3567.4290	3672.8038

G2. MTPAa *Anion* Vibrational Frequencies in cm^{-1} (being recalculated)

	1	2	3
Frequencies --	-22.0528	14.9294	22.1998
	4	5	6
Frequencies --	26.7895	27.4960	33.8273
	7	8	9
Frequencies --	44.7845	49.6142	54.4453
	10	11	12
Frequencies --	60.8810	75.2092	99.9912
	13	14	15
Frequencies --	128.9555	140.5560	163.5157
	16	17	18
Frequencies --	175.6708	198.4684	214.0370
	19	20	21
Frequencies --	239.6151	263.4179	271.2125
	22	23	24
Frequencies --	296.2845	309.3209	334.9278

	25	26	27
Frequencies --	340.0774	355.7167	357.7267
	28	29	30
Frequencies --	380.7536	390.7900	421.4552
	31	32	33
Frequencies --	421.8030	426.4682	436.6299
	34	35	36
Frequencies --	455.8127	463.2276	486.8472
	37	38	39
Frequencies --	495.2675	501.3706	519.0174
	40	41	42
Frequencies --	532.2211	560.5565	597.0837
	43	44	45
Frequencies --	644.6752	649.3089	652.1110
	46	47	48
Frequencies --	654.8783	658.6999	673.4579
	49	50	51
Frequencies --	699.2888	717.2813	719.3507
	52	53	54
Frequencies --	724.4113	739.7868	777.1652
	55	56	57
Frequencies --	787.1323	789.2653	794.4331
	58	59	60
Frequencies --	798.2963	808.7926	814.8669
	61	62	63
Frequencies --	826.5620	829.2879	831.6582
	64	65	66
Frequencies --	836.3337	838.9941	839.8183
	67	68	69
Frequencies --	869.1907	919.3526	920.2179

	70	71	72
Frequencies --	921.7901	940.1538	943.2384
	73	74	75
Frequencies --	950.2040	953.0893	958.0596
	76	77	78
Frequencies --	973.6169	976.3783	998.5238
	79	80	81
Frequencies --	1005.4672	1005.6376	1007.5400
	82	83	84
Frequencies --	1024.2026	1025.1989	1057.9352
	85	86	87
Frequencies --	1058.4652	1086.5418	1119.0263
	88	89	90
Frequencies --	1138.4290	1141.1517	1141.8010
	91	92	93
Frequencies --	1170.5602	1188.0790	1195.5798
	94	95	96
Frequencies --	1198.7531	1205.6763	1212.7651
	97	98	99
Frequencies --	1232.7576	1234.4881	1242.8773
	100	101	102
Frequencies --	1269.7638	1277.5208	1289.1596
	103	104	105
Frequencies --	1297.8354	1303.9747	1309.1620
	106	107	108
Frequencies --	1332.9238	1338.4551	1339.1068
	109	110	111
Frequencies --	1343.0866	1351.5558	1356.7330
	112	113	114
Frequencies --	1371.2434	1414.1239	1414.9417

	115	116	117
Frequencies --	1439.4197	1449.7567	1452.0304
	118	119	120
Frequencies --	1460.9460	1481.6863	1482.4202
	121	122	123
Frequencies --	1487.2040	1489.8902	1501.7089
	124	125	126
Frequencies --	1514.8398	1523.6416	1533.7444
	127	128	129
Frequencies --	1543.2684	1559.0841	1588.8368
	130	131	132
Frequencies --	1596.2194	1607.9697	1622.6733
	133	134	135
Frequencies --	1635.1573	1645.5025	1647.8994
	136	137	138
Frequencies --	1655.2397	3023.7979	3024.1158
	139	140	141
Frequencies --	3080.4700	3080.5478	3110.4846
	142	143	144
Frequencies --	3110.8682	3126.0969	3136.0410
	145	146	147
Frequencies --	3147.7214	3147.9895	3149.9170
	148	149	150
Frequencies --	3161.3260	3166.6969	3167.2679
	151	152	153
Frequencies --	3167.7043	3168.5566	3169.2918
	154	155	156
Frequencies --	3175.7278	3187.0275	3188.2499
	157	158	159
Frequencies --	3204.0532	3205.6883	3208.1432

	160	161	162
Frequencies --	3208.5772	3526.7569	3623.3617

G3. MTPAo *Neutral* Vibrational Frequencies in cm^{-1}

	1	2	3
Frequencies --	14.2630	18.4142	23.4293
	4	5	6
Frequencies --	26.3471	28.2427	37.0107
	7	8	9
Frequencies --	39.8751	43.6576	52.2202
	10	11	12
Frequencies --	57.1508	78.0948	83.5180
	13	14	15
Frequencies --	102.3498	130.3360	143.1898
	16	17	18
Frequencies --	163.9751	172.2866	185.2325
	19	20	21
Frequencies --	196.9239	240.6482	256.4714
	22	23	24
Frequencies --	264.6345	287.6999	297.2097
	25	26	27
Frequencies --	331.7284	340.8288	348.3804
	28	29	30
Frequencies --	364.1418	387.8064	389.9232
	31	32	33
Frequencies --	420.7220	423.4012	426.4322
	34	35	36
Frequencies --	427.6028	439.3614	464.5782
	37	38	39
Frequencies --	487.8118	503.6706	510.3758
	40	41	42
Frequencies --	520.5449	542.6133	557.2860
	43	44	45
Frequencies --	575.3540	601.0369	645.9839

	46	47	48
Frequencies --	649.1210	651.2202	655.6919
	49	50	51
Frequencies --	669.5422	714.2836	721.8824
	52	53	54
Frequencies --	727.7802	736.0141	772.2393
	55	56	57
Frequencies --	791.8068	810.4090	816.3809
	58	59	60
Frequencies --	827.6537	830.2617	833.9869
	61	62	63
Frequencies --	834.9489	841.5908	843.2580
	67	68	69
Frequencies --	888.5628	933.0667	935.5518
	70	71	72
Frequencies --	949.7812	959.7106	964.3551
	73	74	75
Frequencies --	964.7689	970.7909	977.4545
	76	77	78
Frequencies --	980.4742	981.3539	995.3624
	79	80	81
Frequencies --	1007.0442	1008.8000	1019.8460
	82	83	84
Frequencies --	1023.6528	1030.2593	1031.0412
	85	86	87
Frequencies --	1049.7594	1059.9938	1060.6966
	88	89	90
Frequencies --	1137.8289	1138.7854	1140.7336
	91	92	93
Frequencies --	1144.3225	1170.0251	1189.1993
	94	95	96
Frequencies --	1199.8281	1201.3324	1202.1938
	97	98	99
Frequencies --	1203.4838	1216.1460	1219.3158
	100	101	102

Frequencies --	1232.7694	1234.4610	1253.6791
	103	104	105
Frequencies --	1278.3128	1294.7686	1298.7695
	106	107	108
Frequencies --	1307.7948	1311.8942	1334.0528
	109	110	111
Frequencies --	1338.1289	1339.8440	1343.8846
	112	113	114
Frequencies --	1350.3414	1353.2612	1362.5970
	115	116	117
Frequencies --	1382.5378	1414.7441	1415.2638
	118	119	120
Frequencies --	1438.7066	1447.0232	1454.8034
	121	122	123
Frequencies --	1462.9090	1476.9848	1480.9165
	124	125	126
Frequencies --	1483.0033	1488.2730	1488.5399
	127	128	129
Frequencies --	1490.3933	1501.2301	1536.9875
	130	131	132
Frequencies --	1540.0011	1543.8124	1549.0341
	133	134	135
Frequencies --	1591.8616	1607.6276	1610.9612
	136	137	138
Frequencies --	1615.6940	1638.3094	1649.4443
	139	140	141
Frequencies --	1650.6839	1657.9085	1683.9366
	142	143	144
Frequencies --	3030.4627	3030.9533	3032.8171
	145	146	147
Frequencies --	3087.3751	3089.0178	3099.1488
	148	149	150
Frequencies --	3118.4533	3118.4990	3151.5219
	151	152	153

Frequencies --	3159.7973	3161.2590	3175.4686
	154	155	156
Frequencies --	3175.6821	3176.5573	3177.1469
	157	158	159
Frequencies --	3178.0050	3180.8233	3192.3007
	160	161	162
Frequencies --	3193.5365	3203.5814	3203.7484
	163	164	165
Frequencies --	3205.2223	3205.3753	3208.4019
	166	167	168
Frequencies --	3208.9200	3210.2040	3225.6207

G4. MTPAo *Anion* Vibrational Frequencies in cm^{-1}

	1	2	3
Frequencies --	13.4125	21.8330	27.9246
	4	5	6
Frequencies --	28.5150	29.3880	33.6538
	7	8	9
Frequencies --	40.7110	44.7505	53.8252
	10	11	12
Frequencies --	56.5557	70.4302	76.3724
	13	14	15
Frequencies --	103.1987	125.6496	138.5495
	16	17	18
Frequencies --	161.5451	170.8784	191.1669
	19	20	21
Frequencies --	227.1288	254.7131	259.5548
	22	23	24
Frequencies --	266.0303	274.8938	296.8842
	25	26	27
Frequencies --	322.3898	337.6941	345.3378
	28	29	30
Frequencies --	357.5794	363.9375	387.4220

	31	32	33
Frequencies --	421.5017	426.3489	427.2567

	34	35	36
Frequencies --	433.7033	435.9612	456.4874

	37	38	39
Frequencies --	464.6725	486.2880	502.5962

	40	41	42
Frequencies --	507.4873	519.1338	548.7484

	43	44	45
Frequencies --	560.7760	598.0147	643.8209

	46	47	48
Frequencies --	647.5440	649.8753	654.2508

	49	50	51
Frequencies --	659.3266	673.3847	702.2145

	52	53	54
Frequencies --	718.1055	720.4940	737.3283

	55	56	57
Frequencies --	753.1089	778.8567	787.4485

	58	59	60
Frequencies --	791.8761	796.2603	807.6603

	61	62	63
Frequencies --	808.4443	826.8060	827.0541

	64	65	66
Frequencies --	831.4423	836.3047	839.6691

	67	68	69
Frequencies --	840.5144	868.9805	919.5741

	70	71	72
Frequencies --	921.5705	922.2923	939.6637

	73	74	75
Frequencies --	944.0168	951.1623	953.3088

	76	77	78
Frequencies --	958.0423	973.4951	976.3419

	79	80	81
Frequencies --	999.1187	1002.2349	1005.2107

	82	83	84
Frequencies --	1007.5554	1024.4487	1025.2441
	85	86	87
Frequencies --	1057.9124	1058.1692	1058.5708
	88	89	90
Frequencies --	1119.2019	1123.5246	1138.5397
	91	92	93
Frequencies --	1141.2476	1170.5042	1170.7558
	94	95	96
Frequencies --	1189.6243	1195.7229	1198.1932
	97	98	99
Frequencies --	1198.9710	1204.1730	1212.9110
	100	101	102
Frequencies --	1232.8462	1234.4788	1238.2988
	103	104	105
Frequencies --	1258.3345	1280.9900	1289.7099
	106	107	108
Frequencies --	1298.2107	1303.7482	1308.5665
	109	110	111
Frequencies --	1327.2301	1333.5716	1338.3206
	112	113	114
Frequencies --	1339.5251	1344.6168	1351.9270
	115	116	117
Frequencies --	1374.9189	1414.0815	1414.8960
	118	119	120
Frequencies --	1439.4871	1446.4913	1450.2391
	121	122	123
Frequencies --	1456.5871	1475.2381	1481.7796
	124	125	126
Frequencies --	1482.5266	1484.8950	1487.3842
	127	128	129
Frequencies --	1490.0398	1502.1494	1504.6704
	130	131	132
Frequencies --	1516.0064	1522.7666	1533.9551

	133	134	135
Frequencies --	1543.3316	1551.8751	1591.4359

	136	137	138
Frequencies --	1596.6362	1608.2205	1620.4268

	139	140	141
Frequencies --	1630.7032	1645.6894	1655.3284

	142	143	144
Frequencies --	3010.1150	3023.9565	3024.2119

	145	146	147
Frequencies --	3068.7946	3080.8805	3080.9087

	148	149	150
Frequencies --	3110.6363	3111.0305	3127.5914

	151	152	153
Frequencies --	3137.2086	3142.3539	3148.9716

	154	155	156
Frequencies --	3158.4102	3162.6042	3167.3614

	157	158	159
Frequencies --	3167.8359	3168.5831	3169.3836

	160	161	162
Frequencies --	3173.2459	3176.6582	3187.8074

	163	164	165
Frequencies --	3193.8481	3204.1197	3205.7402

	166	167	168
Frequencies --	3206.2372	3207.9961	3208.3727

G5. MTPA *Neutral* Vibrational Frequencies in cm^{-1} (being recalculated)

	1	2	3
Frequencies --	-31.6259	16.9770	21.9487

	4	5	6
Frequencies --	24.5921	27.4748	35.8698

	7	8	9
Frequencies --	40.4521	50.9368	59.1436

	10	11	12
Frequencies --	69.6824	79.8186	90.2414
	13	14	15
Frequencies --	140.7193	147.0333	168.8188
	16	17	18
Frequencies --	181.3421	230.7035	251.4018
	19	20	21
Frequencies --	258.6156	292.3461	301.2349
	22	23	24
Frequencies --	328.5556	350.5472	358.9404
	25	26	27
Frequencies --	367.1820	392.0401	414.4912
	28	29	30
Frequencies --	420.1440	423.2088	426.7497
	31	32	33
Frequencies --	459.8629	481.2358	494.0441
	34	35	36
Frequencies --	506.2423	516.2222	539.6292
	37	38	39
Frequencies --	573.5310	575.5573	612.4193
	40	41	42
Frequencies --	630.9671	648.9495	649.1704
	43	44	45
Frequencies --	655.5055	678.1833	698.9329
	46	47	48
Frequencies --	720.8511	727.3879	728.9347
	49	50	51
Frequencies --	764.0672	791.8663	809.3623
	52	53	54
Frequencies --	827.3760	833.5058	834.4236

	55	56	57
Frequencies --	837.1601	837.5256	842.5940
	58	59	60
Frequencies --	843.8145	850.4534	881.5769
	61	62	63
Frequencies --	886.1029	927.2446	933.2443
	64	65	66
Frequencies --	935.8151	960.2970	964.5631
	67	68	69
Frequencies --	965.1299	978.0506	980.8314
	70	71	72
Frequencies --	981.6476	984.9096	994.8826
	73	74	75
Frequencies --	1005.2221	1007.5174	1008.1406
	76	77	78
Frequencies --	1008.9689	1023.4360	1030.3454
	79	80	81
Frequencies -	1031.1143	1048.9275	1059.9790
	82	83	84
Frequencies --	1060.0888	1104.3133	1138.3130
	85	86	87
Frequencies --	1140.4093	1145.2288	1178.4422
	88	89	90
Frequencies --	1189.1652	1200.9498	1202.4700
	91	92	93
Frequencies --	1204.5144	1215.9584	1216.7398
	94	95	96
Frequencies --	1232.4748	1234.1712	1257.4731
	97	98	99
Frequencies --	1294.3565	1298.5102	1309.2507

	100	101	102
Frequencies --	1311.7514	1335.3885	1337.9708
	103	104	105
Frequencies --	1339.5913	1350.1955	1353.4258
	106	107	108
Frequencies --	1359.7416	1367.6400	1379.6264
	109	110	111
Frequencies --	1415.1352	1415.3411	1438.5464
	112	113	114
Frequencies --	1446.4867	1461.1293	1481.5921
	115	116	117
Frequencies --	1482.3022	1483.1161	1487.9187
	118	119	120
Frequencies --	1489.5013	1527.6951	1539.4792
	121	122	123
Frequencies --	1540.2434	1547.8602	1591.7644
	124	125	126
Frequencies --	1610.5493	1615.6147	1616.0165
	127	128	129
Frequencies --	1633.8247	1646.9343	1649.4685
	130	131	132
Frequencies --	1657.6784	1685.0363	3031.1810
	133	134	135
Frequencies --	3032.2083	3089.1375	3089.5483
	136	137	138
Frequencies --	3118.8369	3118.9360	3153.9797
	139	140	141
Frequencies --	3162.2478	3176.0780	3176.1767
	142	143	144
Frequencies --	3176.2790	3177.0178	3177.3339

	145	146	147
Frequencies --	3178.7948	3183.2142	3192.2813
	148	149	150
Frequencies --	3193.6322	3200.9715	3203.6693
	151	152	153
Frequencies --	3203.8197	3205.1766	3205.3278

G6. MTPA *Anion* Vibrational Frequencies in cm^{-1}

	1	2	3
Frequencies --	16.6717	23.4415	28.9712
	4	5	6
Frequencies --	30.7605	34.4778	38.0579
	7	8	9
Frequencies --	45.3023	55.5905	58.7205
	10	11	12
Frequencies --	67.4716	76.0028	117.1305
	13	14	15
Frequencies --	135.3936	143.0010	168.2841
	19	20	21
Frequencies --	265.8845	279.3778	299.4922
	22	23	24
Frequencies --	318.5976	339.6889	357.1559
	25	26	27
Frequencies --	363.7605	392.5273	421.4549
	28	29	30
Frequencies --	425.5156	426.4127	434.9080

	31	32	33
Frequencies --	452.5316	463.5180	483.9542
	34	35	36
Frequencies --	503.0998	504.9618	519.0789
	37	38	39
Frequencies --	562.6227	564.6903	608.4017
	40	41	42
Frequencies --	628.0423	646.1460	649.6817
	43	44	45
Frequencies --	654.2824	667.3223	680.7369
	46	47	48
Frequencies --	691.2159	716.2710	721.1479
	49	50	51
Frequencies --	721.3525	756.3429	785.7218
	52	53	54
Frequencies --	791.7030	804.7471	808.0607
	55	56	57
Frequencies --	809.6777	823.1743	827.4148
	58	59	60
Frequencies --	831.6229	835.1776	837.0784
	61	62	63
Frequencies --	839.9854	852.0131	867.7495
	64	65	66
Frequencies --	920.9019	923.4693	946.4906
	67	68	69
Frequencies --	953.9611	954.4567	958.4666
	70	71	72
Frequencies --	958.9255	963.0934	974.3946

	73	74	75
Frequencies --	976.7213	984.9262	1002.2879
	76	77	78
Frequencies --	1005.7998	1007.9393	1025.0404
	79	80	81
Frequencies --	1025.6777	1026.3520	1058.2871
	82	83	84
Frequencies --	1058.6979	1089.9976	1121.6791
	85	86	87
Frequencies --	1138.9122	1141.6086	1159.2698
	88	89	90
Frequencies --	1171.9603	1190.3669	1196.6672
	91	92	93
Frequencies --	1199.6467	1206.8737	1213.5789
	94	95	96
Frequencies --	1232.8984	1234.7232	1246.0570
	97	98	99
Frequencies --	1282.4577	1290.5559	1299.8415
	100	101	102
Frequencies --	1304.4644	1312.1230	1334.2382
	103	104	105
Frequencies --	1338.9208	1340.5060	1346.1739
	106	107	108
Frequencies --	1351.9266	1361.3696	1376.1896
	109	110	111
Frequencies --	1414.2443	1414.9412	1439.5716
	112	113	114
Frequencies --	1450.0802	1454.4994	1471.6504

	115	116	117
Frequencies --	1482.2473	1482.7127	1487.5556
	118	119	120
Frequencies --	1490.1167	1502.4721	1518.7100
	121	122	123
Frequencies --	1522.0930	1534.5468	1543.6452
	124	125	126
Frequencies --	1551.4749	1596.8356	1598.1225
	127	128	129
Frequencies --	1605.8815	1609.1749	1627.5865
	130	131	132
Frequencies --	1646.3184	1655.6247	3024.7443
	133	134	135
Frequencies --	3024.9993	3081.0900	3081.7496
	136	137	138
Frequencies --	3111.5254	3111.6149	3130.5741
	139	140	141
Frequencies --	3137.9036	3147.5271	3152.3572
	142	143	144
Frequencies --	3154.8178	3165.7848	3167.3799
	145	146	147
Frequencies --	3168.2020	3168.5297	3169.6439
	148	149	150
Frequencies --	3170.0842	3179.2772	3185.5349
	151	152	153
Frequencies --	3189.9769	3194.8851	3204.3475
	154	155	156
Frequencies --	3205.8427	3207.8238	3208.3665

G7. MTPAcl *Neutral* Vibrational Frequencies in cm^{-1} (being recalculated)

	1	2	3
Frequencies --	-33.4489	14.8625	19.5245

	4	5	6
Frequencies --	24.4114	24.9488	34.3972

	7	8	9
Frequencies --	38.4647	43.8007	49.9656

	10	11	12
Frequencies --	57.7490	77.8961	84.3766

	13	14	15
Frequencies --	126.9733	144.4579	155.2863

	16	17	18
Frequencies --	162.8120	183.6723	206.1339

	19	20	21
Frequencies --	257.5390	286.0992	287.9670

	22	23	24
Frequencies --	295.0722	323.1312	337.3739

	25	26	27
Frequencies --	346.0396	363.2824	375.4747

	28	29	30
Frequencies --	383.2244	418.7322	420.5523

	31	32	33
Frequencies --	423.2367	426.6432	439.2971

	34	35	36
Frequencies --	462.6848	484.8531	497.0540

	37	38	39
Frequencies --	515.8953	516.5018	538.2969

	40	41	42
Frequencies --	574.3758	592.5653	642.9321
	43	44	45
Frequencies --	646.6696	649.6372	651.1548
	46	47	48
Frequencies --	655.6510	699.9958	707.1459
	49	50	51
Frequencies --	721.4165	728.1764	734.4101
	52	53	54
Frequencies --	791.6841	809.7134	821.4886
	55	56	57
Frequencies --	827.9214	828.6944	834.2240
	58	59	60
Frequencies --	834.6085	838.6716	841.9139
	61	62	63
Frequencies --	843.4891	846.1128	882.6485
	64	65	66
Frequencies --	893.1030	933.2339	935.7695
	67	68	69
Frequencies --	959.1917	961.4612	965.3408
	70	71	72
Frequencies --	965.5017	977.4272	978.1927
	73	74	75
Frequencies --	981.0379	981.8528	996.8889
	76	77	78
Frequencies -	1007.6675	1008.9753	1018.0854
	79	80	81
Frequencies --	1023.2449	1030.3685	1031.1418
	82	83	84
Frequencies --	1060.0028	1060.0968	1098.0814

	85	86	87
Frequencies --	1134.5254	1138.0446	1140.1539
	88	89	90
Frequencies --	1146.0449	1189.0915	1200.6812
	91	92	93
Frequencies --	1202.2883	1205.0156	1215.7353
	94	95	96
Frequencies --	1217.7179	1232.2847	1233.9896
	97	98	99
Frequencies --	1258.6803	1294.0971	1298.3129
	100	101	102
Frequencies --	1310.0744	1311.4821	1328.2198
	103	104	105
Frequencies --	1334.6729	1337.7477	1339.4916
	106	107	108
Frequencies --	1350.1844	1353.7035	1363.2924
	109	110	111
Frequencies --	1378.2010	1415.0978	1415.5229
	112	113	114
Frequencies --	1437.9743	1439.8362	1446.2060
	115	116	117
Frequencies --	1463.2941	1481.6344	1483.0853
	118	119	120
Frequencies --	1487.8701	1489.4867	1523.2061
	121	122	123
Frequencies --	1538.9896	1540.3084	1547.6955
	124	125	126
Frequencies --	1590.8556	1604.1212	1611.0862
	127	128	129
Frequencies --	1615.8520	1627.0394	1643.3637

	130	131	132
Frequencies --	1649.4469	1657.4861	1684.3778

	133	134	135
Frequencies --	3031.3576	3032.3547	3089.3298

	136	137	138
Frequencies --	3089.7947	3119.0481	3119.1423

	139	140	141
Frequencies --	3155.5658	3164.9349	3176.2609

	142	143	144
Frequencies --	3176.5709	3177.3120	3177.7422

	145	146	147
Frequencies --	3179.1067	3188.6057	3194.2029

	148	149	150
Frequencies --	3203.0493	3203.6914	3203.8395

	151	152	153
Frequencies --	3205.1596	3205.3215	3211.6493

	154	155	156
Frequencies --	3212.6814	3217.8029	3219.3995

G8. MTPAcl *Anion* Vibrational Frequencies in cm^{-1} (being recalculated)

	1	2	3
Frequencies --	-16.1683	3.3734	13.6966

	4	5	6
Frequencies --	22.7671	25.7711	33.3786

	7	8	9
Frequencies --	44.1009	44.2635	54.5433

	10	11	12
Frequencies --	57.4473	76.1968	91.6486

	13	14	15
Frequencies --	123.5397	139.1811	159.5580

	16	17	18
Frequencies --	163.8025	201.6397	228.6761
	19	20	21
Frequencies --	262.6471	267.9318	285.6081
	22	23	24
Frequencies --	291.3908	294.3180	326.5223
	25	26	27
Frequencies --	333.8546	357.7852	365.4889
	28	29	30
Frequencies --	381.3209	421.4187	426.1690
	31	32	33
Frequencies --	427.5971	433.0428	435.3421
	34	35	36
Frequencies --	452.8071	456.7213	486.6460
	37	38	39
Frequencies --	497.1369	511.7945	519.1192
	40	41	42
Frequencies --	562.9982	588.2799	637.4097
	43	44	45
Frequencies --	639.8217	646.9712	650.3999
	46	47	48
Frequencies --	654.5618	662.2646	682.0121
	49	50	51
Frequencies --	703.9695	718.4619	721.9336
	52	53	54
Frequencies --	745.7245	779.5938	786.3746
	55	56	57
Frequencies --	794.5567	795.6458	808.0842
	58	59	60
Frequencies --	816.8757	823.2123	828.0169

	61	62	63
Frequencies --	831.6571	837.2510	840.3267
	64	65	66
Frequencies --	850.1293	868.4236	921.3085
	67	68	69
Frequencies --	924.5148	931.1902	946.6174
	70	71	72
Frequencies --	948.1050	954.4722	956.3371
	73	74	75
Frequencies --	958.6044	974.7125	977.2288
	76	77	78
Frequencies --	992.1471	1003.6682	1005.3063
	79	80	81
Frequencies --	1008.0500	1025.4122	1025.9712
	82	83	84
Frequencies --	1058.2413	1058.9034	1075.6925
	85	86	87
Frequencies --	1119.8737	1123.9704	1139.2010
	88	89	90
Frequencies --	1141.9288	1172.1750	1188.8922
	91	92	93
Frequencies --	1197.0986	1200.1030	1207.9377
	94	95	96
Frequencies --	1213.9300	1233.1501	1235.0695
	97	98	99
Frequencies --	1247.1632	1283.4170	1291.4361
	100	101	102
Frequencies --	1301.5238	1303.5834	1308.7896
	103	104	105
Frequencies --	1317.9822	1335.0888	1339.2116

	106	107	108
Frequencies --	1341.0898	1345.9825	1351.8066
	109	110	111
Frequencies --	1375.7387	1413.7034	1414.3275
	112	113	114
Frequencies --	1439.5448	1442.1386	1450.2278
	115	116	117
Frequencies --	1456.5795	1481.3395	1482.0368
	118	119	120
Frequencies --	1487.5214	1490.4065	1497.3324
	121	122	123
Frequencies --	1517.0355	1525.1604	1528.3589
	124	125	126
Frequencies --	1534.9647	1543.9320	1596.1897
	127	128	129
Frequencies --	1598.5446	1602.6880	1609.7417
	130	131	132
Frequencies --	1624.9352	1646.7424	1655.7650
	133	134	135
Frequencies --	3025.0353	3025.7476	3081.2919
	136	137	138
Frequencies --	3081.8772	3111.6753	3111.8785
	139	140	141
Frequencies --	3133.3050	3140.9647	3154.4474
	142	143	144
Frequencies --	3162.5530	3167.7818	3168.4708
	145	146	147
Frequencies --	3168.6764	3170.0560	3170.6195
	148	149	150
Frequencies --	3181.0411	3183.8802	3191.1838

	151	152	153
Frequencies --	3196.9734	3201.0160	3204.3606
	154	155	156
Frequencies --	3205.8257	3207.6374	3208.4287

G9. MTPAc *Neutral* Vibrational Frequencies in cm^{-1}

	1	2	3
Frequencies --	12.8605	18.5731	23.9429
	4	5	6
Frequencies --	26.4369	29.4855	32.7623
	7	8	9
Frequencies --	39.0828	42.0249	49.1063
	10	11	12
Frequencies --	56.7756	76.5085	84.3301
	13	14	15
Frequencies --	124.1058	137.3008	143.9451
	16	17	18
Frequencies --	157.4226	168.6533	183.1432
	19	20	21
Frequencies --	237.2638	257.3716	271.6316
	22	23	24
Frequencies --	292.8706	296.7402	328.9979
	25	26	27
Frequencies --	349.1995	357.2240	365.2211
	28	29	30
Frequencies --	386.6257	411.0067	420.2188
	31	32	33
Frequencies --	423.0149	426.2016	458.9711
	34	35	36
Frequencies --	467.7316	476.0884	486.0238
	37	38	39
Frequencies --	510.8755	523.2949	531.5916
	40	41	42

Frequencies --	564.4303	565.6967	576.3005
	43	44	45
Frequencies --	596.2096	647.4954	648.6970
	46	47	48
Frequencies --	655.3124	659.1279	663.5428
	49	50	51
Frequencies --	717.6560	722.4907	727.0019
	52	53	54
Frequencies --	738.7230	749.6330	792.3747
	55	56	57
Frequencies --	810.2147	826.2191	829.2966
	58	59	60
Frequencies --	834.6827	834.7791	840.7209
	61	62	63
Frequencies --	842.9302	843.9110	844.1707
	64	65	66
Frequencies --	850.4330	885.0631	897.4037
	67	68	69
Frequencies --	933.2727	935.8067	961.4757
	70	71	72
Frequencies --	965.3838	966.2038	976.3379
	73	74	75
Frequencies --	979.4216	981.9019	982.6963
	76	77	78
Frequencies --	987.9055	997.6896	1007.8662
	79	80	81
Frequencies --	1009.2846	1021.9652	1027.1446
	82	83	84
Frequencies --	1031.0327	1031.8388	1060.1632
	85	86	87
Frequencies --	1060.9778	1137.7278	1139.9307
	88	89	90
Frequencies --	1143.6957	1148.4751	1187.8248
	91	92	93
Frequencies --	1195.1689	1200.6788	1203.6151

	94	95	96
Frequencies --	1215.3152	1223.4351	1232.2565
	97	98	99
Frequencies --	1233.5174	1234.1292	1263.7252
	100	101	102
Frequencies --	1292.9206	1303.2435	1313.1451
	103	104	105
Frequencies --	1313.6380	1335.4224	1336.7672
	106	107	108
Frequencies --	1338.2721	1339.6800	1350.3234
	109	110	111
Frequencies --	1355.6100	1363.6161	1383.7761
	112	113	114
Frequencies --	1414.8804	1415.6708	1438.6250
	115	116	117
Frequencies --	1445.6113	1450.6613	1466.0402
	118	119	120
Frequencies --	1481.1877	1483.2220	1488.0216
	121	122	123
Frequencies --	1490.4568	1535.0202	1540.6087
	124	125	126
Frequencies --	1541.3634	1548.5282	1581.7435
	127	128	129
Frequencies --	1591.2613	1611.1963	1615.8931
	130	131	132
Frequencies --	1623.8960	1648.8893	1649.5349
	133	134	135
Frequencies --	1657.9768	1680.8243	2309.9437
	136	137	138
Frequencies --	3032.2967	3034.2656	3088.8255
	139	140	141
Frequencies --	3090.5226	3120.0299	3120.1853
	142	143	144
Frequencies --	3159.8160	3170.3852	3176.7473

	145	146	147
Frequencies --	3177.3377	3178.1885	3179.3757
	148	149	150
Frequencies --	3180.6299	3193.4335	3196.1490
	151	152	153
Frequencies --	3203.7409	3203.8044	3204.9901
	154	155	156
Frequencies --	3205.2177	3205.3146	3214.2725
	157	158	159
Frequencies --	3215.5466	3216.4344	3219.2317

G10. MTPAc *Anion* Vibrational Frequencies in cm^{-1}

	1	2	3
Frequencies --	14.1523	22.5717	26.0899
	4	5	6
Frequencies --	27.1387	32.8860	40.1889
	7	8	9
Frequencies --	42.2421	43.1695	54.3618
	10	11	12
Frequencies --	55.9978	76.8055	87.4837
	13	14	15
Frequencies --	121.9855	139.6670	149.6284
	16	17	18
Frequencies --	157.1012	167.9078	211.8192
	19	20	21
Frequencies --	235.3681	262.8580	273.3579
	22	23	24
Frequencies --	282.7799	292.6527	319.3417
	25	26	27
Frequencies --	337.6696	359.5146	364.5977
	28	29	30
Frequencies --	386.2149	421.4964	423.7231
	31	32	33
Frequencies --	426.2921	430.2417	440.5344

	34	35	36
Frequencies --	454.0149	468.2746	485.3785
	37	38	39
Frequencies --	501.6491	517.1256	518.9279
	40	41	42
Frequencies --	523.6575	568.0610	572.1651
	43	44	45
Frequencies --	595.2751	646.1909	649.4935
	46	47	48
Frequencies --	652.9333	655.6578	659.1237
	49	50	51
Frequencies --	680.5866	716.3442	721.9592
	52	53	54
Frequencies --	722.7161	739.0063	770.4845
	55	56	57
Frequencies --	789.6737	791.1509	803.4857
	58	59	60
Frequencies --	808.2280	812.7243	825.2294
	61	62	63
Frequencies --	829.8727	831.9785	835.3815
	64	65	66
Frequencies --	838.6310	840.5854	871.0904
	67	68	69
Frequencies --	892.4648	925.0784	928.4754
	70	71	72
Frequencies --	951.4943	953.1185	957.1097
	73	74	75
Frequencies --	959.5726	959.6580	964.0413
	76	77	78
Frequencies --	976.1945	978.0422	991.4262
	79	80	81
Frequencies --	1005.6640	1006.8604	1013.1517
	82	83	84
Frequencies --	1026.9412	1027.3980	1059.0620

	85	86	87
Frequencies --	1059.9770	1126.4619	1130.8639
	88	89	90
Frequencies --	1139.8111	1142.1530	1175.1762
	91	92	93
Frequencies --	1187.7404	1198.6532	1201.3337
	94	95	96
Frequencies --	1214.2808	1217.1007	1233.0816
	97	98	99
Frequencies --	1234.9255	1241.3358	1257.1408
	100	101	102
Frequencies --	1286.2232	1294.9671	1303.6737
	103	104	105
Frequencies --	1305.1162	1311.2334	1320.7959
	106	107	108
Frequencies --	1336.7618	1339.7535	1344.3609
	109	110	111
Frequencies --	1349.5117	1351.7776	1383.1469
	112	113	114
Frequencies --	1414.5452	1414.9133	1439.5910
	115	116	117
Frequencies --	1449.9523	1454.4105	1480.2514
	118	119	120
Frequencies --	1482.7818	1484.0041	1488.4135
	121	122	123
Frequencies --	1491.4295	1491.6266	1505.7599
	124	125	126
Frequencies --	1528.9922	1536.4789	1544.7349
	127	128	129
Frequencies --	1552.2937	1586.1196	1601.6983
	130	131	132
Frequencies --	1611.8538	1624.8866	1638.1810
	133	134	135
Frequencies --	1647.8863	1656.3040	2198.7331
	136	137	138

Frequencies --	3027.0221	3028.6796	3081.5791
	139	140	141
Frequencies --	3083.6663	3113.6626	3113.8712
	142	143	144
Frequencies --	3136.1163	3148.5146	3160.7065
	145	146	147
Frequencies --	3164.0151	3169.8895	3170.5498
	148	149	150
Frequencies --	3172.3826	3172.9906	3176.3803
	151	152	153
Frequencies --	3177.4894	3189.0918	3189.2625
	154	155	156
Frequencies --	3196.7198	3197.3522	3204.5872
	157	158	159
Frequencies --	3205.7873	3206.7628	3207.8230

G11. MTPAcc *Neutral* Vibrational Frequencies in cm^{-1}

	1	2	3
Frequencies --	6.5055	8.2548	15.3068
	4	5	6
Frequencies --	17.9474	27.4007	32.6649
	7	8	9
Frequencies --	34.2891	41.9434	5.9670
	10	11	12
Frequencies --	47.0709	52.7576	61.0438
	13	14	15
Frequencies --	74.4263	82.2365	92.8979
	16	17	18
Frequencies --	109.9583	120.1883	145.3035
	19	20	21
Frequencies --	158.3494	162.7965	186.2227

	22	23	24
Frequencies --	199.9094	215.1490	245.0815
	25	26	27
Frequencies --	255.5020	282.3498	289.1199
	28	29	30
Frequencies --	297.5964	319.6520	343.5611
	31	32	33
Frequencies --	349.2924	357.9069	374.8697
	34	35	36
Frequencies --	386.7036	402.2803	420.5184
	37	38	39
Frequencies --	421.7886	425.1485	427.2504
	40	41	42
Frequencies --	434.8824	466.0729	485.6421
	43	44	45
Frequencies --	498.7622	500.5935	512.8894
	46	47	48
Frequencies --	516.5511	528.4881	544.1257
	49	50	51
Frequencies --	573.2338	575.7132	607.2713
	52	53	54
Frequencies --	611.4252	641.6541	647.8291
	55	56	57
Frequencies --	648.6288	655.3565	668.5698
	58	59	60
Frequencies --	690.5109	718.3059	722.7231
	61	62	63
Frequencies --	728.3063	739.7227	770.7337
	64	65	66
Frequencies --	789.0217	791.8769	810.4353
	67	68	69
Frequencies --	826.3724	829.6755	833.7353
	70	71	72
Frequencies --	834.4748	836.6363	837.1127

	73	74	75
Frequencies --	842.7014	843.8517	849.8587
	76	77	78
Frequencies --	866.7150	887.3136	899.4809
	79	80	81
Frequencies --	933.2045	935.2165	962.1820
	82	83	84
Frequencies --	965.8952	966.3756	970.0079
	85	86	87
Frequencies --	980.6729	982.1968	982.9435
	88	89	90
Frequencies --	986.9752	994.4012	999.7806
	91	92	93
Frequencies --	1007.3208	1007.8923	1020.0626
	94	95	96
Frequencies --	1022.2066	1030.8743	1031.4885
	97	98	99
Frequencies --	1059.7372	1060.6268	1079.8770
	100	101	102
Frequencies --	1137.5804	1138.8907	1148.4239
	103	104	105
Frequencies --	1153.3641	1168.0058	1187.6565
	106	107	108
Frequencies --	1196.9063	1199.8880	1208.3871
	109	110	111
Frequencies --	1215.3055	1231.5015	1233.3646
	112	113	114
Frequencies --	1233.7637	1261.8232	1272.7001
	115	116	117
Frequencies --	1291.3513	1309.6252	1315.0651
	118	119	120
Frequencies --	1318.2442	1337.0711	1338.8478
	121	122	123
Frequencies --	1339.2636	1346.3565	1349.3630

	124	125	126
Frequencies --	1356.8937	1361.1105	1374.5672
	127	128	129
Frequencies --	1391.8437	1414.1970	1414.6517
	130	131	132
Frequencies --	1421.7158	1438.3630	1444.6350
	133	134	135
Frequencies --	1461.8304	1470.4532	1482.6590
	136	137	138
Frequencies --	1482.8146	1487.1873	1489.2627
	139	140	141
Frequencies --	1534.3190	1540.4600	1540.7853
	142	143	144
Frequencies --	1548.7305	1569.5581	1579.1656
	145	146	147
Frequencies --	1590.9680	1611.4732	1616.0685
	148	149	150
Frequencies --	1630.0300	1649.3808	1651.2268
	151	152	153
Frequencies --	1658.3954	1675.6978	1734.1227
	154	155	156
Frequencies --	2312.6119	3032.2541	3033.6185
	157	158	159
Frequencies --	3090.8725	3091.1867	3119.7554
	160	161	162
Frequencies --	3121.0810	3161.9884	3172.0141
	163	164	165
Frequencies --	3177.7781	3177.8260	3178.9304
	166	167	168
Frequencies --	3179.2187	3182.0381	3186.5904
	169	170	171
Frequencies --	3198.0794	3200.6487	3202.8294
	172	173	174
Frequencies --	3203.5029	3204.0719	3204.8913

	175	176	177
Frequencies --	3205.4336	3210.3939	3217.3241

	178	179	180
Frequencies --	3218.2914	3244.8561	3758.1626

G12. MTPAcc *Anion* Vibrational Frequencies in cm^{-1} (being recalculated)

	1	2	3
Frequencies --	-36.2378	10.9434	12.0037
	4	5	6
Frequencies --	17.5509	25.1130	29.5404
	7	8	9
Frequencies --	34.2863	36.8406	40.6823
	10	11	12
Frequencies --	47.4677	50.4667	70.6007
	13	14	15
Frequencies --	81.5498	87.7615	91.4728
	16	17	18
Frequencies --	116.6816	120.4859	142.7389
	19	20	21
Frequencies --	157.5892	163.6082	189.2540
	22	23	24
Frequencies --	199.0541	214.7211	240.7498
	25	26	27
Frequencies --	259.0111	283.2732	289.1764
	28	29	30
Frequencies --	299.1242	314.8086	337.8297
	31	32	33
Frequencies --	346.3362	356.4424	372.8527
	34	35	36
Frequencies --	378.2241	402.2064	421.1660
	37	38	39
Frequencies --	422.8924	427.1229	431.9936
	40	41	42

Frequencies --	446.9204	460.8455	482.2630
	43	44	45
Frequencies --	489.6331	491.6284	504.1219
	46	47	48
Frequencies --	512.6787	514.4148	529.6318
	49	50	51
Frequencies --	569.0494	570.8764	574.2785
	52	53	54
Frequencies --	605.5474	639.1214	648.5337
	55	56	57
Frequencies --	648.8539	655.0688	666.4485
	58	59	60
Frequencies --	682.6220	706.5548	720.7705
	61	62	63
Frequencies --	726.6111	732.9844	741.4475
	64	65	66
Frequencies --	780.1190	790.4589	797.3458
	67	68	69
Frequencies --	809.0725	817.4538	825.4761
	70	71	72
Frequencies --	829.6057	830.2971	833.8996
	73	74	75
Frequencies --	834.9063	842.5223	843.3445
	76	77	78
Frequencies --	847.4164	863.1548	871.8110
	79	80	81
Frequencies --	878.8242	931.6538	933.5039
	82	83	84
Frequencies --	953.7733	959.5281	963.1884
	85	86	87
Frequencies --	964.2512	973.0114	974.0749
	88	89	90
Frequencies --	976.9152	980.4917	980.9631

	91	92	93
Frequencies --	1002.5876	1006.3411	1007.4203
	94	95	96
Frequencies --	1021.0318	1029.2517	1029.3972
	97	98	99
Frequencies --	1046.4299	1059.3667	1059.6008
	100	101	102
Frequencies --	1136.6004	1139.0625	1140.4961
	103	104	105
Frequencies --	1141.2944	1163.7036	1182.9518
	106	107	108
Frequencies --	1190.0667	1200.3169	1200.8490
	109	110	111
Frequencies --	1215.0455	1225.4045	1232.1398
	112	113	114
Frequencies --	1234.0221	1253.1089	1265.6192
	115	116	117
Frequencies --	1298.6918	1302.4042	1303.3128
	118	119	120
Frequencies --	1309.2432	1320.9784	1325.2041
	121	122	123
Frequencies --	1337.3307	1339.1982	1342.6155
	124	125	126
Frequencies --	1349.9162	1350.7410	1366.9064
	127	128	129
Frequencies --	1381.0210	1385.5646	1414.2579
	130	131	132
Frequencies --	1414.5309	1438.3293	1447.5976
	133	134	135
Frequencies --	1456.4840	1474.2036	1481.3094
	136	137	138
Frequencies --	1482.7294	1487.5798	1489.4631
	139	140	141
Frequencies --	1502.1870	1529.1081	1534.0976

	142	143	144
Frequencies --	1539.0378	1546.1551	1555.7920
	145	146	147
Frequencies --	1569.1046	1589.4654	1607.9210
	148	149	150
Frequencies --	1614.3691	1637.6137	1643.3928
	151	152	153
Frequencies --	1649.0779	1651.9695	1658.0881
	154	155	156
Frequencies --	2240.9730	3029.4388	3030.3284
	157	158	159
Frequencies --	3086.3618	3087.5898	3116.5384
	160	161	162
Frequencies --	3116.6506	3143.2236	3156.6561
	163	164	165
Frequencies --	3158.8350	3173.4200	3173.5903
	166	167	168
Frequencies --	3174.8821	3175.5375	3176.6358
	169	170	171
Frequencies --	3177.1251	3183.8931	3190.0346
	172	173	174
Frequencies --	3194.5521	3203.7644	3204.2703
	175	176	177
Frequencies --	3204.5053	3205.4530	3205.7164
	178	179	180
Frequencies --	3206.3829	3230.7534	3774.7311

G13. MTPAn *Neutral* Vibrational Frequencies in cm^{-1}

	1	2	3
Frequencies --	11.1321	16.0553	19.4366
	4	5	6
Frequencies --	23.3518	31.1533	34.0344

	7	8	9
Frequencies --	40.2262	40.9026	47.1389
	10	11	12
Frequencies --	56.7190	62.4251	77.7444
	13	14	15
Frequencies --	86.1475	123.7909	144.5256
	16	17	18
Frequencies --	151.3888	165.0600	183.1346
	19	20	21
Frequencies --	195.4510	255.7267	268.2921
	22	23	24
Frequencies --	287.1634	290.8737	308.6286
	25	26	27
Frequencies --	332.8568	348.4170	357.7215
	28	29	30
Frequencies --	367.4837	382.0089	420.0561
	31	32	33
Frequencies --	420.7998	423.3256	426.2337
	34	35	36
Frequencies --	435.6955	462.8610	478.4432
	37	38	39
Frequencies --	493.2994	513.5681	517.4280
	40	41	42
Frequencies --	537.2822	541.0192	573.1344
	43	44	45
Frequencies --	592.3079	640.9840	645.8155
	46	47	48
Frequencies --	649.0305	650.2383	656.0947
	49	50	51
Frequencies --	693.9158	696.4420	721.4263

	52	53	54
Frequencies --	729.5260	730.4350	755.3111
	55	56	57
Frequencies --	793.1553	808.6876	825.6006
	58	59	60
Frequencies --	830.0190	831.2198	834.3482
	61	62	63
Frequencies --	834.9446	836.2455	844.0485
	64	65	66
Frequencies --	844.2948	856.0791	859.2980
	67	68	69
Frequencies --	887.7147	900.0965	933.1559
	70	71	72
Frequencies --	935.5125	962.5002	966.4964
	73	74	75
Frequencies --	967.1334	980.2055	982.9475
	76	77	78
Frequencies --	983.0342	984.2041	994.3161
	79	80	81
Frequencies --	998.2651	1007.8894	1009.5883
	82	83	84
Frequencies --	1020.0144	1020.6187	1031.7086
	85	86	87
Frequencies --	1032.4854	1060.2272	1061.2082
	88	89	90
Frequencies --	1122.5147	1137.5978	1138.4762
	91	92	93
Frequencies --	1139.5684	1150.1998	1188.2131
	94	95	96
Frequencies --	1199.8922	1200.5705	1210.0933

	97	98	99
Frequencies --	1214.1810	1224.7311	1232.2268
	100	101	102
Frequencies --	1233.9381	1264.4677	1290.6597
	103	104	105
Frequencies --	1308.1470	1310.4132	1316.4850
	106	107	108
Frequencies --	1323.8267	1332.7259	1337.7372
	109	110	111
Frequencies --	1339.6571	1351.2707	1352.9925
	112	113	114
Frequencies --	1359.4293	1366.5273	1394.4564
	115	116	117
Frequencies --	1414.7324	1416.1062	1438.7674
	118	119	120
Frequencies --	1444.9237	1453.7801	1469.4800
	121	122	123
Frequencies --	1479.6652	1483.2251	1488.2763
	124	125	126
Frequencies --	1491.1021	1522.3808	1527.5977
	127	128	129
Frequencies --	1539.1218	1540.9513	1547.5997
	130	131	132
Frequencies --	1585.5797	1609.1817	1612.5400
	133	134	135
Frequencies --	1616.9270	1620.0616	1646.7380
	136	137	138
Frequencies --	1649.5345	1657.4227	1674.7531
	139	140	141
Frequencies --	3033.1570	3035.6176	3089.0710

	142	143	144
Frequencies --	3091.2922	3120.9084	3121.4952
	145	146	147
Frequencies --	3163.0001	3173.8904	3177.4923
	148	149	150
Frequencies --	3178.0291	3179.0582	3180.4846
	151	152	153
Frequencies --	3182.2446	3197.7592	3199.4409
	154	155	156
Frequencies --	3203.7068	3203.9498	3205.1230
	157	158	159
Frequencies --	3205.3776	3216.0978	3217.3376
	160	161	162
Frequencies --	3218.9779	3243.6290	3244.1374

G14. MTPAn *Anion* Vibrational Frequencies in cm^{-1}

	1	2	3
Frequencies --	11.7784	17.1025	23.6254
	4	5	6
Frequencies --	24.0547	34.8023	37.1875
	7	8	9
Frequencies --	39.8540	44.8654	52.5901
	10	11	12
Frequencies --	55.9558	81.8322	87.0137
	13	14	15
Frequencies --	104.7157	122.2137	142.1391
	16	17	18
Frequencies --	160.4394	162.3931	187.9088
	19	20	21
Frequencies --	197.5127	257.7031	264.2858

	22	23	24
Frequencies --	283.6827	288.0130	308.0204
	25	26	27
Frequencies --	326.7123	341.7539	357.7822
	28	29	30
Frequencies --	366.7541	382.0544	420.5620
	31	32	33
Frequencies --	423.3454	427.5226	434.8975
	34	35	36
Frequencies --	436.2142	443.0582	458.5192
	37	38	39
Frequencies --	481.1045	509.2503	514.7914
	40	41	42
Frequencies --	526.2145	537.7938	551.6651
	43	44	45
Frequencies --	574.4627	591.2191	633.8629
	46	47	48
Frequencies --	642.1344	649.1208	649.8199
	49	50	51
Frequencies --	655.4051	676.0484	703.3788
	52	53	54
Frequencies --	721.1698	726.8232	733.4067
	55	56	57
Frequencies --	775.4512	790.7034	810.0573
	58	59	60
Frequencies --	811.0058	815.5251	827.5739
	61	62	63
Frequencies --	832.7635	833.6338	836.6220
	64	65	66
Frequencies --	838.6819	841.7952	842.8515
	67	68	69
Frequencies --	876.1943	880.5280	931.9427
	70	71	72
Frequencies --	934.3951	955.3839	959.1095

	73	74	75
Frequencies --	963.0774	963.9111	973.4994
	76	77	78
Frequencies --	974.7515	979.6353	980.3134
	79	80	81
Frequencies --	980.6291	1003.4714	1007.0838
	82	83	84
Frequencies --	1008.1402	1022.3582	1029.3648
	85	86	87
Frequencies —	1029.9022	1059.4716	1059.7428
	88	89	90
Frequencies —	1067.2632	1122.3286	1138.6416
	91	92	93
Frequencies --	1140.5649	1141.2165	1186.8919
	94	95	96
Frequencies --	1189.7500	1200.7355	1201.5879
	97	98	99
Frequencies --	1215.3162	1216.3190	1232.5899
	100	101	102
Frequencies --	1234.3346	1255.2384	1283.2970
	103	104	105
Frequencies --	1297.6374	1301.4663	1303.7662
	106	107	108
Frequencies --	1311.1236	1324.6802	1337.6987
	109	110	111
Frequencies —-	1339.5119	1341.6386	1350.0650
	112	113	114
Frequencies --	1351.9118	1354.6330	1381.6891
	115	116	117
Frequencies --	1390.0390	1414.6356	1414.9789
	118	119	120
Frequencies --	1438.5925	1447.7277	1456.4181
	121	122	123
Frequencies --	1467.8251	1483.0526	1483.0769
	124	125	126

Frequencies --	1487.3370	1489.4258	1515.4372
	127	128	129
Frequencies --	1537.7080	1539.2668	1546.7933
	130	131	132
Frequencies --	1556.0753	1582.6461	1596.2882
	133	134	135
Frequencies --	1608.7518	1614.8271	1639.6297
	136	137	138
Frequencies --	1648.9833	1654.1199	1660.0533
	139	140	141
Frequencies --	3029.6691	3029.9288	3087.4811
	142	143	144
Frequencies --	3088.0223	3116.8904	3116.9187
	145	146	147
Frequencies --	3145.4165	3157.3900	3169.7722
	148	149	150
Frequencies --	3174.1529	3174.2908	3175.1985
	151	152	153
Frequencies --	3175.5219	3176.1220	3189.8496
	154	155	156
Frequencies --	3190.4228	3203.5407	3204.2573
	157	158	159
Frequencies --	3205.0644	3205.3381	3205.4414
	160	161	162
Frequencies --	3206.7812	3233.9248	3235.7590

APPENDIX H

PREDICTED EXCITATION ENERGIES OF THE 7 MTPA DERIVATIVES USING B3LYP/TD-CAMB3LYP AND 6-31+G (d,p) BASIS SET

H1. Excited State Energies with Oscillator Strength of MTPAa

```
Excited State   1:    Singlet-A       3.3924 eV  365.48 nm  f=1.5281
     104 ->105         0.67409

Excited State   2:    Singlet-A       3.9833 eV  311.26 nm  f=0.0662
     103 ->106        -0.24567
     104 ->106         0.62010
     104 ->113         0.10882

Excited State   3:    Singlet-A       4.2698 eV  290.38 nm  f=0.3607
     103 ->107        -0.31324
     104 ->107         0.60370

Excited State   4:    Singlet-A       4.2842 eV  289.40 nm  f=0.0124
     103 ->105         0.51672
     103 ->108        -0.14534
     104 ->108        -0.36912

Excited State   5:    Singlet-A       4.4980 eV  275.64 nm  f=0.1506
      98 ->105         0.16061
     103 ->105         0.31686
     103 ->108         0.32681
     104 ->108         0.34604
     104 ->110        -0.21386
     104 ->111         0.17544

Excited State   6:    Singlet-A       4.5743 eV  271.05 nm  f=0.0413
      97 ->105        -0.13583
     102 ->106         0.14041
     103 ->106         0.20402
     103 ->108        -0.11496
     103 ->113        -0.11614
     104 ->113         0.55425

Excited State   7:    Singlet-A       4.7131 eV  263.06 nm  f=0.0191
      97 ->107         0.11009
     101 ->106        -0.13708
     103 ->112        -0.30948
     104 ->112         0.53810

Excited State   8:    Singlet-A       4.9413 eV  250.91 nm  f=0.0015
     103 ->110         0.12967
     103 ->111         0.14239
```

```
     104 ->109         0.60200
     104 ->115        -0.17703

Excited State   9:    Singlet-A       5.0568 eV  245.18 nm  f=0.0016
     102 ->111        -0.10119
     103 ->105         0.13353
     103 ->109         0.22038
     103 ->110         0.17636
     103 ->111         0.20754
     104 ->108         0.12763
     104 ->110         0.48229
     104 ->111         0.18614

Excited State  10:    Singlet-A       5.0784 eV  244.14 nm  f=0.0017
     103 ->105        -0.25435
     103 ->109         0.12113
     103 ->110         0.10899
     104 ->108        -0.20243
     104 ->110        -0.16721
     104 ->111         0.48417

Excited State  11:    Singlet-A       5.2970 eV  234.07 nm  f=0.0097
     102 ->105        -0.15601
     103 ->110        -0.17055
     103 ->111         0.15263
     104 ->116         0.52047
     104 ->117         0.15054
     104 ->121         0.13778

Excited State  12:    Singlet-A       5.3634 eV  231.17 nm  f=0.0095
     102 ->109        -0.10347
     103 ->109        -0.17792
     103 ->110         0.12008
     103 ->111         0.14382
     103 ->119        -0.11240
     104 ->115         0.51476
     104 ->118        -0.20864
     104 ->124         0.13528
```

H2. Excited State Energies with Oscillator Strength of MTPAo

```
Excited State   1:    Singlet-A       3.4360 eV  360.84 nm  f=1.4743
     107 ->109         0.12161
     108 ->109         0.66846

Excited State   2:    Singlet-A       4.0012 eV  309.87 nm  f=0.0640
     107 ->110        -0.17903
     108 ->110         0.64290
```

```
Excited State   3:    Singlet-A       4.2877 eV  289.17 nm  f=0.3576
     107 ->111        -0.24852
     108 ->111         0.63329

Excited State   4:    Singlet-A       4.4095 eV  281.18 nm  f=0.0597
     107 ->109         0.54127
     107 ->112         0.12675
     108 ->112         0.27507
     108 ->114        -0.24261

Excited State   5:    Singlet-A       4.5966 eV  269.73 nm  f=0.1164
     101 ->109        -0.14063
     107 ->109         0.17273
     107 ->110        -0.20388
     108 ->112        -0.18508
     108 ->116         0.48040
     108 ->117        -0.22044

Excited State   6:    Singlet-A       4.6514 eV  266.55 nm  f=0.0784
     102 ->109         0.19234
     102 ->114        -0.10086
     107 ->109        -0.17976
     107 ->112         0.38692
     108 ->112         0.35433
     108 ->114         0.19568
     108 ->116         0.18235

Excited State   7:    Singlet-A       4.7273 eV  262.27 nm  f=0.0122
     101 ->111         0.10739
     106 ->110        -0.13477
     107 ->115        -0.25183
     108 ->115         0.55835

Excited State   8:    Singlet-A       4.9908 eV  248.43 nm  f=0.0023
     107 ->113        -0.10065
     108 ->113         0.61904
     108 ->120         0.16593
     108 ->122        -0.10912

Excited State   9:    Singlet-A       5.1084 eV  242.71 nm  f=0.0103
     107 ->109         0.28915
     108 ->109        -0.13605
     108 ->112        -0.14201
     108 ->114         0.53550

Excited State  10:    Singlet-A       5.3723 eV  230.78 nm  f=0.0120
     107 ->113        -0.18234
     107 ->114         0.14189
     107 ->117         0.11504
     108 ->116         0.16362
     108 ->117         0.36817
     108 ->119         0.21529
```

```
     108 ->120        -0.31993
     108 ->121         0.11494
     108 ->122        -0.14380
     108 ->129         0.11510

Excited State  11:    Singlet-A       5.3755 eV  230.65 nm  f=0.0102
     107 ->113         0.16182
     107 ->114         0.12434
     108 ->116        -0.14959
     108 ->117        -0.23107
     108 ->119         0.48276
     108 ->121         0.18778

Excited State  12:    Singlet-A       5.4765 eV  226.39 nm  f=0.1009
     101 ->109        -0.25187
     103 ->109        -0.28475
     106 ->109         0.29515
     107 ->110        -0.13118
     107 ->116         0.15252
     108 ->116        -0.16572
     108 ->118         0.16842
     108 ->119        -0.16312
```

H3. Excited State Energies with Oscillator Strength of MTPA

```
Excited State   1:    Singlet-A       3.4291 eV  361.56 nm  f=1.3539
      99 ->101         0.15536
     100 ->101         0.66016

Excited State   2:    Singlet-A       4.0230 eV  308.19 nm  f=0.0573
      99 ->102        -0.12123
     100 ->102         0.65554

Excited State   3:    Singlet-A       4.3111 eV  287.59 nm  f=0.3492
      99 ->103        -0.19420
     100 ->103         0.65229

Excited State   4:    Singlet-A       4.4985 eV  275.61 nm  f=0.0729
      99 ->101         0.52836
     100 ->104        -0.32312
     100 ->105         0.18924
     100 ->108        -0.13141

Excited State   5:    Singlet-A       4.6273 eV  267.94 nm  f=0.0882
      94 ->101        -0.15247
      95 ->101        -0.10223
      99 ->101         0.17392
      99 ->102         0.19822
     100 ->105         0.13616
```

```
     100 ->108         0.53290

Excited State   6:    Singlet-A       4.7399 eV  261.58 nm  f=0.0152
      94 ->103         0.10616
      98 ->102        -0.13827
      99 ->107        -0.21294
     100 ->107         0.58394

Excited State   7:    Singlet-A       4.8506 eV  255.61 nm  f=0.0258
      93 ->104         0.11092
      96 ->101         0.36560
      96 ->105         0.13740
      99 ->101        -0.13255
      99 ->104        -0.29699
      99 ->105        -0.18622
     100 ->104        -0.27241
     100 ->105        -0.23344
     100 ->108         0.12246

Excited State   8:    Singlet-A       5.0311 eV  246.43 nm  f=0.0029
     100 ->106         0.62294
     100 ->112        -0.18395

Excited State   9:    Singlet-A       5.0920 eV  243.49 nm  f=0.0299
      99 ->101        -0.32073
     100 ->101         0.18033
     100 ->104        -0.31198
     100 ->105         0.42489

Excited State  10:    Singlet-A       5.4075 eV  229.28 nm  f=0.0156
      94 ->101        -0.12674
      95 ->101        -0.14034
      98 ->101         0.12738
      99 ->104         0.10902
      99 ->105        -0.13483
     100 ->108        -0.10720
     100 ->111         0.54916
     100 ->113        -0.13678

Excited State  11:    Singlet-A       5.4525 eV  227.39 nm  f=0.1164
      94 ->101        -0.27529
      95 ->101        -0.30543
      98 ->101         0.31002
      99 ->108         0.13455
     100 ->108        -0.18520
     100 ->111        -0.25645

Excited State  12:    Singlet-A       5.4831 eV  226.12 nm  f=0.0208
      99 ->106         0.22095
     100 ->109         0.48722
     100 ->112        -0.26552
     100 ->114        -0.20389
```

```
     100 ->120         0.13347
```

H4. Excited State Energies with Oscillator Strength of MTPAcl

```
Excited State   1:    Singlet-A       3.3827 eV  366.53 nm  f=1.4443
     107 ->109         0.16365
     108 ->109         0.65700
     108 ->113         0.13176

Excited State   2:    Singlet-A       4.0309 eV  307.58 nm  f=0.0553
     107 ->110        -0.11676
     108 ->110         0.65425

Excited State   3:    Singlet-A       4.3246 eV  286.69 nm  f=0.3448
     107 ->111        -0.11823
     107 ->112        -0.14925
     108 ->111         0.41597
     108 ->112         0.50384

Excited State   4:    Singlet-A       4.4545 eV  278.33 nm  f=0.0780
     107 ->109         0.52866
     108 ->111         0.18286
     108 ->112        -0.15271
     108 ->113        -0.29903

Excited State   5:    Singlet-A       4.6285 eV  267.87 nm  f=0.0827
     102 ->109        -0.14139
     104 ->109        -0.10276
     107 ->109         0.12962
     107 ->110         0.19957
     108 ->111        -0.10134
     108 ->116        -0.21900
     108 ->117         0.50652

Excited State   6:    Singlet-A       4.7360 eV  261.79 nm  f=0.0670
     101 ->109        -0.23023
     101 ->113         0.10071
     107 ->109         0.10418
     107 ->111        -0.24822
     107 ->112         0.20410
     107 ->115        -0.11082
     108 ->111        -0.25007
     108 ->112         0.21053
     108 ->113        -0.11996
     108 ->115         0.32148
     108 ->117        -0.13061

Excited State   7:    Singlet-A       4.7523 eV  260.89 nm  f=0.0051
     101 ->109         0.15236
     106 ->110         0.10967
     107 ->109        -0.14689
     107 ->111         0.15910
     107 ->112        -0.12727
```

```
     107 ->115        -0.16744
     108 ->111         0.15440
     108 ->112        -0.13333
     108 ->115         0.45818
     108 ->116        -0.16759

Excited State   8:    Singlet-A       5.0326 eV  246.36 nm  f=0.0341
     107 ->109         0.28903
     108 ->109        -0.17059
     108 ->113         0.44734
     108 ->114         0.29862

Excited State   9:    Singlet-A       5.0505 eV  245.49 nm  f=0.0102
     107 ->109        -0.15622
     108 ->113        -0.24817
     108 ->114         0.54255
     108 ->122        -0.13662

Excited State  10:    Singlet-A       5.3868 eV  230.16 nm  f=0.0574
     102 ->109        -0.12053
     103 ->109        -0.19079
     104 ->109        -0.22820
     106 ->109         0.21568
     107 ->113         0.17176
     108 ->113         0.11055
     108 ->117        -0.15047
     108 ->120         0.41429

Excited State  11:    Singlet-A       5.4365 eV  228.06 nm  f=0.0809
     102 ->109         0.17582
     103 ->109         0.15350
     104 ->109         0.25283
     106 ->109        -0.25068
     108 ->117         0.10979
     108 ->120         0.41501

Excited State  12:    Singlet-A       5.4854 eV  226.02 nm  f=0.0109
     107 ->114         0.23432
     108 ->115         0.13712
     108 ->116         0.36540
     108 ->117         0.13102
     108 ->119         0.37000
     108 ->123         0.18588
     108 ->128         0.12302
```

H5. Excited State Energies with Oscillator Strength of MTPAc

```
Excited State   1:    Singlet-A       3.1836 eV  389.45 nm  f=1.5889
     105 ->107        -0.19795
```

```
     106 ->107         0.64365
     106 ->109         0.14106

Excited State   2:    Singlet-A       4.0530 eV  305.91 nm  f=0.0449
     106 ->108         0.62240
     106 ->109        -0.20289

Excited State   3:    Singlet-A       4.3438 eV  285.43 nm  f=0.0895
     100 ->107        -0.11764
     105 ->107         0.53748
     106 ->109         0.28552
     106 ->110         0.24468

Excited State   4:    Singlet-A       4.3628 eV  284.19 nm  f=0.3322
     105 ->111         0.17113
     106 ->111         0.65186

Excited State   5:    Singlet-A       4.6284 eV  267.88 nm  f=0.0353
      99 ->107         0.14476
     101 ->107         0.15631
     105 ->108         0.21751
     106 ->109        -0.23195
     106 ->110         0.15390
     106 ->115         0.46134

Excited State   6:    Singlet-A       4.6969 eV  263.97 nm  f=0.0118
      99 ->107         0.38134
     100 ->110         0.11267
     105 ->109         0.16464
     105 ->110        -0.27160
     106 ->108        -0.10781
     106 ->109        -0.16437
     106 ->110         0.25583
     106 ->115        -0.26782

Excited State   7:    Singlet-A       4.7655 eV  260.17 nm  f=0.0024
     104 ->108         0.12248
     105 ->107        -0.17356
     105 ->114         0.17053
     106 ->107        -0.11142
     106 ->109         0.13504
     106 ->110         0.11869
     106 ->114         0.52256
     106 ->115         0.11722

Excited State   8:    Singlet-A       4.7936 eV  258.65 nm  f=0.1294
     105 ->107        -0.30554
     105 ->114        -0.10195
     106 ->107        -0.22090
     106 ->108         0.11933
     106 ->109         0.35165
     106 ->110         0.26890
```

```
     106 ->114        -0.25814

Excited State   9:    Singlet-A       5.0857 eV  243.79 nm  f=0.0024
     106 ->112         0.59006
     106 ->113         0.19699
     106 ->118         0.14593
     106 ->120        -0.10509

Excited State  10:    Singlet-A       5.2512 eV  236.11 nm  f=0.1615
      99 ->107         0.18787
     101 ->107         0.29355
     102 ->107         0.26909
     104 ->107         0.25095
     105 ->109        -0.12956
     106 ->108         0.13103
     106 ->109         0.12453
     106 ->110        -0.13192
     106 ->115        -0.18656
     106 ->117         0.17039

Excited State  11:    Singlet-A       5.3541 eV  231.57 nm  f=0.0180
      99 ->107         0.40701
     101 ->107        -0.15061
     102 ->107        -0.15922
     104 ->107        -0.16582
     105 ->109        -0.10197
     106 ->109         0.18907
     106 ->110        -0.30196
     106 ->115         0.15131

Excited State  12:    Singlet-A       5.4006 eV  229.58 nm  f=0.0835
      99 ->107        -0.18974
     104 ->107        -0.10584
     105 ->109        -0.12334
     105 ->110        -0.13966
     106 ->110         0.18383
     106 ->116         0.27915
     106 ->117         0.42651
     106 ->119         0.11630
```

H6. Excited State Energies with Oscillator Strength of MTPAcc

```
Excited State   1:     Singlet-A      2.7236 eV  455.22 nm  f=1.8771
     123 ->125        -0.25906
     124 ->125         0.61803
     124 ->126        -0.18831

Excited State   2:    Singlet-A       3.8065 eV  325.72 nm  f=0.0660
```

```
     119 ->125         0.19210
     121 ->125         0.13016
     123 ->125         0.52814
     124 ->125         0.13159
     124 ->126        -0.33905

Excited State   3:    Singlet-A       4.0324 eV  307.47 nm  f=0.0532
     123 ->125         0.16867
     123 ->127         0.10125
     124 ->125         0.15010
     124 ->126         0.25657
     124 ->127         0.55341
     124 ->134         0.11863

Excited State   4:    Singlet-A       4.1467 eV  298.99 nm  f=0.2249
     123 ->125         0.21004
     123 ->126        -0.13269
     124 ->125         0.25023
     124 ->126         0.45051
     124 ->127        -0.33660

Excited State   5:    Singlet-A       4.3392 eV  285.73 nm  f=0.0336
     117 ->125         0.61428
     123 ->129        -0.17495
     124 ->129         0.21377

Excited State   6:    Singlet-A       4.3699 eV  283.73 nm  f=0.3025
     123 ->128         0.19211
     124 ->128         0.64772

Excited State   7:    Singlet-A       4.6301 eV  267.78 nm  f=0.0427
     118 ->125         0.16006
     118 ->126        -0.14688
     120 ->125         0.10278
     123 ->126        -0.12409
     123 ->127        -0.17438
     124 ->127        -0.10010
     124 ->129        -0.17221
     124 ->132        -0.17826
     124 ->133         0.18700
     124 ->134         0.43150

Excited State   8:    Singlet-A       4.7253 eV  262.39 nm  f=0.0474
     116 ->125        -0.20137
     117 ->125        -0.14599
     119 ->125         0.29863
     120 ->125         0.10970
     121 ->125         0.18865
     123 ->125        -0.10635
     123 ->126         0.30873
     124 ->129         0.20197
     124 ->133        -0.16479
```

```
     124 ->134         0.22792

Excited State   9:    Singlet-A       4.7800 eV  259.38 nm  f=0.0328
     122 ->127         0.12654
     123 ->133         0.18701
     124 ->132         0.30240
     124 ->133         0.48231

Excited State  10:    Singlet-A       4.9910 eV  248.41 nm  f=0.1031
     116 ->125         0.17000
     117 ->125        -0.16180
     119 ->125        -0.35759
     121 ->125        -0.20774
     123 ->125         0.17911
     123 ->129        -0.13915
     124 ->126        -0.11549
     124 ->129         0.36318

Excited State  11:    Singlet-A       5.0634 eV  244.87 nm  f=0.0171
     118 ->125        -0.15541
     120 ->125        -0.17270
     122 ->125         0.17505
     124 ->130        -0.18801
     124 ->131         0.47564
     124 ->134         0.17087
     124 ->139         0.15537

Excited State  12:    Singlet-A       5.1253 eV  241.91 nm  f=0.0437
     118 ->125         0.24453
     118 ->126        -0.10417
     120 ->125         0.25368
     120 ->126        -0.11365
     122 ->125        -0.26319
     122 ->126         0.10621
     124 ->130        -0.13453
     124 ->131         0.34792
     124 ->134        -0.21862
     124 ->139         0.10846
```

H7. Excited State Energies with Oscillator Strength of MTPAn

```
Excited State   1:    Singlet-A       2.8241 eV  439.03 nm  f=1.4711
     110 ->112         0.23208
     111 ->112         0.61923
     111 ->113         0.21791

Excited State   2:    Singlet-A       3.8127 eV  325.19 nm  f=0.0000
     102 ->112         0.63918
```

```
     102 ->113        -0.26432

Excited State   3:    Singlet-A       3.9414 eV  314.57 nm  f=0.0108
     105 ->112         0.15973
     110 ->112        -0.37217
     111 ->113         0.49993
     111 ->114         0.14239
     111 ->118         0.10788

Excited State   4:    Singlet-A       4.0788 eV  303.97 nm  f=0.0303
     110 ->112         0.27494
     111 ->112        -0.12530
     111 ->114         0.57047
     111 ->120         0.10369

Excited State   5:    Singlet-A       4.1741 eV  297.03 nm  f=0.2915
     105 ->112        -0.10548
     110 ->112         0.37516
     110 ->113         0.16636
     111 ->112        -0.29787
     111 ->113         0.35019
     111 ->114        -0.27386

Excited State   6:    Singlet-A       4.3360 eV  285.94 nm  f=0.0194
     104 ->112         0.63929
     110 ->115         0.15829
     111 ->115         0.18426

Excited State   7:    Singlet-A       4.3960 eV  282.04 nm  f=0.3101
     110 ->116        -0.16698
     111 ->116         0.65573

Excited State   8:    Singlet-A       4.6434 eV  267.01 nm  f=0.0381
     106 ->112         0.17255
     106 ->113         0.16710
     107 ->112         0.11512
     110 ->114         0.19471
     111 ->114        -0.11259
     111 ->115         0.13765
     111 ->118        -0.13964
     111 ->119         0.12000
     111 ->120         0.47599

Excited State   9:    Singlet-A       4.7804 eV  259.36 nm  f=0.0152
     109 ->114         0.13274
     109 ->116        -0.10228
     110 ->119        -0.19379
     111 ->117         0.11674
     111 ->118         0.17182
     111 ->119         0.55296

Excited State  10:    Singlet-A       4.8481 eV  255.74 nm  f=0.0193
```

```
     103 ->112         0.12719
     104 ->112        -0.16689
     105 ->112         0.12327
     106 ->112        -0.11764
     110 ->113         0.31906
     110 ->115         0.11563
     111 ->115         0.33026
     111 ->117        -0.17517
     111 ->118        -0.24569
     111 ->120        -0.13791

Excited State  11:    Singlet-A       5.0776 eV  244.18 nm  f=0.0012
     104 ->112        -0.13386
     105 ->112        -0.11012
     106 ->112         0.18863
     107 ->112         0.18791
     109 ->112         0.19973
     110 ->115         0.19896
     111 ->115         0.28868
     111 ->117        -0.13880
     111 ->118         0.27574
     111 ->120        -0.18812

Excited State  12:    Singlet-A       5.0960 eV  243.30 nm  f=0.0748
     103 ->112        -0.12556
     104 ->112        -0.12012
     105 ->112        -0.18268
     106 ->112        -0.10090
     107 ->112        -0.10953
     109 ->112        -0.12212
     110 ->113        -0.17211
     110 ->115         0.19370
     111 ->115         0.28732
     111 ->117         0.38206
     111 ->120         0.12171
     111 ->124         0.10355
```

VITA

Graduate School
Southern Illinois University

Pamela C. Ubaldo

pamela.ubaldo@outlook.com

University of Santo Tomas, Manila, Philippines
Bachelor of Science, Chemical Engineering, March 2003

Special Honors and Awards:

C. David Schmulbach Award for Outstanding Teaching Assistant in 2012

Dissertation Title:

Towards Combined Computational and Experimental Studies on Toxicity of Silver Nanoparticles

Major Professor: Lichang Wang

Publications:

Peer Reviewed Journal Articles

Ubaldo, P. C., Mason, C. A., Chun, S. H., Wang, L.; Toxicity of Ag cations; "A Computational Study of the Interaction between Silver and Lipids present in HepG2 cells" Chem. Phys. Lett. (2015) – to be submitted

Ubaldo, P. C., Abshiro, H. D., Cavender, F. A., Means, J. C., Hales, D. B., Wang, L.; " Mechanistic Studies on the Toxicity of Citrate Stabilized Silver Nanoparticles to HepG2 cells" *Toxicol. Lett*. (2015) – to be submitted

Ubaldo, P. C., Harrell, B. L., Zhang, Q., Colley, N. D., Dick, B. J., Wang, L..; "The Best Functionals to Predict Optoelectronic Properties of MTPA Derivatives" *J. Chem. Theory Comput.,* **(2015)** – submitted

Ubaldo, P. C., Colley, N. D., Plunkett, K. N., Wang, L.; "Electron Acceptability of Cyclopenta-fused Polycyclic Aromatic Hydrocarbons: Effect of One Electron" J. Phys. Chem. **(2015)** – submitted

Wang, T., Weerasinghe, K. C., Ubaldo, P. C., Liu, D., Li, W., Zhou, X., Wang, L.; "Tuning electron-hole distance of the exitons in organic molecules using functional groups" *Chem. Phys. Lett.,* **(2015)**, *618*, 142-146

Book Chapter

Wang, L. and Ubaldo, P. C. In Silico Studies of Functional Transition Metal Nanoclusters. *Functional Nanometer-Sized Clusters of Transition Metals: Synthesis, Properties and Applications*; Chen, W., Chen, S., Ed.; Royal Society of Chemistry, Cambridge, U. K. **2014**; pp 323-351

Presentations:

Pamela C. Ubaldo, Nathan Colley, Kyle Plunkett, and Lichang Wang, "DFT and TDDFT studies of functionalized cyclopenta[hi]aceanthrylenes and dicylopenta[de,mn]tetracenes" (**poster**) at ACS National Meeting and Exposition, March 16-20, **2014**, Dallas, Texas

Pamela C. Ubaldo, Franklin Cavender, Henok Abshiro, Sarah Ladley, D.B. Hales, Jay Means, and Lichang Wang, " Computational and Experimental Studies on the toxicity of AgNP to HepG2 Cells" (**oral presentation**) at ACS National Meeting and Exposition, March 25-29, **2012**, San Diego, California

Pamela C. Ubaldo, Christian Mason, Ryan Chun, and Lichang Wang, "Theoretical and Experimental Studies of Interaction between Nano-Silver and Model HepG2" (**poster**) at Midwest Theoretical Chemistry Conference 2011, June 9-11, **2011**, University of Notre Dame, Indiana

Pamela C. Ubaldo, Christian Mason, and Lichang Wang, "Theoretical Studies of the Interaction between Nano-Silver and Model HepG2" (**poster**) at the 2010 Pacifichem Conference, December 15-20, **2010**, Honolulu, Hawaii

Pamela C. Ubaldo, Jennifer Yukna, Hongmei Tang, Jianbo Li, and Lichang Wang, "DFT Studies of Silver Clusters and their Binding with Model HepG2" (**poster**) at Midwest Theoretical Chemistry Conference 2010, May 20-22, **2010**, Purdue University, Indiana